UNIVERSIDAD TECNICA
FEDERICO SANTA MARIA

NUMERICAL AND EXPERIMENTAL INVESTIGATION OF SOLAR THERMOCHEMICAL GASIFICATION OF SOLID FUELS IN A HYBRID POROUS MEDIA REACTOR

by

Andrés Ignacio Arriagada Romero

A thesis submitted in partial fulfillment of the requirements under the institutional agreement within the framework of the dual doctoral program to obtain the degrees of

Doctor of Philosophy in Chemical Engineering

Department of Chemical and Materials Engineering

University of Alberta

and

Doctor of Philosophy in Mechanical Engineering

Department of Mechanical Engineering

Universidad Técnica Federico Santa María

Abstract

Within the framework of the ANID/FONDECYT/1241030 project, an experimental and numerical investigation was performed on the thermochemical gasification of solid fuels in a hybrid porous media reactor exposed to concentrated solar energy and in a chemically reacting fixed-bed for hydrogen (H_2) and syngas production.

An up-to-date literature review on H_2 and syngas production by thermochemical processes, including filtration combustion, porous media combustion, and hybrid filtration combustion (HFC), is presented from an experimental and numerical perspective. Incorporating solar energy and biomass, two of the most important Chilean renewable resources, is discussed as a key element for allothermal gasification. Building on the current state of the art in thermochemical gasification, **this thesis aims to address key gaps in understanding the fundamentals of heat and mass transfer inside inert and hybrid porous media reactors**.

In particular, this work aims to develop new permeability-based models, including intrinsic reacting particles using a porous media model (PMM) approach. The assessment of Reynolds number, inflow gas temperature and oxidative atmosphere, and the feasibility of a 2D axisymmetric porous media numerical model to represent a 3D particle-resolved approach of carbon char gasification are investigated. **The novelty of this research is tailoring a PMM approach, making results close to those obtained using a PRS model, opening new perspectives for the simulation of chemically reacting fixed-beds.**

Due to the complexity and the lack of literature regarding the use of biomass as a solid fuel for solar-driven gasification, all numerical studies were performed using carbon char particles. In this regard, a comprehensive study of the gasification of carbon char particles inside a fixed-bed reactor was performed using a three-dimensional model to analyze the effect of the inflow gas temperature, oxidative atmosphere ($Y_{O_2,in}$ = 0.05, 0.11, and 0.233), and Reynolds number (Re_{in} = 10, 50, 75, and 100). This work is next extended using a 2D

axisymmetric geometry and a continuum approach to investigate the use of simplified models to represent complex multiphysics reactive processes. Also, a macro-pore-resolved approach was studied against a porous media model using a single carbon char particle. These studies were performed to better understand the heat and mass transfer behavior of the phenomenon, specially at a pore-scale level, where porosity, tortuosity, effective diffusivity, dispersion, and thermal conductivity play a crucial role.

Regarding experimental-specific goals, this work aims to perform experiments in a hybrid porous media reactor exposed to concentrated solar energy, focusing on hydrogen and syngas production, and identify the most significant operational parameters according to experimental and numerical results to propose improvements to the processes for further research. In this regard, experimental research was conducted on the interaction of different mixtures of solid fuels inside a solar-driven gasifier for H_2 and syngas production at low temperatures ($\sim$ 600K). Since the ultimate numerical approach is the simulation of the solar-driven gasification reactor, a 3D-CFD based porous media model including char reacting particles treated as porous and inert solid particles is mathematically described.

Finally, an extension of this thesis and future recommendations are given regarding experiment designing, chemical kinetics, use of new solid and gaseous fuels, and key aspects to achieve a continuous operation of the system.

Keywords: Heterogeneous combustion, Hybrid filtration combustion, Solar-driven gasification, Fixed-bed reactor, Hydrogen production, Renewable energy, Computational fluid dynamics (CFD).

Preface

The present thesis is an original work by Andrés Ignacio Arriagada Romero. Chapters are presented in chronological order as they were published as original review/research articles. The computational models of Chapters 2, 3, and 4 have been designed and analysed by myself, with the assistance of Prof. Petr A. Nikrityuk, Prof. Robert E. Hayes (Department of Chemical and Materials Engineering, University of Alberta, Canada), and Prof. Mario Toledo (Department of Mechanical Engineering, Universidad Técnica Federico Santa María, Chile).

The content presented in Chapter 1 is based on the review article published in the Journal Renewable and Sustainable Energy Reviews. The article, titled **"Hydrogen and syngas production by hybrid filtration combustion: Progress and Challenges"**, may be accessed here: M. Toledo, A. Arriagada, N. Ripoll, E. Salgansky, and M.A. Mujeebu, Renewable and Sustainable Energy Reviews, **2023**. I composed the original draft, sequentially polished and refined under the valuable guidance of Dr. Mario Toledo, Dr. Nicolás Ripoll, Dr. Eugene Salgansky, and Dr. M. Abdul Mujeebu. My contributions constitute about 60% of the total work in this chapter, including the original draft and text writing, visualization and formal analysis.

The content in Chapter 2 is reproduced form an original manuscript entitled **"3D chemically reacting fixed-bed under gasification conditions for non-porous char: Laminar flow"**. The access can be obtained here: A. Arriagada, M. Toledo, R.E. Hayes, and P.A. Nikrityuk, Journal of the Energy Institute, **2023**. Andrés Arriagada Romero is responsible for CFD simulations, post-processing the results, original draft and text writing, validation, and visualization, which constitute about 80% of the total work in this chapter.

Chapter 3 of this work has been published as **"Modeling of a moving reacting carbon char particle using macro-pore-resolved and porous media approaches"**. The

access can be obtained here: A. Arriagada, M. Toledo, R.E. Hayes, and P.A. Nikrityuk, Industrial & Engineering Chemistry Research, **2024**. Andrés Arriagada Romero is responsible for CFD simulations, in-house code development, post-processing the results, original draft and text writing, validation, and visualization, which constitute about 85% of the total work in this chapter.

The content in Chapter 4 is based on an original manuscript entitled **"Verification of a porous media model for the partial oxidation of a chemically reacting fixed-bed"**. The access can be obtained here: A. Arriagada, M. Toledo, R.E. Hayes, D. Paschenko and P. Nikrityuk, Fuel **2024**. Andrés Arriagada Romero is responsible for CFD simulations, in-house code development, post-processing the results, original draft and text writing, validation, and visualization, which constitute about 85% of the total work in this chapter.

In all aforementioned chapters, my major technical contribution was developing CFD models using the ANSYS Fluent 22R2 commercial package, developing in-house user-defined function codes, and post-processing data using Tecplot 360 EX software. Dr. Petr Nikrityuk, as the supervising author, made significant contributions to the conceptualization of the research topic, provided valuable supervision and steering throughout its development, and contributed to the review and editing of the manuscript. I composed the original draft, sequentially polished and refined under the valuable guidance of Dr. Petr Nikrityuk, Dr. Robert E. Hayes, and Dr. Mario Toledo.

Chapter 5 of this work has been published as **"Solar-driven gasification for syngas production at low temperatures using a rotary hybrid porous media reactor"**. The access can be obtained here: A. Arriagada, R. Mena, N. Ripoll, R.E. Hayes, P. Nikrityuk and M. Toledo, Chemical Engineering Journal **2024**. Andrés Arriagada Romero is responsible for writing – original draft, visualization, investigation, formal analysis, and data curation, which constitute about 70% of the total work in this chapter.

In this chapter, Dr. Mario Toledo, as the supervising author, made significant contributions to the conceptualization of the research topic, provided valuable supervision and steering throughout its development, and contributed to the review and editing of the manuscript. I composed the original draft, sequentially polished and refined under the valuable guidance of Dr. Mario Toledo, Dr. Robert E. Hayes, and Dr. Petr Nikrityuk.

Para mis padres Bernardo y Elizabeth

El futuro es de aquellos que creen en la belleza de sus sueños.

Gracias por siempre creer en mí.

Acknowledgments

This journey started in April 2021 after two years of thinking about my future and what I really want to do for the next 35 years. As a challenge itself, this dual doctoral degree program has brought knowledge, experience, tools and new perspectives to my life. After a pandemic, several crises, 14 courses, a professional development program, teaching three undergraduate courses, working as a teaching assistant for three undergraduate courses, four conferences, one international forum, eleven research articles, two candidacy exams, several seminars, mixers, and working on a few research grants, I have some words for those who have been crucial during this time.

I extend my heartfelt appreciation to my esteemed thesis advisors and supervisors, Dr. Robert E. Hayes, Dr. Petr A. Nikrityuk, and Dr. Mario Toledo. Your guidance, expertise, and patience were instrumental in shaping this research. Your continuous encouragement, insightful feedback, and willingness to engage in discussions were invaluable. I am genuinely grateful for the knowledge and skills I have gained under your mentorship.

I acknowledge the financial support of the National Agency for Research and Development (ANID) / Scholarship Program / DOCTORADO BECAS CHILE/2021 – 21211230, SERC Chile FONDAP 1523A0006, Dirección de Postgrado (DPP) and Proyecto Ingeniería 2030 at Universidad Técnica Federico Santa María, the Faculty of Graduate & Postdoctoral Studies (GPS) at the University of Alberta, and the Natural Science and Engineering Research Council of Canada (NSERC, RGPIN-2019-03914). Also, to the faculty, staff and students in the Department of Chemical and Materials Engineering at the University of Alberta, and the Department of Mechanical Engineering at Universidad Técnica Federico Santa María, who provided me with an enriching academic environment and prompt administrative support. Special thanks to Prof. Joe Mmbaga, Fabián Guerrero, Prof. Patricio Reveco, Lorena

Espinoza, and the students who I worked with for their constant support, and great talks during these years. I am grateful for the opportunities I have had to explore the world at different conferences throughout my tenure program; Madrid, Spain, Darmstadt, Germany, Kyoto, Japan, Princeton, USA, and of course, Edmonton, Canada.

I immensely thank my dear friends in Chile and Canada. Thanks to Gonzalo, Pablo, Kevin, José, Agustín, Ricardo for their moral support and friendship throughout this journey. Also, I thank Edmar, Sergio, and Angélica for all the talks and activities we did during my two-year stay in Canada. I wish to extend my thanks to my friends and teammates, Chinmay and Doston, for their fruitful collaboration and informative discussion sessions. Thank you for being my sounding board and celebrating the milestones together. I am fortunate to be surrounded by such reliable, genuine, and trustworthy people.

I sincerely thank my family for the unwavering support and encouragement. Specially to my parents Bernardo and Elizabeth, my brother Pablo, Nala, Paulina, and those who are taking care of us from heaven: Mama, Tata. Your belief in me has been a constant source of motivation. Your presence in my life made the challenging moments bearable and the joyous moments more delightful.

Finalmente, fuera de la formalidad de la tesis en inglés, me parece justo tener un pequeño espacio para escribir algo en español. La tesis de doctorado es más que conocimiento científico. Es aprendizaje para toda la vida. Aprender a luchar frente a las adversidades, las constantes injusticias y malos ratos. Ahí es donde sin la familia no somos nada. Embarcarse en este viaje es también valorar y disfrutar el enseñar, transmitir, conversar, conocer lo que hay detrás de las caras en el día a día. Por mucho que se haya aprendido en lo técnico, los mayores aprendizajes están en el proceso: Caerse está permitido, escuchar, decir que no, y por sobretodo, agradecer, porque la vida es corta, y se debe matar viviendo.

Es gibt immer etwas Neues zu entdecken. There is always something new to discover. Siempre hay algo nuevo por descubrir.

Table of Contents

List of Tables

List of Figures

Chapter 1

Hydrogen and syngas production by thermochemical processes[*]

[*]This chapter is based on the review article published in M. Toledo, A. Arriagada, N. Ripoll, E. Salgansky, and M.A. Mujeebu, Renewable and Sustainable Energy Reviews, **2023**.

1.1 Abstract

Hydrogen (H_2) and syngas (a mixture of H_2 and carbon monoxide) can be thermochemically produced from various sources, such as fossil fuels, biomass, water, and solid wastes, via steam reforming, dry reforming, and partial oxidation. In this scenario, hybrid filtration combustion (HFC), where aleatory solid fuel and inert particles compose a porous bed, has been identified as a robust and feasible alternative for sustainable energy production from solid and gaseous fuels, thus glimpsing new opportunities for the development of new reactors. This technology has been studied for different applications using several solid fuels, analyzing the effect of varying the gasifying agents inside the reactor (mainly tested for carbon dioxide, steam, and premixed air/fuel flows) both empirically and numerically. The latter has a promising future since no three-dimensional approaches have been found in the literature. After providing a brief conceptual background, this chapter presents a review focused on hydrogen and syngas production by thermochemical processes, including gasification, HFC technology, numerical approaches, fuel diversity, operational conditions, and the incorporation of renewable energy in HFC technology, such as solar and energy from biomass. This could help identify future challenges ahead regarding this technology and decide on new directions for further research.

Keywords: Hydrogen, Hybrid filtration combustion, Porous media reactor, Computational Fluid Dynamics, Renewable energy.

Nomenclature

Roman Symbols	Definition
B_f	Solid fuel combustion rate
C	Specific heat capacity
D	Species diffusion coefficient
H	Enthalpy
Q	Standard heat of reaction
r	Reaction rate
S	Source term for species
t	Time
T	Temperature
$\vec{u}$	Filtration velocity
v	Velocity of reaction wave
Y	Mole fraction of species
W	Molecular weight

Greek Symbols	Definition
γ	Stoichiometric coefficient
ε	Fraction of heat retained in solid phase
θ	Porosity
λ	Thermal conductivity
ξ	Heat transfer coefficient
ρ	Density
ϕ	Equivalence ratio
η	Solid fuel conversion

Abbreviations	Definition
FC	Filtration combustion
FCL	Forward combustion linking
GHG	Greenhouse gas
HFC	Hybrid filtration combustion
HSC	HYbrid solar combustor
IPM	Inert porous media
MSW	Municipal solid wastes
N_{HE}	Number of heterogeneous reactions
N_{SP}	Number of species considered
PMC	Porous media combustion
RCL	Reverse combustion linking
RL	Reaction leading
RT	Reaction trailing
ST	Stationary thermal
SMR	Steam methane reforming
UCG	Underground coal gasification

Subscripts	Definition
f	Fuel
g	Gas
i	Inert component in the solid
j	Ordinal number
s	Solid

1.2 Introduction

Global carbon dioxide (CO_2) emissions increase every year, profoundly impacting the climate scenario given by climate change. As a matter of fact, and after the oscillating scenario caused partly by the COVID-19 pandemic, CO_2 emissions grew by 321 Mt in 2022, reaching a new high of over 36.8 Gt [1, 2]. The energy sector contributes the most considerable amount of greenhouse gas (GHG) emissions to this phenomenon, adversely affecting biodiversity and human health [3–6]. Moreover, climate change negatively impacts the photovoltaic solar energy potential, one of the most important sources of climate change mitigation at present [7, 8]. Therefore, the energy sector plays a crucial role when facing this global concern [9], where novel energy utilization processes are at the forefront of modern technological

development to address this challenge. New efficient and eco-friendly processes must be developed and implemented in the transport, industrial, commercial, and residential sectors. In this context, several countries are implementing new energy policies to decarbonize their energy matrix, considering the depletion of fossil fuels, and understanding its crucial role towards 2050 [10–12].

Porous media combustion (PMC), an extension to filtration combustion (FC), is a sufficiently well-known technology that has been extensively studied during the last decades, including its applications [13–16], being a feasible alternative for tackling technical and energy perspectives of the problems described above. It is defined as a combustion wave that travels through a medium composed of an inert solid and interstitial spaces (porosity) that percolate through the solid occupied space. Hybrid filtration combustion, hereafter abbreviated as HFC, establishes a relationship between inert porous media combustion and solid fuels gasification, combining the properties of these processes by replacing a fraction of the inert solid volume with solid fuel, producing a simultaneous conversion of the solid and gaseous fuels to energy [17, 18]. In this case, a combustion wave is produced by a flow that can contain hot air, water-steam, and/or gaseous fuel-air mixture [19] and propagates, reforming the solid fuel contained in the porous medium within a wide range of thermal power with a high energy concentration per unit of volume, and with high efficiency. Researchers have studied inert porous media (IPM) and HFC technology, detecting many essential advantages, such as low pollutant emissions, high thermal stability, increased reaction temperature due to its internal heat recirculation, and extended flammability limits, among others [20–22]. Abdul Mujeebu [13] reviewed H_2 and syngas production by superadiabatic combustion with and without a porous medium, partially covering HFC. Haugen et al. [23] have made a thorough review on numerical approaches for thermochemical conversion of char, which may be understood as the baseline of HFC technology, where there are chemically reacting particles inside the reactor. Accordingly, hybrid filtration combustion technology can be successfully used for producing energy from wastes that are economically unsuitable for processing by traditional technologies. This opens new perspectives for the valorization of energy from solid fuels to obtain valuable chemical compounds and those already developed [24, 25], which offers a broad scope for future research in this field, recognizing HFC as a green technique

for energy production from solid sources.

The aim of this chapter is giving a comprehensive review on hydrogen and syngas production by thermochemical processes, particularly exploring inert porous media combustion (PMC), hybrid filtration combustion (HFC), and solar-driven gasification, from both experimental and numerical perspectives to highlight the research gap covered by this doctoral thesis, finishing this chapter with the hypothesis and research objectives.

1.3 Theoretical framework and conceptual background

1.3.1 Hydrogen/syngas production methods

This section gives a brief outline of the various methods of H_2/syngas production. However, by considering the specific aim of this chapter, a detailed comparative analysis of all these techniques is excluded. H_2 and syngas are not readily available in nature in its pure form; therefore, the use of specifically devised processes is necessary to obtain them to be used as feedstock for the chemical industry and/or as fuel. In general terms, H_2/syngas production routes can be thermochemical, electrolytic, direct solar water splitting, and biological. Previous review articles have covered the details of these processes, while providing detailed comparisons and discussions [26–28]. Furthermore, Epelle et al. [29] reviewed the recent advances in renewable hydrogen production methods with a specific focus on the comparison of different nanomaterials used to enhance H_2 production. The thermochemical processes of H_2/syngas production mainly include steam reforming, dry reforming, and partial oxidation [30, 31] from various feedstocks such as fossil fuels, biomass, hydrogen sulfide (H_2S), and water [26, 32–34]. Depending on the process employed, the source of the fuel, the environmental impact, and efficiency, an appropriate color is assigned to the produced H_2, which is summarized in Table 1.1. For instance, gray H_2 is produced from fossil fuels, mainly natural gas, by steam methane reforming (SMR) process, which emits significant amount of CO_2. Currently, more than 70% of the global H_2 production is by large-scale SMR processes [35]. The H_2 production methods from both natural gas and coal are similar [27], and the products comprise CO, H_2, and CO_2 along with steam or methane (CH_4) [36]. For each ton of H_2

generated from coal, the amount of carbon released to the atmosphere is 5 tons, while it is 2.5 tons from other hydrocarbons [37]. Blue H_2 refers to that produced from fossil fuels with CO_2 capture during the process, and it is less polluting than gray H_2. However, green H_2 is produced from renewable sources such as solar, wind, or biomass, and also by electrolysis and different other methods [27, 32]. In this regard, water is one of the most abundant and inexhaustible raw materials on Earth and can be used for H_2 production through water electrolysis, which is one of the most basic methods to generate almost pure hydrogen [26, 38]. If the energy input is provided from renewable sources, H_2 produced by water-electrolysis will be the cleanest (greenest) energy carrier [39, 40].

Table 1.1: Overview of hydrogen production methods: Environmental impact, efficiency, and cost [41].

Hydrogen Production	Primary Resources	kg CO_2eq/kgH_2	Efficiency (%)
Gray Hydrogen	Natural Gas, Coal	7.5 - 25	60 - 85 % (Natural Gas) 74-85% (coal gasification)
Blue Hydrogen	Natural Gas + CCS	$3.97 - 6.87$	$55 - 80\%$ (with CCUS)
Turquoise Hydrogen	Methane	$3.94 - 9.91$	Not specified
Green hydogen	Water electrolysis	~ 0	60 - 85%
Pink/Red Hydrogen	Nuclear Energy	$0.1 - 0.6$	Not specified
Yellow Hydrogen	Solar Energy	~ 0	Variable
Biohydrogen (BmH_2, BwH_2)	Biomass, Biowaste	6.7 - 9.8 (biogas reforming)	Not specified
White hydrogen	Nuclear Energy	0.87 (Cu-Cl cycle)	Not specified

1.3.2 Gasification of solid fuels

Gasification is the process of transforming organic or fossil-based carbonaceous materials such as coal or biomass into a gaseous fuel (syngas) in the presence of steam, CO_2, oxygen (O_2), air, or mixture of these gasifying agents [42, 43] at high temperature (around 1100 K) and moderate pressure (from atmospheric pressure to 70 bars) [44–46], and it is shown in Figure 1.1.

Being an endothermic process, the heat for gasification can be produced by partial oxidation of the fuel inside the reactor (autothermal gasification) or can be supplied by an external heat source (allothermal gasification) [47, 48]. Conventional gasifiers are classified based on the type of bed and the direction of the gaseous flow [49]; their functioning principles and main features are well documented [50]. Biomass gasification differs from

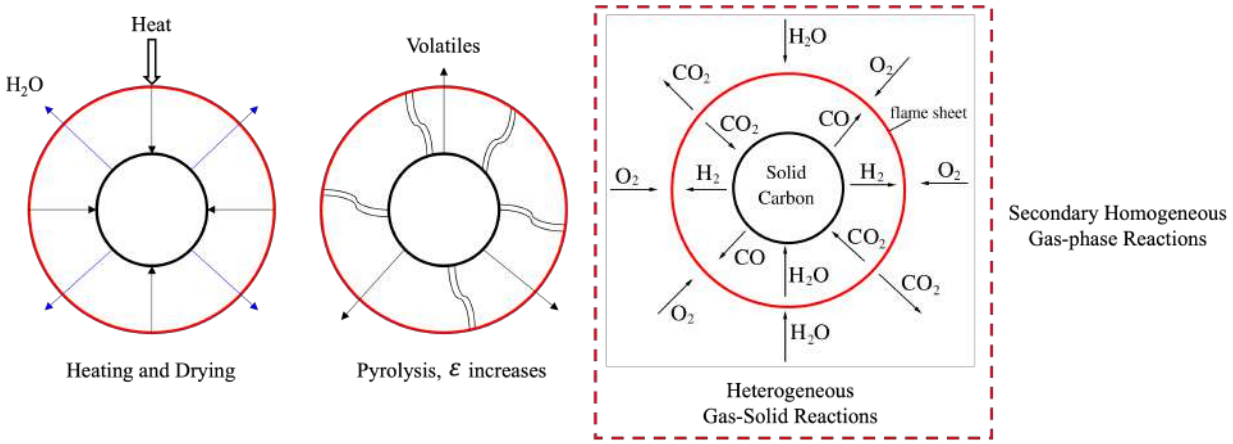

Figure 1.1: Schematics of the gasification of a single coal particle.

coal gasification mainly because biomass is a carbon-neutral and sustainable energy source [49, 51]. Moreover, as biomass is more reactive and has a higher volatile content than coal, the gasification can occur at lower temperatures, which reduces heat loss, undesired emissions, and material problems associated with high temperatures [49]. Biomass also has a low sulfur content, which results in less sulfur oxide (SO_X) emissions [49]. However, due to specific inorganic species, slagging, fouling, and corrosion are common problems in biomass gasification [49, 52]. Other challenging issues of biomass gasification are tar formation and moisture content [42, 53]. At high temperatures, tar exists in gaseous state, uniformly mixed with the gaseous products [54], whereas at low temperatures (< 500 K), tar condenses and bonds with water and char, blocking gas pipelines [55]. Moreover, tar formation causes severe problems in downstream particle removal devices (e.g., filters and cyclones), gas turbines, and engines [51]. Nonetheless, several methods to reduce tar are currently known: fast pyrolysis [51, 52], thermal cracking [56–58], high-temperature steam reforming [52, 59], dry reforming [60], catalytic cracking [61], partial oxidation [62], and plasma reforming [63]. Excessive moisture in biomass reduces the quality and yield of the produced gas and the system performance, besides other issues [53]. Also, lower energy density and the presence of heteroatoms (especially oxygen) can reduce the potential for biomass gasification compared to coal gasification. On the other hand, the main disadvantage of conventional autothermal gasification technology is the production of undesired species such as particulate matter, tar, and char [64, 65]. The emission of these species is highly associated with operating condi-

tions such as temperature, pressure, heating rate, and residence time [66]. Thus, gasification as a process still requires further optimizations to enhance its energy efficiency by overcoming the aforementioned challenges [67, 68]. Since temperature, residence time, and oxygen availability are key factors that govern the destruction of tar produced during biomass/solid fuel gasification [57], the process could be improved by techniques that can effectively control these parameters. Accordingly, gasification by FC/PMC under superadiabatic condition has been explored and successfully demonstrated [69, 70]. Besides being more environment friendly and efficient, this method allows gasification of high-ash and humid fuels [71]. Later on, the FC technique was developed into HFC, where the gasification of solid fuel alone or concurrently with gaseous fuel occurs in a hybrid porous media reactor [72, 73]. Hydrogen/syngas production from carbonaceous feedstocks by HFC reactors offers high reaction temperatures (900-1800 K) for different equivalence ratios (due to enhanced heat transfer by conduction, convection, and radiation) and low solid particle emissions [73, 74]. The FC or HFC reactors work on thermal partial oxidation [75, 76], which has gained wide recognition as one of the effective methods for tar reduction during biomass gasification.

1.3.3 Filtration combustion with heat recuperation

The term filtration combustion (FC) was first reported by Russian researchers to explain the process of combustion synthesis of refractory nitrides by oxidizing metal powders in the presence of a nitrogen atmosphere [77]. Afterwards, the term was used to describe the in-situ underground coal gasification (UCG) by forward or reverse combustion linking (FCL or RCL) [78–80]. However, processes that involve filtration of gases through porous media with chemical reactions are generally regarded as filtration combustion [81, 82]. Depending on the relative directions of propagation of the combustion wave, the oxidant, and the product gas, FC is classified as coflow FC and counter-flow FC [80, 83, 84]. In the coflow FC, there is a possibility of heat recuperation from the reacted zone to the incoming fresh oxidant. Nevertheless, the excess enthalpy theory of Weinberg [85] suggested the possibility of preheating the fresh air-fuel mixture by heat recirculation (by internal or external means) from the combustion products without direct mixing of the products with the reactants. This borrowing of enthalpy from the combustion products could increase the reaction temperature

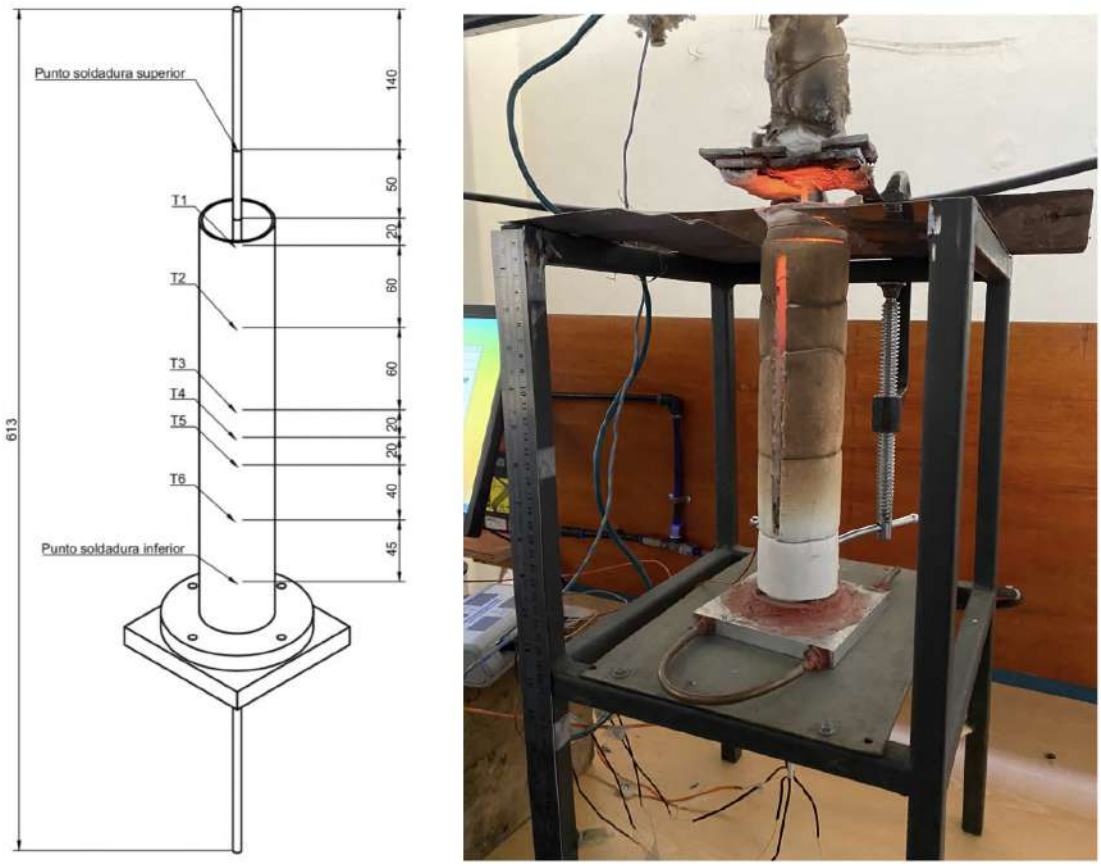

Figure 1.2: Inert porous media combustion reactor used in experiments at UTFSM, Chile.

above that of the thermodynamically possible flame temperature of a given fuel/air ratio of the mixture, thereby realizing an excess enthalpy or superadiabatic flame [86]. In this case, the maximum temperature in the combustion zone can exceed the adiabatic temperature of the mixture by several hundred degrees. Thus, by incorporating the Weinberg theory, the coflow FC was later extended for combustion of gaseous and liquid fuels, as well as powdered solid fuel within an inert/catalytic porous medium (abbreviated previously as PMC in this chapter). In PMC, the internal self-organized heat recuperation from the reaction zone to preheat the incoming fresh fuel-air mixture is facilitated by the solid porous medium. In fact, PMC is often named in the literature as inert filtration combustion, lean filtration combustion, and/or rich filtration combustion [87–90]. Figure 1.2 shows an example of a PMC reactor used for experimental work at Universidad Técnica Federico Santa María (UTFSM), Chile.

1.3.4 Hybrid filtration combustion

Hybrid filtration combustion (HFC) is a multiphase, multiscale, and multiphysics process that stablishes a relationship between inert porous media combustion and solid fuels gasification, replacing an inert solid fraction volume with solid fuel, producing a simultaneous conversion of the solid and gaseous fuels to energy (lean combustion) or hydrogen and syngas (rich combustion) [17]. This process, depicted in Figure 1.3, describes a simultaneous thermal conversion of gaseous and solid fuels when the gaseous fuel-oxidant mixture filters through a porous packed bed composed of solid fuel and inert particles, but also the thermal conversion of solid fuel when only gaseous oxidant filters through the porous packed bed composed of solid fuel and inert particles [91]. Hybrid filtration combustion can be successfully used for producing green energy from wastes that are economically unsuitable for processing by traditional technologies. A gaseous oxidant flow produces a reaction wave through the process, which can be hot air, water steam, or a gaseous fuel-air mixture that propagates along the reactor reforming the solid fuel inside within a wide power range, high efficiency, high energy concentration per unit of volume and stable combustion over a wide range of equivalence ratios [92–94]. As a result of a composing porous medium, observed combustion temperatures can be lower when compared to IPM values. Upstream and downstream wave propagations are present in the hybrid porous reactor. The upstream wave propagation in the composite bed is similar to the inert bed, but the downstream wave propagation shows a flat temperature profile with practically constant temperature along the reactor. As almost all fuels contain chemically inert admixtures (e.g., ash) from the very beginning, the porous medium ahead of the reaction zone in the general case is a mixture of solid fuel and inert material. The substances formed behind the combustion front are a porous residue containing ash and solid combustion products. The heat released during the reaction is transferred to nonreacted layers of the substance with a lower temperature and initiates their own heat release, which results in self-sustaining propagation of the reaction wave. Due to the solid fuel's heterogeneous interaction with the gaseous oxidizer can form both solid and gaseous products in the filtration combustion wave [95, 96]. The most important operational parameters through the HFC process are injection velocity for the premixed flow and the equivalence

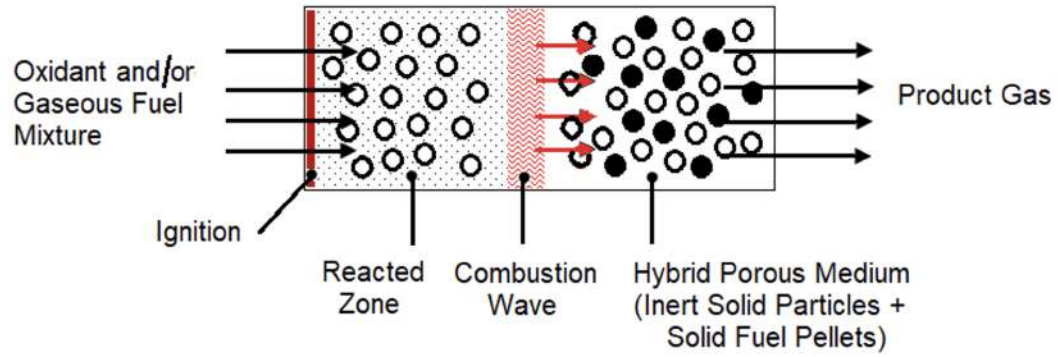

(a)

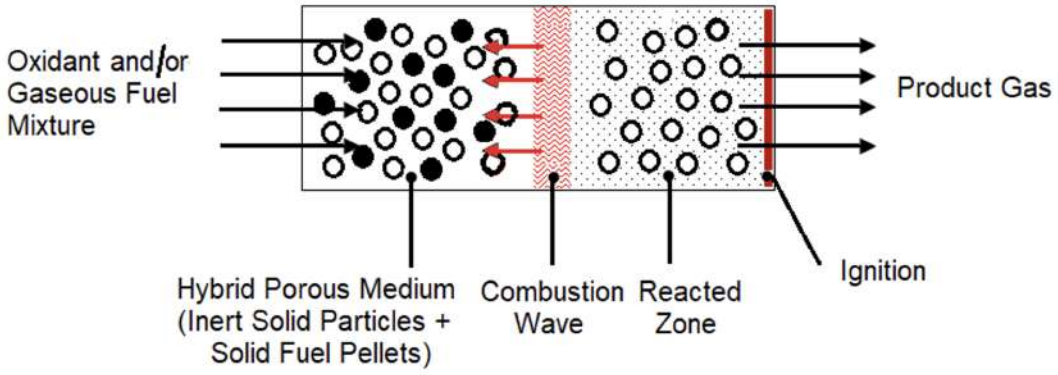

(b)

Figure 1.3: Hybrid filtration combustion for coflow (a) and counterflow (b) combustion of gaseous and solid fuels.

ratio (φ), both playing a crucial role in the process, obtaining a different temperature for the wave combustion and the gaseous mixture.

The combustion temperature in composite bed decreases from rich to ultra-rich gas fuel-air mixtures, and the increase of solid fuel volume fraction in the porous media. At high downstream propagation velocities close to the stoichiometric conditions, the role of the gaseous phase kinetics is controlled. In these conditions, the upstream wave propagation suppresses the heterogeneous processes by the total consumption of the oxidizer agent. At higher equivalence ratios, the wave propagation is slower. This remarks the role of heterogeneous kinetics, which results in the ignition and combustion temperatures drop, impacting the wave velocity. The mechanism of heterogeneous combustion becomes prevalent for downstream wave propagation. The slowly reacting solid fuel is directly exposed to the oxidizer agent. The ignition initiated over the solid phase is further transferred to the gaseous phase.

In this case, it is possible to suggest that the wave structure involves a heterogeneous reaction front followed by the gas phase reaction front. These fronts are followed by a slow endothermic reaction between the forms of steam and solid/gaseous fuels. The propagation of downstream hybrid combustion waves in the fuel loaded medium result in broad combustion fronts with superadiabatic combustion temperatures. The flat temperature profile remarks that the fuel particles are burning upstream of the front. Lean combustion results in the complete burnout of the hydrocarbon fuel, with CO_2 and water production being both the composition of the final products and the heat release properly defined [97]. In contrast to lean combustion, the partial oxidation products of rich and ultra-rich waves are not clearly defined. In this case, fuel is only partially oxidized in the wave, and the total heat release could be kinetically controlled by the degree of oxidation. As a result, chemical kinetics, heat release, and heat transfer are strongly coupled in the rich and ultra-rich waves, turning it into a more complicated phenomenon than the lean wave [17]. As a multiphysics problem, heat transfer is deeply involved in HFC technology. Figure 1.4 depicts how the well-known heat transfer mechanisms, i.e., conduction, convection and radiation, play a crucial role inside a hybrid porous media reactor. In particular, black and white circles represent a solid fuel and inert material, respectively. Moreover, conduction and radiation act as a heat recirculation mechanism, preheating inflow gaseous phase and therefore, achieving superadiabatic temperatures along the reactor. Convection is mainly driven by the direction of the inlet condition of the reactor.

Frequently an unstable combustion wave is observed. This instability is caused both by the difference in the gas permeabilities of the solid porous material ahead of the combustion zone and the solid combustion products [98] and by the dependence of the total gas permeability of the mixture on the fraction composition. The gas permeability of the solid can change because of the melting of the solid products and the formation of channels whose characteristic size is larger than the particle size in the initial mixture [99]. Combustion front stability might create difficulties in technologies based on filtration combustion. Current combustion theory dismisses the motion of the solid phase or considers uniform motion in the direction perpendicular to the combustion front. However, if one succeeds in creating conditions under which the velocity of radial motion of particles of the material in the

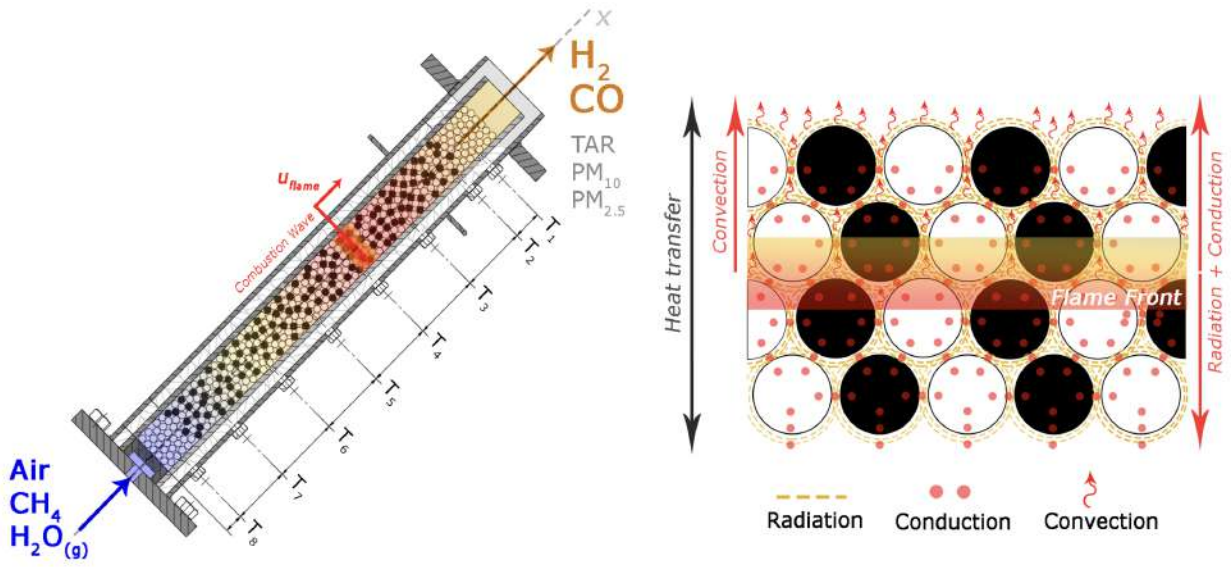

Figure 1.4: Autothermal HFC process scheme and heat transfer mechanisms interaction between solid particles.

combustion zone exceeds the instability development rate, then one can avoid the formation of regions emptied by burning. For this purpose, the reactor can be placed at an angle to the horizontal and may be rotated about its axis [100, 101]. The inclined position of the reactor causes the formation of a single burning-emptied region in the upper part of the combustion zone, and the rotation of the reactor ensures the filling of the burning-emptied region by unburned material. Stirring promotes both filling of cavities and channels and the redistribution of red-hot solid particles in a reactor section plane, making the combustion wave stable [102, 103].

The main advantages of hybrid filtration combustion include a wider power range, higher efficiency, higher energy concentration per unit of volume, and stable combustion over a wide range of equivalence ratios due to the capacity of the porous media to recirculate the heat within the reactor. Therefore, temperature exceeding adiabatic values can be attained at equilibrium due to a larger superficial area offered by the porous media, which is responsible for heat transfer between gaseous and inert solid phases. Various mathematical models regarding HFC modeling have been proposed and analytically and numerically solved. Salgansky et al. [95, 104] described a model based on the original one proposed by Aldushin et al. [82] with the first approach to filtration combustion with a hybrid porous bed. Toledo

and Rosales [17] extended these models for the general case of HFC technology. In both models, apart from the governing equations representing gas-phase energy, inert solid phase energy, and conservation of mass for the gaseous phase [90, 105, 106], a fourth equation is introduced to represent mass conservation of the solid fuel. A novel feature of the HFC model is the relatively complex chemical kinetics that couples three types of reactions: homogeneous, devolatilization, and heterogeneous. The relevance of this coupling is due to the sustaining simultaneous reactions (combustion, gasification and/or pyrolysis) involving gaseous and solid fuels.

The main control parameters of HFC are presented in Table 1.2. The solid phase usually consists of a mixture of combustible and inert particles. Materials such as coal, peat, biomass, polymers etc. can be used as fuel. The mass content of combustible material in the mixture can vary from 5 to 100%. An inert material can be both fuel ash and an added refractory material (alumina, chamotte, porcelain and others). The gas to be filtered can generally contain both an oxidizing agent (air, steam, carbon dioxide) and a combustible gas (methane, butane etc.). The HFC process is carried out for both lean ($\varphi < 1$) and rich mixtures ($\varphi > 1$). In this case, the gas filtration velocity through the porous filling can reach a value of 1 m/s. Most of the reactors are of the batch type and have a cylindrical geometry.

Table 1.2: HFC controlling parameters.

Reference	Solid Fuel	Mass fraction of solid fuel in porous medium, %	Inert particles	Gaseous Oxidant (equivalence ratio)	Filtration velocity, cm/s	Reactor type
Toledo et al. [91]	Wood pellets	50	Alumina spheres	Butane/air $1.0 \leq \varphi \leq 2.6$	$13 - 14.4$	Batch
Toledo et al. [107]	Coal particles	$0 - 75$	Alumina spheres	Natural gas/air $1.0 \leq \varphi \leq 3.8$	$12 - 19$	Batch
Gentillon et al. [108]	Polyethylene pellets	50	Alumina spheres	Propane/air $1.0 \leq \varphi \leq 1.65$	11.7	Batch
Araus et al. [109]	Wood pellets	50	Alumina spheres	Natural/air $0.3 \leq \varphi \leq 1.0$	15	Batch
Caro et al. [110]	Oat cane, wheat cane, Eucalyptus nitens and Pinus radiata pellets	50	Alumina spheres	Natural gas/air, $\varphi = 1.1$ and steam	$26.1 - 36.5$	Batch
Toledo et al. [72]	Biomass	12.5– 62.5	Alumina spheres	Natural/air $0.2 \leq \varphi \leq 1.1$	15	Batch
Ripoll et al. [111]	Algae biomass particles with moisture content $(0 - 100\%)$	$0 - 100$	Alumina spheres	Natural/air, $\varphi = 1.2$	27.6	Batch
Toledo et al. [74]	Waste tires particles	50	Alumina spheres	Air, steam and natural gas $(0.3 \leq \varphi \leq 1.4)$	$4.2 - 33.2$	Batch
Salgansky et al. [71]	Coal dust/Peat dust	$5 - 100$	Porcelain rings/ Alumina spheres	Air/steam	$10 - 100$	Continuous

Having gained an understanding of FC, PMC, and HFC from the preceding sections, there need to be clarifications on how these processes differ from smoldering ('smouldering' in British English) [112]. Accordingly, a comparison of all these techniques has been made as summarized in Table 1.3. Unlike FC, PMC, and HFC, smoldering is basically a fire hazard and is characterized by a low temperature and burning rate [112–114]. The oxidation process occurs mainly in heterogeneous reactions, while the reactions in the gas phase can be neglected. With an increase in the rate of homogeneous reactions, a transition from

smoldering to combustion occurs. Also, the transition to combustion can be caused by the acceleration of the coke oxidation reaction with an increase in the gas flux [98, 115, 116]. Smoldering is initiated and sustained at the surface of the solid, and it creeps through the porous matrix under favorable conditions. Smoldering can also happen to liquid fuels soaked by inert porous materials [113]. Though smoldering is a natural or accidental phenomenon, its chemistry has been a topic of intensive research, which has reached to the consensus that further research is needed to understand it completely and to explore its potential applications.

Table 1.3: Comparison of smoldering with FC, PMC and HFC.

Characteristic	**Combustion type**			
	Smoldering	Filtration combustion	Porous media combustion	Hybrid filtration combustion
Oxidant	Natural air	Supplied air	Supplied air	Supplied oxidant or oxidant-gaseous fuel mixture
Reactant	Solid or liquid fuel	Solid fuel	Supplied gaseous or liquid	Solid fuel particles contained by the hybrid porous bed with or without supplied gaseous fuel
Reaction medium	Solid surface or porous matrix	Porous material	Inert or catalytic porous medium	Hybrid porous bed made of solid fuel and inert solid particles
Oxidation Level	Partial	Partial or full	Partial or full	Partial or full
Occurrence	Natural or accidental	Manual initiation	Manual initiation	Manual initiation
Controllability	Uncontrollable and can lead to flaming combustion	Controllable	Controllable	Controllable
Relative propagation of oxidant and combustion wave	Forward or reverse	Forward or Reverse	Forward or reverse	Forward or reverse
Temperature	Low	Average	High	High
Combustion rate	Low	Average	High	High
Homogeneous reactions	Negligible	Important	Important	Important
Heterogeneous reactions	Important	Important	Negligible	Important
Products	Unintended products of partial combustion	Combustible gas (H_2, CO)	Combustible gas (H_2, CO) in partial combustion	Combustible gas (H_2 CO, tar) in partial combustion
References	[112–114]	[77–80]	[16, 22, 117, 118]	[72, 73]

1.3.5 Numerical approaches

Hybrid filtration combustion is a multiphase, multiscale, and multiphysics challenge, thus requires a proper analysis on the problem to ensure that its most relevant characteristics are well recognized, such as the complex chemical kinetics (homogeneous, devolatilization, and heterogeneous reactions), enhancement of the heat transfer mechanisms (thermal radiation, heat convection and conduction), the thermal, structural and hydrodynamic properties, and the coupling of simultaneous reactions involving different phases. Various studies have reported mathematical models of HFC, being analytically and numerically solved. Salgansky [95, 104] developed the first approach to a porous media combustion model based on the one proposed by Aldushin et al. [82]. Further on, Toledo and Rosales [17] extended the general case of this phenomenon, where coexists the partial oxidation of gaseous and solid fuels inside a reactor. These models consider four governing equations representing gas phase energy, inert solid phase energy, conservation of mass for the gaseous phase [90, 105, 106], and mass conservation of the solid fuel. Depending on the gaseous oxidizer utilized for each study, slight variations in the chemical kinetic schemes were found. These models do not consider a thermal equilibrium among the solid and gaseous phases, so the term H_V is added as a boundary condition, referring to the energy sources per unit of bulk volume, where $H_V = H_{V,v} + H_{V,HE} + H_{V,Q}$, where $H_{V,v}$ is the enthalpy received by the gas from the volatiles evolved from the solid fuel, $H_{V,HE}$ is the energy released towards the gas from reactions of the solid fuel, and $H_{V,Q}$ is the heat transfer from the solid to the gaseous phase, where $H_{V,Q} = \xi F (T_s - T_g)$. Thus, the fundamental equations governing the process are the following [17]:

Conservation of mass for gaseous species equation:

$$\frac{\partial \theta \rho_g Y_j}{\partial t} = \nabla \cdot (\theta \rho_g D_j \nabla Y_j) - \nabla \cdot (\theta \rho_g Y_j \vec{u}) + S_j \tag{1.1}$$

Conservation of mass for solid fuel species equation:

$$\frac{\partial \left[\rho_f (1-\theta)\right]}{\partial t} + \nabla \cdot \left[\rho_f (1-\theta)\right] \vec{v} = -B_f \tag{1.2}$$

Gas phase energy equation:

$$\frac{\partial \theta \rho_g C_{p_g} T_g}{\partial t} + \nabla \cdot \left(\theta \rho_g C_{p_g} T_g \vec{u}\right) = \nabla \cdot \left(\theta \lambda_g \nabla T_g\right) + \nabla \cdot \left(\theta \rho_g \sum_{j=1}^{N_{SP}} C_{p_j} T_g D_j \nabla Y_j\right) + H_V \quad (1.3)$$

Solid phase energy equation:

$$\begin{aligned} \frac{\partial \left[\left(\rho_f C_f + \rho_i C_i\right)(1-\theta) T_s\right]}{\partial t} + \nabla \cdot \left[\left(\rho_f C_f + \rho_i C_i\right)(1-\theta) \vec{v} T_s\right] = \\ \nabla \cdot \left[(1-\theta) \lambda_s \nabla T_s\right] - \frac{\varepsilon}{W_s} \sum_{\gamma=1}^{N_{HE}} r_\gamma^H Q_{R\gamma} - \xi F \left(T_s - T_g\right) \end{aligned} \quad (1.4)$$

In Equations 1.1 to 1.4, θ is porosity, ρ is density, Y is mole fraction of specie, t is simulation time, D is the diffusion coefficient of the species in the gas mixture, $\vec{u}$ is filtration velocity, S is the source term for species considered, $\vec{v}$ is velocity of the reaction wave, B_f is rate of solid fuel consumption by volatilization and heterogeneous reactions, T is temperature, λ is thermal conductivity, $\mathrm{N_{SP}}$ is the number of species considered, $\mathrm{H_V}$ refers to the sources of energy per unit of bulk volume, where $H_V = H_{V,v} + H_{V,HE} + H_{V,Q}$, where $\mathrm{H_{V,v}}$ is the enthalpy received by the gas from the volatiles evolved from the solid fuel, $\mathrm{H_{V,HE}}$ is the energy released towards the gas from reactions of the solid fuel, and $H_{V,Q}$ is the heat transfer from the solid to the gaseous phase, where $H_{V,Q} = \xi F \left(T_s - T_g\right)$, C is specific heat capacity, F is the solid fuel area, $\mathrm{N_{HE}}$ is the number of heterogeneous reactions, r is reaction rate, Q is standard heat of reaction, and ξ is the heat transfer coefficient. The subscripts (j) refer to the j species considered in the reactor, (g) to the gas phase, (s) to the solid phase, (f) to the fuel component in the solid, and (i) to the inert component in the solid. The system of equations is presented for the adiabatic case.

These mathematical models do not consider boundary conditions describing gas-solid interface interactions at pore-scale for mass and energy balances. Since the computational resources, power, and technology have exponentially increased over time, it is feasible to simulate complex engineering applications regarding fixed-bed reactors for engineering applications and the chemical industry, such as catalysis, steam methane reforming, and energy storage, among others [119–121]. As a matter of fact, numerical simulations for studying

carbon combustion have been previously reported in the literature for a one-particle model [122]. Nevertheless, and to the best of the authors' knowledge, there is no actual research found in the literature regarding three-dimensional chemically reacting particles in a fixed-bed reactor, being a tremendous opportunity to deeply explore these units from a numerical perspective. Numerical studies in this thesis will consider three stages with increasing complexity; the first one is related to the analysis of a chemically reacting fixed-bed reactor using solid carbonaceous materials in a three-dimensional approach, followed by studying the impact of intrinsic chemical reactions inside solid particles in both one-particle and fixed-bed reactor models. Since there is an important interaction between gaseous and solid phases on the surface of the particles (pore-scale level), mass and energy balances at the interface are affected by the heterogeneous chemical reactions. The production and destruction rates of gaseous species caused by these interactions, along with convective and diffusive mass fluxes of the gas phase species at the surface, are essential to set the following boundary conditions:

$$\rho_{\text{wall}}\, D_i \frac{\partial Y_{i,\,\text{wall}}}{\partial n} - \dot{m}''_C Y_{i,\,\text{wall}} \;= M_i \widehat{R}_{i,s} \tag{1.5}$$

$$\dot{m}''_C = \sum_{i=1}^{N_R} M_i \widehat{R}_{i,s} \tag{1.6}$$

$$\mathbf{n} \cdot \lambda \nabla T\big|_{\text{gas}} \;= \sum_{j=1}^{N} M_i \widehat{R}_{i,s} h_j^0 + \epsilon_{\text{s}} \sigma \left(T_{in}^4 - T_{\text{surf}}^4 \right) \tag{1.7}$$

Furthermore, heterogeneous reactions may modify the 'no-slip' condition used typically for zero velocity for fluids on chemically non-reacting surfaces. In this case, the velocity may be nonzero, also called Stefan flow, which characterizes the net mass flux between surface and gas [123]. This induced velocity is represented as $\boldsymbol{n} \cdot \vec{u} = \frac{\dot{m}''_c}{\rho}$, where $\boldsymbol{n}$ is the normal vector to the wall, and $\dot{m}''_c$ is the net mass flux between surface and gas. The kinetics of the carbonaceous feedstocks devolatilization involved could be approached via pyrolysis and gasification reactions, obtained through thermogravimetric analysis (TGA), being processed utilizing a specific software such as Gpyro [124], Thermakin [125], or FireFOAM pyrolysis model [126], and further contrasted with the modelled values that may be found in literature,

coming from several studies based on similar techniques [127–130]. This method has been used to characterize thermal decomposition of biomass under oxidative conditions, and to assess their potential combustibility as natural fuels [131–133]. This kind of kinetics mechanism provides a better prediction of the temperature profiles, products, and energy fluxes in the process [134]. Specific inorganic species, slagging, fouling, corrosion, tar formation, and moisture content are common problems in biomass gasification and must be considered in the chemical kinetics mechanisms regarding solar-driven gasification of biomass [42, 49, 52, 53]. Expected results include the temperature profiles, major product characterization profile, reactor behavior prediction for different operational conditions and utilized feedstocks, and a derived description of several multi-step reaction mechanisms for the gaseous and solid species involved. Through a sensitivity analysis, critical parameters might be identified, and a thorough analysis of how heat transfer mechanisms interact inside the reactor will be assessed in order to improve the renewable hydrogen production process and other applications, since temperature, residence time, and oxygen availability are key factors that govern the destruction of undesirables by-products produced during biomass/solid fuel gasification [57]. Toledo et al. [72] investigated the hybrid filtration combustion of biomass from a numerical perspective, solving governing equations using an implicit finite difference scheme, considering a forward first order scheme for the time related terms, a backward scheme for the convective terms and a second order central difference scheme for the diffusion terms. The resulting tridiagonal matrix was solved using the TDMA algorithm via a Fortran 90 code. The authors found a good agreement between numerical solutions predictions and experimental data for temperature and chemical products profiles. Important assumptions were made in this study, such as no pyrolysis model for biomass, a simplified kinetic mechanism for the thermal decomposition of biomass. Moreover, a higher biomass fraction inside the HFC reactor leads to a higher hydrogen production (4.17% for equivalence ratio of 0.2 and biomass fraction of 62.5%).

Ripoll et al. [135] investigated the gasification of carbonaceous feedstocks inside a batch reactor operating on a HFC mode in presence of solar steam aiming to hybridize conventional process. The governing equations were discretized and solved using the TDMA algorithm. Results showed that an increase on the coal presence favored a normal thermal structure,

observing a maximum temperature of 1,638 K at a 70% coal mass fraction, while an increase on the steam content led from normal to inverse thermal structure recording a peak temperature of 1618 K at a 0.95 H_2O/O_2 fraction and 50% coal presence.

1.4 Further applications of HFC technology

1.4.1 Use of renewable energies

Throughout this chapter, it has been widely commented that fossil fuels contribute to global warming, GHG emissions, and climate change. In this context, incorporating renewable energies in the HFC process, such as solar and energy from biomass, could help in the migration from gray to blue and green hydrogen, replacing fossil fuels and being an urgent challenge to address [136]. The literature has widely reported efforts to understand the effect of hybridizing the combustion process with direct solar irradiation. Nathan et al. [137] state that synergies between renewable and fossil energies through a Hybrid Solar Combustor (HSC) have the potential to ease the transition from conventional technologies to a renewable future thanks to the use of shared infrastructure and lower thermal losses by ensuring a continuous process thus lowering the overall CO_2 emissions. Furthermore, Medwell et al. [138] informed that adding direct solar irradiation to free flames directly affected the behavior of flames and soot formation, which presents itself as one of the current issues to be solved to develop a mature HSC technology effectively. An alternative approach to integrating solar energy into conventional thermal power plants is theoretically and numerically evaluated by Hosseini et al. [27] through preheating air in a combined cycle power plant operating in a flameless combustion mode. This approach enables ultra-low NO_X emissions due to its homogeneous heat distribution and more compact designs. Solar-driven gasification has been demonstrated as a promising technology to use solar energy for hydrogen and syngas production [139]. Ruiz et al. [140] investigated temperature profiles and heat fluxes in a packed bed heated by radiation that simulates a solar energy flux. A radiant porous burner was placed at the bottom of the packed bed to simulate an imposed concentrated solar heat flux. Incorporating other solid renewable fuels, such as biomass, exploring native and

exotic forest species that could reduce the emissions levels, having a CO_2 capture system, and migrating from a system that uses fossil fuels to biomass [141, 142]. Most recently, Arriagada et al. [143] studied the solar-driven gasification of carbon for hydrogen and syngas production using a hybrid porous media reactor at low temperatures (Approximately 600 K). The highest ratio of hydrogen and carbon monoxide (H_2/CO) was 0.163 when the rotation speed was 20 rpm.

1.4.2 Waste to energy

It is important to give this technology a social and environmental purpose, with little devices that can take garbage from schools or social buildings and produce H_2, which greatly impacts society, considering the economic feasibility. Furthermore, the hybrid filtration combustion technology can be the last step to recycling and utilizing the highest energy from a matrix. This can be important for municipal solid wastes (MSW), which have a regular composition depending on the city and economic activities developed in different areas [144]. Since municipal solid waste is a global issue, its treatment, and utilization are widely investigated [24, 25, 145–147]. A conventional approach to waste to energy treatment is the direct combustion of waste (incineration), which aims to recover the energetic value of waste. Other thermochemical treatment methods, i.e., pyrolysis and gasification, may additionally be used for recovering the chemical value of wastes. In this context, gasification is related to the production of syngas, where hybrid filtration combustion could be implemented [148]. As a matter of fact, industrial applications of HFC have been successfully implemented in NothernEuropean countries, such as Finland and Russia, where two reactors that can process up to 15000 ton/yr of MSW were engineered by the IPCP-RAS (Russia) and developed by Europrofile Ltd. In Lappeenranta (Finland) and Moscow (Russia) [70, 149]. Many researchers have studied the filtration combustion technology of solid fuel in countercurrent reactors [149, 150]. Further studies using residential waste for hydrogen and syngas production could be an important research line, considering tons of municipal waste per year with serious health risks for the population.

1.4.3 Valorization of metallic compounds

The hybrid filtration combustion technology allows efficient mass transfer of compounds [151, 152]. Thanks to this feature, it is possible to implement an entirely new process of separating valuable metals and their compounds in a wave of filtration combustion. It was shown in [153] that if mixtures containing metals that form relatively volatile products are subjected to filtration combustion, the corresponding metals can be effectively extracted from the original mixture. In the example of metal-containing mixtures, the separation in the space of the processes of oxidation, evaporation, and condensation, the separation of target products have been stablished [154]. It becomes possible to selectively concentrate and isolate metals and their derivatives when metal compounds accumulate in a particular reactor zone due to the continuous evaporation and condensation of these compounds [155]. It was shown that under HFC wave conditions, it is possible to extract compounds of such metals as zinc, cadmium, molybdenum, etc. [150, 154, 156, 157]. Technological possibilities of using HFC to separate valuable elements from various traditional and, most importantly, unconventional sources (poor ores, production wastes, heavy oil residues, coal waste, etc.) are opening up.

1.4.4 Miscellaneous and innovative applications

Hybrid filtration combustion has a broad scope of applications adequately described in this review. Nonetheless, several miscellaneous and innovative applications show how versatile HFC as a feasible alternative could be. Wood has been used for centuries; residential wood combustion is one of the most polluting activities in many countries [158, 159]. Hybrid filtration combustion can be extended to utilize hybrid pellets (e.g., wood and alumina spheres) that could act in these devices as feedstocks, enhancing the radiation as a dominating heat transfer mechanism. Moreover, radiant porous burners can impact the gastronomic industry when using hybrid mixtures in wood-burning cookers. This could be key in the energy transition process, highlighting less polluting activities.

1.5 Concluding remarks

A review of hydrogen (H_2) and syngas production by hybrid filtration combustion (HFC) has been made. Shifting the current production of H_2 mainly from fossil fuels towards a green alternative represents a baseline for the development of the HFC technology. Hybrid filtration combustion has been investigated to produce H_2 and syngas from different solid fuels such as biomass, algae, polyethylene, and coal, and different gasifying agents such as water steam, air, and gaseous fuel-air mixtures. As analyzed in this review, three parameters are crucial to optimize the HFC process: the temperature along the reactor, combustion wave velocity, and H_2 and syngas yield. Remarkably, H_2 and CO production is totally related to the thermal behavior of the reactor and the type of gasifying agent used. It could be concluded from the reviewed studies of HFC that, when using a mixture of air with steam as an oxidizer, the maximum H_2 content in the gaseous products was 25% by volume, being variable for different fuels. Catalysts and/or an oxygen-enriched oxidant could enhance the H_2 yield. For filtration regimes, when the front velocity is limited by the supply of oxidizer to the combustion zone, gas-dynamic instability of a flat front is possible. Instability during HFC occurs when the hydrodynamic resistance of the initial solid backfill is higher than the resistance of the solid ash residue. The development of instability leads to an alternative combustion mode featured by the propagation of a separate channel or inclined front. A feasible solution to this problem was to facilitate the HFC process in a rotating cylindrical reactor with a certain angle of inclination, which enhances mixing of the solid material by change in gravity. Lateral feeding of powdered solid fuel mixed with the secondary oxidant stream and replacing the fixed bed by a moving one are also among the improvements explored in the reactor design and operation. Many challenges have been identified in this chapter. Extended research is needed in the characterization of HFC reactors, modeling and simulation of different systems and operational conditions, economic analysis, and environmental impact assessment before materializing a complex matrix for H_2 production. Further studies aiming to optimize the operation of the reactor in a continuous solid fuel feed with the stabilization of the combustion wave at an optimum position regime would be of significant interest. Finally, a necessary transition from gray to green hydrogen production could be aided by using solar and other

renewable energy sources to produce hydrogen and syngas.

1.6 Hypothesis

The hypothesis of this doctoral thesis postulates:

1. The porous structure of carbonaceous materials, where heterogeneous chemical reactions take place, among with diffusivity, porosity and flow conditions influence the mass transfer of reactants and products during gasification.

2. A hybrid porous media reactor exposed to concentrated solar energy will enhance allothermal gasification of carbonaceous materials at low temperatures for renewable hydrogen generation.

1.7 Research objectives

The main goal of this doctoral project is to study experimentally and numerically the thermochemical conversion of solid carbonaceous materials, using hybrid porous media reactor exposed to concentrated solar energy and a chemically reacting fixed-bed towards a renewable hydrogen and syngas generation.

Specific goals of this doctoral project are listed below:

1. Understand the fundamentals of the theory of inert porous media combustion, hybrid filtration combustion and solar-driven gasification through a literature review.

2. Numerically study heat and mass transfer inside a chemically reacting fixed-bed assessing Reynolds number, inflow gas temperature and oxidative atmosphere.

3. Study heat and mass transfer inside a carbon char particle using macro-pore-resolved and porous media numerical approaches.

4. Investigate the feasibility of a 2D axisymmetric porous media numerical model to represent a 3D particle-resolved approach of carbon char gasification.

5. Perform experiments in a hybrid porous media reactor exposed to concentrated solar energy, focusing on hydrogen and syngas production.

6. Identify the most significant operational parameters according to experimental and numerical results to propose improvements to the processes for further research.

Acknowledgments

The authors would like to thank the support of the National Agency of Research and Development (ANID) of Chile (FONDAP SERC-Chile N°15110019, FONDECYT N°1190654, and Scholarship Program / DOCTORADO BECAS CHILE/2021 - 21211230) and state assignment of Ministry of Education and Science of Russia, no. 0089-2019-0018 (registration number AAAA-A19-119-022690098-3).

References

[1] International Energy Agency. Co2 emissions in 2022, 2022. URL `www.iea.org`.

[2] M. Younas, M. Rezakazemi, M. Daud, M.B. Wazir, S. Ahmad, N. Ullah, Inamuddin, and S. Ramakrishna. Recent progress and remaining challenges in post-combustion co2 capture using metal-organic frameworks (mofs). *Progress in Energy and Combustion Science*, 80, 2020. ISSN 03601285.

[3] T. Wernberg, B.D. Russell, P.J. Moore, S.D. Ling, D.A. Smale, A. Campbell, M.A. Coleman, P.D. Steinberg, G.A. Kendrick, and S.D. Connell. Impacts of climate change in a global hotspot for temperate marine biodiversity and ocean warming. *Journal of Experimental Marine Biology and Ecology*, 400:7–16, 4 2011. ISSN 00220981.

[4] D. Marazziti, P. Cianconi, F. Mucci, L. Foresi, I. Chiarantini, and A. Della Vecchia. Climate change, environment pollution, covid-19 pandemic and mental health. *Science of the Total Environment*, 773, 6 2021. ISSN 18791026.

[5] S.I. Zandalinas, F.B. Fritschi, and R. Mittler. Global warming, climate change, and environmental pollution: Recipe for a multifactorial stress combination disaster. *Trends in Plant Science*, 26:588–599, 6 2021. ISSN 13601385.

[6] D.L. Swain, D. Singh, D. Touma, and N.S. Diffenbaugh. Attributing extreme events to climate change: A new frontier in a warming world. *One Earth*, 2:522–527, 6 2020. ISSN 25903322.

[7] K. Oka, W. Mizutani, and S. Ashina. Climate change impacts on potential solar energy production: A study case in fukushima, japan. *Renewable Energy*, 153:249–260, 6 2020. ISSN 18790682.

[8] X. Zhao, G. Huang, C. Lu, X. Zhou, and Y. Li. Impacts of climate change on photovoltaic energy potential: A case study of china. *Applied Energy*, 280:115888, 2020. ISSN 03062619.

[9] J.N. Kang, Y.M. Wei, L.C. Liu, R.H., B.Y. Yu, and J.W. Wang. Energy systems for climate change mitigation: A systematic review. *Applied Energy*, 263, 4 2020. ISSN 03062619.

[10] T. Raksha, U. Bünger, U. Albrecht, J. Michalski, and J. Zerhusen. International hydrogen strategies: A study commissioned by and in cooperation with the world energy council germany, 2020.

[11] J. Andrews and B. Shabani. The role of hydrogen in a global sustainable energy strategy. *Wiley Interdisciplinary Reviews: Energy and Environment*, 3:474–489, 2014. ISSN 2041840X.

[12] K. Espegren, S. Damman, P. Pisciella, I. Graabak, and A. Tomasgard. The role of hydrogen in the transition from a petroleum economy to a low-carbon society. *International Journal of Hydrogen Energy*, 46:23125–23138, 7 2021. ISSN 03603199.

[13] M.A. Mujeebu. Hydrogen and syngas production by superadiabatic combustion - a review. *Applied Energy*, 173:210–224, 7 2016. ISSN 03062619.

[14] J. Zanganeh, B. Moghtaderi, and H. Ishida. Combustion and flame spread on fuel-soaked porous solids. *Progress in Energy and Combustion Science*, 39:320–339, 2013. ISSN 03601285.

[15] Z. Al-Hamamre and A. Al-Zoubi. The use of inert porous media based reactors for hydrogen production. *International Journal of Hydrogen Energy*, 35:1971–1986, 3 2010. ISSN 03603199.

[16] M.A. Mujeebu, M.Z. Abdullah, M.Z. Abu Bakar, A.A. Mohamad, and M.K. Abdullah. Applications of porous media combustion technology - a review. *Applied Energy*, 86: 1365–1375, 2009. ISSN 03062619.

[17] M. Toledo and C. Rosales. Hybrid filtration combustion. *Hydrogen Energy - Challenges and Perspectives*, 10 2012.

[18] M. Toledo, A. Arriagada, N. Ripoll, E.A. Salgansky, and M.A. Mujeebu. Hydrogen and syngas production by hybrid filtration combustion: Progress and challenges. *Renewable and Sustainable Energy Reviews*, 177, 5 2023. ISSN 18790690.

[19] M. Saidi, M.H. Gohari, and A.T. Ramezani. Hydrogen production from waste gasification followed by membrane filtration: a review. *Environmental Chemistry Letters*, 18:1529–1556, 9 2020. ISSN 16103661.

[20] T. Carvalho, M. Costa, C. Casaca, R. C. Catapan, and A. A.M. Oliveira. Destruction of the tar present in syngas by combustion in porous media. *Energy and Fuels*, 29: 1130–1136, 2 2015. ISSN 15205029.

[21] M.M. Kamal and A.A. Mohamad. Combustion in porous media. *Proceedings of the Institution of Mechanical Engineers, Part A: Journal of Power and Energy*, 220:487–508, 8 2006. ISSN 09576509.

[22] S. Wood and A.T. Harris. Porous burners for lean-burn applications. *Progress in Energy and Combustion Science*, 34:667–684, 10 2008. ISSN 03601285.

[23] N. Haugen, B. Loong, and R. Mitchell. Numerical approaches for thermochemical conversion of char. *Progress in Energy and Combustion Science*, 91, 7 2022. ISSN 03601285.

[24] K. Kaya, E. Ak, Y. Yaslan, and S.F. Oktug. Waste-to-energy framework: An intelligent energy recycling management. *Sustainable Computing: Informatics and Systems*, 30, 6 2021. ISSN 22105379.

[25] W.A. Mahari, E. Azwar, S.Y. Foong, A. Ahmed, W. Peng, M. Tabatabaei, M. Aghbashlo, Y. Park, C. Sonne, and S. Lam. Valorization of municipal wastes using co-pyrolysis for green energy production, energy security, and environmental sustainability: A review. *Chemical Engineering Journal*, 421, 10 2021. ISSN 13858947.

[26] P. Nikolaidis and A. Poullikkas. A comparative overview of hydrogen production processes. *Renewable and Sustainable Energy Reviews*, 67:597–611, 1 2017. ISSN 18790690.

[27] S.E. Hosseini, H. Barzegaravval, B. Chehroudi, and M.A. Wahid. Hybrid solar flameless combustion system: Modeling and thermodynamic analysis. *Energy Conversion and Management*, 166:146–155, 2018. ISSN 01968904.

[28] D. Banerjee, N. Kushwaha, N.P. Shetti, T.M. Aminabhavi, and E. Ahmad. Green hydrogen production via photo-reforming of bio-renewable resources. *Renewable and Sustainable Energy Reviews*, 167, 10 2022. ISSN 18790690.

[29] E.I. Epelle, K.S. Desongu, W. Obande, A.A. Adeleke, P.P. Ikubanni, J.A. Okolie, and B. Gunes. A comprehensive review of hydrogen production and storage: A focus on the role of nanomaterials. *International Journal of Hydrogen Energy*, 47:20398–20431, 6 2022. ISSN 03603199.

[30] K. Liu, C. Song, and V. Subramani. *Hydrogen and syngas production and purification technologies*. Wiley, 2010. ISBN 9780471719755.

[31] I. Dincer and C. Acar. Innovation in hydrogen production. *International Journal of Hydrogen Energy*, 42:14843–14864, 6 2017. ISSN 03603199.

[32] I. Dincer. Green methods for hydrogen production. *International Journal of Hydrogen Energy*, 37:1954–1971, 1 2012. ISSN 03603199.

[33] F. Dawood, M. Anda, and G.M. Shafiullah. Hydrogen production for energy: An overview. *International Journal of Hydrogen Energy*, 45:3847–3869, 2 2020. ISSN 03603199.

[34] S. Dutta. A review on production, storage of hydrogen and its utilization as an energy resource. *Journal of Industrial and Engineering Chemistry*, 20:1148–1156, 2014. ISSN 22345957.

[35] International Energy Agency. The future of hydrogen, 2019.

[36] M. Appl. *Ammonia: Principles and Industrial Practice*. Wiley-VCH, 2007. ISBN 978-3-527-61388-5.

[37] D. Scott. *Smelling Land: The Hydrogen Defense Against Climate Catastrophe*. Queen's Printer Publishing, 2008. ISBN 9780980967401.

[38] A. Steinfeld. Solar thermochemical production of hydrogen - a review. *Solar Energy*, 78:603–615, 2005. ISSN 0038092X.

[39] C. Acar, Y. Bicer, M. Demir, and I. Dincer. Transition to a new era with light-based hydrogen production for a carbon-free society: An overview. *International Journal of Hydrogen Energy*, 44:25347–25364, 2019. ISSN 03603199.

[40] D. Gielen, F. Boshell, D. Saygin, M.D. Bazilian, N. Wagner, and R. Gorini. The role of renewable energy in the global energy transformation. *Energy Strategy Reviews*, 24: 38–50, 4 2019. ISSN 2211467X.

[41] Z. Hammi, N. Labjar, M. Dalimi, Y. El Hamdouni, and S. El Hajjaji. Green hydrogen: A holistic review covering life cycle assessment, environmental impacts, and color analysis. *International Journal of Hydrogen Energy*, 80:1030–1045, 2024.

[42] N. Hanchate, S. Ramani, C.S. Mathpati, and V.H. Dalvi. Biomass gasification using dual fluidized bed gasification systems: A review. *Journal of Cleaner Production*, 280, 1 2021. ISSN 09596526.

[43] S. Safarian, R. Unnþórsson, and C. Richter. A review of biomass gasification modelling. *Renewable and Sustainable Energy Reviews*, 110:378–391, 8 2019. ISSN 18790690.

[44] R. Luque and J.G. Speight. *Gasification for Synthetic Fuel Production: Fundamentals, Processes and Applications*. Woodhead Publishing Series in Energy, 2015. ISBN 978-0-85709-802-3.

[45] M. Préndez, V. Carvajal, K. Corada, J. Morales, F. Alarcón, and H. Peralta. Biogenic volatile organic compounds from the urban forest of the metropolitan region, chile. *Environmental pollution (Barking, Essex : 1987)*, 183:143–150, 2013. ISSN 18736424.

[46] J. A. Ruiz, M. C. Juárez, M. P. Morales, P. Muñoz, and M. A. Mendívil. Biomass gasification for electricity generation: Review of current technology barriers. *Renewable and Sustainable Energy Reviews*, 18:174–183, 2013. ISSN 13640321.

[47] R.S. Volkov and P.A. Strizhak. Planar laser-induced fluorescence diagnostics of water droplets heating and evaporation at high-temperature. *Applied Thermal Engineering*, 127:141–156, 2017. ISSN 13594311.

[48] Z. Yang, Y. Wu, Z. Zhang, H. Li, X. Li, R.I. Egorov, P.A. Strizhak, and X. Gao. Recent advances in co-thermochemical conversions of biomass with fossil fuels focusing on the synergistic effects. *Renewable and Sustainable Energy Reviews*, 103:384–398, 4 2019. ISSN 18790690.

[49] A. Kumar, D.D. Jones, and M.A. Hanna. Thermochemical biomass gasification: A review of the current status of the technology. *Energies*, 2:556–581, 9 2009. ISSN 19961073.

[50] C. Higman. *Gasification. Elsevier*. Gulf Professional Publishing, 2003.

[51] X. Ma, X. Zhao, J. Gu, and J. Shi. Co-gasification of coal and biomass blends using dolomite and olivine as catalysts. *Renewable Energy*, 132:509–514, 3 2019. ISSN 18790682.

[52] V. Sikarwar, M. Zhao, P. Clough, J. Yao, X. Zhong, M. Memon, N. Shah, E.J. Anthony, and P.S. Fennell. An overview of advances in biomass gasification. *Energy and Environmental Science*, 9:2939–2977, 2016. ISSN 17545706.

[53] E. Pereira, J. Da Silva, J.L. De Oliveira, and C.S. MacHado. Sustainable energy: A review of gasification technologies. *Renewable and Sustainable Energy Reviews*, 16: 4753–4762, 2012. ISSN 13640321.

[54] S.S. Siwal, Q. Zhang, C. Sun, S. Thakur, V. Gupta, and V. Thakur. Energy production from steam gasification processes and parameters that contemplate in biomass gasifier – a review. *Bioresource Technology*, 297, 2 2020. ISSN 18732976.

[55] L. Liu, Y. Huang, J. Cao, C. Liu, L. Dong, L. Xu, and J. Zha. Experimental study of biomass gasification with oxygen-enriched air in fluidized bed gasifier. *Science of the Total Environment*, 626:423–433, 2018. ISSN 18791026.

[56] C. Di Blasi. Modeling chemical and physical processes of wood and biomass pyrolysis. *Progress in Energy and Combustion Science*, 34:47–90, 2 2008. ISSN 03601285.

[57] J. Han and H. Kim. The reduction and control technology of tar during biomass gasification/pyrolysis: An overview. *Renewable and Sustainable Energy Reviews*, 12: 397–416, 2 2008. ISSN 13640321.

[58] A.S. Al-Rahbi and P.T. Williams. Hydrogen-rich syngas production and tar removal from biomass gasification using sacrificial tyre pyrolysis char. *Applied Energy*, 190: 501–509, 2017. ISSN 03062619.

[59] L. Pala, Q. Wang, G. Kolb, and V. Hessel. Steam gasification of biomass with subsequent syngas adjustment using shift reaction for syngas production: An aspen plus model. *Renewable Energy*, 101:484–492, 2 2017. ISSN 18790682.

[60] N. Aramouni, J.G. Touma, B. Tarboush, J. Zeaiter, and M.N. Ahmad. Catalyst design for dry reforming of methane: Analysis review. *Renewable and Sustainable Energy Reviews*, 82:2570–2585, 2 2018. ISSN 18790690.

[61] F. Guo, X. Li, Y. Liu, K. Peng, C. Guo, and Z. Rao. Catalytic cracking of biomass pyrolysis tar over char-supported catalysts. *Energy Conversion and Management*, 167: 81–90, 7 2018. ISSN 01968904.

[62] S. Sengodan, R. Lan, J. Humphreys, D. Du, W. Xu, H. Wang, and S. Tao. Advances in reforming and partial oxidation of hydrocarbons for hydrogen production and fuel cell applications. *Renewable and Sustainable Energy Reviews*, 82:761–780, 2018. ISSN 18790690.

[63] Y. X. Zeng, L. Wang, C. F. Wu, J. Q. Wang, B. X. Shen, and X. Tu. Low temperature reforming of biogas over k-, mg- and ce-promoted ni/al2o3 catalysts for the production of hydrogen rich syngas: Understanding the plasma-catalytic synergy. *Applied Catalysis B: Environmental*, 224:469–478, 2018. ISSN 09263373.

[64] B.B. Krishna, B. Biswas, and T. Bhaskar. *Gasification of lignocellulosic biomass*. Elsevier Inc., 2 edition, 2019. ISBN 9780128168561.

[65] S. Ciuta, D. Tsiamis, and M.J. Castaldi. *Fundamentals of gasification and pyrolysis*. Elsevier, 1 2017. ISBN 9780128127162.

[66] P. Mondal, G. S. Dang, and M. O. Garg. Syngas production through gasification and cleanup for downstream applications - recent developments. *Fuel Processing Technology*, 92:1395–1410, 2011. ISSN 03783820.

[67] B. Dou, H. Zhang, Y. Song, L. Zhao, B. Jiang, M. He, C. Ruan, H. Chen, and Y. Xu. Hydrogen production from the thermochemical conversion of biomass: Issues and challenges. *Sustainable Energy and Fuels*, 3:314–342, 2019. ISSN 23984902.

[68] S. Farzad, M. Mandegari, and J. Görgens. A critical review on biomass gasification, co-gasification, and their environmental assessments. *Biofuel Research Journal*, 3:483–495, 2016. ISSN 22928782.

[69] E. A. Salgansky, V. M. Kislov, S. V. Glazov, and M. V. Salganskaya. Formation of liquid products at the filtration combustion of solid fuels. *Journal of Combustion*, 2016, 2016. ISSN 20901976.

[70] V. M. Kislov, S. V. Glazov, N. A. Chervonnaya, L. I. Patronova, M. V. Salganskaya, and G. B. Manelis. Biomass gasification under combustion conditions with superadiabatic heating. *Solid Fuel Chemistry*, 42:135–139, 2008. ISSN 03615219.

[71] E. A. Salgansky, A. Yu Zaichenko, D. N. Podlesniy, M. V. Salganskaya, and M. Toledo. Coal dust gasification in the filtration combustion mode with syngas production. *International Journal of Hydrogen Energy*, 42:11017–11022, 4 2017. ISSN 03603199.

[72] M. Toledo, C. Rosales, C. Silvestre, and S. Caro. Numerical simulation of the hybrid filtration combustion of biomass. *International Journal of Hydrogen Energy*, 41:21131–21139, 12 2016. ISSN 03603199.

[73] M. Toledo and N. Ripoll. *Syngas Fuel Production from Carbonaceous Feedstocks Using Hybrid Porous Media*. IntechOpen, 9 2019.

[74] M. Toledo, N. Ripoll, J. Céspedes, A. Zbogar-Rasic, N. Fedorova, V. Jovicic, and A. Delgado. Syngas production from waste tires using a hybrid filtration reactor under different gasifier agents. *Energy Conversion and Management*, 172:381–390, 2018. ISSN 01968904.

[75] J. Ahrenfeldt, H. Egsgaard, W. Stelte, T. Thomsen, and U. Henriksen. The influence of partial oxidation mechanisms on tar destruction in twostage biomass gasification. *Fuel*, 112:662–680, 2013. ISSN 00162361.

[76] Y. Su, Y. Luo, Y. Chen, W. Wu, and Y. Zhang. Experimental and numerical investigation of tar destruction under partial oxidation environment. *Fuel Processing Technology*, 92:1513–1524, 8 2011. ISSN 03783820.

[77] A.P. Aldushin, A.G. Merzhanov, and B.S. Seplyarskii. Theory of filtration combustion of metals. *Combustion, Explosion, and Shock Waves*, 12:285–294, 1976.

[78] M.S. Blinderman and A.Y. Klimenko. Theory of reverse combustion linking. *Combustion and Flame*, 150:232–245, 8 2007. ISSN 00102180.

[79] M.S. Blinderman, D.N. Saulov, and A.Y. Klimenko. Forward and reverse combustion linking in underground coal gasification. *Energy*, 33:446–454, 2008. ISSN 03605442.

[80] A.P-Aldushin. *Filtration Combustion*, pages 95–115. 1 edition, 1996. ISBN 9781600866456.

[81] A. Lebedev, G. Sukhov, and P. Yarin. Theory of filtration combustion. *Combustion Explosion Schock and Waves*, 4:7–11, 1977.

[82] A.P. Aldushin, B.S. Seplyarskii, and K.G. Shkadinskii. Theory of filtrational combustion. *Combustion, Explosion, and Shock Waves*, 16:33–40, 1980. ISSN 00105082.

[83] C. Lu and Y.C. Yortsos. Pattern formation in reverse filtration combustion. *Physical Review E - Statistical, Nonlinear, and Soft Matter Physics*, 72, 9 2005. ISSN 15393755.

[84] D.A. Schult, A. Bayliss, B.J. Matkowsky, and Siam. Traveling waves in natural counterflow filtration combustion and their stability *. *and Applied Mathematics*, 58:806–852, 1998.

[85] F.J. Weinberg. Combustion temperatures: The future? *Nature*, 233:239–241, 1971. ISSN 00280836.

[86] D.R. Hardesty and F.J. Weinberg. Burners producing large excess enthalpies. *Combustion Science and Technology*, 8:201–214, 12 1973. ISSN 1563521X.

[87] R.B. Slimane, F.S. Lau, M. Khinkis, J.P. Bingue, A.V. Saveliev, and L.A. Kennedy. Conversion of hydrogen sulfide to hydrogen by superadiabatic partial oxidation: Thermodynamic consideration. *International Journal of Hydrogen Energy*, 29:1471–1477, 11 2004. ISSN 03603199.

[88] K.V. Dobrego, N.N. Gnesdilov, S.H. Lee, and H.K. Choi. Overall chemical kinetics model for partial oxidation of methane in inert porous media. *Chemical Engineering Journal*, 144:79–87, 2008. ISSN 13858947.

[89] J.P. Bingue, A.V. Saveliev, and L.A. Kennedy. Optimization of hydrogen production by filtration combustion of methane by oxygen enrichment and depletion. *International Journal of Hydrogen Energy*, 29:1365–1370, 2004. ISSN 03603199.

[90] L.A. Kennedy, J.P. Bingue, A.V. Saveliev, A.A. Fridman, and S.I. Foutko. Chemical structures of methane-air filtration combustion waves for fuel-lean and fuel-rich conditions. *Proceedings of the Combustion Institute*, 28:1431–1438, 2000. ISSN 15407489.

[91] M. Toledo, E. Vergara, and A.V. Saveliev. Syngas production in hybrid filtration combustion. *International Journal of Hydrogen Energy*, 36:3907–3912, 3 2011. ISSN 03603199.

[92] M. Toledo, K. Araus, and D. Vasconcelo. Syngas production from coal in presence of steam using filtration combustion. *International Journal of Hydrogen Energy*, 40: 6340–6345, 2015. ISSN 03603199.

[93] M.V. Salganskaya, S.V. Glazov, E.A. Salganskii, V.M. Kislov, A.F. Zholudev, and G.B. Manelis. Filtration combustion of humid fuels. *Russian Journal of Physical Chemistry B*, 2:71–76, 2008. ISSN 19907923.

[94] V. Jovicic, N. Fedorova, A. Zbogar-Rasic, D. Nloka, and A. Delgado. Combustion of solid fuel in a hybrid porous reactor. *Energy Procedia*, 120:431–438, 2017. ISSN 18766102.

[95] E.A. Salganskii, V.P. Fursov, S.V. Glazov, M.V. Salganskaya, and G.B. Manelis. Model of vapor-air gasification of a solid fuel in a filtration mode. *Combustion, Explosion and Shock Waves*, 42:55–62, 2006. ISSN 00105082.

[96] V.A. Levin and N.A. Lutsenko. Two-dimensional gas flows under heterogeneous combustion of solid porous media. *Doklady Physics*, 62:425–429, 9 2017. ISSN 10283358.

[97] I. Amelin, E. Salgansky, N. Volkova, A. Zholudev, A. Alekseev, E. Polianczyk, and G. Manelis. Parametric domain of the stationary filtration combustion wave in the charge with a low carbon content. *Izvestiya Akademii Nauk. Seriya Khimicheskaya*, 60:1125–1132, 2011.

[98] A.P. Aldushin and B. Braverman. Hydrodynamic instability of filtration combustion wave. *Doklady Physical Chemistry*, 427:125–128, 2009. ISSN 00125016.

[99] S.V. Glazov, V.M. Kislov, E.A. Salgansky, O.S. Rabinovich, A.I. Malinouski, M.V. Salganskaya, E.N. Pilipenko, and Y.Y. Kolesnikova. Effect of local rearrangements in the particle bed on the stability of filtration combustion of solid fuel. *International Journal of Heat and Mass Transfer*, 108:1602–1609, 2017. ISSN 00179310.

[100] D.N. Podlesniy, A.Y. Zaichenko, E.A. Salgansky, and M.V. Salganskaya. Stability of the front of filtration combustion of bidisperse fuel mixture in an inclined rotating gas generator. *Russian Journal of Applied Chemistry*, 90:1783–1788, 11 2017. ISSN 10704272.

[101] A.Y. Zaichenko, A.A. Zhirnov, G.B. Manelis, E.V. Polianchik, and A.F. Zholudev. Filtration combustion front stabilization. *Doklady Chemistry*, 418:37–39, 2008. ISSN 0012-5008.

[102] S.O. Dorofeenko, E.V. Polianczyk, and G.B. Manelis. Numerical simulation of bidisperse granular material flow in a rotating reactor. *Doklady Physics*, 53:510–512, 10 2008. ISSN 10283358.

[103] G.B. Manelis, S.V. Glazov, E.A. Salgansky, and D.B. Lempert. Autowave processes in the filtration combustion in counterflow systems. *Russian Chemical Reviews*, 81: 855–873, 2012. ISSN 0036-021X.

[104] E.A. Salgansky, V.M. Kislov, S.V. Glazov, A.F. Zholudev, and G.B. Manelis. Filtration combustion of a carbon-inert material system in the regime with superadiabatic heating. *Combustion, Explosion and Shock Waves*, 44:273–280, 2008. ISSN 00105082.

[105] M.R. Henneke and J.L. Ellzey. Modeling of filtration combustion in a packed bed. *Combustion and Flame*, 117:832–840, 1999. ISSN 00102180.

[106] J.R. Howell, M.J. Hall, and J.L. Ellzey. Combustion of hydrocarbon fuels within porous inert media. *Progress in Energy and Combustion Science*, 22:121–145, 1996. ISSN 03601285.

[107] M. Toledo, K. Utria, F. González, J. Zuñiga, and A. Saveliev. Hybrid filtration combustion of natural gas and coal. *International Journal of Hydrogen Energy*, 37:6942–6948, 2012. ISSN 03603199.

[108] P. Gentillon and M.Toledo. Hydrogen and syngas production from propane and polyethylene. *International Journal of Hydrogen Energy*, 38:9223–9228, 7 2013. ISSN 03603199.

[109] K. Araus, F. Reyes, and M. Toledo. Syngas production from wood pellet using filtration combustion of lean natural gas-air mixtures. *International Journal of Hydrogen Energy*, 39:7819–7825, 2014. ISSN 03603199.

[110] S. Caro, D. Torres, and M.Toledo. Syngas production from residual biomass of forestry and cereal plantations using hybrid filtration combustion. *International Journal of Hydrogen Energy*, 40:2568–2577, 2015. ISSN 03603199.

[111] N. Ripoll, C. Silvestre, E. Paredes, and M. Toledo. Hydrogen production from algae biomass in rich natural gas-air filtration combustion. *International Journal of Hydrogen Energy*, 42:5513–5522, 2017. ISSN 03603199.

[112] J.L. Torero, J.I. Gerhard, M.F. Martins, M. Zanoni, T.L. Rashwan, and J.K. Brown. Processes defining smouldering combustion: Integrated review and synthesis. *Progress in Energy and Combustion Science*, 81, 11 2020. ISSN 03601285.

[113] G. Rein. Smouldering combustion phenomena in science and technology. *International Review of Chemical Engineering*, 1:3–18, 2009.

[114] M.J. Hurley, D. Gottuk, J.R. Hall, K. Harada, E. Kuligowski, M. Puchovsky, J. Torero, J.M. Watts, and C. Wieczorek. *SFPE handbook of fire protection engineering, fifth edition*. Springer New York, 1 2016. ISBN 9781493925650.

[115] A.P. Aldushin, A. Bayliss, and B.J. Matkowsky. On the mechanism of triggering the transition from smoldering to flaming. *Proceedings of the Combustion Institute*, 31 II: 2661–2668, 2007. ISSN 15407489.

[116] A.P. Aldushin, A. Bayliss, and B.J. Matkowsky. On the transition from smoldering to flaming. *Combustion and Flame*, 145:579–606, 5 2006. ISSN 00102180.

[117] M.A. Mujeebu, M.Z. Abdullah, M.Z. Abu Bakar, A.A. Mohamad, R. Muhad, and M.K. Abdullah. Combustion in porous media and its applications - a comprehensive survey. *Journal of Environmental Management*, 90:2287–2312, 2009. ISSN 03014797.

[118] M.A. Mujeebu, M.Z. Abdullah, M.Z. Abu Bakar, A.A. Mohamad, and M.K. Abdullah. A review of investigations on liquid fuel combustion in porous inert media. *Progress in Energy and Combustion Science*, 35:216–230, 2009. ISSN 03601285.

[119] A.G. Dixon, M. Nijemeisland, and E.H. Stitt. Packed tubular reactor modeling and catalyst design using computational fluid dynamics, 2006. ISSN 00652377.

[120] J. Wang, S. Wei, Q. Wang, and B. Sundén. Transient numerical modeling and model predictive control of an industrial-scale steam methane reforming reactor. *International Journal of Hydrogen Energy*, 46:15241–15256, 4 2021. ISSN 03603199.

[121] A.G. Dixon. Local transport and reaction rates in a fixed bed reactor tube: Endothermic steam methane reforming. *Chemical Engineering Science*, 168:156–177, 2017.

[122] R. Stauch and U. Maas. Transient detailed numerical simulation of the combustion of carbon particles. *International Journal of Heat and Mass Transfer*, 52:4584–4591, 9 2009. ISSN 00179310.

[123] P.A. Nikrityuk, M. Gräbner, M. Kestel, and B. Meyer. Numerical study of the influence of heterogeneous kinetics on the carbon consumption by oxidation of a single coal particle. *Fuel*, 114:88–98, 2013. ISSN 00162361.

[124] C.W. Lautenberger. Gpyro : A three dimensional generalized pyrolysis model gpyro - open source pyrolysis model. *IAFSS Workshop on MaCFP (Condensed Phase Subgroup)*, 2017.

[125] S.I. Stoliarov and R.E. Lyon. Thermo-kinetic model of burning for pyrolyzing materials. pages 1141–1152, 2008.

[126] N. Grange, K. Chetehouna, N. Gascoin, A. Coppalle, I. Reynaud, and S. Senave. One-dimensional pyrolysis of carbon based composite materials using firefoam. *Fire Safety Journal*, 97:66–75, 4 2018. ISSN 03797112.

[127] C. Herce, B. De Caprariis, S. Stendardo, N. Verdone, and P. De Filippis. Comparison of global models of sub-bituminous coal devolatilization by means of thermogravimetric analysis. *Journal of Thermal Analysis and Calorimetry*, 117:507–516, 2014. ISSN 13886150.

[128] M. Lapuerta, J.Hernández, and J. Rodríguez. Comparison between the kinetics of devolatilisation of forestry and agricultural wastes from the middle-south regions of spain. *Biomass and Bioenergy*, 31:13–19, 2007. ISSN 09619534.

[129] J.M. Johansen, R. Gadsbøll, J. Thomsen, P.A. Jensen, P. Glarborg, P. Ek, N. De Martini, M. Mancini, R. Weber, and R.E. Mitchell. Devolatilization kinetics of woody biomass at short residence times and high heating rates and peak temperatures. *Applied Energy*, 162:245–256, 2016. ISSN 03062619.

[130] S. Benkorichi, T. Fateh, F. Richard, J.L. Consalvi, and A. Nadjai. Investigation of thermal degradation of pine needles using multi-step reaction mechanisms. *Fire Safety Journal*, 91:811–819, 2017. ISSN 03797112.

[131] V. Tihay and P. Gillard. Pyrolysis gases released during the thermal decomposition of three mediterranean species. *Journal of Analytical and Applied Pyrolysis*, 88:168–174, 2010. ISSN 01652370.

[132] G. Gerandi, V. Tihay-Felicelli, P.A. Santoni, V. Leroy-Cancellieri, and D. Cancellieri. Multi-scale modeling of the degradation of thermally thin wood plates. *Fire Safety Journal*, 108, 9 2019. ISSN 03797112.

[133] K. Burra and A.K. Gupta. Modeling of biomass pyrolysis kinetics using sequential multi-step reaction model. *Fuel*, 237:1057–1067, 2 2019. ISSN 00162361.

[134] A. Mohammadi and A. Jazayeri. *Numerical Simulation of Combustion in Porous Media*. IntechOpen, 9 2012. ISBN 978-953-51-0749-1.

[135] N. Ripoll, E. Salgansky, and M. Toledo. Volatiles effects on the thermal and chemical structures of h2 production in a hybrid porous media reactor using solar steam. *International Journal of Heat and Mass Transfer*, 177, 10 2021. ISSN 00179310.

[136] S.K. Ngoh and D. Njomo. An overview of hydrogen gas production from solar energy. *Renewable and Sustainable Energy Reviews*, 16:6782–6792, 12 2012. ISSN 13640321.

[137] G. J. Nathan, M. Jafarian, B. B. Dally, W. L. Saw, P. J. Ashman, E. Hu, and A. Steinfeld. Solar thermal hybrids for combustion power plant: A growing opportunity. *Progress in Energy and Combustion Science*, 64:4–28, 2018. ISSN 03601285.

[138] P.R. Medwell, G.J. Nathan, Q.N. Chan, Z.T. Alwahabi, and B.B. Dally. The influence on the soot distribution within a laminar flame of radiation at fluxes of relevance to concentrated solar radiation. *Combustion and Flame*, 158:1814–1821, 2011. ISSN 00102180.

[139] P.G. Loutzenhiser and A.P. Muroyama. A review of the state-of-the-art in solar-driven gasification processes with carbonaceous materials. *Solar Energy*, 156:93–100, 2017. ISSN 0038092X.

[140] G. Ruiz, N. Ripoll, N. Fedorova, A. Zbogar-Rasic, V. Jovicic, A. Delgado, and M. Toledo. Experimental and numerical analysis of the heat transfer in a packed bed exposed to the high thermal radiation flux. *International Journal of Heat and Mass Transfer*, 136:383–392, 2019. ISSN 00179310.

[141] X. Wu and A.F. Ghoniem. Mixed ionic-electronic conducting (miec) membranes for thermochemical reduction of co2: A review. *Progress in Energy and Combustion Science*, 74:1–30, 2019. ISSN 03601285.

[142] X. Zhu, S. Li, Y. Shi, and N. Cai. Recent advances in elevated-temperature pressure swing adsorption for carbon capture and hydrogen production. *Progress in Energy and Combustion Science*, 75, 2019. ISSN 03601285.

[143] A. Arriagada, R. Mena, N. Ripoll, R.E. Hayes, P.A. Nikrityuk, and M. Toledo. Solar-driven gasification for syngas production at low temperatures using a rotary hybrid porous media reactor. *Chemical Engineering Journal*, page 153011, 2024.

[144] H. Khandelwal, H. Dhar, A. Thalla, and S. Kumar. Application of life cycle assessment in municipal solid waste management: A worldwide critical review. *Journal of Cleaner Production*, 209:630–654, 2019. ISSN 09596526.

[145] J.I. Gug, D. Cacciola, and M.J. Sobkowicz. Processing and properties of a solid energy fuel from municipal solid waste (msw) and recycled plastics. *Waste Management*, 35: 283–292, 2015. ISSN 18792456.

[146] Z. Shareefdeen, A. Elkamel, and S. Tse. Review of current technologies used in municipal solid waste-to-energy facilities in canada. *Clean Technologies and Environmental Policy*, 17:1837–1846, 10 2015. ISSN 16189558.

[147] W. Ma, T. Wenga, F.J. Frandsen, B. Yan, and G. Chen. The fate of chlorine during msw incineration: Vaporization, transformation, deposition, corrosion and remedies. *Progress in Energy and Combustion Science*, 76:100789, 2020. ISSN 03601285.

[148] V. Jovicic, N. Fedorova, A. Zbogar-Rasic, M. Toledo, and A. Delgado. Experimental investigation of solid fuel combustion process in a hybrid porous reactor. *Journal of Energy and Power Engineering*, 11:589–596, 2017. ISSN 19348975.

[149] G. B. Manelis, S. V. Glazov, D. B. Lempert, and E. A. Salgansky. Filtration combustion of solid fuel in countercurrent reactors. *Russian Chemical Bulletin*, 60:1301–1317, 2011. ISSN 10665285.

[150] A. S. Rozenberg, L. A. Grigor'Yan, I. Yu Gudkova, D. B. Lempert, and G. B. Manelis. Mass transfer of zinc-containing compounds during filtration combustion in the counterflow regime: 3. mass transfer at a low content of the zinc-containing component in the initial stock. *Russian Journal of Physical Chemistry B*, 3:802–806, 10 2009. ISSN 19907931.

[151] M. Martínez, M. Toledo, and M. Cabrera. Molybdenum oxide reduction using syngas and heat from an inert porous media reactor. *International Journal of Hydrogen Energy*, 41:12747–12761, 2016. ISSN 03603199.

[152] P. Palacios, M. Toledo, and M. Cabrera. Iron ore reduction by methane partial oxidation in a porous media. *International Journal of Hydrogen Energy*, 40:9621–9633, 2015. ISSN 03603199.

[153] D. Lempert, S. Glazov, and G. Manelis. Mass transfer in filtration combustion processes. *Mass Transfer in Multiphase Systems and its Applications*, 2011.

[154] S. I. Soglasnova, A. S. Rozenberg, and D. B. Lempert. Mass transfer of zinc-containing compounds during filtration combustion in the counterflow regime. 1. mass transfer in the zno-inert component system during co filtration. *Russian Journal of Physical Chemistry B*, 3:615–619, 2009. ISSN 19907931.

[155] E.A. Salgansky, N.A. Lutsenko, and M. Toledo. The model of the extraction process of rare metals under condition of filtration combustion wave. *Frontiers in Chemistry*, 8, 11 2020. ISSN 22962646.

[156] I.Y. Gudkova, D.B. Lempert, and A.S. Rozenberg. Burning chromium-containing compounds in the filtration combustion mode. *Russian Journal of Applied Chemistry*, 84: 1855–1859, 2011. ISSN 10704272.

[157] G. B. Manelis, S. V. Glazov, E. A. Salgansky, D. B. Lempert, I. Yu Gudkova, I. A. Domashnev, A. M. Kolesnikova, V. M. Kislov, and Y. Y. Kolesnikova. Extraction of molybdenum-containing species from heavy oil residues using the filtration combustion method. *International Journal of Heat and Mass Transfer*, 92:744–750, 2016. ISSN 00179310.

[158] F. Guerrero, A. Arriagada, F. Muñoz, P. Silva, N. Ripoll, and M. Toledo. Particulate matter emissions reduction from residential wood stove using inert porous material inside its combustion chamber. *Fuel*, 289, 4 2021. ISSN 00162361.

[159] A. Cincinelli, C. Guerranti, T. Martellini, and R. Scodellini. Residential wood combustion and its impact on urban air quality in europe. *Current Opinion in Environmental Science and Health*, 8:10–14, 2019. ISSN 24685844.

Chapter 2

Chemically reacting fixed-bed under gasification conditions for non-porous char[*]

[*]This chapter is a facsimile of the research article published in A. Arriagada, M. Toledo, R.E. Hayes, and P. Nikrityuk, Journal of the Energy Institute, **2023**.

2.1 Abstract

This chapter reports a computational investigation of the combustion of char particles in a fixed-bed using a three-dimensional model. Numerical simulations were carried out using the commercial software Ansys® Fluent, implementing a six semi-global kinetic scheme, where carbon monoxide combustion, forward and backward water-gas-shift reaction (WGS), Boudouard reaction, and two other heterogeneous reactions take place inside the reactor composed of 85 spherical particles. The diameter of the particles is 5.6 mm. Laminar flow regime (Re_{in} = 50, 75 and 100), inflow gas temperature in the range of 900-1500 K, and mass fraction of oxygen at the inlet ($Y_{O_2,in}$) of 0.05, 0.11, and 0.233 are the parameters of interest to study the heterogeneous combustion of carbon char particles inside the unit. The Boudouard reaction and oxidation of carbon monoxide are dominant among heterogeneous and homogeneous chemical reactions, respectively, being the inflow gas temperature a critical parameter to assess, since the kinetic scheme is dramatically activated at higher temperatures. A linear dependency has been found for species concentration and temperature profile in most of the simulations using $Y_{O_2,in} = 0.05$. Further studies are necessary to extend this research to intrinsic chemical reactions (tracking of porosity and particle radius), and the hybridization of the bed zone by incorporating inert solid particles into the system.

Keywords: Heterogeneous combustion, Fixed-bed reactor, Computational fluid dynamics (CFD), Carbon char particles, Chemical kinetics.

Nomenclature

Roman Symbols	Definition	Greek Symbols	Definition
A	Pre-exponential factor	ϵ	Emissivity
C	Concentration, $\text{kmol} \cdot \text{m}^{-3}$	λ	Thermal conductivity, $\text{W} \cdot \text{m}^{-1} \cdot \text{K}^{-1}$
D	Mass diffusion coefficient, $\text{m}^2 \cdot \text{s}^{-1}$	μ	Viscosity, $\text{Pa} \cdot \text{s}$
d	Diameter, m	ρ	Density, $\text{kg} \cdot \text{m}^{-3}$
E_a	Activation energy, $\text{J} \cdot \text{mol}^{-1}$	σ	Stefan-Boltzmann constant, $\text{W} \cdot \text{m}^{-2} \cdot \text{K}^{-4}$
h	Enthalpy, $\text{J} \cdot \text{kg}^{-1}$	τ	Stress tensor, Pa
k	Reaction rate constant	**Abbreviations**	**Definition**
M	Molecular weight, $\text{kg} \cdot \text{mol}^{-1}$	CFD	Computational fluid dynamics
$\dot{m}''$	Net mass flux gas-surface, $\text{kg} \cdot \text{m}^{-2} \cdot \text{s}^{-1}$	HFC	Hybrid filtration combustion
$\mathbf{n}$	Normal vector	SMR	Steam methane reforming
p	Pressure, Pa	**Subscripts**	**Definition**
R	Universal gas constant, $\text{J} \cdot \text{mol}^{-1} \cdot \text{K}^{-1}$	*bed zone*	Bed zone
$\widehat{R}$	Production rate, $\text{mol} \cdot \text{m}^{-2} \cdot \text{s}^{-1}$	C	at carbon char particle
Re	Reynolds number	i	species i
$\vec{u}$	Velocity, $\text{m} \cdot \text{s}^{-1}$	in	Inlet
T	Temperature, K	p	Particle
Y	Mass fraction	$surf$	Particle surface

2.2 Introduction

Fixed-bed reactors have great research interest since their multiphase and multiscale modeling have been widely studied on typical applications in the chemical industry, including steam methane reforming (SMR), and energy storage, among others [1–3], and for thermochemical conversion of carbonaceous materials under pyrolysis conditions, where thermogravimetric analysis (TGA) has similar kinetic approaches when compared to fixed-bed units [4, 5]. Modeling a multiscale and multiphysics phenomenon, such as a chemically reacting fixed-bed requires the understanding of transport properties in the gaseous phase and the coupling of boundary conditions at the surface of the solid fuel particles, which describe heterogeneous chemical interactions. This research focuses on the heterogeneous combustion of carbon char particles in a fixed-bed. Previous computational fluid dynamics (CFD) studies have been carried out for this fuel using a single spherical particle [6–8]. Gururajan et al. [6] explored the steady-state combustion of a coal particle, using a detailed model in which surface oxidation and volatilization of the coal particle were included. To the best of the authors'

knowledge, there is no reported research regarding a three-dimensional approach for chemically reacting particles in a fixed-bed, which offers a tremendous opportunity to explore these units using advanced computational methods. Safronov et al. [7] studied the oxidation of a single moving particle in a laminar flow regime, assessing the effect of the particle Reynolds number ($\mathrm{Re_{in}}$), finding a strong relationship between this parameter and oxidation regimes (kinetically, diffusion, transitional). Furthermore, Richter et al. [8] investigated the influence of particle velocity, temperature, and species composition of the gaseous phase on the consumption rate of a single carbon particle, showing how increasing the $\mathrm{Re_{in}}$ enhances species transport to the particle surface, going from a diffusion to a kinetically controlled regime.

On the other hand, the heterogeneous combustion phenomenon has been identified as a challenge specifically to char since an important amount of physical processes are taking place on the surface of the particles [9]. This process has been the focus of numerical studies for roughly one hundred years. The first approaches developed by Nusselt [10], and Burke and Schuman [11] proposed one and two-film analytical models, respectively. Since currently the computational resources, power, and technology have dramatically increased, it is now feasible to simulate complex engineering applications. The pioneer models are nowadays used only for validation. Furthermore, numerical simulations for studying carbon thermochemical conversion have been reported in the literature [12–18], where a complex phenomenon on the surface of the particles resulting from the interaction of the gaseous and solid phases could be observed, in addition to the transport properties and the radiation as dominant heat transfer mechanism. Libby and Blake [12] studied the carbon consumption in a hot atmosphere considering the effect of water vapor, while Cho et al. [14] obtained information regarding the interaction of multicomponent molecular diffusion, heterogeneous chemical reactions in and around chemically reacting particles. Stauch and Maas [15] investigated the burning process of a single carbon particle in air at isobaric conditions, observing a linear relationship between the burning rate and oxygen concentration of the inflow gas with negligible dependency on ambient pressure. Most recently, Qian et al. [17, 18] studied the pyrolysis of sub-bituminous coal in a fixed-bed reactor, remarking the relevance of phase change for water and due to heterogeneous reactions, also recognizing radiation as dominant

heat transfer mechanism for volatiles release.

To improve the understanding of coupling complex interactions between gaseous and solid phases, the effects of different flow regimes and ambient conditions on a chemically reacting fixed-bed must be assessed. The aim of this study is to analyze the heterogeneous combustion of carbon char particles, proposing a three-dimensional CFD particle resolved model using a fixed-bed reactor assessing inflow gas temperature, Reynolds number, and mass fraction of oxygen at inlet conditions.

2.3 Model Formulation

2.3.1 Chemical and Physical modeling

The model was formulated to simulate the heterogeneous combustion of carbon char particles in a fixed-bed reactor. For these purposes, all simulations were carried out using a commercial software package. Figure 2.1a depicts the geometry used for all simulations, where 85 spherical particles were located in the bed zone, and subsequently placed in a stationary position. The inflow gas consisted of several mass fractions of O_2 ($Y_{O_2,in}$ = 0.05, 0.11, and 0.233), 0.001 mass fraction of H_2O, the rest is nitrogen ($Y_{N_2} = 1 - \sum_i Y_i$). The diameter of each particle (d_p) was set to 5.6 mm, following experimental data found in the literature for porous media combustion [19, 20] and hybrid filtration combustion (HFC) [21, 22] applications since this study is a first three-dimensional numerical approach based on these multiphysics phenomena. HFC was also the reference process for determining the inflow gas temperature (T_{in}) selecting the range of 900-1500 K, since transforming organic or fossil-based materials such as coal into a gaseous fuel in the presence of an oxidant mixture/gasifying agent [23, 24] require high temperature (around 1100 K) [25, 26]. In particular, for the application of hydrogen/syngas production from carbonaceous feedstocks using this technology, a temperature range of 900-1800 K can be achieved for different equivalence ratios due to the intensification of heat transfer mechanisms inside the reactor [27, 28].

The Reynolds number (Re) was defined based on the particle size as described in Equation

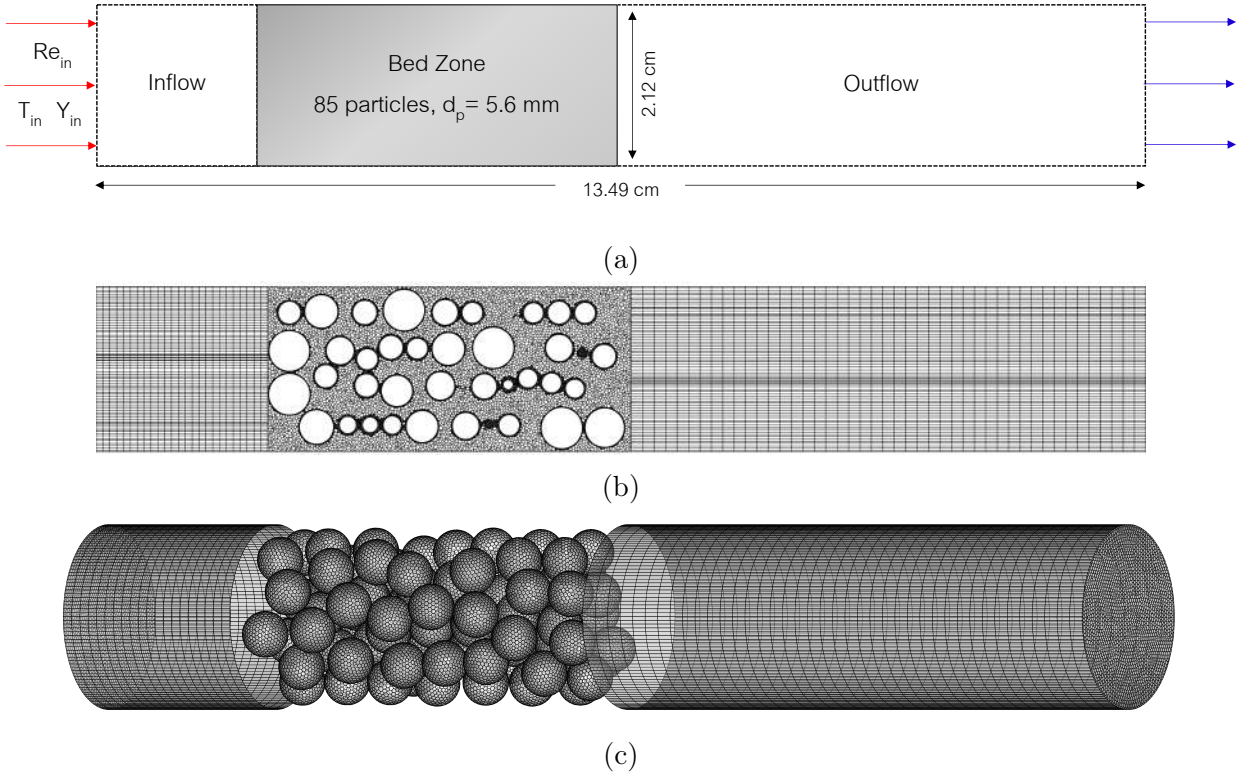

Figure 2.1: Schematics of the domain (a), 2D mesh slice (b) and 3D geometry (c) of the fixed-bed reactor model.

2.1:

$$\mathrm{Re_{in}} = \frac{\rho_{\mathrm{in}} |\vec{u}_{\mathrm{in}}| d_{\mathrm{p}}}{\mu_{\mathrm{in}}} \tag{2.1}$$

where ρ_{in} is the density, $\vec{u}_{\mathrm{in}}$ is the inlet velocity, and μ_{in} is the viscosity of the inflow gas mixture.

The chemical kinetic mechanism is modeled using a semi-global scheme, with three heterogeneous reactions at each particle surface (Reactions R1 to R3), and three homogeneous reactions (Reactions R4 to R6) taking place in the gaseous phase. R2 is the Boudouard reaction, R4 describes the oxidation of carbon monoxide (CO), where water acts as a catalyst species in the oxidation of CO, R5 and R6 represent the forward and backward water-gas shift (WGS) reaction, respectively. The global reaction scheme is properly described below:

$$\begin{aligned}
\text{R1:} &\quad 2\mathrm{C_{(s)}} + \mathrm{O_2} \longrightarrow 2\mathrm{CO} \\
\text{R2:} &\quad \mathrm{C_{(s)}} + \mathrm{CO_2} \longrightarrow 2\mathrm{CO} \\
\text{R3:} &\quad \mathrm{C_{(s)}} + \mathrm{H_2O} \longrightarrow \mathrm{CO} + \mathrm{H_2} \\
\text{R4:} &\quad \mathrm{CO} + 0.5\mathrm{O_2} \xrightarrow{\mathrm{H_2O}} \mathrm{CO_2} \\
\text{R5:} &\quad \mathrm{CO} + \mathrm{H_2O} \longrightarrow \mathrm{CO_2} + \mathrm{H_2} \\
\text{R6:} &\quad \mathrm{CO_2} + \mathrm{H_2} \longrightarrow \mathrm{CO} + \mathrm{H_2O}
\end{aligned}$$

Kinetic parameters and reaction rates of both heterogeneous and homogeneous reactions were based on the Arrhenius law, mathematically described by Equation 2.2, and listed in Table 2.1 as follows [12, 29, 30]:

$$k = AT^{n_r} e^{-\frac{E_a}{RT}} \tag{2.2}$$

where k is the rate constant for reaction, A is the pre-exponential factor, E_a is the activation energy, R is the universal gas constant, T is the temperature, and n_r is the temperature exponent.

Table 2.1: Kinetics parameters and reaction rates for heterogeneous combustion of char carbon particles.

Equation	$R_i \left[\frac{\text{mol}}{\text{m}^2 \cdot \text{s}}\right]$	A	$E_a \left[\frac{\text{J}}{\text{mol}}\right]$	n_r
R1	$k_{r,O_2} C_{O_2}, s$	$1.5 \cdot 10^5$	$1.494 \cdot 10^5$	0
R2	$k_{r,\text{CO}_2} C_{\text{CO}_2}, s$	4.605	$1.751 \cdot 10^5$	1
R3	$k_{r,\text{H}_2\text{O}} C_{\text{H}_2\text{O}}, s$	11.25	$1.751 \cdot 10^5$	1
R4	$k_{r,CO} C_{CO} C_{\text{H}_2O}^{0.5} C_{0_2}^{0.25}$	$1.25 \cdot 10^{11}$	$1.67 \cdot 10^5$	0
R5	$k_{r,CO} C_{CO} C_{H_2O}$	$2.74 \cdot 10^6$	$8.36 \cdot 10^4$	0
R6	$k_{r,\text{CO}_2} C_{CO_2} C_{H_2}$	$1.0 \cdot 10^8$	$6.28 \cdot 10^4$	0

2.3.2 Governing equations

Numerical simulations require assumptions to save time and computational resources. In particular, for a chemically reacting fixed-bed model, this is an essential step for reaching convergence considering the geometry and complexity of this multiphysics phenomenon. The following assumptions were applied to the steady-state model for the set of all the conservation equations (Equations 2.3 to 2.6), also described below:

1. The fixed-bed of the reactor is composed entirely of spherical non-porous carbon char particles.

2. The volatilization of fuel particles is not included, due to the steady-state feature of the model.

3. The density (ρ) follows the incompressible ideal-gas law.

4. The gaseous phase behaves as an incompressible flow with $p = 10^5$ Pa.

5. The buoyancy effect is neglected.

Conservation equation for mass transport:

$$\nabla \cdot (\rho \vec{u}) = 0 \tag{2.3}$$

Conservation equation for momentum transport:

$$\nabla \cdot (\rho \vec{u} \vec{u}) = -\nabla p + \nabla \cdot \tau \tag{2.4}$$

Conservation equation for species transport:

$$\nabla \cdot (\rho \vec{u} Y_i) = \nabla \cdot (\rho D_i \nabla Y_i) + R_i \tag{2.5}$$

Conservation equation for energy transport:

$$\nabla \cdot (\rho \vec{u} h) = \nabla \cdot (\lambda \nabla T) - \sum_i \frac{h_i^0}{M_i} R_i \tag{2.6}$$

where $\tau = \mu \left(\nabla \vec{u} + \nabla \vec{u}^{\mathrm{T}} \right)$ is the stress tensor. Species i is any reacting participant involved in the heterogeneous combustion process, i.e., O_2, CO_2, CO, N_2, H_2O, D_i is the mass diffusion coefficient, λ is the thermal conductivity, h_i is enthalpy, h^0 is the enthalpy of formation, M_i is molecular weight, Y_i is mass fraction, R_i is the net production rate, and $\widehat{R}_{i,r}$ is the Arrhenius molar rate of creation/destruction for species i, respectively. The last two terms are calculated using Equations 2.7-2.8, where $v''_{i,r}$ and $v'_{i,r}$ are the stoichiometric coefficients for reactants and products in the reaction r, $\eta'_{j,r}$ and $\eta''_{j,r}$ are the forward and backward rate exponents in the reaction r for each chemical species j.

$$R_i = M_i \sum_r \widehat{R}_{i,r} \tag{2.7}$$

$$\widehat{R}_{i,r} = \left(v''_{i,r} - v'_{i,r} \right) \left[k_r \prod_{j=1}^{N} C_{j,r}^{\left(\eta'_{j,r} - \eta''_{j,r} \right)} \right] \tag{2.8}$$

2.3.3 Boundary conditions

At the inlet of the fixed-bed reactor, the following Dirichlet boundary conditions are considered for inflow gas velocity, species mass fractions, and temperature, described by Equation

2.9. No heat flux has been imposed for the reactor walls.

$$\vec{u} = \vec{u}_{\text{in}}, \quad Y_i = Y_{i,\text{in}}, \quad T = T_{\text{in}} \tag{2.9}$$

Since there is an important interaction between gaseous and solid phases on the surface of the particles, mass and energy balance at the interface are affected by the heterogeneous chemical reactions (R1 to R3). The production and destruction rates of gaseous species caused by these reactions along with convective and diffusive mass fluxes of the gas phase species at the surface are crucial to set the boundary conditions shown in Equations 2.10 to 2.12 [31]. Heterogeneous reactions may modify also the 'no-slip' condition used typically for zero velocity for fluids on chemically non-reacting surfaces, notably affecting combustion of carbon char particles [32, 33]. In this case, the velocity may be nonzero, also called Stefan flow, which characterizes the net mass flux between surface and gas, and may be mathematically represented by Equation 2.13 [34, 35].

$$\rho_{\text{wall}}\, D_i \frac{\partial Y_{i,\text{ wall}}}{\partial n} - \dot{m}''_C Y_{i,\text{ wall}} \; = M_i \widehat{R}_{i,s} \tag{2.10}$$

$$\dot{m}''_C = \sum_{i=1}^{N_R} M_i \widehat{R}_{i,s} \tag{2.11}$$

$$\mathbf{n} \cdot \lambda \nabla T|_{\text{gas}} \; = \sum_{j=1}^{N} M_i \widehat{R}_{i,s} h_j^0 + \epsilon_{\text{s}} \sigma \left(T_{surf}^4 - T_{\text{in}}^4 \right) \tag{2.12}$$

$$\mathbf{n} \cdot \vec{u} = \frac{\dot{m}''_C}{\rho} \tag{2.13}$$

where $\mathbf{n}$ is the normal vector to the wall, ϵ_{s} is the emissivity ($\epsilon_{\text{s}} \approx 1.0$ for solid carbon), σ is the Stefan-Boltzmann constant, $\widehat{R}_{i,s}$ is the production rate of species i due to surface chemical reactions, $\dot{m}''_C$ is the net mass flux between surface and gas, indexes $wall$ and $surf$ refer to gas side at the wall and surface of the particles, respectively.

2.3.4 Numerics and validation

Simulations were carried out using the commercial software Ansys® Fluent 2022R2 [36], where the aforementioned governing equations were solved by applying an implicit finite volume technique. The scheme of the computational domain, grid structure, and resolution of the fixed-bed reactor is schematically depicted in Figure 2.1. Coordinates of particles were generated using the open source DEM software YADE [37]. Mechanical properties of the particles and validation of the software may be found in the literature [38]. To avoid deformation of the cells by contact point, gap size of less than 1% of the particle diameter have been imposed between spheres after shrinking the particles [39, 40]. A grid independence study was carried out by using several mesh sizes, specifically using 619,461, 1,972,845, and 3,677,036 polyhedral cells, being the 1,972,845 cells mesh selected for further simulations (See section 3.1). As a first three-dimensional numerical approach, only surface of the particles is meshed. For the same size of the reactor, a particle size smaller than 5.6 mm would increase the mesh size and thus, simulation times will increase. As three-dimensional CFD projects require an important amount of computational resources, this model is used to understand the phenomenon in a lower scale when compared to experiments. As a matter of fact, including the real amount of particles (200 particles normally used in experiments) and reactor dimensions will lead to an unacceptably large increase in the number of control volumes to simulate, therefore several months will be necessary to achieve convergence in such cases using a high-performance computing system. The solution method for coupling pressure and velocity was the semi-implicit method for pressure-linked equations (SIMPLE) scheme [41]. Radiation was considered using the P-1 model [42] since it plays a crucial role as a heat transfer mechanism inside the fixed-bed reactor, specially due to gas-to-gas radiation. Convective terms, species, and energy were discretized using an upwind second-order scheme. The under-relaxation factors were set at 0.5 for momentum, energy 0.8, and species 0.5, except for carbon dioxide (0.7), and oxygen (0.3), as the kinetic scheme involved in the process has a critical effect on these species' conservation. The iterations were stopped when the residual for all equations was less than 10^{-5}, which required approximately $5 \cdot 10^4$ iterations until convergence.

2.4 Results and discussion

2.4.1 Grid independence study

As shown in Figure 2.1, the chemically reacting fixed-bed reactor is composed of three zones: in, bed, and out (from left to right), being the bed zone the most critical section of the reactor, since here is where the 85 spherical particles are located, and therefore, where heterogeneous chemical reactions take place. A grid independence study was performed by analyzing coarse and fine mesh sizes, using 619,461, 1,972,845, and 3,677,036 polyhedral cells, which were obtained by locally refining the surface of the particles. Figure 2.2 shows the mesh of the bed zone of the reactor in its original form (619,461 polyhedral cells), using one (1,972,845 polyhedral cells) and two levels of refinement (3,677,036 polyhedral cells), respectively. The criteria for deciding which mesh size is more suitable for the setup under study is a difference below 5% between two grids. This was evaluated for crucial variables, such as temperature and mass fraction of CO_2 (Y_{CO_2}) on the surface of the particles (Area-weighted averaged) and in the bed zone (Volume averaged). Figure 2.3 and Tables 2.2 and 2.3 summarize the results for grids 1,972,845 and 3,677,036 polyhedral cells, observing difference no higher than 2.5% between both of them. As a matter of fact, the highest difference in the registered values was 2.147%. Therefore, all numerical simulations were carried out using the mesh size of 1,972,845 polyhedral cells.

Table 2.2: Results for temperature grid independence study.

	T_{surf}, K			$T_{bedzone}$, K		
T_{in}, K	$1,972,845$ cells	$3,677,036$ cells	Dif., %	$1,972,845$ cells	$3,677,036$ cells	Dif., %
900	1205.161	1205.153	0.001	1209.243	1209.178	0.005
1100	1210.695	1212.084	0.115	1220.637	1222.167	0.125
1300	1224.219	1225.405	0.097	1238.694	1240.187	0.120
1500	1247.065	1245.843	0.098	1267.398	1266.0634	0.105

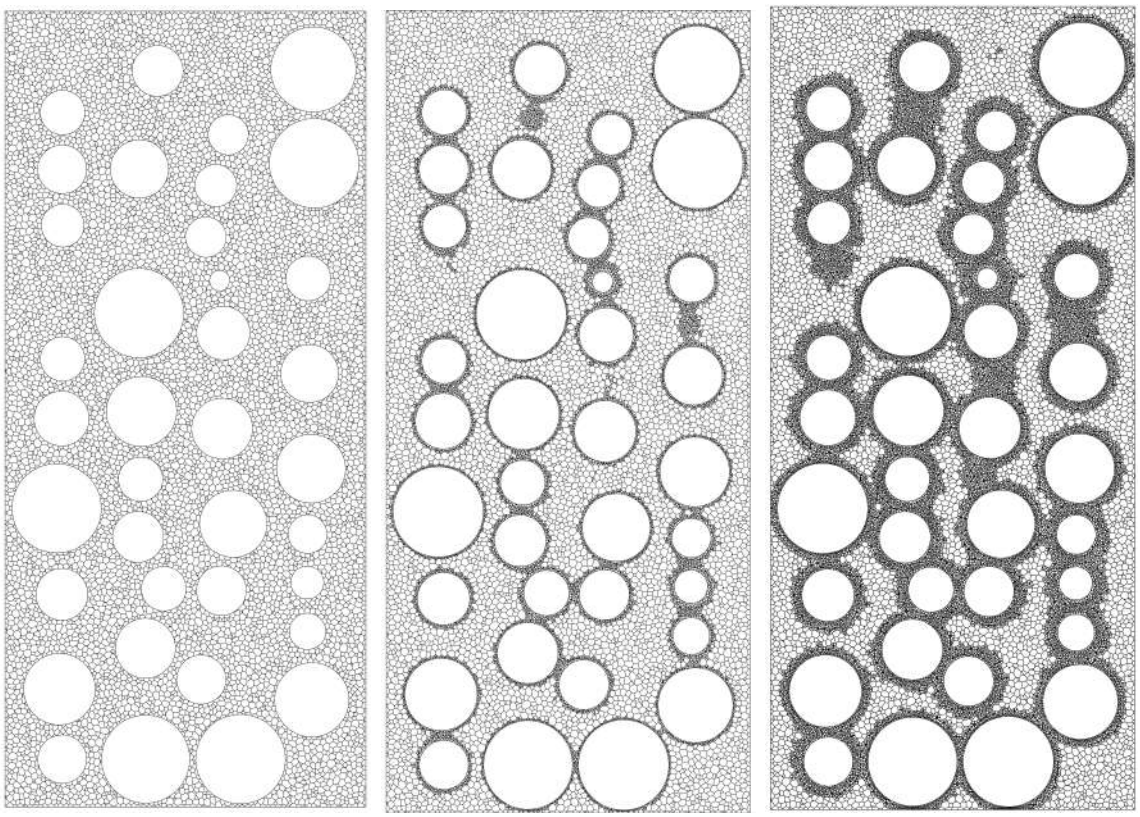

(a) (b) (c)

Figure 2.2: Mesh of bed zone of the reactor with different levels of refinement on particles surface (a) 619,461 polyhedral cells, (b) 1,972,845 polyhedral cells, and (c) 3,677,036 polyhedral cells.

Table 2.3: Results for Y_{CO_2} grid independence study.

	$Y_{CO_2,surf}$, [-]			$Y_{CO_2,bedzone}$, [-]		
T_{in}, K	$1,972,845$ cells	$3,677,036$ cells	Dif., %	$1,972,845$ cells	$3,677,036$ cells	Dif., %
900	0.0437289	0.0438657	0.312	0.0445701	0.0447017	0.294
1100	0.0585866	0.0597813	1.998	0.0594507	0.0606297	1.945
1300	0.0815193	0.0833133	2.153	0.0821038	0.0839054	2.147
1500	0.1183061	0.1183432	0.031	0.117745	0.1177906	0.039

2.4.2 Influence of inflow gas temperature

Simulations were carried out testing different inflow gas temperatures (T_{in}), particularly in the range of 1100-1500 K, which results are shown in Figure 2.4. Regarding oxygen concentration along the reactor (Y_{O_2}), Figure 2.4a shows the concentration profile of oxygen

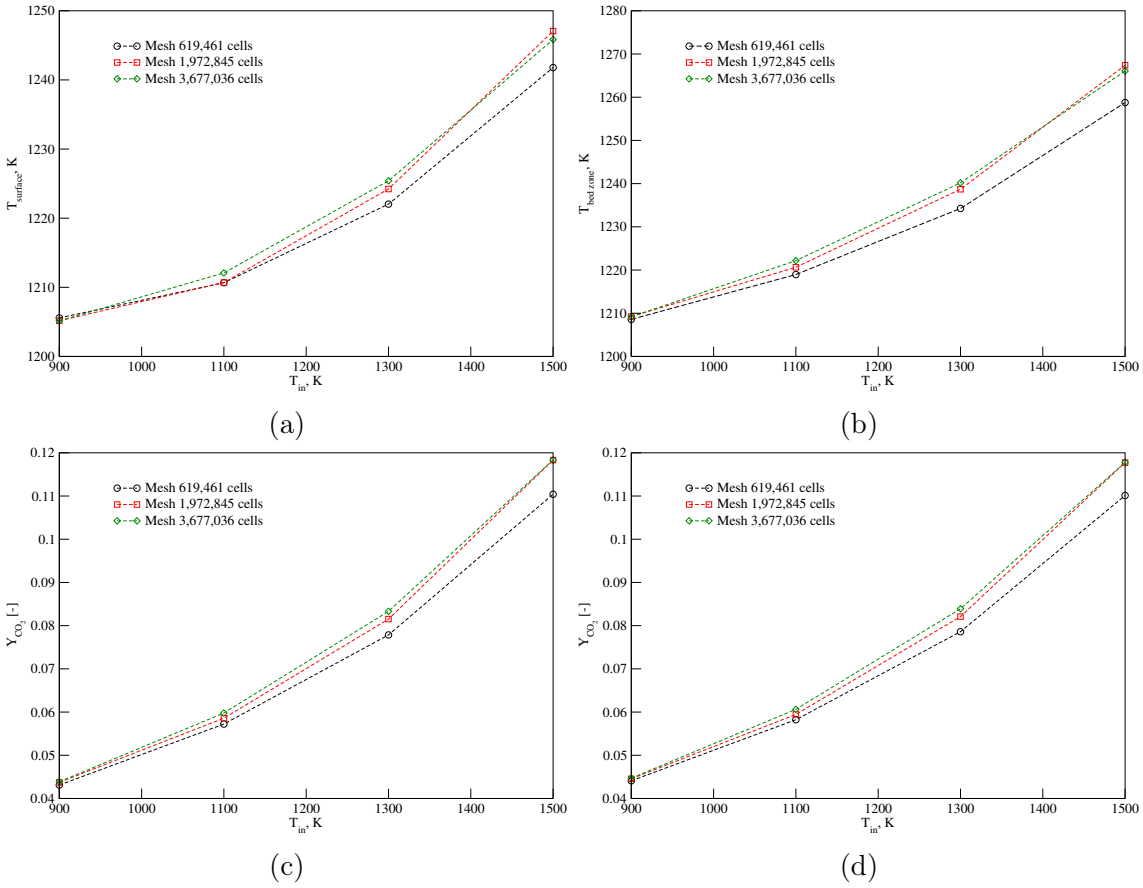

Figure 2.3: Temperature on surface of particles (a), and bed zone (b). Mass fraction of CO_2 on surface of particles (c), and bed zone (d) for several mesh sizes.

decreasing as the inflow gas meets the carbon char particles in the bed zone. Moreover, the consumption of oxygen is greater for higher values of T_{in}, observing almost complete consumption of oxygen along the reactor for 1500 K. The mass fraction of hydrogen (Y_{H_2}) is depicted for $Y_{O_2,\text{in}} = 0.11$ in Figure 2.4b, where profiles show how production of H_2 increases with the inflow gas temperature. Furthermore, hydrogen is produced particularly in R3 and R5, so it is involved both in heterogeneous and homogeneous chemical reactions. Carbon monoxide mass fraction Y_{CO} profiles are quite consistent with the literature since all heterogeneous reactions (R1 to R3) produce CO, so it is produced basically due to the gas-solid interactions on the surface of the particles. This is depicted in Figure 2.4c, where a positive evolution over the inlet temperature is observed. In the case of CO_2, it can be noticed that the mass fraction of carbon dioxide (Y_{CO_2}) increases with the inflow gas temperature for all cases under study as shown in Figure 2.4d, no matter the Reynolds number or mass fraction of oxygen at the inlet of the reactor.

2.4.3 Influence of Reynolds number

Reynolds numbers based on particle size (Re_{in}) of 50, 75, and 100 were numerically studied in the reactor. From an elemental perspective, as Re_{in} increases, a higher inlet velocity ($\vec{u}_{\text{in}}$) is observed. Thus, the possibility to experiment external limitations of the chemical kinetic scheme exists. This phenomenon is consistent with what has been found in the literature by assessing external Damköhler number [7]. The inlet temperature in the of range 1100-1500 K was assessed for all simulations. Figure 2.5 shows results for the concentration profile of chemical species involved in both homogeneous and heterogeneous reactions taking place inside the fixed-bed reactor. It can be observed in Figure 2.5b that there is an inverse proportional relationship between Y_{H_2} and Re_{in}, achieving volume-averaged values of magnitude 10^{-6} for the lowest Reynolds number evaluated in this study. In the case of carbon monoxide and as shown in Figure 2.5c, the concentration decreases with Re_{in}. For the outlet zone, the concentration shows some variations since CO is involved in all homogeneous chemical reactions. Regarding the mass fraction of carbon dioxide (Y_{CO_2}), it decreases with the Reynolds number as the maximum value is found for $\text{Re}_{\text{in}} = 50$ as depicted in Figure 2.5d. Moreover, the concentration has been found to be lower on the particle surfaces, which is consistent

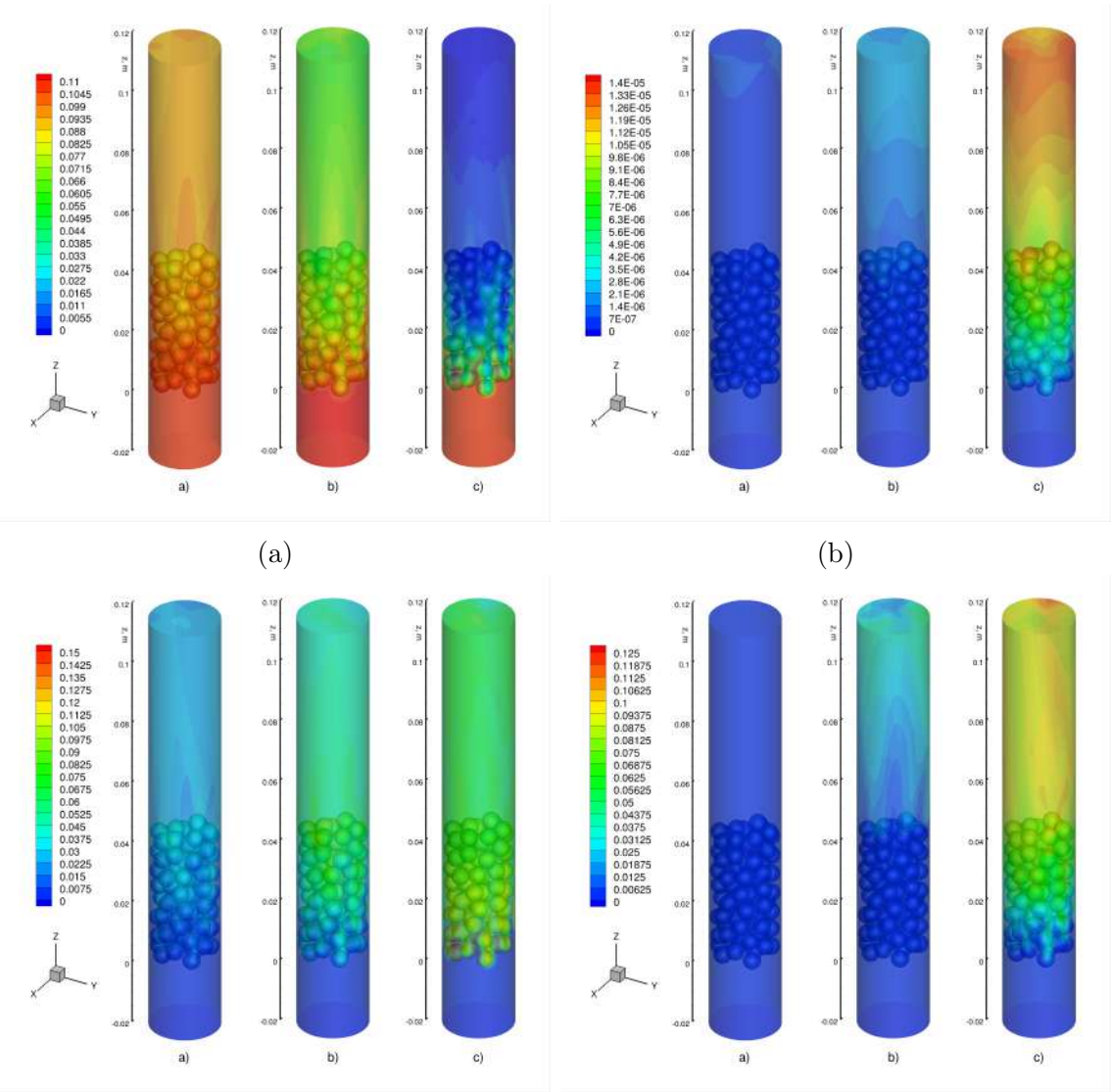

(a) (b)

(c) (d)

Figure 2.4: Y_{O_2} (a), Y_{H_2} (b), Y_{CO} (c), and Y_{CO_2} (d) for $Y_{O_2,in} = 0.11$, $Re_{in} = 75$ and $T_{in} = 1100$ K (a), 1300 K (b), and 1500 K (c).

with the kinetic scheme since the Boudouard reaction (R2) represents the consumption of carbon along with CO_2. Results confirm what Higuera [43] showed in his research, particularly for the effect of the Reynolds number in the performance of the combustion of a coal char particle in the presence of dry gas.

2.4.4 Influence of mass fraction of oxygen at inlet condition

Thermochemical processes can be classified according to the ambient mass fraction of oxygen Y_{O_2}. In this regard, it is essential to evaluate the behavior of the domain using several values based on combustion and gasification, so values of 0.05, 0.11, and 0.233 have been studied in this research. As stated previously, the numerical setup is based on steady-state and laminar regime simulations. Nevertheless, some of the cases tested did not converge for the conditions mentioned above, since oscillating residuals have been observed leading to a transition regime. This happened specifically for all Reynolds numbers, $Y_{O_2,in} = 0.233$, and inlet temperatures of 1300 K and 1500 K. The influence of $Y_{O_2,in}$ is shown in Figure 2.6, where mass fraction of chemical species were assessed using $Re_{in} = 75$ and inflow gas temperature of $T_{in} = 1100$ K. In the case of oxygen, the difference is quite evident since this parameter will drive the mass fraction of oxygen along the reactor, as clearly depicted in Figure 2.6a. Moreover, results for hydrogen mass fraction are shown in Figure 2.6b, where an increase in $Y_{O_2,in}$ leads to a higher concentration of H_2, specially for the zone after the bed of carbon char particles, which is attributed to the homogeneous chemical reactions taking place in that part of the computational domain. The same scenario may be observed in Figure 2.6c as the amount of carbon monoxide increases over $Y_{O_2,in}$. Regarding CO_2, it can be observed how the concentration is affected by the mass fraction of oxygen at the inlet of the fixed-bed reactors. In particular, keeping constant a value for $Re_{in} = 75$, the mass fraction of carbon dioxide increases with $Y_{O_2,in}$. This could be attributed to the oxidation of CO (R4) where oxygen is required, being the dominant homogeneous reaction along the reactor.

It can be observed in Figure 2.7 how both the variables of Re_{in} and $Y_{O_2,in}$ affect both the mass fraction of chemical species on the surface of the particles and the net mass flux between surface and gas ($\dot{m}''_C$). In particular, oxygen decreases over the inflow gas temperature,

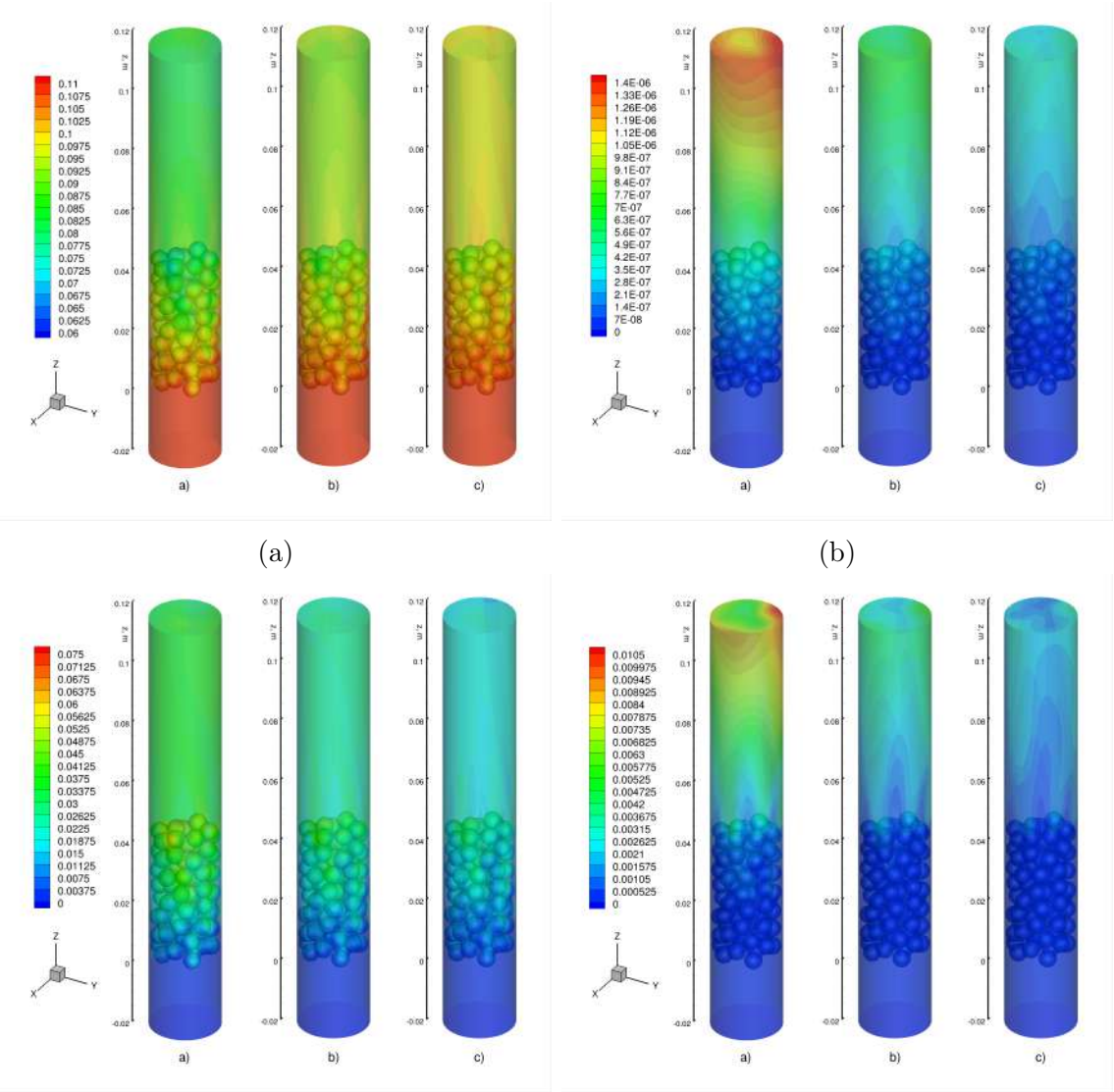

Figure 2.5: Y_{O_2} (a), Y_{H_2} (b), Y_{CO} (c), and Y_{CO_2} (d) for $Y_{O_2,in} = 0.11$, $T_{in} = 1100$ K and Re_{in} and $= 50$ (a), 75 (b), 100 (c).

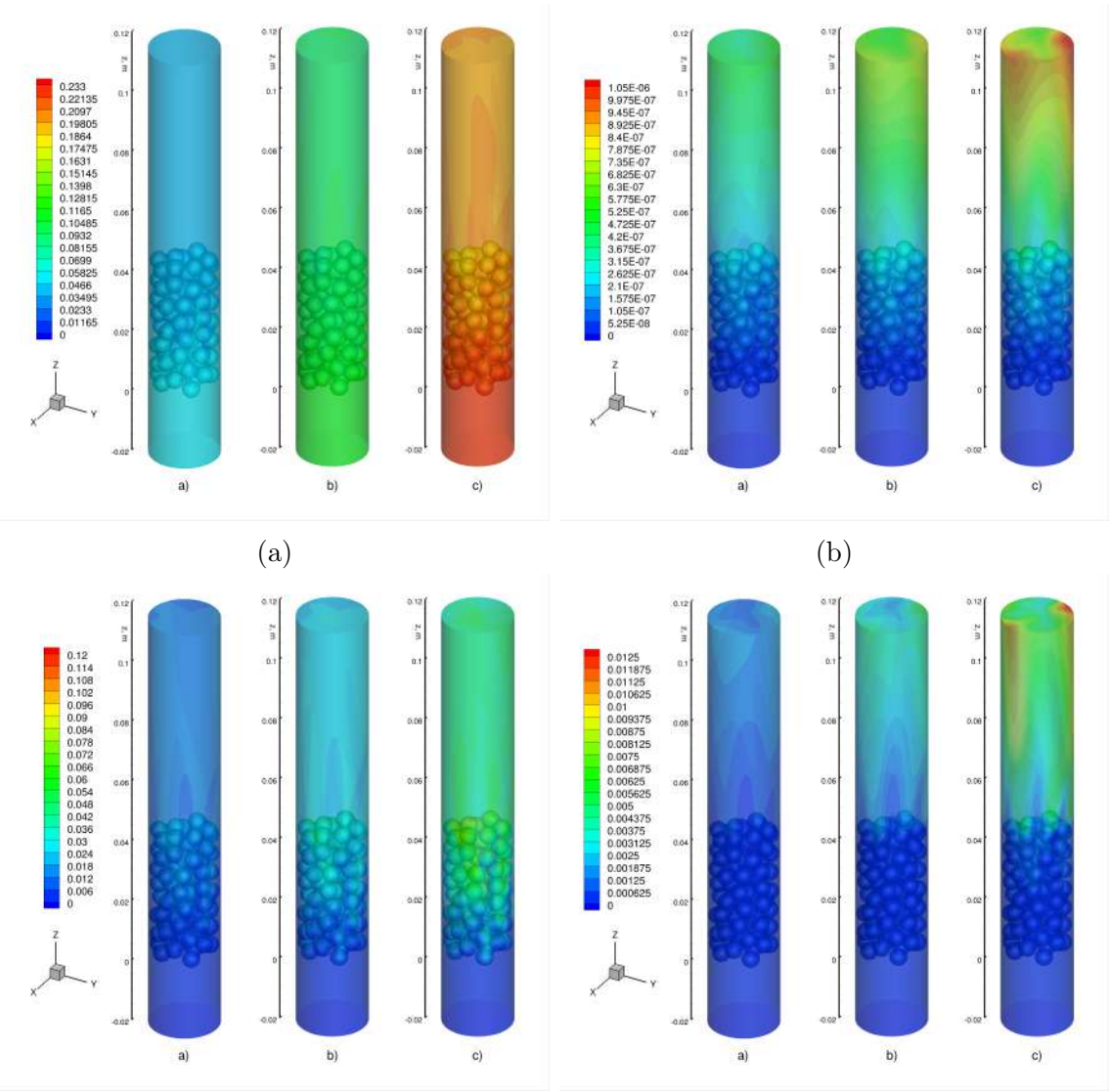

Figure 2.6: Y_{O_2} (a), Y_{H_2} (b), Y_{CO} (c), and Y_{CO_2} (d) for $Re_{in} = 75$, $T_{in} = 1100$ K and $Y_{O_2,in}$ = 0.05 (a), 0.11 (b), 0.233 (c).

more dramatically between 1100 K and 1300 K. In the case of hydrogen, the slope of the curves is higher for $\mathrm{Re_{in}} = 50$ as observed in Figure 2.7b, which may be attributed to the lower velocity of the flow, which leads to a higher conversion of R3 and R5. Carbon monoxide profile (See Figure 2.7c) shows interesting results since for $\mathrm{Re_{in}} = 50$ between 1300 K and 1500 K the mass fraction does not increase as for the rest of the temperature range, which could be attributed to the activation of R4 and R5. Moreover, carbon dioxide on the surface of the particles is related directly to the mass fraction of oxygen at the inlet of the reactor, and inversely with the Reynolds number (See Figure 2.7d). Moreover, the effect of the inflow gas temperature is strongly recognized as it increases dramatically from 1100 K to 1500 K. In general terms, and observing the semi-global kinetic scheme used for this study, the Boudouard reaction (R2) and oxidation of carbon monoxide (R4) are the most dominant chemical reactions (with higher reaction rates) among heterogeneous and homogeneous reactions, respectively. Figure 2.7e shows the net mass flux between surface and gas (or carbon consumption rate) as a function of the inflow gas temperature. Curves show clear differences between $\mathrm{Y_{O_2,in}}$ under study, being all values of $\dot{m}''_C$ positively related with the presence of oxygen in the inflow gas. Furthermore, a greater slope for all curves related to $\mathrm{Y_{O_2,in}} = 0.11$ is observed, specially in the range of 1100-1500 K. Below 1100 K, there is no significant effect of the Reynolds number, which may lead to a combined effect at 1300 K. There could be an important effect of the particle size since magnitude achieved for $\dot{m}''_C$ gets higher for a smaller size of spherical particles [7]. In particular, highest values are close to 0.003 $\mathrm{kg \cdot m^{-2} s^{-1}}$ at $\mathrm{Re_{in}} = 100$, $\mathrm{Y_{O_2,in}} = 0.11$, and $T_{\mathrm{in}} = 1500$ K. It can also be observed that for a low amount of oxygen in the inflow gas, i.e., $\mathrm{Y_{O_2,in}} = 0.05$, a linear dependency of the results is shown for most of the numerical simulations (See Figure 2.7f).

Regarding the temperature achieved inside the reactor, Figure 2.8a shows how the temperature in the bed zone of the reactor slightly increases with the mass fraction of oxygen at the inlet ($\mathrm{Y_{O_2,in}}$). The curves are almost similar in the range of 900-1100 K, showing a more pronounced difference in the range of 1100-1500 K. The same phenomenon is observed for the temperature on the surface of the carbon char particles (See Figure 2.8b), where the temperature increases almost without significant difference in the range of 900-1100 K, and then the temperature increases at higher Reynolds number. Figure 2.8c shows the tempera-

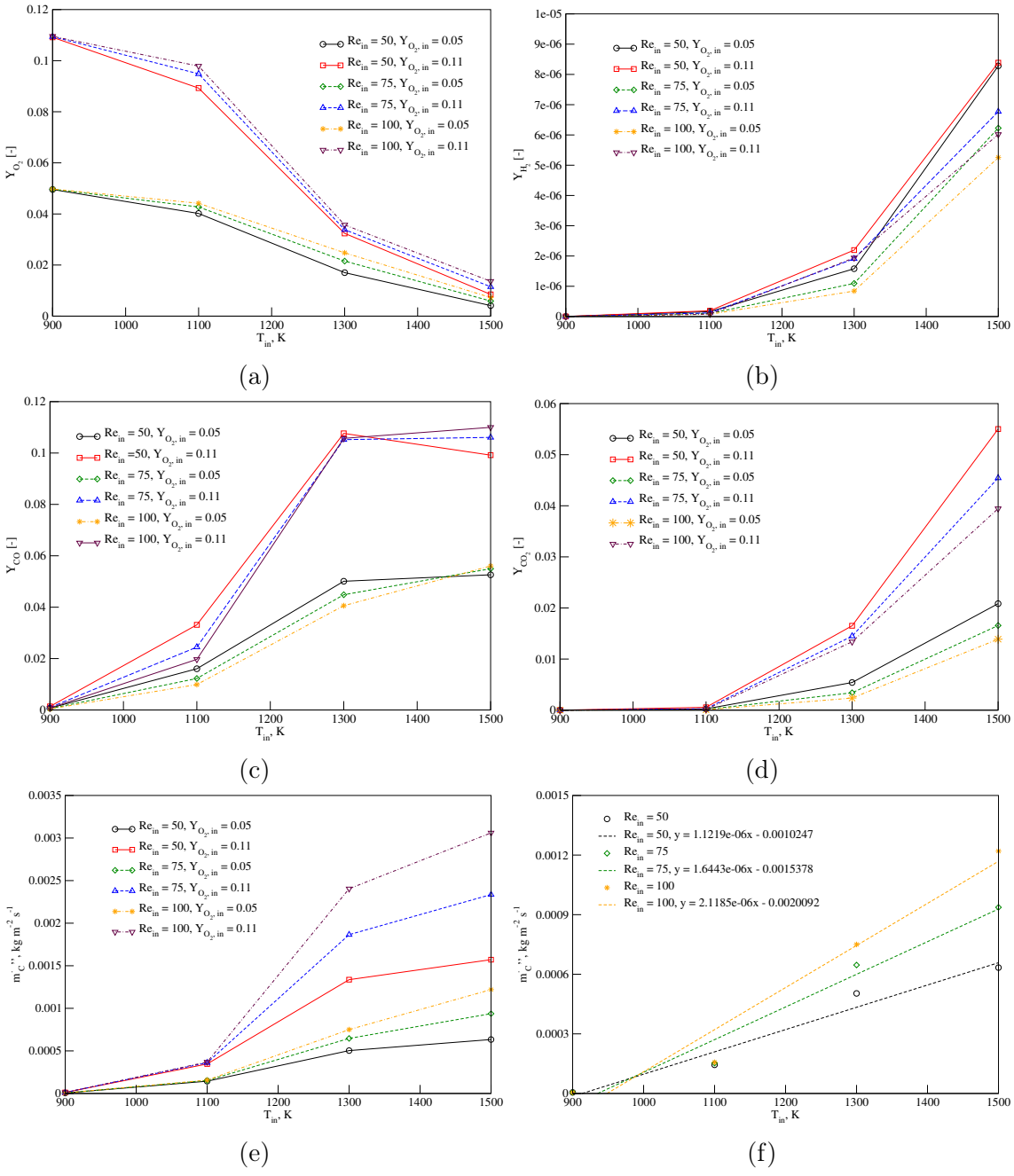

Figure 2.7: Y_{O_2} (a), Y_{H_2} (b), Y_{CO} (c), and Y_{CO_2} (d) on surface of particles, surface-averaged carbon mass flux ($\dot{m}''_C$) (e) for several $Y_{O_2,in}$ and Re_{in}, and $\dot{m}''_C$ regression for $Y_{O_2,in} = 0.05$ (f).

ture at the outlet of the reactor, where the tendency is similar to the previous zones by not observing a crucial effect of either $\mathrm{Re_{in}}$ or $\mathrm{Y_{O_2,in}}$. Nevertheless, it can be observed a steep slope at higher values for inflow gas temperature, which may be attributed to the effect of the homogeneous chemical reactions (R4 to R6). Furthermore, the mass fraction of species is depicted in Figure 2.9, where interesting results may be discussed. In particular, Figure 2.9a shows how oxygen is completely consumed for an inflow gas temperature of 1300 K no matter the Reynolds number for $\mathrm{Y_{O_2,in}} = 0.11$, presenting a strong decrease in the range of temperature from 1100 K to 1300 K. Moreover, the mass fraction of hydrogen increases with T_{in} in all cases under study. The same scenario may be observed for carbon monoxide (See Figure 2.9c), where the maximum amount of CO was achieved overall for $\mathrm{Re_{in}} = 50$, $\mathrm{Y_{O_2,in}} = 0.11$. Mass fraction of CO_2 at the outlet of the reactor is depicted in Figure 2.9d, where the effect of $\mathrm{Y_{O_2,in}}$ appears to be dominant when compared to the Reynolds number. The inflow gas temperature has clearly an impact on the performance of the heterogeneous combustion in a fixed-bed reactor. This has been observed in several works found in the literature with different configurations. As a matter of fact, Yi et al. [16] evaluated for one carbon particle how particle diameter, T_{in} and velocities affected the performance of carbon combustion.

Figure 2.10 describes the temperature and mass fraction of oxygen and carbon dioxide along the reactor (left) and particularly in the bed zone (right). The temperature of the gaseous phase is depicted in Figure 2.10a, where for the outlet zone (after nearly 0.05 m) a constant slope may be observed for all the results, highlighting the homogeneous chemical reactions taking place inside the reactor. Moreover, in the case of the bed zone, Figure 2.10b shows how the temperature of the gaseous phase is slightly higher than the temperature on the surface of the particles, observing an average and highest difference of 0.085% and 0.391%, respectively. This was tested as an example for $\mathrm{Re_{in}} = 50$ and considering that all curves would show the same tendency. Traditional species involved in combustion processes were also evaluated as a function of the z coordinate, observing in the case of oxygen (See Figure 2.10c) how this species is consumed in the bed zone due to the heterogeneous interactions occurring there. Interesting result is showed for $\mathrm{Y_{O_2}}$ since a slight increase after the bed zone is observed. As a matter of fact, and following the pattern described below, the mass fraction

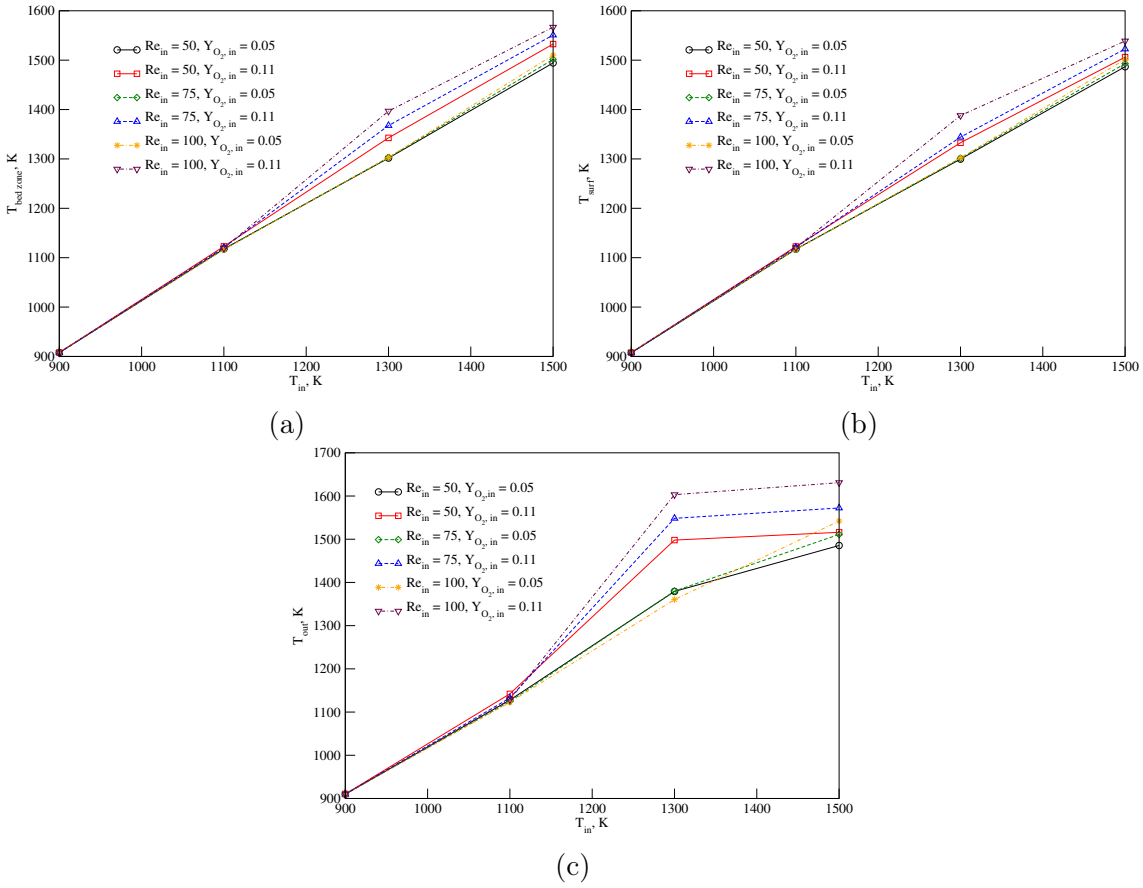

Figure 2.8: Temperature on the surface of carbon char particles (a) in the bed zone of the reactor (b) and at the outlet of the unit (c) at several $Y_{O_2,in}$ and Re_{in}.

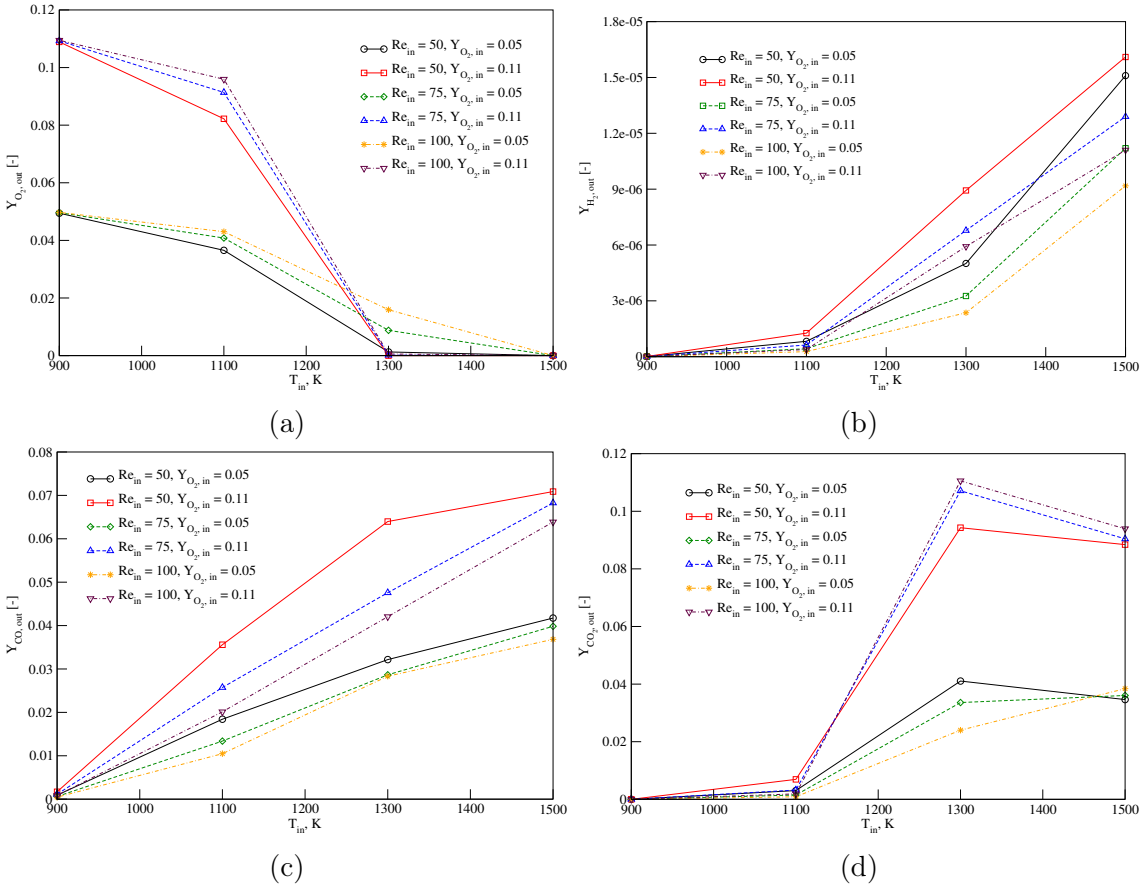

Figure 2.9: Y_{O_2} (a), Y_{H_2} (b), Y_{CO} (c), and Y_{CO_2} (d) at the outlet of the reactor for several $Y_{O_2,in}$ and Re_{in}.

of oxygen is higher in the gaseous phase rather than on the surface of the particles, achieving a maximum difference of 1.70% (See Figure 2.10d). In contrast, Figure 2.10e shows how carbon dioxide is produced along the reactor, where a more pronounced increase is observed in the outlet zone being affected entirely by the homogeneous kinetic scheme proposed in this study. Combustion of carbon char particles leads to a higher amount of CO_2 on the surface of the particles when compared to the gaseous phase with an average and maximum difference of 9.70% and 29.7%, respectively, as shown in Figure 2.10f.

All of the presented results show the effect of the $\mathrm{Re_{in}}$, $\mathrm{Y_{O_2,in}}$ and T_{in}, considering a particle size of 5.6 mm and no mesh inside particles. Regarding this particular features, the role of particle porosity is crucial to study how the conversion process behaves over time. In particular, Dierich et al. [44] presented a CFD-based model for tracking the chemically reacting interface and porosity of a single spherical particle of carbon moving in a hot CO_2 gas, where it has been demonstrated that Stefan flow inside the particles play a crucial role in the mass transfer process, and Reynolds number is relevant for accelerating the particle conversion time. Moreover, Nguyen et al. [45] explored the morphology evolution of char particles during fuel conversion at different operating conditions using the Random Pore Model for describing how the specific surface area varies over carbon consumption [46, 47]. Both of the aforementioned works were simulated using a 2D axisymmetric model. In the current study, there is no mesh inside particles, since assessing surface of the particles is the first step of an increasing complexity process. On the other hand, particle shape has been discussed in the past years [48], where non-spherical char particles where considered for evaluating the conversion process in the flame zone of an entrained-flow gasifier. Main findings are related to the shape development (transient simulation) over the conversion process, where the Reynolds number is the crucial parameter to consider (drag coefficient will change). Furthermore, ellipsoidal, cylindrical, conical, rhomboidal, among other particle shapes have been considered for evaluating the performance of the pseudo-steady state approach for carbon particle combustion/gasification [49]. Even considering the same volume of a particle, the surface area will be changing depending on the shape of the particle, therefore the effect of heterogeneous chemical reactions may be intensified in some cases when compared to a spherical particle. In terms of computational resources, the more complex and irregular the

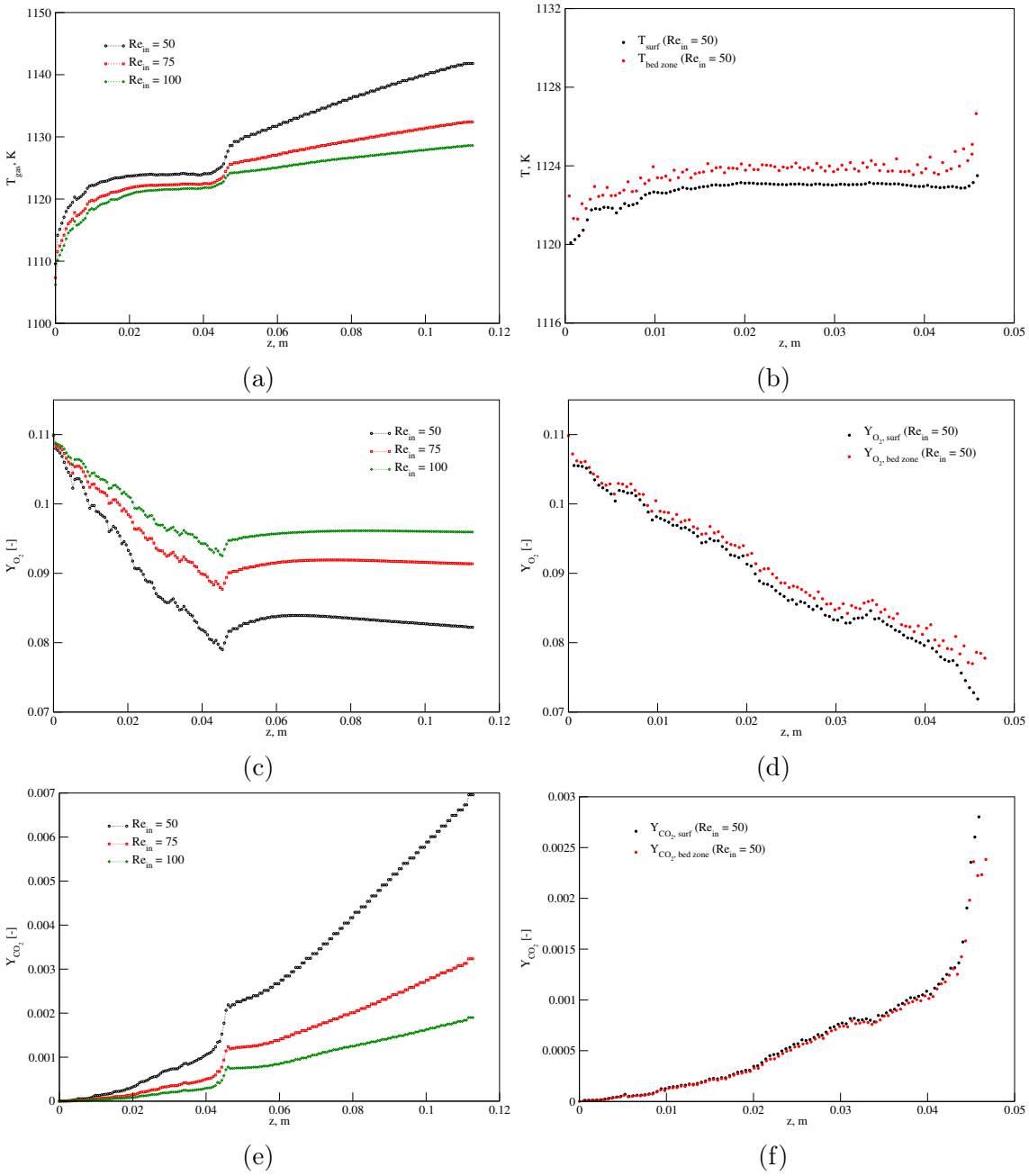

Figure 2.10: Temperature of the gaseous phase (T_{gas}) along the reactor for several Re_{in} (a), Temperature of gas and solid phases in the bed zone of the reactor for $\text{Re}_{\text{in}} = 50$ (b), Y_{O_2} along the reactor for several for Re_{in} (c), Y_{O_2} in the bed zone of the reactor for $\text{Re}_{\text{in}} = 50$ (d), Y_{O_2} along the reactor for several for Re_{in} (e), Y_{CO_2} in the bed zone of the reactor for $\text{Re}_{\text{in}} = 50$ (f), $\text{Y}_{\text{O}_2,\text{in}} = 0.11$ and $T_{\text{in}} = 1100$ K.

geometry, the more cell volumes are necessary to have a suitable numerical approach. No matter the particles shape, it would be expected a higher mass fraction of carbon dioxide (Y_{CO_2}) closed to the particles when the inflow gas temperature is higher. Here the endothermic Boudouard reaction may impact negatively in the temperature surface due to the high presence of CO_2 in the downstream part of the particles. Finally, results of this case will be enhanced to Large Eddy Simulation (LES) and Reynolds-Averaged Navier-Stokes (RANS) modeling approaches of turbulent heterogeneous combustion.

2.5 Concluding remarks

In this work, the heterogeneous combustion of a chemically reacting fixed-bed reactor using 85 spherical carbon char particles was investigated using a three-dimensional CFD-based approach under steady-state and laminar flow regime conditions. Critical parameters of Re_{in}, $Y_{O_2,in}$, and T_{in} were assessed, observing interesting results. Based on the proposed semi-global chemical kinetic scheme, the mass fraction of species (Y_i) showed consistency when describing the heterogeneous combustion of carbon char particles. Boudouard reaction (R2) was the dominant chemical reaction among the heterogeneous interactions taking place on the surface of the particles, while oxidation of carbon monoxide (R4) was dominant among homogeneous chemical reactions. There is a relevant influence of the inflow gas temperature (T_{in}) in the performance of the kinetic scheme since chemical reactions are dramatically activated from 1300 K. It was found that for $Y_{O_2,in} = 0.05$ almost all dependencies had a linear behavior. The highest difference between surface of particles and gaseous phase in the bed zone of the reactor was found for carbon dioxide, achieving a maximum value of 29.7%. This research shows a remarkable potential for various applications since this three-dimensional approach can successfully predict the heterogeneous combustion of carbon char particles using a fixed-bed reactor in terms of thermal and concentration of species profiles, showing an important place to further explore using different flow regimes and boundary conditions. This study may be considered as a benchmark case for validation of 1D and 2D models, where a continuum numerical approach (porous media model) might be validated against 3D particle-resolved simulations. Further studies are necessary to assess turbulent

flow regime, intrinsic chemical reactions (tracking of porosity and particle radius), a wider range of inflow gas temperature, a more detailed chemical kinetics mechanism, and the hybridization of the bed by incorporating inert solid particles into these type of units.

Acknowledgments

The authors would like to thank the support of the National Agency for Research and Development (ANID) / Scholarship Program / DOCTORADO BECAS CHILE/2021 – 21211230 and the Digital Research Alliance of Canada for the computational infrastructure used in this research.

References

[1] A.G. Dixon, M. Nijemeisland, and E.H. Stitt. Packed tubular reactor modeling and catalyst design using computational fluid dynamics. *Advances in Chemical Engineering*, 31:307–389, 2006.

[2] J. Wang, S. Wei, Q. Wang, and B. Sunden. Transient numerical modeling and model predictive control of an industrial-scale steam methane reforming reactor. *International Journal of Hydrogen Energy*, 46:15241–15256, 2021.

[3] A.G. Dixon. Local transport and reaction rates in a fixed bed reactor tube: Endothermic steam methane reforming. *Chemical Engineering Science*, 168:156–177, 2017.

[4] R. Meijer, H.J. Miihlen, F. Kapteijn, and J.A. Moulijn. Burn-off behaviour in alkali-catalysed co2 gasification of bituminous coal char: A comparison of tga and fixed-bed reactor. *Fuel Processing Technology*, 28:5–17, 1991.

[5] D.K. Park, S.D. Kim, S. Hoon Lee, and J. Goo Lee. Co-pyrolysis characteristics of sawdust and coal blend in tga and a fixed bed reactor. *Bioresource Technology*, 101: 6151–6156, 8 2010. ISSN 09608524.

[6] V.S. Gururajan, T.F. Wall, R.P. Gupta, and J.S. Truelove. Mechanisms for the ignition of pulverized coal particles. *Combustion and Flame*, 81(2):119–132, 1990. ISSN 0010-2180.

[7] Dmitry Safronov, Matthias Kestel, Petr Nikrityuk, and Bernd Meyer. Particle resolved simulations of carbon oxidation in a laminar flow. *Canadian Journal of Chemical Engineering*, 92:1669–1686, 10 2014. ISSN 1939019X.

[8] A. Richter, P.A. Nikrityuk, and M. Kestel. Numerical investigation of a chemically reacting carbon particle moving in a hot o2/co2 atmosphere. *Industrial and Engineering Chemistry Research*, 52:5815–5824, 4 2013. ISSN 08885885.

[9] C. Hasse, P. Debiagi, X. Wen, K. Hildebrandt, M. Vascellari, and T. Faravelli. Advanced modeling approaches for cfd simulations of coal combustion and gasification. *Progress in Energy and Combustion Science*, 86, 9 2021. ISSN 03601285.

[10] Nusselt W. Der verbrennungsvorgang in der kohlenstaubfeuerung. *Zeitschrift des Vereins Deutsche Ingenieure*, 68:124–8, 1924.

[11] S.P. Burke and T.E. Schumann. Kinetics of a type of heterogeneous reactions' the mechanism of combustion of pulverized fuel. *Industrial and Engineering Chemistry*, 23, 1931.

[12] P.A. Libby and T.R. Blake. Burning carbon particles in the presence of water vapor. *Combustion and Flame*, 41:123, 1981.

[13] J.C. Lee, R.A. Yetter, and F.L. Dryer. Transient numerical modeling of carbon particle ignition and oxidation. *Combustion and Flame*, 101:387–98, 1995.

[14] S.Y. Cho, R.A. Yetter, and F.L. Dryer. A computer model for one-dimensional mass and energy transport in and around chemically reacting particles, including complex gas-phase chemistry, multicomponent molecular diffusion, surface evaporation, and heterogeneous reaction. *Journal of Computational Physics*, 102:160–179, 1992.

[15] R. Stauch and U. Maas. Transient detailed numerical simulation of the combustion of carbon particles. *International Journal of Heat and Mass Transfer*, 52:4584–4591, 9 2009. ISSN 00179310.

[16] F. Yi, J. Fan, D. Li, S. Lu, and K. Luo. Three-dimensional time-dependent numerical simulation of a quiescent carbon combustion in air. *Fuel*, 90:1522–1528, 4 2011. ISSN 00162361.

[17] Y. Qian, Y. Yu, G. Xu, and X. Liu. Cfd modeling of coal pyrolysis in externally heated fixed-bed reactor. *Fuel*, 233:685–694, 12 2018. ISSN 00162361.

[18] Y. Qian, J. Zhan, Y. Yu, G. Xu, and X. Liu. Cfd model of coal pyrolysis in fixed bed reactor. *Chemical Engineering Science*, 200:1–11, 6 2019. ISSN 00092509.

[19] M.A. Mujeebu, M.Z. Abdullah, A.A. Mohamad, and M.Z. Abu Bakar. Trends in modeling of porous media combustion. *Progress in Energy and Combustion Science*, 36: 627–650, 2010. ISSN 03601285.

[20] M.A. Mujeebu, M.Z. Abdullah, M.Z. Abu Bakar, A.A. Mohamad, R.M. Muhad, and M.K. Abdullah. Combustion in porous media and its applications - a comprehensive survey. *Journal of Environmental Management*, 90:2287–2312, 2009. ISSN 03014797.

[21] M. Toledo and C. Rosales. Hybrid filtration combustion. *Hydrogen Energy - Challenges and Perspectives, in Hydrogen Energy - Challenges and Perspectives, 1st ed., IntechOpen*, pages 201–222, 2012.

[22] M. Toledo, A. Arriagada, N. Ripoll, E.A. Salgansky, and M.A. Mujeebu. Hydrogen and syngas production by hybrid filtration combustion: Progress and challenges. *Renewable and Sustainable Energy Reviews*, 177, 5 2023. ISSN 18790690.

[23] N. Hanchate, S. Ramani, C.S. Mathpati, and V.H. Dalvi. Biomass gasification using dual fluidized bed gasification systems: A review. *Journal of Cleaner Production*, 280, 1 2021. ISSN 09596526.

[24] S. Safarian, R. Unnpórsson, and C. Richter. A review of biomass gasification modelling. *Renewable and Sustainable Energy Reviews*, 110:378–391, 8 2019. ISSN 18790690.

[25] J.A. Ruiz, M.C. Juárez, M.P. Morales, P. Muñoz, and M.A. Mendívil. Biomass gasification for electricity generation: Review of current technology barriers. *Renewable and Sustainable Energy Reviews*, 18:174–183, 2013. ISSN 13640321.

[26] R. Luque and J.G. Speight. *Gasification for Synthetic Fuel Production: Fundamentals, Processes and Applications*. Woodhead Publishing Series in Energy, 2015. ISBN 978-0-85709-802-3.

[27] M. Toledo and N. Ripoll. *Syngas Fuel Production from Carbonaceous Feedstocks Using Hybrid Porous Media*. IntechOpen, 9 2019.

[28] M. Toledo, N. Ripoll, J. Céspedes, A. Zbogar-Rasic, N. Fedorova, V. Jovicic, and A. Delgado. Syngas production from waste tires using a hybrid filtration reactor under different gasifier agents. *Energy Conversion and Management*, 172:381–390, 9 2018. ISSN 01968904.

[29] S.R. Turns. *An Introduction to Combustion: Concepts and Applications*. McGraw-Hill, 2006. ISBN 9780072350449.

[30] W.P. Jones and R.P. Lindstedt. Global reaction schemes for hydrocarbon combustion. *Combustion and Flame*, 73:233–249, 1988.

[31] R.J. Kee, M.E. Coltrin, and P. Glarborg. *Chemically Reacting Flow: Theory and Practice*. Wiley, 2005. ISBN 9780471461302.

[32] A. Ermoline, D. Yildiz, and E.L. Dreizin. Model of heterogeneous combustion of small particles. *Combustion and Flame*, 160:2982–2989, 12 2013. ISSN 00102180.

[33] T.R. Jayawickrama, M.A. Chishty, N. Haugen, M.U. Babler, and K. Umeki. The effects of stefan flow on the flow surrounding two closely spaced particles. *International Journal of Multiphase Flow*, 166, 104499, 9 2023. ISSN 03019322.

[34] P.A. Nikrityuk, M. Gräbner, M. Kestel, and B. Meyer. Numerical study of the influence of heterogeneous kinetics on the carbon consumption by oxidation of a single coal particle. *Fuel*, 114:88–98, 2013. ISSN 0016-2361. Advances in Coal Science and Technology, ICCS&T 2011.

[35] J. Yu, K. Zhou, and W. Ou. Effects of stefan flow and co oxidation on char particle combustion in o2/co2 atmosphere. *Fuel*, 106:576–585, 2013. ISSN 00162361.

[36] Inc. ANSYS. ANSYS-FLUENT™ V 2022R2 – Commercially available CFD software package based on the Finite Volume method. Southpointe, 275 Technology Drive, Canonsburg, PA 15317, U.S.A., 2022.

[37] Jan Kozicki and Frederic V. Donze. YADE-OPEN DEM: An open-source software using a discrete element method to simulate granular material. *Engineering Computations*, 26(7):786 – 805, 2009.

[38] Y.R. Lu and P.A. Nikrityuk. DEM-based model for steam methane reforming. *Chemical Engineering Science*, 247:116903, 2022.

[39] A.G. Dixon, M. Nijemeisland, and E.H. Stitt. Systematic mesh development for 3D CFD simulation of fixed beds: contact points study. *Comput. Chem. Eng.*, 48:135–153, 2013.

[40] M. Pichler, B. Haddadi, C. Jordan, H. Norouzi, and M. Harasek. Effect of particle contact point treatment on the CFD simulation of the heat transfer in packed beds. *Chem. Eng. Res. and Design*, 165:242–253, 2021.

[41] S.V. Patankar. *Numerical heat transfer and fluid flow*. Series on Computational Methods in Mechanics and Thermal Science. Hemisphere Publishing Corporation (CRC Press, Taylor & Francis Group), 1980. ISBN 978-0891165224.

[42] G. Krishnamoorthy, R. Rawat, and P. Smith. Parallelization of the p-1 radiation model. *Numerical Heat Transfer, Part B: Fundamentals*, 49:1–17, 1 2006. ISSN 10407790.

[43] F.J. Higuera. Combustion of a coal char particle in a stream of dry gas. *Combustion and Flame*, 152:230–244, 1 2008. ISSN 00102180.

[44] F. Dierich, A. Richter, and P. Nikrityuk. A fixed-grid model to track the interface and porosity of a chemically reacting moving char particle. *Chemical Engineering Science*, 175:296–305, 1 2018. ISSN 00092509.

[45] C.B. Nguyen, J. Scherer, M. Hartwich, and A. Richter. The morphology evolution of char particles during conversion processes. *Combustion and Flame*, 226:117–128, 4 2021. ISSN 15562921.

[46] S.K. Bhatia and D.D. Perlmutter. A rondom pore model for fluid-solid reactions: I. isothermal, kinetic control. *AlChE Journal*, 26:379–386, 1980.

[47] S.K. Bhatia and D.D. Perlmutter. A random pore model for fluid-solid reactions : Ii. diffusion and transport effects. *AlChE Journal*, 27:247–254, 1981.

[48] C. Nguyen, J. Scherer, Q. Guo, S. Kriebitzsch, and A. Richter. The shape development of spherical and non-spherical char particles in the flame zone of an entrained-flow gasifier – a numerical study. *International Journal of Heat and Mass Transfer*, 149, 3 2020. ISSN 00179310.

[49] P. Nikrityuk and B. Meyer. Pseudo-steady-state approach for carbon particle combustion/gasification. In *Gasification Processes: Modeling and Simulation*, pages 205–244. Willey-VCH Verlag GmbH & Co, Weinheim, Germany, 9 2014. ISBN 9783527335503.

Chapter 3

Modeling of a moving reacting carbon char particle using macro-pore-resolved and porous media approaches[*]

[*]This chapter is a facsimile of the research article published in A. Arriagada, M. Toledo, R.E. Hayes, and P. Nikrityuk, Industrial & Engineering Chemistry Research, **2024**.

3.1 Abstract

This work presents a comparative computational study of the heterogeneous combustion of a single spherical carbon char particle in hot atmospheres with different O_2 concentrations using porous media model (PMM) and macro-pore-resolved simulations (PRS). A two-dimensional axisymmetric computational fluid dynamics model (2D CFD) in a pseudo-steady-state approach (PSS) is performed. In both cases, a semi-global kinetic scheme is implemented, including three heterogeneous and three homogeneous chemical reactions. Several Reynolds numbers (Re_{in} = 10, 50, and 100), inflow gas temperatures (T_{in} = 1100-2000 K), and inlet mass fractions of oxygen ($Y_{O_2,in}$ = 0.05 and 0.11) are assessed. Results show good agreement between PMM and PRS, specially for T_{in} = 2000 K, where the deviation in the values for species was not higher than 8.3%. Maximum deviation for CO_2 was 1.54% when evaluating the maximum values for species concentration. In addition, the effects of the gasifying conditions, oxidative regime, and tortuosity on the partial oxidation process are discussed.

Keywords: Chemical kinetics, Heterogeneous combustion, Mass diffusivity, Pore-resolved simulation, Porous media model.

Nomenclature

Roman Symbols	Definition	Greek Symbols	Definition
A	Pre-exponential factor	α	Permeability, m^2
C	Concentration, $kmol \cdot m^{-3}$	ϵ	Emissivity
D	Molecular diffusivity, $m^2 \cdot s^{-1}$	ε	Porosity
d	Diameter, m	λ	Thermal conductivity, $W \cdot m^{-1} \cdot K^{-1}$
E_a	Activation energy, $J \cdot mol^{-1}$	μ	Viscosity, $Pa \cdot s$
h	Enthalpy, $J \cdot kg^{-1}$	ρ	Density, $kg \cdot m^{-3}$
k	Reaction rate constant	$\overline{\overline{\tau}}$	Stress tensor, Pa
M	Molecular weight, $kg \cdot mol^{-1}$	τ	Tortuosity
$\dot{m}''$	Net mass flux gas-surface, $kg \cdot m^{-2} \cdot s^{-1}$	**Abbreviations**	**Definition**
N	Number	CFD	Computational fluid dynamics
n_r	Temperature exponent	HFC	Hybrid filtration combustion
p	Pressure, Pa	PMM	Porous media model
R	Universal gas constant, $J \cdot mol^{-1} \cdot K^{-1}$	PRS	Pore-resolved simulation
$\widehat{R}$	Production rate	**Subscripts**	**Definition**
Re	Reynolds number	g	Gas phase
S	Source term	i	species i
S'''	Specific surface area, m^{-1}	in	Inlet
T	Temperature, K	m	Mass
$\vec{u}$	Velocity, $m \cdot s^{-1}$	p	Particle
Y	Mass fraction	R	Reaction

3.2 Introduction

Coal is one of the most relevant solid fuels since it supplies more than one-third of the global electricity generation, playing a relevant role in the economy and industrial sector. The global coal demand reached a record high in 2022, rising by 4% year-on-year to 8.42 billion tonnes, and it is expected to reach a new record in 2023 (an increase of 1.4%) [1]. Carbon char particle combustion stands as a fundamental research topic that has been extensively explored [2–8], specifically the heterogeneous combustion of char. This challenge arises since several physical processes are taking place on the surface of the particles, being widely studied for approximately a hundred years now [9].

Numerical simulations for studying carbon thermochemical conversion have been widely documented in the literature [10–15]. In particular, studies have assessed the steady-state combustion of a coal particle [3], the oxidation of a single moving particle under laminar

regime conditions [4], the consumption rate of carbon based on the effect of critical parameters such as inlet velocity, composition, and temperature [5] using a detailed model that integrates surface oxidation and volatilization processes of the coal particle. The individual effect of oxygen and steam concentration on the reaction behaviors of a single coal char particle and the particle motion (translation and rotation) has also been assessed in recent years [6, 8]. Furthermore, a strong relationship between the particle Reynolds number (Re_{in}) and oxidation regimes (kinetically-controlled, transition, diffusion-controlled) related to species transport to the particle surface has been found. In addition, interesting findings relate to the relationship between burning rate and oxygen concentration at the inlet of the reactor [13]. For the thermochemical conversion at a low oxygen concentration in a fixed-bed reactor, radiation has been identified as the dominant heat transfer mechanism, highlighting the relevance of heterogeneous reactions and the phase change of water along the process [14, 15].

The role of particle porosity (ε) is crucial to studying how the conversion of carbon occurs over time. A CFD-based model for tracking the reacting interface and porosity in a hot CO_2 gas has been explored, highlighting the relevance of Stefan flow inside carbon particles in diffusion phenomena, where also Re_{in} is a parameter of interest when accelerating the particle conversion rate [16]. The random pore model (RPM) has also been studied in extension for modeling the porosity and specific surface development under a kinetically-controlled regime and three-dimensional geometry of a spherical carbon char particle, where fragmentation of the particle depends on instantaneous porosity and carbon conversion due to disaggregation of the pore walls [17]. However, it should be noted that one of the first 2D and 3D pore-resolved CFD-based simulations of chemically reacting char particles was reported by Richter et al. [5] and [18, 19], respectively. It was shown that endothermic heterogeneous reactions such as $C + CO_2$ and $C + H_2O$ and the Stefan flow inside and around the particle play a significant role in the heat and mass transfer balances.

The numerical simulation of gasifiers has been assessed based on the inherent complexity of the interactions between a hot oxidant gaseous mixture and coal particles, where particle trajectory, flow field, and size of particles have been objects of study when pyrolysis, devolatilization, and thermal conversion occur [19]. Reynolds number is essential to con-

sider when the particle shape is considered as non-spherical, since the drag coefficient will change depending on the shape, along with its shape development in a transient state over the conversion of the particle in the flame zone of an entrained-flow gasifier [20]. Most recently, carbon char thermochemical conversion has been studied in a fixed-bed gasifier using surface-based reactions [21]. Moreover, Lattice Boltzmann simulations have been performed to represent catalytic reactions inside a single particle [22] and inert porous media combustion [23]. Nevertheless, the complexity of the computational domain does not allow for conducting a study with a large number of particles (250-300 solid fuel particles are commonly used in laboratory-scale experiments) or even intrinsic chemical reactions for heterogeneous combustion. Thus, this research focuses on applying a porous media model (PMM) to the heterogeneous combustion of a single spherical carbon char particle using air and steam as oxidant agents and its validation against Pore-resolved simulations (PRS), since pore-resolved CFD simulations of chemically reacting particles are extremely expensive in terms of computational resources. This validation is necessary and could potentially enable the use of the PMM approach in particle-resolved fixed-bed units with porous particles [24, 25]. In particular, Fong et al. [24] reported a hybrid PRS-PMM approach where macro-pores were directly resolved by computational mesh and the micro- and meso-porous were taken into account by effective diffusion coefficient within effective-continuum equations. It should be noted that validation of porous media-based models for a single particle against pore-resolved simulations is widely used in the heat and mass transfer theory. For example, Wittig et al. [26, 27] compared Nusselt numbers for porous and non-porous particles using pore-resolved 3D CFD simulations.

Finally, the novelty of this work consists of performing comparative numerical studies of the intraparticle heat and mass transfer in a chemically reacting porous particle moving in a hot gas, where numerical models are based on the so-called pore-resolved and porous media approach CFD simulations. The main objective of this research is the illustration of differences between the porous media approach, which is computationally suitable for modeling a large number of reacting porous particles, and direct numerical modeling of a chemically porous particle resolving macro-pores directly. To validate the applicability of PMM in an intrinsic heterogeneous combustion process, the effects of different flow regimes under several

gasification conditions and a thorough comparison with a PRS numerical approach must be assessed, as pore-resolved CFD simulations of chemically reacting particles are extremely expensive in terms of computational resources. This numerical study aims to analyze the heterogeneous combustion of a single spherical carbon char particle under partial oxidative conditions in a 2D axisymmetric pseudo-state approach, assessing inflow gas temperature, Reynolds number, and mass fraction of oxygen at inlet conditions.

3.3 Model Formulation

3.3.1 Problem description

The numerical model was implemented to simulate the heterogeneous combustion of a single spherical carbon char particle under various gasification conditions within a laminar flow regime. Figure 3.1 depicts the schematics of the 2D axisymmetric numerical domain used within two different models, being Pore-resolved simulation (PRS) and the porous media model (PMM) module available in the commercial software Ansys® Fluent. The diameter of the particle (d_p) was set to 5.6 mm, following theoretical data found in the literature for filtration and hybrid filtration combustion (HFC) processes [28–31]. The inflow gas temperature (T_{in}) selected for this study was in the range of 1100-2000 K [29, 32, 33]. The dimensions of the computational domain were set to $130d_p$ x $40d_p$. The characteristics of the fuel particle can be found in Table 3.1 [20, 34], where inertial resistance, inverse of permeability, porosity and specific surface were calculated using the geometrical features of the particle. The inflow gas consisted of two different oxidative atmospheres ($\text{Y}_{\text{O}_2,\text{in}}$ = 0.05, and 0.11), and mass fraction of H_2O ($\text{Y}_{\text{H}_2\text{O},\text{in}}$ = 0.001 and 0.074), the rest is nitrogen ($\text{Y}_{\text{N}_2} = 1 - \sum_i \text{Y}_\text{i}$). The inflow gas temperature (T_{in}) was set in the range of 1100-2000 K, and the operating pressure was 1 bar.

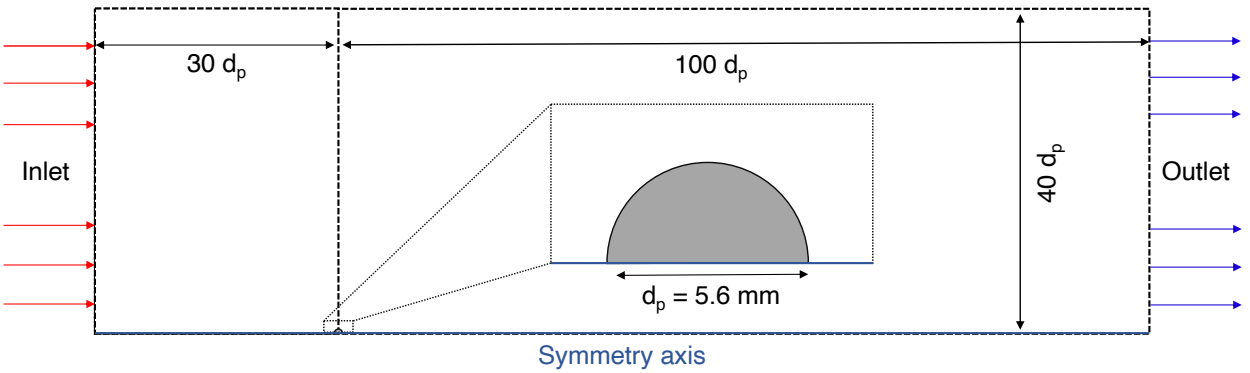

Figure 3.1: Schematics of 2D axisymmetric geometry.

Table 3.1: Porous characteristics of carbon char particle.

Parameter	Symbol	Value
Diameter	d_p	5.6 mm
Density	ρ	1532.8 kg $\cdot$ m^{-3}
Inertial resistance	C_2	1835.65 m^{-1}
Inverse of permeability	$\frac{1}{\alpha}$	6.47 $\cdot 10^6$ m^{-2}
Particle porosity	ε	0.5393
Specific surface area	S'''	8214.64 m^{-1}

The Reynolds numbers ($\mathrm{Re_{in}}$) selected for this study were 50, 75, and 100. The mathematical description is given in Equation 3.1, considering the superficial velocity ($\vec{u}_{\mathrm{in}}$), which was calculated using $\mathrm{Re_{in}}$, particle size (d_p), and physical characteristics of the incoming gas flow, i.e., density (ρ_{in}) and viscosity (μ_{in}).

$$\mathrm{Re_{in}} = \frac{\rho_{\mathrm{in}} |\vec{u}_{\mathrm{in}}| d_{\mathrm{p}}}{\mu_{\mathrm{in}}} \tag{3.1}$$

Carbon char gasification kinetics is modeled by implementing a six semi-global reactions scheme, with three heterogeneous reactions (Reactions R1 to R3) and three homogeneous reactions (Reactions R4 to R6) taking place in the porous (inside carbon char particle) and gaseous phase, respectively. Key reactions are R2 (Boudouard reaction), R4 (oxidation of carbon monoxide) and R5-R6 (Forward and reverse Water-gas shift, respectively). Kinetic parameters and reaction rates of both heterogeneous and homogeneous reactions were based on the Arrhenius law (See Equation 3.2). The kinetic parameters of the mechanism are given

in Table 2.1 [10, 35, 36]:

$$k = AT^{n_r} e^{-\frac{E_a}{RT}} \tag{3.2}$$

where A is the pre-exponential factor, E_a is the activation energy, k is the rate constant for reaction, n_r is the temperature exponent, R is the universal gas constant, and T is the temperature.

$$\begin{aligned}
\text{R1:} &\quad 2C_{(s)} + O_2 \longrightarrow 2CO \\
\text{R2:} &\quad C_{(s)} + CO_2 \longrightarrow 2CO \\
\text{R3:} &\quad C_{(s)} + H_2O \longrightarrow CO + H_2 \\
\text{R4:} &\quad CO + 0.5O_2 \xrightarrow{H_2O} CO_2 \\
\text{R5:} &\quad CO + H_2O \longrightarrow CO_2 + H_2 \\
\text{R6:} &\quad CO_2 + H_2 \longrightarrow CO + H_2O
\end{aligned}$$

3.3.2 Governing equations of pore-resolved approach

Next, we present a system of equations describing the heat and mass transfer inside and around the porous particle. One of the important limitations of that model in comparison to the work [24] is the neglecting of the mass transfer inside solid parts of particles representing porous structures. To proceed, equations 3.3 to 3.6 describe the mathematical conservation of mass, momentum, species, and energy for the PRS model [5, 20], taking into consideration the following assumptions:

1. The spherical carbon char particle structure is modeled using macro-pores only.
2. Drying and devolatilization are not included, due to the steady-state feature of the model.
3. Thermal equilibrium is assumed inside the particle for solid and gas phases.
4. The gas flow behaves as laminar and incompressible ($p = 10^5$ Pa) [37].
5. The buoyancy effect is neglected.

Conservation equation for mass transport:

$$\nabla \cdot (\rho \vec{u}) = 0 \tag{3.3}$$

Conservation equation for momentum transport:

$$\nabla \cdot (\rho \vec{u}\vec{u}) = -\nabla p + \nabla \cdot \overline{\overline{\tau}} \tag{3.4}$$

Conservation equation for species transport:

$$\nabla \cdot (\rho \vec{u} Y_i) = \nabla \cdot (\rho D_i \nabla Y_i) + R_i \tag{3.5}$$

Conservation equation for energy transport:

$$\nabla \cdot (\rho \vec{u} h) = \nabla \cdot (\lambda \nabla T) - \sum_i \frac{h_i^0}{M_i} R_i \tag{3.6}$$

where $\overline{\overline{\tau}} = \mu \left(\nabla \vec{u} + \nabla \vec{u}^{\mathrm{T}} \right)$ is the stress tensor. Regarding the PRS approach, Stefan flow has been considered, i.e., when the velocity is non-zero at chemically reacting surfaces, defining the net mass flux between the solid and gas phases [38, 39]. The mathematical description of the boundary conditions for chemically reacting surfaces has the form [40]:

$$\rho_{\mathrm{wall}} \, D_i \frac{\partial Y_{i,\,\mathrm{wall}}}{\partial n} - \dot{m}_C'' Y_{i,\,\mathrm{wall}} \; = M_i \widehat{R}_{i,s} \tag{3.7}$$

$$\dot{m}_C'' = \sum_{i=1}^{N_R} M_i \widehat{R}_{i,s} \tag{3.8}$$

$$\mathbf{n} \cdot \lambda \nabla T|_{\mathrm{gas}} \; = \sum_{j=1}^{N} M_i \widehat{R}_{i,s} h_j^0 + \epsilon_{\mathrm{s}} \sigma \left(T_{surf}^4 - T_{\mathrm{in}}^4 \right) \tag{3.9}$$

$$\mathbf{n} \cdot \vec{u} = \frac{\dot{m}_C''}{\rho} \tag{3.10}$$

where $\mathbf{n}$ is the normal vector to the wall, ϵ_{s} is the emissivity ($\epsilon_{\mathrm{s}} \approx 1.0$ for solid carbon), σ is

the Stefan-Boltzmann constant, $\widehat{R}_{i,s}$ is the production rate of species i due to heterogeneous reactions, $\dot{m}''_C$ is the net mass flux between surface and gas. The indexes $wall$ and $surf$ refer to the gas side at the wall and the surface inside the char particle, respectively. Due to the laminar regime ($\mathrm{Re_{in}} < 100$), and a low thermal diffusivity inside the solid fuel particle, the heat flux into the solid is neglected in Equation 3.9.

3.3.3 Governing equations of porous media approach

The following assumptions were applied to the 2D axisymmetric steady-state model for the set of all the conservation equations (Equations 3.11 to 3.14), describing the porous media model mathematically [34, 41]:

1. The single spherical carbon char particle is porous.
2. Drying and devolatilization are not considered.
3. The solid and gas phases inside the char particle are in thermal equilibrium.
4. The ambient gas phase is assumed to be isobaric with $p = 10^5$ Pa.
5. The gas flow is laminar, and the flow field is axisymmetric.
6. The intrinsic heterogeneous reaction rate constants are modeled using the surface-based reaction rate multiplied by the specific surface area [16, 34, 42].

Conservation equation for mass transport:

$$\nabla \cdot (\varepsilon \rho_g \vec{u}) = S_m \tag{3.11}$$

Conservation equation for momentum transport:

$$\nabla \cdot (\varepsilon \rho_g \vec{u}\vec{u}) = -\varepsilon \nabla p + \nabla \cdot (\varepsilon \overline{\overline{\tau}}) - \left(\frac{\varepsilon^2 \mu}{\alpha} \vec{u} + \frac{\varepsilon^3 C_2}{2} \rho_g |\vec{u}| \vec{u} \right) + S_m \vec{u} \tag{3.12}$$

Conservation equation for species transport:

$$\nabla \cdot (\varepsilon \rho_g \vec{u} Y_i) = \nabla \cdot (\varepsilon \rho_g D_{eff} \nabla Y_i) + \varepsilon R_i \tag{3.13}$$

Conservation equation for energy transport:

$$\nabla \cdot (\varepsilon \rho_g \vec{u} h_g) = \nabla \cdot (\lambda_{eff} \nabla T) - \sum_i \varepsilon \frac{h_i^0}{M_i} R_i \tag{3.14}$$

Species i is any reacting participant involved in the heterogeneous combustion process, i.e., H_2O, O_2, H_2, CO, CO_2, D_{eff} is the mass diffusion coefficient, λ is the thermal conductivity, h_i is enthalpy, h^0 is the enthalpy of formation, M_i is molecular weight, Y_i is mass fraction, R_i is the net production rate, and $\widehat{R}_{i,r}$ is the Arrhenius molar rate of creation/destruction for species i, respectively, which depends if the chemical reaction is heterogeneous ($R_i\left[\frac{\text{mol}}{\text{m}^2\cdot\text{s}}\right]$) or homogeneous ($R_i\left[\frac{\text{mol}}{\text{m}^3\cdot\text{s}}\right]$). The last two terms are described below, where $v''_{i,r}$ and $v'_{i,r}$ are the stoichiometric coefficients for reactants and products in the reaction r, $\eta'_{j,r}$ and $\eta''_{j,r}$ are the forward and backward rate exponents in the reaction r for each chemical species j.

$$R_i = M_i \sum_r \widehat{R}_{i,r} \tag{3.15}$$

$$\widehat{R}_{i,r} = \left(v''_{i,r} - v'_{i,r}\right) \left[k_r \prod_{j=1}^{N} C_{j,r}^{\left(\eta'_{j,r} - \eta''_{j,r}\right)} \right] \tag{3.16}$$

The source term incorporated in the continuity equation may be expressed as [43, 44]:

$$S_m = S''' \left(\rho_g \frac{2M_{\text{C}}}{M_{\text{O}_2}} k_{\text{R1}} Y_{\text{O}_2} + \rho_g \frac{M_{\text{C}}}{M_{\text{CO}_2}} k_{\text{R2}} Y_{\text{CO}_2} + \rho_g \frac{M_{\text{C}}}{M_{\text{H}_2O}} k_{\text{R3}} Y_{\text{H}_2O} \right) \tag{3.17}$$

The density of the gaseous mixture was calculated as stated by Equation 3.18. Viscosity and thermal conductivity were calculated using the kinetic theory [45].

$$\rho_g = \frac{P}{RT \sum_i \frac{Y_i}{M_i}} \tag{3.18}$$

Regarding the PMM approach, the porosity ($\varepsilon = 0.5393$) significantly influences the gaseous flow through the carbon char particle. The value of the porosity was calculated using the macro-pore geometry (PRS) for the carbon char particle, considering the volume of gas inside the particle and its total volume. To determine the pressure drop, the Blake-Kozeny equation may be used, as described in Equation 3.19 [46]. The permeability (α) and

inertial loss coefficient of flow (C_2) in the porous zone are described by Equation 3.20 and 3.21, respectively, where D_p was considered as 1% of the particle diameter [47].

$$\frac{|\Delta p|}{L} = \frac{150\mu}{D_p^2}\frac{(1-\varepsilon)^2}{\varepsilon^3}v_\infty \tag{3.19}$$

$$\alpha = \frac{D_p^2}{150}\frac{\varepsilon^3}{(1-\varepsilon)^2} \tag{3.20}$$

$$C_2 = \frac{3.5}{D_p}\frac{(1-\varepsilon)}{\varepsilon^3} \tag{3.21}$$

The effective diffusivity ($D_{m,i}^{eff}$) was calculated using user-defined-function (UDF) as follows:

$$D_{m,i}^{eff} = \frac{\varepsilon}{\tau}\frac{1-x_i}{\sum \frac{x_i}{D_{ij}}} \tag{3.22}$$

where ε is porosity; τ is tortuosity; x_i is molar fraction of i-th species; D_{ij} is binary diffusivity for $i-j$-th pair. D_{ij} is calculated from the Fuller correlation [47]:

$$D_{ij} = \frac{0.01013T^{1.75}}{pM^{0.5}\left(V_i^{1/3}+V_j^{1/3}\right)^2} \tag{3.23}$$

where $V_{i,j}$ - diffusion volume for i,j-th species [48], which may be found in Table 3.2. The thermal conductivity (λ_{eff}) inside the porous particle was calculated accordingly:

$$\lambda_{eff} = \varepsilon\lambda \tag{3.24}$$

Table 3.2: Diffusion volume (V_i) for gaseous species involved in kinetic scheme.

Species	Diffusion volume, V_i
Carbon dioxide (CO_2)	26.9
Carbon monoxide (CO)	18.9
Hydrogen (H_2)	7.07
Nitrogen (N_2)	17.9
Oxygen (O_2)	16.6
Water (H_2O)	12.7

3.3.4 Boundary conditions

The inlet boundary conditions are specified as Dirichlet conditions for inflow gas velocity, species mass fractions, and temperature, respectively:

$$\vec{u} = \vec{u}_{\text{in}}, \quad Y_i = Y_{i,\text{in}}, \quad T = T_{\text{in}} \tag{3.25}$$

At the symmetry axis as well as at the upper side of the domain, the following Neumann boundary conditions must be specified for the PMM approach:

$$\frac{\partial p}{\partial r} = 0, \quad \frac{\partial \vec{u}}{\partial r} = 0, \quad \frac{\partial Y_i}{\partial r} = 0, \quad \frac{\partial T}{\partial r} = 0 \tag{3.26}$$

Furthermore, the interaction between gaseous and solid phases on the surface of the carbon char particle affects the mass and energy balance at the interface. This impact is a result of heterogeneous chemical reactions (R1 to R3), influencing the production and destruction rates of gaseous species caused by these reactions along with convective and diffusive mass fluxes of the gas phase species at the surface of the particle [40]. A crucial parameter for heterogeneous chemical reactions is the specific surface area (S''') of the porous particle. In the literature, the normal value has the order of magnitude of 10^8 m^{-1} [34, 49]. In our work, the specific surface area was calculated taking into consideration the macro PRS model based on geometrical data, being $S''' = 8214.64$ m^{-1}, which was also used in the PMM approach when selecting porous zone with the reaction for the domain inside the carbon char particle. This is a lower value when compared to the literature since it is used for comparison between PMM and PRS approaches, and only macro pores are solved.

3.3.5 Numerics and validation

Simulations were carried out using the commercial software Ansys® Fluent 2022R2 [45], where Equations 3.3 to 3.6 were solved. The number of cells was 24610 and 63761 for the PMM and PRS, respectively. The mesh structure is shown in Figure 3.2 for both numerical approaches. In particular, Figure 3.2a and 3.2b depict the mesh of the PRS model, with and without considering the ten-layer solid mesh inside the particle White spaces represent solid

mesh inside the particle, the rest is occupied by the gas. Each macro-pore has a dimension of 0.14 mm, i.e., 2.5% of the particle diameter (d_p), while the space between macro-pores in the radial direction have a size of 0.084 mm (60% of each macro-pore). Specific surface area (S''') was used to consider wall-surface reactions in the porous zone. The solution technique adopted for coupling pressure and velocity was the semi-implicit method for pressure-linked equations (SIMPLE) [50]. The P-1 model [51] was used to incorporate radiation, given its significant role as a heat transfer mechanism within the fixed-bed reactor, particularly in the context of solid-to-gas radiation. A second-order upwind scheme was used to discretize convective, species, and energy terms. The under-relaxation factors were set at 0.5 for momentum, energy 0.8, and species 0.5, except for CO_2 (0.7) and O_2 (0.3), as the kinetic scheme involved in the process critically affects these species' conservation. Initialization values for carbon dioxide and carbon monoxide were 0.2 and 0.1, respectively. The iterative process was stopped upon achieving relative residuals of less than 10^{-6}, which required approximately 10^5 iterations until convergence for some of the cases under study. The software was validated both against analytical solutions [4] and experimental data [5, 7, 52]. Functions for effective diffusivity and thermal conductivity in the porous zone were implemented into the software through a user-defined-function (UDF), where the DEFINE macros of DEFINE_DIFFUSIVITY and DEFINE_PROPERTY were used, respectively.

3.4 Results and discussion

The simulations were conducted to test various inflow gas temperatures (T_{in}), particularly 1100, 1500 and 2000 K, oxygen concentration at the inlet of the reactor ($Y_{O_2,\text{in}} = 0.05$ and 0.11), and Reynolds numbers (Re_{in}) of 10, 50 and 100. The upcoming sections show the effect of each of these variables on the temperature and species profile along the reactor, also validating the use of a continuum model against a pore-resolved simulation setup assessing effective molecular diffusivity and tortuosity. In particular, for all PRS cases, 2D contour plots are depicted without considering the ten-layer solid mesh inside the particle.

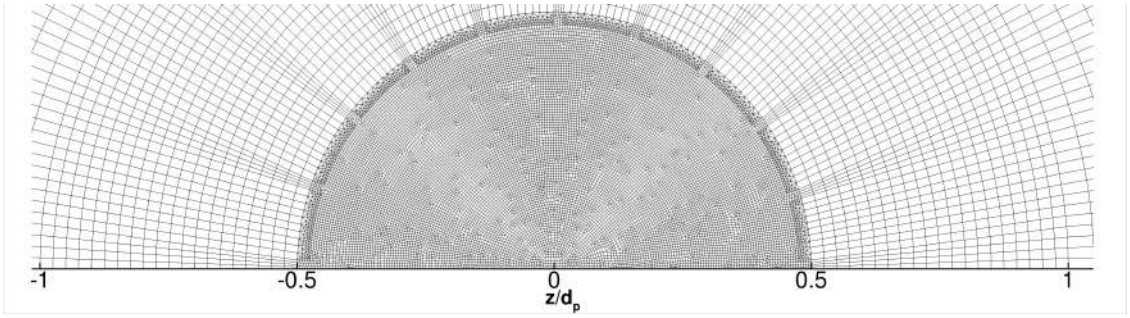

(a)

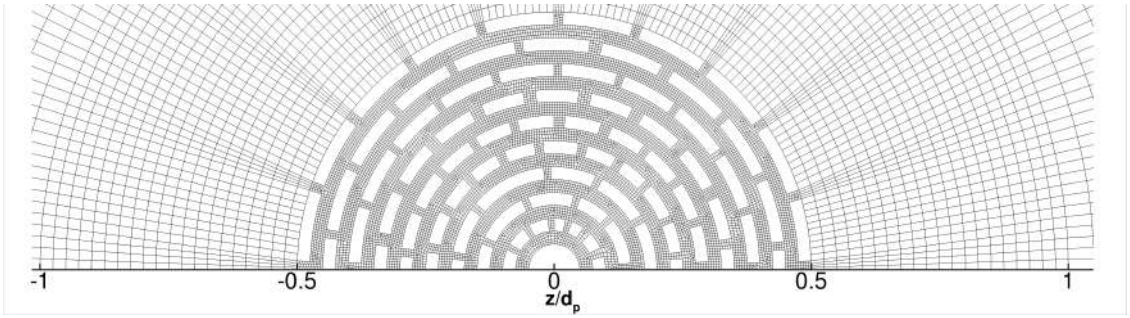

(b)

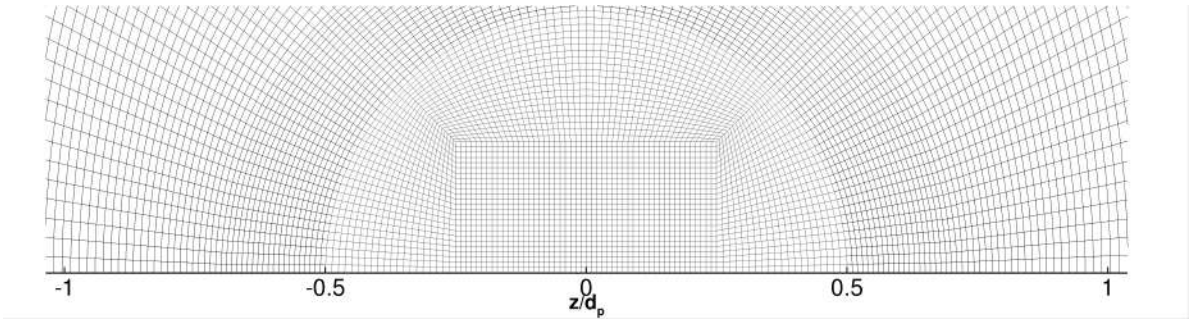

(c)

Figure 3.2: Mesh of carbon char particle for (a) PRS (including solid mesh), (b) PRS (without solid mesh), and (c) PMM.

3.4.1 Influence of Reynolds number and inflow gas temperature

In this research, several Reynolds numbers based on particle size ($\mathrm{Re_{in}} = 10, 50, 100$) were numerically studied. Figure 3.3 depicts the effect of the inflow gas temperature and Reynolds number on the volume-averaged species concentration and temperature inside the carbon char porous particle. At very high inlet temperatures, the capability of the porous media model to reproduce a pore-resolved simulation becomes more accurate. It can be observed how at low inflow gas temperatures ($T_{\mathrm{in}} = 1100$ K) results deviate considerably when comparing PRS and PMM model approaches. From the literature, it would be expected to have a sustained increase in the temperature (Figure 3.3a), and both hydrogen (Figure 3.3b) and carbon monoxide (Figure 3.3c) concentration inside the porous domain, which takes place in all the cases. Nevertheless, and certainly due to the effect of temperature, the mass fraction of CO_2 undergoes an important difference between PRS and PMM (See Figure 3.3d). A profile for oxygen is not reported since the volume-averaged value inside the particle is negligible. The influence of Reynolds number on the combustion efficiency of a coal char particle in a dry gas atmosphere is corroborated with the results of Higuera [53].

Furthermore, Figure 3.4 shows the species concentration profiles for oxygen, hydrogen, carbon monoxide and carbon dioxide ($\mathrm{Y_{O_2}}$, $\mathrm{Y_{H_2}}$, $\mathrm{Y_{CO}}$, and $\mathrm{Y_{CO_2}}$, respectively) near and inside the porous char particle both for pore-resolved simulations (See Figure 3.4a) and using the porous media model approach (See Figure 3.4b) for $\mathrm{Y_{O_2,in}} = 0.11$, $\mathrm{Re_{in}} = 10$ and $T_{\mathrm{in}} = 2000$ K. In particular, it could be observed how all the chemical species involved in the gasification of carbon char are consistent with the semi-global kinetic scheme but also between the two approaches under study. Moreover, a maximum value for the mass fraction of CO_2 of 0.171 and 0.168 for PRS and PMM models, respectively. This represents a slight difference of 1.54 %, which is not far from the other species, being the difference for maximum values of 1.38% and 1.28% for CO and H_2, respectively.

Figure 3.5a shows contour plots for temperature, which slightly differ inside the porous particle (deviation of 7.4% of PMM compared to PRS case). As a consequence of the achieved temperature, the concentration of CO_2 shows a similar behavior (See Figure 3.5b). The effect of carbon monoxide oxidation (R4) is considered dominant in this kinetic scheme, along with

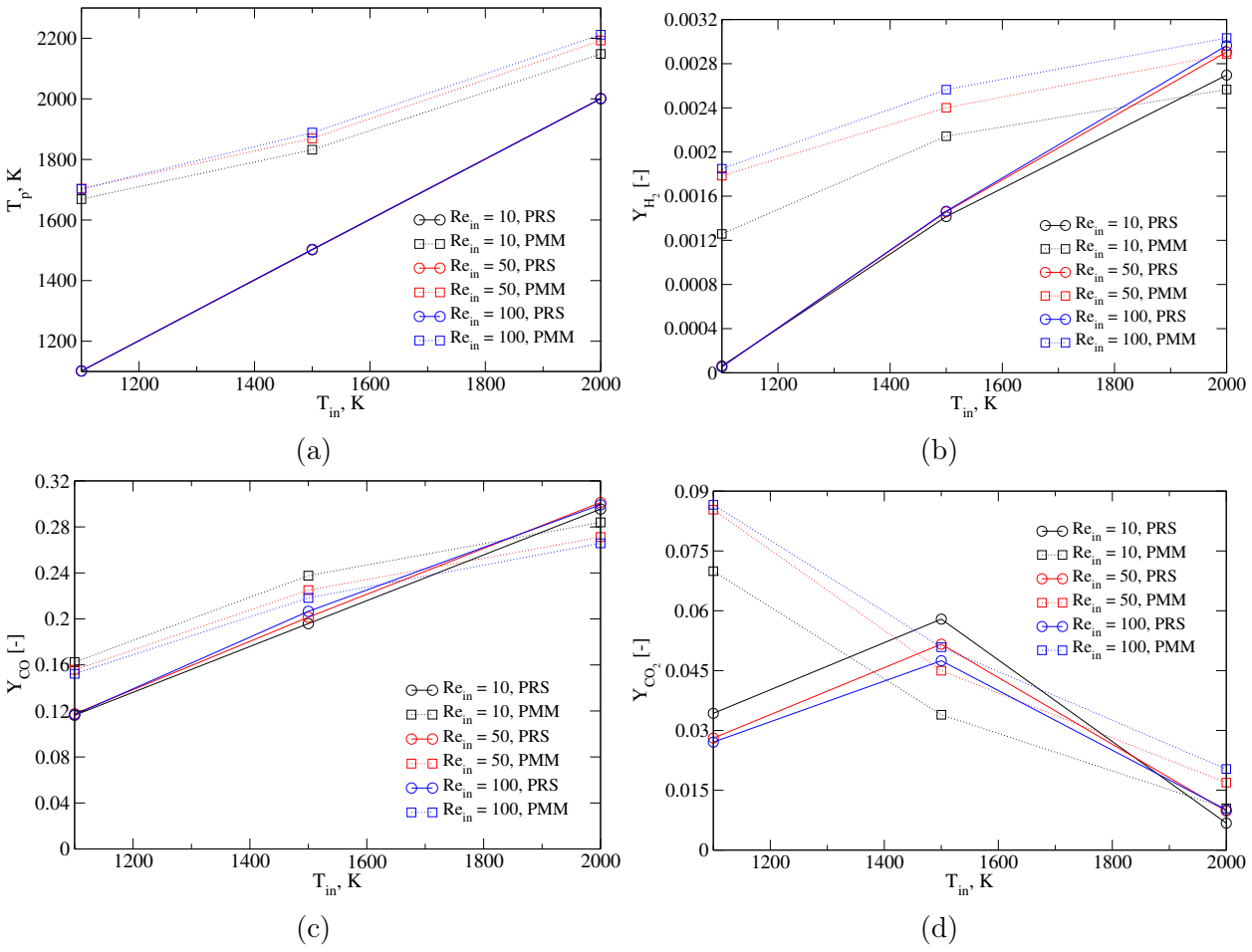

Figure 3.3: Volume-averaged (a) T_{p}, (b) $\mathrm{Y_{H_2}}$, (c) $\mathrm{Y_{CO}}$, and (d) $\mathrm{Y_{CO_2}}$ inside carbon char particle for $\mathrm{Y_{O_2,in}} = 0.11$ and $\mathrm{Re_{in}}$= 10, 50 and 100.

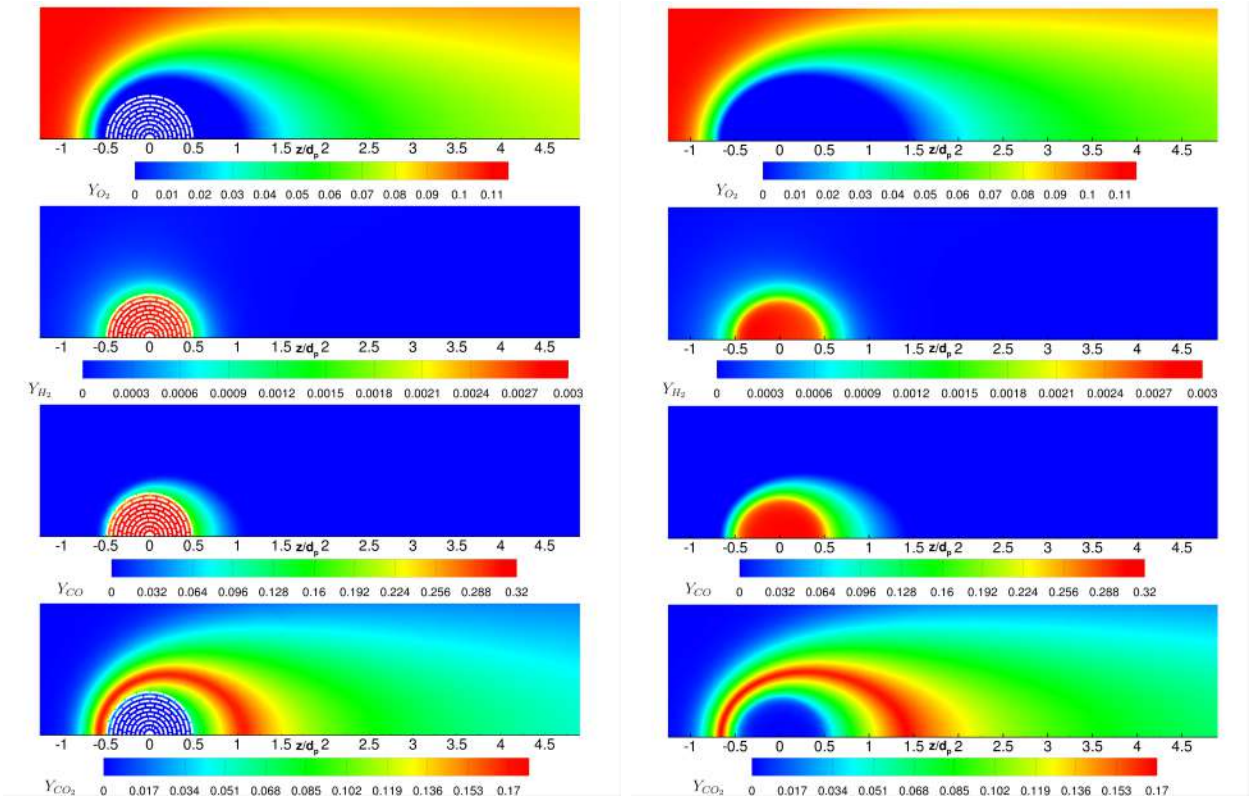

(a) (b)

Figure 3.4: Y_{O_2}, Y_{H_2}, Y_{CO}, and Y_{CO_2} for $Re_{in} = 10$, $T_{in} = 2000$ K, and $Y_{O_2,in} = 0.11$. (a) PRS and (b) PMM.

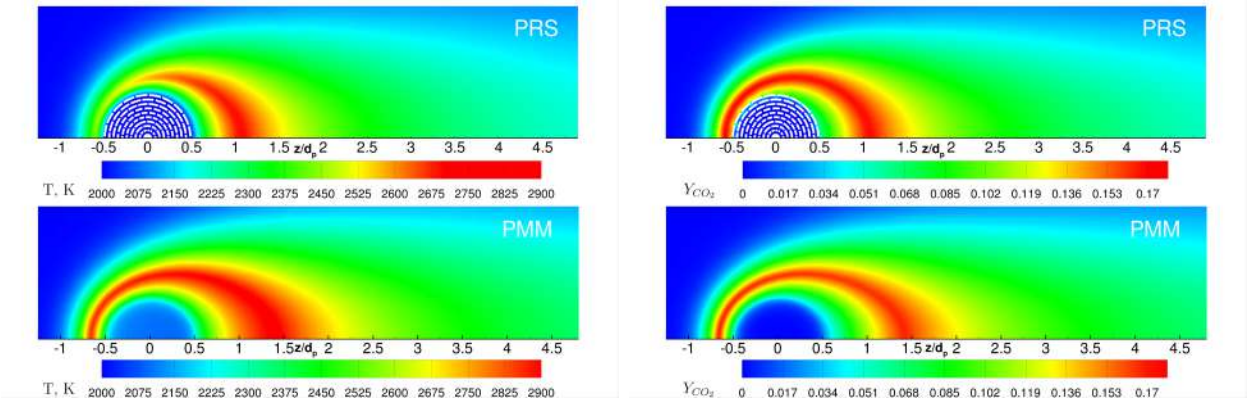

(a) (b)

Figure 3.5: (a) Temperature and (b) Y_{CO_2} inside and near the particle for $Re_{in} = 10$, $Y_{O_2,in} = 0.11$ and $T_{in} = 2000$ K.

the Boudouard reaction, as discussed in the literature [21].

Figure 3.6 shows the flow field surrounding the particle for the same case previously discussed ($Y_{O_2,in} = 0.11$, $Re_{in} = 10$ and $T_{in} = 2000$ K) for PRS (See Figure 3.6a) and PMM (See Figure 3.6b) approaches. Both the magnitude and direction of the velocity at these operating conditions present good agreement, confirming the effect of Stefan flow and the fixed geometry for the macro-PRS approach.

Figure 3.7 shows the influence of the inflow gas temperature on the mass fraction of carbon dioxide for both pore-resolved and porous media model approaches. It could be clearly observed in Figure 3.7a the effect of the inlet temperature as Y_{CO_2} increases with temperature, achieving maximum values of approximately 0.17 for an inflow gas temperature of 2000 K. Moreover, the highest concentration of CO_2 is observed at the surface of the particle and following the fluid dynamics of the system. It can be observed when comparing with Figure 3.7b how the concentration profile starts differing for a lower inflow gas temperature. In particular, for this case, the highest concentration of CO_2 for the porous media model is 0.0754, since for the PRS approach, this achieves a value of 0.050, representing a deviation of 50.2%. This behavior is systematic along the simulations, where the PMM approach fits better with increasing the inflow gas temperature and observing minimum differences, as discussed in the previous paragraphs.

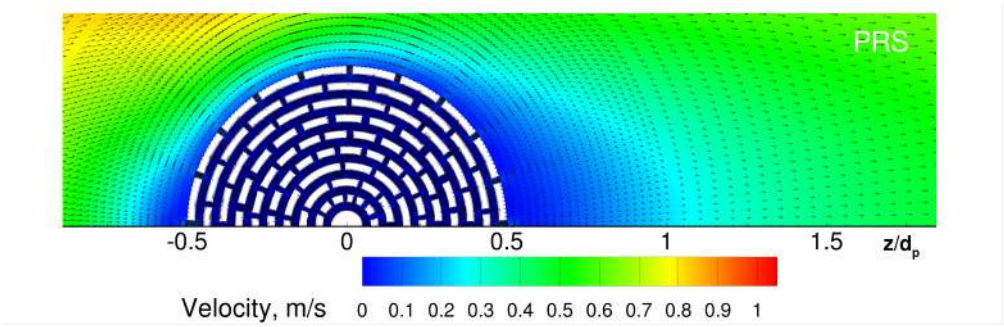

(a)

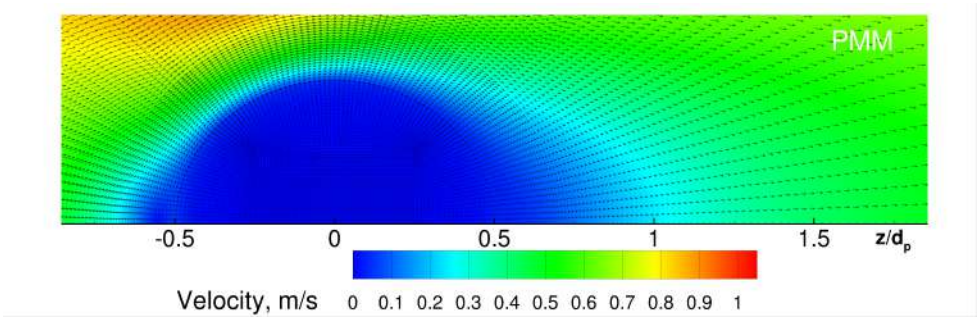

(b)

Figure 3.6: Flow field for velocity surrounding the particle using (a) PRS (without solid mesh), and (b) PMM.

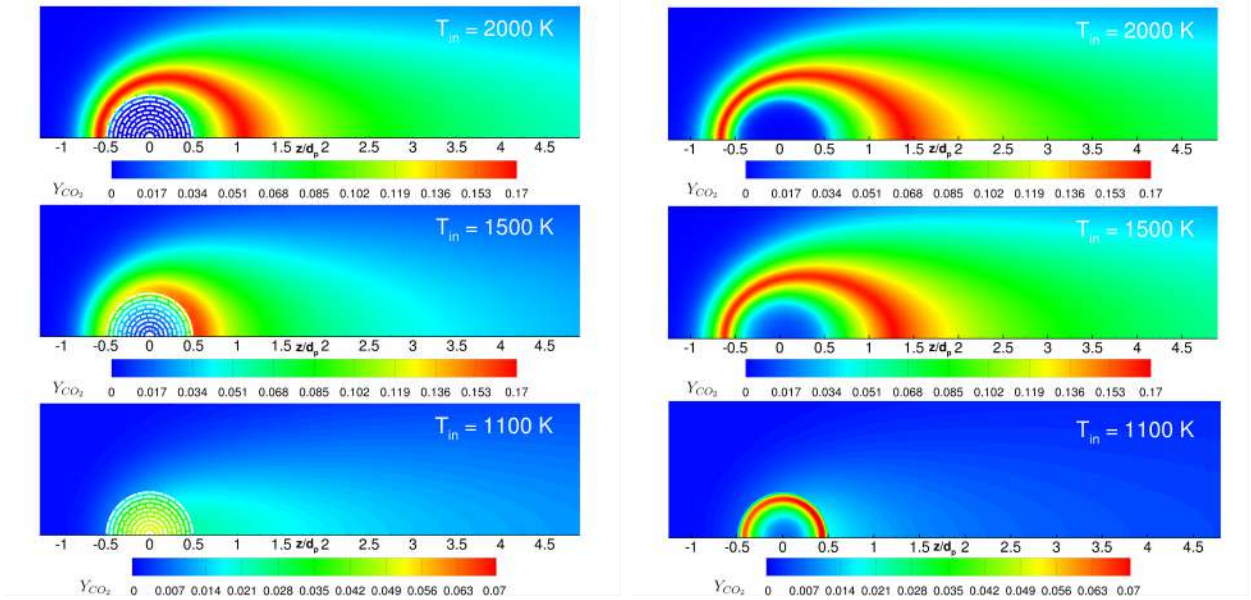

(a) (b)

Figure 3.7: Effect of inflow gas temperature on Y_{CO_2} for $Re_{in} = 10$, $Y_{O_2,in} = 0.11$. (a) PRS and (b) PMM.

3.4.2 Influence of oxygen concentration at inlet

Figure 3.8 shows the results for volume-averaged profiles for temperature (T_p), species concentration of hydrogen (Figure 3.8b), carbon monoxide (Figure 3.8c), carbon dioxide (Figure 3.8d), oxygen (Figure 3.8e), and surface/porous carbon mass flux inside the carbon char particle for Reynolds number of 100, varying the concentration of oxygen at the inlet of the reactor. In particular, two gasifying conditions were studied, i.e., $Y_{O_2,in} = 0.05$ and 0.11. It could be observed how the profiles are consistent for all the plots in terms of tendency following the semi-global kinetic scheme. In particular, the porous media model fits much better for $Y_{O_2,in} = 0.05$, observing higher deviation when the $Y_{O_2,in} = 0.11$, specially at low inflow gas temperatures. The particle size may have an important effect, considering the magnitude achieved for $\dot{m}''_C$, which gets higher for a smaller size of spherical particles [4] (See Figure 3.8f). Moreover, the oxidation regime is a crucial element to analyze for these results since at $T_{in} = 1100$ K, the regime could be identified as kinetically-controlled, for $T_{in} = 1500$ K a transition oxidation regime takes place, and finally for $T_{in} = 2000$ K, the diffusion-controlled regime is dominant [54]. It can also be observed the presence of external limitations of the kinetic scheme due to the elemental increase of the Reynolds number, which is consistent when assessing external Damköhler number. In particular, the higher the inflow gas temperature and particle diameter, the higher Damköhler number. In addition, the oxidative regimes can be identified when Damköhler number is higher than unity (diffusion-controlled regime) and lower than unity (kinetically-controlled regime) [4]. At a low inflow gas temperature ($T_{in} = 1100$ K), the chemical kinetic rate becomes slower than the diffusion rate. The diffusion resistance gets bigger for a large particle, such as the case under study ($d_p = 5.6$ mm). Thus, the PMM approach has significant differences when compared to PRS. It could also be observed the effect of a diffusion-controlled regime ($T_{in} = 2000$ K), where the mass transfer rate is negligible against kinetics, resulting in the absence of oxygen as volume-averaged calculation, even at the surface since it is immediately consumed by the carbon char particle.

This follows the same pattern described in previous sections, where at high values of T_{in} there is a better match for all the cases under study. As a matter of fact, it may be observed

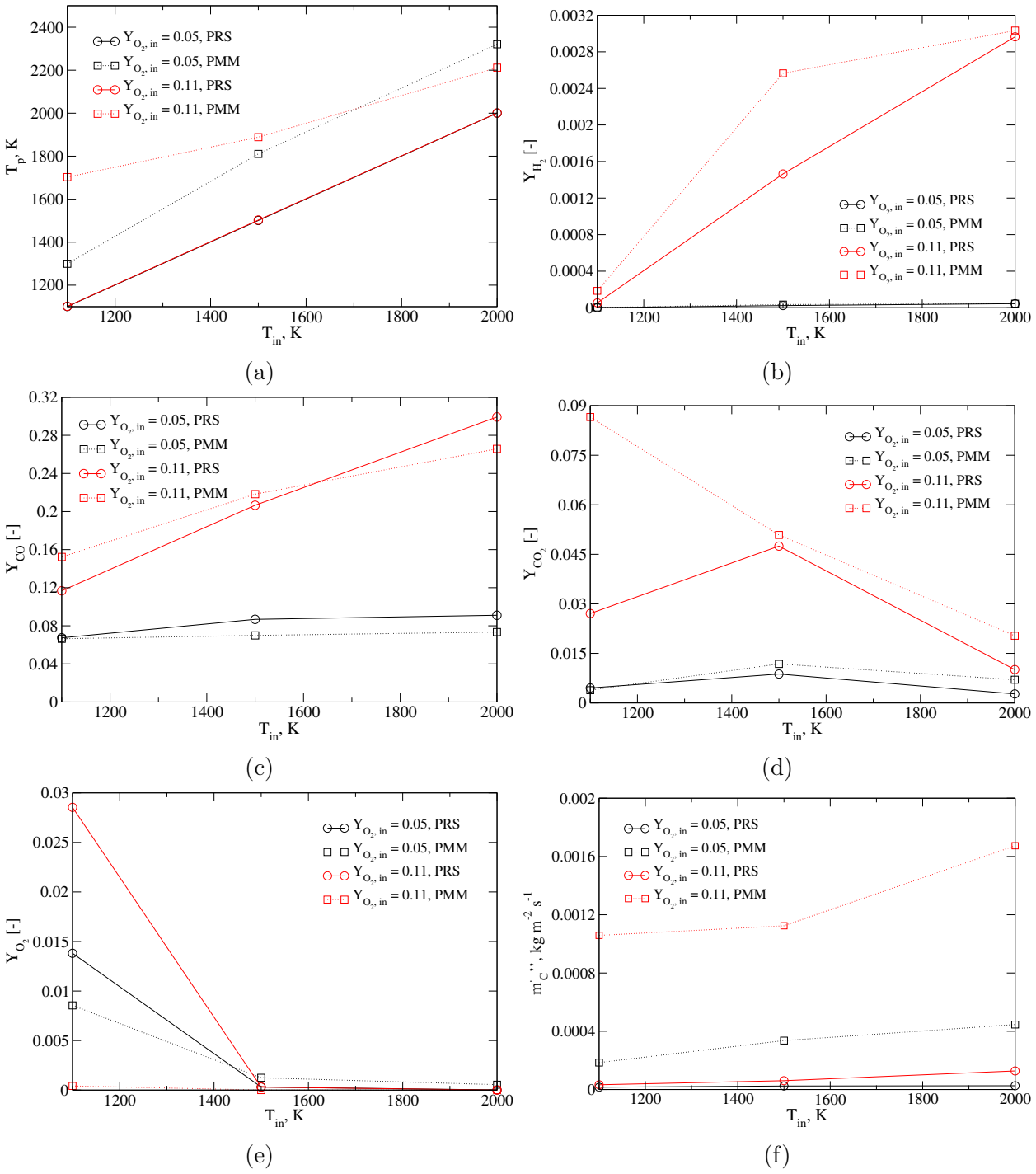

Figure 3.8: Volume-averaged (a) T_{p}, (b) $\mathrm{Y_{H_2}}$, (c) $\mathrm{Y_{CO}}$, and (d) $\mathrm{Y_{CO_2}}$, (e) $\mathrm{Y_{O_2}}$, and (f) Surface/porous carbon mass flux ($\dot{m}_C''$) inside carbon char particle for $\mathrm{Re_{in}} = 100$ and $\mathrm{Y_{O_2,in}}$ = 0.05 and 0.11.

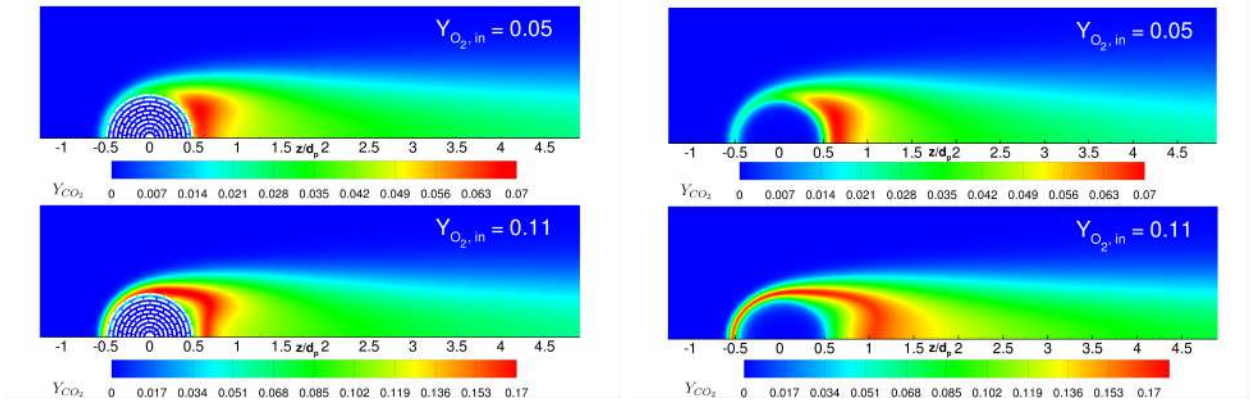

(a) (b)

Figure 3.9: Effect of $Y_{O_2,in}$ on Y_{CO_2} inside and near the particle for $Re_{in} = 100$ and $T_{in} = 2000$ K. (a) PRS and (b) PMM.

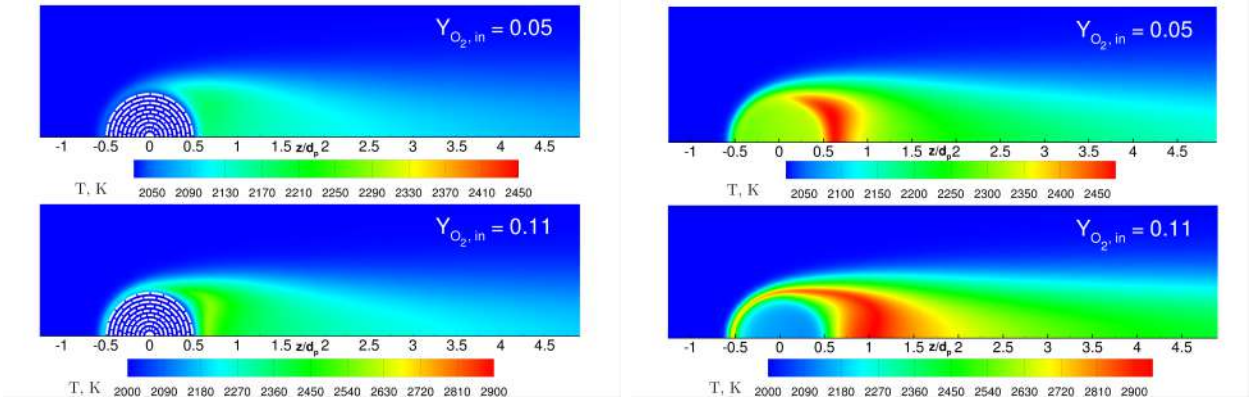

(a) (b)

Figure 3.10: Temperature inside and near the particle for $Re_{in} = 100$, $T_{in} = 2000$ K, and $Y_{O_2,in}$ 0.05 and 0.11. (a) PRS and (b) PMM.

this effect in the mass fraction of carbon dioxide (See Figure 3.9) and temperature (See Figure 3.10), where at high inflow gas temperature (e.g., $T_{in} = 2000$ K) the profiles present minimal differences when comparing PRS and PMM. For example, the maximum values of the mass fraction of all species deviate up to 9.81% (CO), observing slight differences for hydrogen (6.78%) and carbon dioxide (0.09%). Overall, considering all the aspects assessed in the previous sections, the PMM approach fits better with PRS for low oxygen mass fraction at the inlet of the domain and also for high inflow gas temperature, regardless of the Reynolds number, where the best results were found for $Re_{in} = 10$.

3.4.3 Influence of effective molecular diffusivity

The validation of a PMM approach against PRS has been discussed throughout the manuscript. To build the continuum model, the molecular diffusivity was a critical parameter to assess. As it can be observed in Equation 3.22, the effect of tortuosity (τ) might play a crucial role in the performance of PMM. Figure 3.11 shows the effect of tortuosity in both temperature and carbon dioxide profiles. In all the cases under study, the approach of $\tau = 1/\varepsilon$ was used. It can be observed how, when the value of tortuosity increases, the difference between the molecular diffusivity inside and outside the particle starts being higher, thus leading to a remarkable difference in the effect of τ on the kinetic scheme used for both numerical approaches. It can be observed how at $\tau = 50$, the mass fraction of CO_2 gets higher on the surface (See Figure 3.11b) since the molecular diffusivity inside the particle is 50 times less, leading to even a hotter temperature profile inside the porous zone (See Figure 3.11a). Results are showing evidence of the effect of Stefan flow inside the porous particle, which is a crucial element to take into account where heterogeneous chemical reactions occur since the non-zero velocity on the walls of pores might affect the mass transfer process drastically, enhancing a kinetic scheme depending on the Reynolds number as a second relevant variable. This could also be an object of study when tracking of porosity is assessed [16, 17, 34, 55, 56] through the Random Pore Model, where the specific surface area changes over time and conversion of the solid fuel. Moreover, the particle diameter used in this study could also be further assessed, considering that inflow gas temperature and velocity affect the performance of carbon char consumption when d_p changes [57].

3.5 Concluding remarks

In this investigation, the study focused on analyzing the heterogeneous combustion of a single spherical carbon char particle using a two-dimensional CFD-based approach under steady-state and laminar flow regime conditions. Critical parameters of $\mathrm{Re_{in}}$, $\mathrm{Y_{O_2,in}}$, and T_{in} were assessed. Based on the semi-global chemical kinetic scheme, the mass fraction of species ($\mathrm{Y_i}$) showed consistency when describing the thermal conversion process.

The effect of the inflow gas temperature on how the species concentration profile behaves

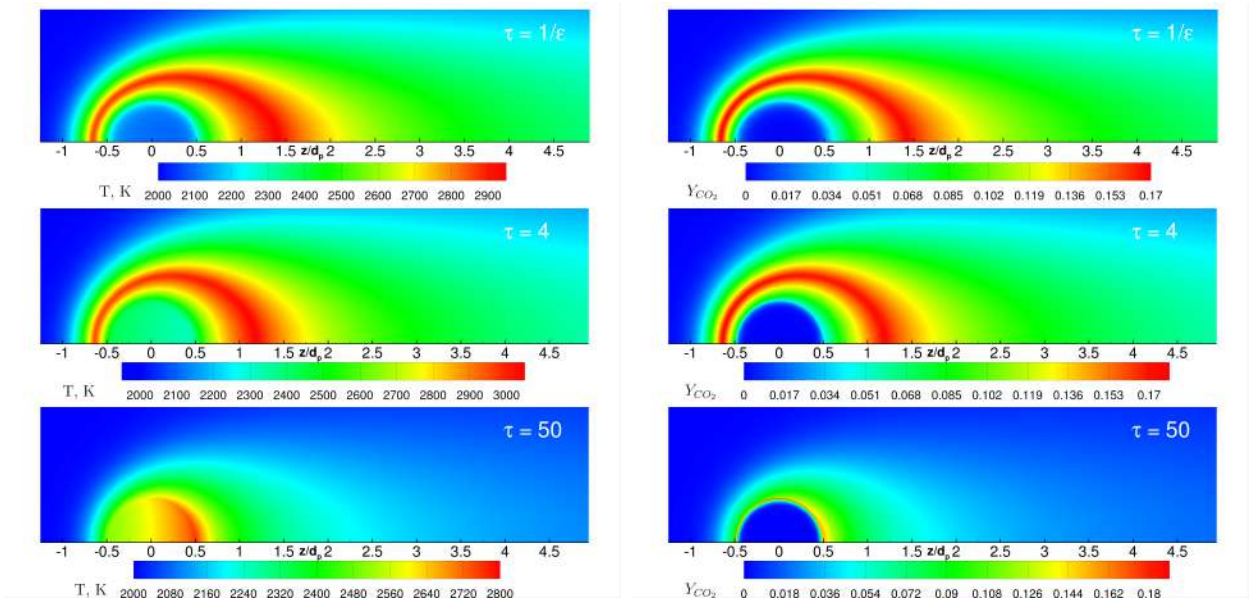

(a) (b)

Figure 3.11: Effect of tortuosity (τ) on (a) Temperature and (b) Y_{CO_2} inside and near the particle for $Re_{in} = 10$, $T_{in} = 2000$ K, and $Y_{O_2,in}$ 0.11.

was assessed, observing a better fit of PMM and PRS for high values of T_{in}. In particular, for $T_{in} = 2000$ K, the deviation in the values for species was not higher than 8.3% (Temperature profile). Maximum values for species concentration were slightly different when comparing both numerical approaches, achieving a maximum deviation of 1.54% for carbon dioxide. A higher deviation is found for lower inflow gas temperature since there is a relevant influence of this parameter on the kinetic scheme performance, considering the activation of these reactions from 1300 K. It could also be observed how PMM fitted better to PRS when $Y_{O_2,in}$ = 0.05, for all cases under study. The role of tortuosity was evaluated at a pore-level scale, observing the effect on the effective molecular diffusivity inside the porous zone, leading to remarkable differences between PRS and PMM at high values of τ.

This research shows the validation of a continuum model (PMM) against pore-resolved simulations (PRS) regarding the thermal and concentration of species profiles. Limitations of the porous media model to predict the heat and mass transfer in reacting particles compared to pore-resolved based models are shown, which are closer to reality. These findings underscore the significance of exploring further using other flow regimes, carbonaceous feedstocks, and boundary conditions. Further research is necessary to comprehensively analyze

a wider range of inflow gas temperatures and a more detailed chemical kinetics mechanism, including changing the carbonaceous solid fuel, tracking of porosity and particle radius, and the effect of intrinsic chemical reactions when escalating the phenomenon to a fixed-bed unit.

Acknowledgments

The authors would like to thank the National Agency for Research and Development (ANID) / Scholarship Program / DOCTORADO BECAS CHILE/2021 – 21211230, FONDECYT Project N°1241030, FONDAP SERC-Chile N°15110019, Project Ingeniería 2030 - P31 UTFSM, and the Natural Science and Engineering Research Council of Canada (NSERC) for their support.

References

[1] IEA International Energy Agency. Coal 2023 - analysis and forecast to 2026, 2023. URL `www.iea.org`.

[2] S. Schulze, M. Kestel, D. Safronov, and P. Nikrityuk. From detailed description of chemical reacting coal particles to subgrid models for CFD: Model development and validation. *Oil & Gas Science and Technology*, 68:1007–1026, 2013.

[3] V.S. Gururajan, T.F. Wall, R.P. Gupta, and J.S. Truelove. Mechanisms for the ignition of pulverized coal particles. *Combustion and Flame*, 81(2):119–132, 1990. ISSN 0010-2180.

[4] D. Safronov, M. Kestel, P. Nikrityuk, and B. Meyer. Particle resolved simulations of carbon oxidation in a laminar flow. *Canadian Journal of Chemical Engineering*, 92: 1669–1686, 10 2014. ISSN 1939019X.

[5] A. Richter, P. Nikrityuk, and M. Kestel. Numerical investigation of a chemically reacting carbon particle moving in a hot o2/co2 atmosphere. *Industrial and Engineering Chemistry Research*, 52:5815–5824, 4 2013. ISSN 08885885.

[6] Z. Zhang, Y. Zhong, Z. Zhao, L. Zhang, X. Li, X. Zha, C. Luo, and F. Wu. Numerical study on heterogeneous reaction characteristics of a single coal char particle under air- and oxy-fuel combustion: Effects of particle motion. *Fuel*, 320:123919, 7 2022. ISSN 00162361.

[7] P.A. Bejarano and Y.A. Levendis. Single-coal-particle combustion in o2/n2 and o2/co2 environments. *Combustion and Flame*, 153:270–287, 4 2008. ISSN 00102180.

[8] Z. Zhang, Z. Zhao, F. Wu, C. Luo, X. Li, Y. Chen, B. Lu, L. Zhang, and C. Zheng. Reaction behaviors of a single coal char particle affected by oxygen and steam under oxy-fuel combustion. *Fuel*, 291:120229, 5 2021. ISSN 00162361.

[9] C. Hasse, P. Debiagi, X. Wen, K. Hildebrandt, M. Vascellari, and T. Faravelli. Advanced modeling approaches for cfd simulations of coal combustion and gasification. *Progress in Energy and Combustion Science*, 86:100938, 9 2021. ISSN 03601285.

[10] P.A. Libby and T.R. Blake. Burning carbon particles in the presence of water vapor. *Combustion and Flame*, 41:123–147, 1981.

[11] J.C. Lee, R.A. Yetter, and F.L. Dryer. Transient numerical modeling of carbon particle ignition and oxidation. *Combustion and Flame*, 101:387–398, 1995.

[12] S.Y. Cho, R.A. Yetter, and F.L. Dryer. A computer model for one-dimensional mass and energy transport in and around chemically reacting particles, including complex gas-phase chemistry, multicomponent molecular diffusion, surface evaporation, and heterogeneous reaction. *Journal of Computational Physics*, 102:160–179, 1992.

[13] R. Stauch and U. Maas. Transient detailed numerical simulation of the combustion of carbon particles. *International Journal of Heat and Mass Transfer*, 52:4584–4591, 9 2009. ISSN 00179310.

[14] Y. Qian, Y. Yu, G. Xu, and X. Liu. Cfd modeling of coal pyrolysis in externally heated fixed-bed reactor. *Fuel*, 233:685–694, 12 2018. ISSN 00162361.

[15] Y. Qian, J. Zhan, Y. Yu, G. Xu, and X. Liu. Cfd model of coal pyrolysis in fixed bed reactor. *Chemical Engineering Science*, 200:1–11, 6 2019. ISSN 00092509.

[16] F. Dierich, A. Richter, and P. Nikrityuk. A fixed-grid model to track the interface and porosity of a chemically reacting moving char particle. *Chemical Engineering Science*, 175:296–305, 1 2018. ISSN 00092509.

[17] K. Wittig, P. Nikrityuk, S. Schulze, and A. Richter. Three-dimensional modeling of porosity development during the gasification of a char particle. *AIChE Journal*, 63: 1638–1647, 5 2017. ISSN 15475905.

[18] A. Richter, M. Kestel, and P.A. Nikrityuk. Pore-resolved simulation of char particle combustion/gasification. In P.A. Nikrityuk and B. Meyer, editors, *Gasification Processes: Modeling and Simulations*, pages 243–270. Wiley-VCH, Verlag GmbH & Co. KGaA, Weinheim, Germany, 2014.

[19] A. Richter, M. Vascellari, P. Nikrityuk, and C. Hasse. Detailed analysis of reacting particles in an entrained-flow gasifier. *Fuel Processing Technology*, 144:95–108, 4 2016. ISSN 03783820.

[20] C. Nguyen, J. Scherer, Q. Guo, S. Kriebitzsch, and A. Richter. The shape development of spherical and non-spherical char particles in the flame zone of an entrained-flow gasifier – a numerical study. *International Journal of Heat and Mass Transfer*, 149: 119220, 3 2020. ISSN 00179310.

[21] A. Arriagada, M. Toledo, R.E. Hayes, and P.A. Nikrityuk. 3d study of a chemically reacting fixed-bed under gasification conditions for non-porous char: Laminar flow. *Journal of the Energy Institute*, 112:101489, 2 2024. ISSN 17439671.

[22] M. Khatoonabadi, N. Prasianakis, and J. Mantzaras. A pore-level 3d lattice boltzmann simulation of mass transport and reaction in catalytic particles used for methane synthesis. *International Journal of Heat and Mass Transfer*, 221:125025, 2024.

[23] S.A. Hosseini and D. Thévenin. Toward pore-scale simulation of combustion in porous

media using a low-mach hybrid lattice boltzmann/finite-difference solver. *Physics of Fluids*, 35(6), 2023.

[24] G.H. Fong, S. Jorgensen, and S.L. Singer. Pore-resolving simulation of char particle gasification using micro-ct. *Fuel*, 224:752–763, 7 2018. ISSN 00162361.

[25] S. Liu, F. Xu, B. Lu, W. Wang, Z. Liu, and Y. Wang. Porous-media model based particle-resolved simulation of a fixed bed with olefin catalytic cracking reaction. *Powder Technology*, 431:119099, 1 2024. ISSN 1873328X.

[26] K. Wittig, A. Golia, and P.A. Nikrityuk. 3D numerical study of the influence of particle porosity on the heat and fluid flow. *Progress in Computational Fluid Dynamics*, 12: 207–19, 2012.

[27] K. Wittig, P.A. Nikrityuk, and A. Richter. Drag coefficient and nusselt number for porous particles under laminar flow conditions. *International Journal of Heat and Mass Transfer*, 112:1005–1016, 2017.

[28] M. Toledo and C. Rosales. Hybrid filtration combustion. In *Hydrogen Energy - Challenges and Perspectives*, pages 201–222. IntechOpen, London, United Kingdom, 2012. ISBN 978-953-51-0812-2.

[29] M. Toledo, A. Arriagada, N. Ripoll, E. Salgansky, and M. Mujeebu. Hydrogen and syngas production by hybrid filtration combustion: Progress and challenges. *Renewable and Sustainable Energy Reviews*, 177:113213, 5 2023. ISSN 18790690.

[30] M.A. Mujeebu, M.Z. Abdullah, A.A. Mohamad, and M.Z. Abu Bakar. Trends in modeling of porous media combustion. *Progress in Energy and Combustion Science*, 36: 627–650, 2010. ISSN 03601285.

[31] M.A. Mujeebu, M.Z. Abdullah, M.Z. Abu Bakar, A.A. Mohamad, R.M.N. Muhad, and M.K. Abdullah. Combustion in porous media and its applications - a comprehensive survey. *Journal of Environmental Management*, 90:2287–2312, 2009. ISSN 03014797.

[32] J. A. Ruiz, M. C. Juárez, M. P. Morales, P. Muñoz, and M. A. Mendívil. Biomass gasification for electricity generation: Review of current technology barriers. *Renewable and Sustainable Energy Reviews*, 18:174–183, 2013. ISSN 13640321.

[33] R. Luque and J.G. Speight. *Gasification for Synthetic Fuel Production: Fundamentals, Processes and Applications*. Woodhead Publishing Series in Energy, 2015. ISBN 978-0-85709-802-3.

[34] C. Nguyen, J. Scherer, M. Hartwich, and A. Richter. The morphology evolution of char particles during conversion processes. *Combustion and Flame*, 226:117–128, 4 2021. ISSN 15562921.

[35] S.R. Turns. *An Introduction to Combustion: Concepts and Applications*. McGraw-Hill, New York City, USA, 2006. ISBN 9780072350449.

[36] W.P. Jones and R.P. Lindstedt. Global reaction schemes for hydrocarbon combustion. *Combustion and Flame*, 73(3):233–249, 1988.

[37] A.G. Tomboulides, J. Lee, and S.A. Orszag. Numerical simulation of low mach number reactive flows. *Journal of Scientific Computing*, 12:139–167, 1997.

[38] P.A. Nikrityuk, M. Gräbner, M. Kestel, and B. Meyer. Numerical study of the influence of heterogeneous kinetics on the carbon consumption by oxidation of a single coal particle. *Fuel*, 114:88–98, 2013. ISSN 0016-2361. Advances in Coal Science and Technology, ICCS&T 2011.

[39] J. Yu, K. Zhou, and W. Ou. Effects of stefan flow and co oxidation on char particle combustion in o2/co2 atmosphere. *Fuel*, 106:576–585, 2013. ISSN 00162361.

[40] R.J. Kee, M.E. Coltrin, and P. Glarborg. *Chemically Reacting Flow: Theory and Practice*. John Wiley & Sons, 2005. ISBN 9780471461302.

[41] S. Kriebitzsch and A. Richter. Les simulation of char particle gasification at reynolds numbers up to 1000. *Combustion and Flame*, 211:185–194, 1 2020. ISSN 15562921.

[42] Q. Xu, S. Pang, and T. Levi. Reaction kinetics and producer gas compositions of steam gasification of coal and biomass blend chars, part 2: Mathematical modelling and model validation. *Chemical Engineering Science*, 66:2232–2240, 5 2011. ISSN 00092509.

[43] A. Arriagada-Romero, M. Toledo, R.E. Hayes, D. Pashchenko, and P.A. Nikrityuk. Verification of a porous media model for the partial oxidation of a chemically reacting fixed-bed. *Fuel*, 375:132582, 2024.

[44] P. Nikrityuk and B. Meyer. Unsteady char gasification/combustion. In *Gasification Processes: Modeling and Simulation*, pages 143–171. Willey-VCH Verlag GmbH & Co, Weinheim, Germany, 9 2014. ISBN 9783527335503.

[45] Inc. ANSYS. ANSYS-FLUENT™ V 2022R2 – Commercially available CFD software package based on the Finite Volume method. Southpointe, 275 Technology Drive, Canonsburg, PA 15317, U.S.A., 2022.

[46] S. Ergun. Fluid flow through packed columns. *Chemical Engineering Progress*, 48(2): 89–94, 1952.

[47] R.E. Hayes and J.P. Mmbaga. *Introduction to Chemical Reactor Analysis*. CRC Press, Taylor & Francis Group, Boca Raton, Florida, 2nd. edition, 2012. ISBN 9780429071515.

[48] E. Fuller, P. Schettler, and J. Giddings. New method for prediction of binary gas-phase diffusion coefficients. *Industrial & Engineering Chemistry*, 58(5):18–27, 1966.

[49] G.S. Liu, H.R. Rezaei, J.A. Lucas, D.J. Harris, and T.F. Wall. Modelling of a pressurised entrained flow coal gasifier: the effect of reaction kinetics and char structure. *Fuel*, 79 (14):1767–1779, 2000.

[50] S.V. Patankar. *Numerical heat transfer and fluid flow*. Series on Computational Methods in Mechanics and Thermal Science. Hemisphere Publishing Corporation (CRC Press, Taylor & Francis Group), Florida, USA, 1980. ISBN 978-0891165224.

[51] G. Krishnamoorthy, R. Rawat, and P. Smith. Parallelization of the p-1 radiation model. *Numerical Heat Transfer, Part B: Fundamentals*, 49:1–17, 1 2006. ISSN 10407790.

[52] S. Schulze, P. Nikrityuk, F. Compart, A. Richter, and B. Meyer. Particle-resolved numerical study of char conversion processes in packed beds. *Fuel*, 207:655–662, 2017. ISSN 00162361.

[53] F. J. Higuera. Combustion of a coal char particle in a stream of dry gas. *Combustion and Flame*, 152:230–244, 1 2008. ISSN 00102180.

[54] P. Nikrityuk and B. Meyer. Pseudo-steady-state approach for carbon particle combustion/gasification. In *Gasification Processes: Modeling and Simulation*, pages 205–244. Willey-VCH Verlag GmbH & Co, Weinheim, Germany, 9 2014. ISBN 9783527335503.

[55] S.K. Bhatia and D.D. Perlmutter. A rondom pore model for fluid-solid reactions: I. isothermal, kinetic control. *AlChE Journal*, 26:379–386, 1980.

[56] S.K. Bhatia and D.D. Perlmutter. A random pore model for fluid-solid reactions : Ii. diffusion and transport effects. *AlChE Journal*, 27:247–254, 1981.

[57] F. Yi, J. Fan, D.Li, S. Lu, and K. Luo. Three-dimensional time-dependent numerical simulation of a quiescent carbon combustion in air. *Fuel*, 90:1522–1528, 4 2011. ISSN 00162361.

Chapter 4

Verification of a porous media model for the partial oxidation of a chemically reacting fixed bed[*]

[*]This chapter is a facsimile of the research article published in A. Arriagada, M. Toledo, R.E. Hayes, D. Paschenko and P. Nikrityuk, Fuel, **2024**.

4.1 Abstract

In this work, two numerical approaches, namely particle-resolved simulations (3D PRS) and porous media model (PMM), are assessed using a 2D axisymmetric CFD pseudo-state approach (PSS) for validation of the gasification of carbon char particles in a chemically reacting fixed-bed. Simulations are performed using the commercial software Ansys® Fluent, implementing a six-reaction semi-global scheme, including three heterogeneous, and three homogeneous chemical reactions. The effects of the inflow gas temperature (T_{in}= 900-1500 K), mass fraction of oxygen ($Y_{O_2,\text{in}}$= 0.05, 0.11), and laminar flow regime (Re_{in} = 50, 75 and 100) reveals a significant role of T_{in}, observing important deviations at T_{in} = 1300 K. Minimum deviations when comparing 3D PRS and 2D PMM models are observed for $Y_{O_2,\text{in}}$ = 0.05, being 3.6% for CO, 5.5% for CO_2 and 0.76% for temperature inside the porous zone at different operating conditions. Thermal conductivity of the solid material, axial dispersion coefficient, and radial variation of porosity are analysed and discussed, showing good agreement between numerical models, remarking the role of geometrical features of the unit in the gasification process.

Keywords: Fixed-bed reactor, Gasification, Particle-resolved simulation, Porosity, Porous media model.

Nomenclature

Roman Symbols	Definition	Greek Symbols	Definition
A	Pre-exponential factor	ϵ	Emissivity
C	Concentration, $\text{kmol} \cdot \text{m}^{-3}$	ε	Porosity
D	Mass diffusion coefficient, $\text{m}^2 \cdot \text{s}^{-1}$	λ	Thermal conductivity, $\text{W} \cdot \text{m}^{-1} \cdot \text{K}^{-1}$
d	Diameter, m	μ	Viscosity, $\text{Pa} \cdot \text{s}$
E_a	Activation energy, $\text{J} \cdot \text{mol}^{-1}$	ρ	Density, $\text{kg} \cdot \text{m}^{-3}$
h	Enthalpy, $\text{J} \cdot \text{kg}^{-1}$	τ	Stress tensor, Pa
k	Reaction rate constant	**Abbreviations**	**Definition**
L	Length, m	CFD	Computational fluid dynamics
M	Molecular weight, $\text{kg} \cdot \text{mol}^{-1}$	FC	Filtration combustion
$\dot{m}''$	Net mass flux gas-surface, $\text{kg} \cdot \text{m}^{-2} \cdot \text{s}^{-1}$	PMM	Porous media model
N	Number	PRS	Particle-resolved simulation
p	Pressure, Pa	**Subscripts**	**Definition**
R	Universal gas constant, $\text{J} \cdot \text{mol}^{-1} \cdot \text{K}^{-1}$	C	Carbon char particle
$\widehat{R}$	Production rate, $\text{mol} \cdot \text{m}^{-2} \cdot \text{s}^{-1}$	i	species i
Re	Reynolds number	in	Inlet
S'''	Specific surface area, m^{-1}	p	Particle
T	Temperature, K	pz	Porous zone
$\vec{u}$	Velocity, $\text{m} \cdot \text{s}^{-1}$	R	Reaction
Y	Mass fraction	t	Tube

4.2 Introduction

Filtration combustion (FC) is the process where an oxidant stream flows through a porous media reactor composed of a solid inert/fuel material, involving exothermic chemical transformations [1], for example, in the gasification of carbonaceous materials in fixed-bed configuration [2]. These units have been widely studied since their multiphase and multiscale modeling for applications such as steam methane reforming (SMR) for hydrogen production and energy storage [3, 4], catalytic combustion [5] and pyrolysis [6], among others, are key for the chemical industry, and specially challenging from a numerical perspective [7]. In particular, for the thermochemical conversion of solid fuels, the thermogravimetric analysis (TGA) has shown similar kinetic modeling of thermochemical processes [8], with applications of coal char gasification [9] and sawdust and coal blend pyrolysis [10]. The heterogeneous interaction between different phases, most likely solid and gas, leads to a transient approach to the excess of enthalpy theory [11]. The theory is based on the intensified radiation heat

transfer mechanism when the inflow gas mixture meets the combustion zone, taking advantage of the high radiant emissivity of the solid fuel. Thus, the combustion temperature may exceed the theoretical adiabatic temperature rise since there is a preheating zone in the inlet section of the unit. There are several experimental studies in this field that have used different fuel/oxidant mixtures, such as methane, air, and oxygen, among others [12]. Filtration combustion may be extended to inert porous media combustion when there are non-chemically reacting particles inside of the reactor [13], e.g., alumina spheres, or to hybrid filtration combustion (HFC), when fuel and inert solid particles coexist inside the bed. Under this configuration, that might be described as the combination of inert porous media combustion and chemically reacting fixed-bed phenomena, both heterogeneous and homogeneous chemical reactions achieve high temperatures in the range of 900-2300 K, observing better performance for H_2 and syngas at temperatures up to 1800 K [14]. Salgansky et al. [15] studied the gasification of a solid fuel using a vapor-air mixture as an oxidant agent in a filtration mode, and assessed the length of the reactor and the relevance of thermodynamics in the mathematical calculations for gasification efficiency. Later, a superadiabatic regime due to filtration combustion was evaluated for a carbon-inert bed. Agreement was observed between theory and experiments by assessing the temperature of the filtration wave, composition of gaseous products, and yield of carbon monoxide and hydrogen [16].

Several studies have been carried out on the oxidation of carbon from a numerical perspective using a single spherical particle. In particular, studies have explored the steady-state combustion of a coal particle [17], the oxidation of a single moving particle under laminar regime conditions [18], and the consumption rate of carbon based on the effect of critical parameters such as inlet velocity, composition, and temperature [19]. using a detailed model in which surface oxidation and volatilization of the coal particle were included. It has been found in the literature a strong relationship between the particle Reynolds number (Re_{in}) and oxidation regimes related to species transport to the particle's surface. Nevertheless, for a chemically reacting porous medium, and to the best of the author's knowledge, research regarding the applicability of a porous media model and its validation against a three-dimensional CFD particle resolved numerical approach is scarce. On the other hand, the heterogeneous combustion phenomenon has been identified as a challenge specifically to

char since an important amount of physical processes are taking place on the surface of the particles, being widely studied for approximately a hundred years now [20]. Furthermore, numerical simulations for studying carbon thermochemical conversion have been reported in the literature in the past decades [21–26]. Libby and Blake [21] studied the effect of water vapor on the carbon consumption in a hot ambient, while Lee et al. [22] and Cho et al. [23] explored the interactions between heterogeneous chemical reactions, mass and energy transport in and around chemically reacting particles. Interesting findings relate to the relationship between burning rate and oxygen concentration at the inlet of the reactor [24]. Furthermore, for the thermochemical conversion at low concentration of oxygen in a fixed-bed reactor, radiation has been identified as the dominant heat transfer mechanism, highlighting the relevance of heterogeneous reactions and the phase change of water along the process [25, 26]. Most recently, a hybrid particle model has been developed to assess the char conversion process, considering the effect of pore diffusion on the carbon consumption rate inside gasifiers [27]. Moreover, carbon char thermochemical conversion has been studied in a fixed-bed gasifier using surface-based reactions [28] using a 3D particle-resolved simulation (PRS) approach, which will be the baseline of future analysis in this present article.

Separately, it should be noted that a comparative study between the so-called 3D particle resolved (PR) CFD-based model and the porous media based model has been presented by Dixon [4]. The study involved conducting 3D CFD-based PR simulation, comparing local heat and mass transport characteristics, and assessing reaction rates in a fixed-bed reactor tube referring to endothermic steam methane reforming. Vardhan Reddy Kuncharam & Dixon [29] presented a new multi-scale non-isothermal heterogeneous steady-state model for steam methane reforming in a packed-bed tube. The model is based on a porous media approach where two-dimensional transport equations describing the heat and mass transfer in the gas phase are directly coupled with the chemical reactions (including the heat and mass transfer) inside the catalyst particle. The results of a sensitivity analysis studying different closure relations (empirical equations) were discussed. The simulations were conducted on a 10 m long packed tube.

The novelty of this work consists of performing numerical studies of the intraparticle heat and mass transfer in a chemically reacting fixed-bed, where numerical models are based

on the so-called particle-resolved (3D PRS) and porous media (2D PMM) approach CFD simulations. The use of a PMM approach, which is computationally suitable for modeling a large number of porous particles (200-300 particles normally used in experiments), is necessary to validate and could potentially enable the use of the PMM approach in particle-resolved fixed-bed units with porous particles [30, 31]. Thus, the effects of different flow regimes, inflow gas temperature, ambient conditions, thermal conductivity of the solid phase, dispersion coefficient and porosity variation over radius on the gasification process and a thorough comparison between 2D and 3D domains must be assessed.

4.3 Model Formulation

4.3.1 Problem description

The model was formulated to simulate the filtration combustion of air over a carbon char packed-bed under a laminar flow regime. Figure 4.1 depicts the geometry and mesh used for all simulations. A 2D continuum numerical approach was used within the porous media model module available in the commercial software Ansys® Fluent. The domain is divided into three cell zones, i.e., inflow, porous (blue color in Figure 4.1b), and outflow zones, where the latter is added to obtain a steady-state and stable converged solution. The continuum model is the physical representation of a volume where solid and gaseous phases coexist. This space can be characterized by a porosity (ε), which elementally indicates the void fraction, i.e., the available volume where the oxidant mixture flows through. For further calculations, the bulk bed porosity was calculated as follows [32]:

$$\varepsilon = 1 - \frac{N_p \cdot \frac{1}{6}\pi d_p^3}{\frac{1}{4}\pi d_t^2 L_t} \tag{4.1}$$

where ε is the bed bulk porosity, N_p is the number of particles, d_p is diameter of particles, d_t and L_t are the diameter and the length of the tube, respectively. Parameters used in this study for the porous zone of the reactor are given in Table 4.1. The diameter of particles inside the packed-bed (d_p) was set to 5.6 mm, following experimental data found in the literature for porous media combustion [12, 13] and HFC technologies [14, 33]. The inflow

gas consisted of several mass fractions of O_2 ($Y_{O_2,in}$ = 0.05 and 0.11), 0.001 mass fraction of H_2O (nearly dry air), the rest is nitrogen ($Y_{N_2} = 1 - \sum_i Y_i$). The inflow gas temperature (T_{in}) was variable in the range of 900-1500 K, taking the temperature requirements ($\sim$ 1100 K) for achieving thermal conversion of coal in the presence of an oxidant mixture/gasifying agent [34–37]. For the particular application of producing H_2/syngas from carbon-based feedstocks using HFC, a temperature range of 900-1800 K can be achieved at different scenarios (Equivalence ratio, filtration velocity) due to the enhanced heat transfer mechanisms within the reactor [38, 39]. The particle Reynolds number (Re_{in}) was defined using Equation 4.2, considering the superficial velocity ($\vec{u}_{in}$), which was calculated using Re_{in}, particle size (d_p), density (ρ_{in}) and viscosity (μ_{in}). Re_{in} of 50, 75, and 100 were tested in this study.

$$Re_{in} = \frac{\rho_{in}|\vec{u}_{in}|d_p}{\mu_{in}} \tag{4.2}$$

The chemical kinetics mechanism uses a semi-global scheme consisting of six reactions, with three heterogeneous occurring in the porous phase (Reactions R1 to R3) and three homogeneous in the gaseous phase (Reactions R4 to R6). Specifically, R2 refers to the Boudouard reaction, R4 characterizes the oxidation of carbon monoxide (CO) with water serving as a catalyst species, and R5 and R6 represent the forward and backward water-gas shift (WGS) reactions, respectively. Reaction mechanism, kinetic parameters and reaction rates of both heterogeneous and homogeneous reactions were based on the extended Arrhenius law, mathematically described by Equation 4.3, and listed in Table 4.2 [21, 40, 41]:

$$k = AT^{n_r}e^{-\frac{E_a}{RT}} \tag{4.3}$$

where k is the rate constant for reaction, A is the pre-exponential factor, E_a is the activation energy, R is the universal gas constant, T is the temperature, and n_r is the temperature exponent.

Table 4.1: Porous zone characteristics and dimensions.

Parameter	Symbol	Value
Bed porosity	ε	0.5063
Inertial resistance	C_2	2378.113 m^{-1}
Inverse of permeability	$\frac{1}{\kappa}$	$8.985 \cdot 10^6$ m^{-2}
Number of particles	N_p	85
Particle diameter	d_p	5.6 mm
Tube diameter	d_t	21.2 mm
Tube length	L_t	45 mm

Table 4.2: Reaction mechanism, reaction rates and kinetics parameters for char gasification.

Equation	Reaction	R_i	A	$E_a\left[\frac{\mathrm{J}}{\mathrm{mol}}\right]$	n_r
R1	$2C_{(s)} + O_2 \longrightarrow 2CO$	$k_{r,O_2} C_{O_2}, s$	$1.5 \cdot 10^5$	$1.494 \cdot 10^5$	0
R2	$C_{(s)} + CO_2 \longrightarrow 2CO$	$k_{r,CO_2} C_{CO_2}, s$	4.605	$1.751 \cdot 10^5$	1
R3	$C_{(s)} + H_2O \longrightarrow CO + H_2$	$k_{r,H_2O} C_{H_2O}, s$	11.25	$1.751 \cdot 10^5$	1
R4	$CO + 0.5O_2 \xrightarrow{H_2O} CO_2$	$k_{r,CO} C_{CO} C_{H_2O}^{0.5} C_{0_2}^{0.25}$	$1.25 \cdot 10^{11}$	$1.67 \cdot 10^5$	0
R5	$CO + H_2O \longrightarrow CO_2 + H_2$	$k_{r,CO} C_{CO} C_{H_2O}$	$2.74 \cdot 10^6$	$8.36 \cdot 10^4$	0
R6	$CO_2 + H_2 \longrightarrow CO + H_2O$	$k_{r,CO_2} C_{CO_2} C_{H_2}$	$1.0 \cdot 10^8$	$6.28 \cdot 10^4$	0

4.3.2 Governing equations of particle-resolved approach

Equations 4.4 to 4.7 describe the mathematical conservation of mass, momentum, species, and energy for the PRS model [28, 42–44], taking into consideration the following assumptions:

1. The volatilization of the particles is not included, due to the steady-state feature of the model.
2. Thermal equilibrium is assumed for solid and gas phases.
3. The gaseous phase behaves as an incompressible flow with $p = 10^5$ Pa.
4. The buoyancy effect is neglected.

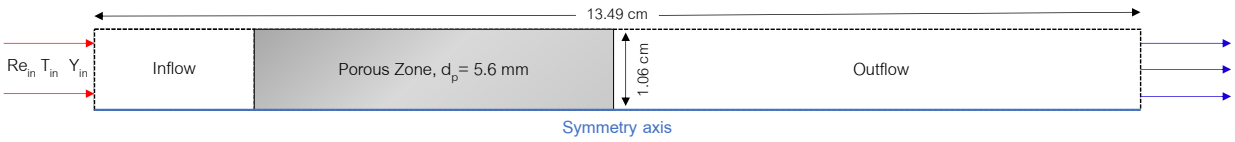

(a)

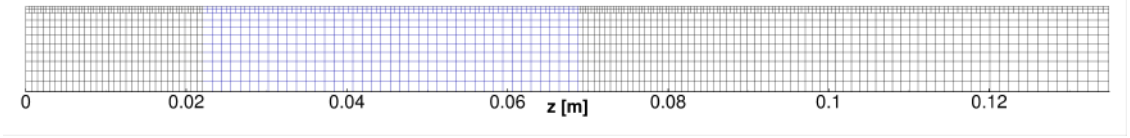

(b)

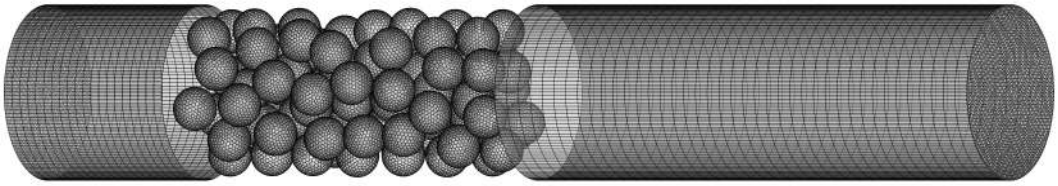

(c)

Figure 4.1: Schematics of computational domain (a) and mesh of fixed-bed reactor (b) using PMM approach. Mesh of 3D PRS approach assessed in [28] (c).

Taking into account all assumptions made, the final system of equations has the following form [28]:

Conservation equation for mass transport:

$$\nabla \cdot (\rho \vec{u}) = 0 \tag{4.4}$$

Conservation equation for momentum transport:

$$\nabla \cdot (\rho \vec{u}\vec{u}) = -\nabla p + \nabla \cdot \tau \tag{4.5}$$

Conservation equation for species transport:

$$\nabla \cdot (\rho \vec{u} Y_i) = \nabla \cdot (\rho D_i \nabla Y_i) + R_i \tag{4.6}$$

Conservation equation for energy transport:

$$\nabla \cdot (\rho \vec{u} h) = \nabla \cdot (\lambda \nabla T) - \sum_i \frac{h_i^0}{M_i} R_i \tag{4.7}$$

In the context of the PRS approach, Stefan flow was considered, i.e., when the velocity is non-zero at chemically reacting surfaces, which characterizes the net mass flux between surface and gas [45, 46]. Below, we outline the mathematical representation of this phenomenon and provide the boundary conditions for heat and mass transfer.

$$\rho_{\text{wall}}\, D_i \frac{\partial Y_{i,\text{ wall}}}{\partial n} - \dot{m}_C'' Y_{i,\text{ wall}} \; = M_i \widehat{R}_{i,s} \tag{4.8}$$

$$\dot{m}_C'' = \sum_{i=1}^{N_R} M_i \widehat{R}_{i,s} \tag{4.9}$$

$$\mathbf{n} \cdot \lambda \nabla T|_{\text{gas}} \; = \sum_{j=1}^{N} M_i \widehat{R}_{i,s} h_j^0 + \epsilon_{\text{s}} \sigma \left(T_{surf}^4 - T_{\text{in}}^4 \right) \tag{4.10}$$

$$\mathbf{n} \cdot \vec{u} = \frac{\dot{m}_C''}{\rho} \tag{4.11}$$

where $\mathbf{n}$ is the normal vector to the wall, ϵ_{s} is the emissivity ($\epsilon_{\text{s}} \approx 1.0$ for solid carbon), σ is the Stefan-Boltzmann constant, $\widehat{R}_{i,s}$ is the production rate of species i due to surface chemical reactions, $\dot{m}_C''$ is the net mass flux between surface and gas, indexes $wall$ and $surf$ refer to gas side at the wall and surface of the particles, respectively.

4.3.3 Governing equations of porous media approach

The 2D axisymmetric steady-state model for the conservation equations (Equations 4.12 to 4.15) describing PMM is based on several assumptions, as outlined in the literature [47, 48]. These assumptions include the composition of the porous zone with spherical carbon char particles, considering fuel particles as a continuously porous medium with initially isotropic properties, excluding drying and devolatilization effects, assuming thermal equilibrium within the char particle between solid and gas phases, setting the ambient gas

phase as isobaric with $p = 10^5$ Pa, and assuming laminar gas flow with an axisymmetric flow field.

Taking into account all assumptions made, the final system of equations has the following form [47, 48]:

Conservation equation for mass transport:

$$\nabla \cdot (\varepsilon \rho_g \vec{u}) = S_m \tag{4.12}$$

Conservation equation for momentum transport:

$$\nabla \cdot (\varepsilon \rho \vec{u} \vec{u}) = -\varepsilon \nabla p + \nabla \cdot (\varepsilon \tau) \tag{4.13}$$

Conservation equation for species transport:

$$\nabla \cdot (\varepsilon \rho \vec{u} Y_i) = \nabla \cdot (\varepsilon \rho D_{eff} \nabla Y_i) + R_i \tag{4.14}$$

Conservation equation for energy transport:

$$\nabla \cdot (\varepsilon \rho \vec{u} h) = \nabla \cdot (\lambda_{eff} \nabla T) - \sum_i \varepsilon \frac{h_i^0}{M_i} R_i \tag{4.15}$$

where $\tau = \mu \left(\nabla \vec{u} + \nabla \vec{u}^{\mathrm{T}} \right)$ is the stress tensor. Species i is any reacting participant involved in the heterogeneous combustion process, i.e., H_2O, O_2, H_2, CO, CO_2, D_{eff} is the mass diffusion coefficient, λ is the thermal conductivity, h_i is enthalpy, h^0 is the enthalpy of formation, M_i is molecular weight, Y_i is mass fraction, R_i is the net production rate, and $\widehat{R}_{i,r}$ is the Arrhenius molar rate of creation/destruction for species i, respectively. The last two terms are described below, where $v''_{i,r}$ and $v'_{i,r}$ are the stoichiometric coefficients for reactants and products in the reaction r, $\eta'_{j,r}$ and $\eta''_{j,r}$ are the forward and backward rate exponents in the reaction r for each chemical species j.

$$R_i = M_i \sum_r \widehat{R}_{i,r} \tag{4.16}$$

$$\widehat{R}_{i,r} = \left(v''_{i,r} - v'_{i,r}\right)\left[k_r \prod_{j=1}^{N} C_{j,r}^{\left(\eta'_{j,r} - \eta''_{j,r}\right)}\right] \tag{4.17}$$

The source term incorporated in the continuity equation may be expressed as:

$$S_m = S'''\left(\rho\frac{2M_{\mathrm{C}}}{M_{\mathrm{O_2}}}k_{\mathrm{R1}}Y_{\mathrm{O_2}} + \rho\frac{M_{\mathrm{C}}}{M_{\mathrm{CO_2}}}k_{\mathrm{R2}}Y_{\mathrm{CO_2}} + \rho\frac{M_{\mathrm{C}}}{M_{\mathrm{H_2}O}}k_{\mathrm{R3}}Y_{\mathrm{H_2}O}\right) \tag{4.18}$$

The density of the gaseous mixture was calculated as stated by Equation 4.19. Viscosity and thermal conductivity were calculated using the kinetic theory [49].

$$\rho = \frac{P}{RT\sum_i \frac{Y_i}{M_i}} \tag{4.19}$$

Regarding the PMM approach, the porosity ($\varepsilon = 0.5063$) impacts on the laminar flow through a packed bed. The Blake-Kozeny equation may be used for calculating pressure drop, as described in Equation 4.20 [50]. The permeability (α) and inertial loss coefficient of flow (C_2) in the porous zone are described by Equation 4.21 and 4.22, respectively.

$$\frac{|\Delta p|}{L} = \frac{150\mu}{D_p^2}\frac{(1-\varepsilon)^2}{\varepsilon^3}v_\infty \tag{4.20}$$

$$\alpha = \frac{D_p^2}{150}\frac{\varepsilon^3}{(1-\varepsilon)^2} \tag{4.21}$$

$$C_2 = \frac{3.5}{D_p}\frac{(1-\varepsilon)}{\varepsilon^3} \tag{4.22}$$

The effective diffusivity ($D_{m,i}^{eff}$) was calculated using Equation 4.23:

$$D_{m,i}^{eff} = \frac{\epsilon}{\tau}\frac{1-x_i}{\sum \frac{x_i}{D_{ij}}} \tag{4.23}$$

where ϵ is porosity; τ is tortuosity; x_i is molar fraction of i th species; D_{ij} is binary diffusivity for $i-j$ th pair. D_{ij} is calculated from the Fuller correlation [51]:

$$D_{ij} = \frac{0.01013T^{1.75}}{p_t M^{0.5}\left(V_i^{1/3} + V_j^{1/3}\right)^2} \tag{4.24}$$

where $V_{i,j}$ - diffusion volume for i, j th species [52], i.e., $V_{CO_2} = 26.9$, $V_{CO} = 18.9$, $V_{H_2} = 7.07$, $V_{N_2} = 17.9$, $V_{O_2} = 16.6$, $V_{H_2O} = 12.7$. The thermal conductivity (λ_{eff}) inside the porous zone was calculated using the porosity of the fixed-bed:

$$\lambda_{eff} = \varepsilon\lambda \tag{4.25}$$

4.3.4 Boundary conditions

At the inlet of the fixed-bed reactor, the following Dirichlet boundary conditions are considered for inflow gas velocity, species mass fractions, and temperature, respectively:

$$\vec{u} = \vec{u}_{\text{in}}, \quad Y_i = Y_{i,\text{in}}, \quad T = T_{\text{in}} \tag{4.26}$$

where $\vec{u}_{\text{in}} = f(\text{Re}_{\text{in}})$, T_{in} = 900-1500 K, and $Y_{i,\text{in}}$ varies depending on the oxidative atmosphere ($\text{Y}_{O_2,\text{in}} = 0.05$ and 0.11). At the outlet of the fixed-bed reactor, the so-called outflow boundary conditions with an overall mass balance correction was implemented [49]. Since there is an important interaction between gaseous and solid phases on the surface of the particles, mass and energy balance at the interface are affected by the heterogeneous chemical reactions (R1 to R3), due to the production and destruction rates of gaseous species caused by these reactions along with convective and diffusive mass fluxes of the gas phase species at the surface of particles [53]. A crucial parameter for heterogeneous chemical reactions is the specific surface area of the porous zone, which was calculated taking into account the number of particles and their occupied volume inside the unit, being $S''' = 528.99$ m^{-1} the value of specific surface area used for both PMM and PRS numerical approaches.

Regarding the PMM approach, at the symmetry axis ($r = 0$) as well as at the upper side of the domain, the following Neumann boundary conditions must be specified for pressure, velocity, concentration, and temperature:

$$\frac{\partial p}{\partial r} = 0, \quad \frac{\partial \vec{u}}{\partial r} = 0, \quad \frac{\partial Y_i}{\partial r} = 0, \quad \frac{\partial T}{\partial r} = 0 \tag{4.27}$$

4.3.5 Numerics and validation

Numerical software Ansys® Fluent 2022R2 [49] was utilized to solve Equations 4.12 to 4.14. The solution method for solving the governing equations by coupling pressure and velocity was the semi-implicit method for pressure-linked equations (SIMPLE) algorithm [54]. The scheme of the computational domain and grid structure are schematically depicted in Figures 4.1a and 4.1b, respectively. The porous zone can be identified in Figure 4.1b for the blue mesh. The number of cells was 1960, to ensure uniform porosity along the bed zone. It should be noted that the grid independence simulations for 3D results have been reported in Arriagada et al. [28]. In terms of 2D grid study, we must emphasise that in porous media models the grid size is limited by the size of particles. In particular, if a grid size in 2D PMM simulation is significantly less than particle diameter, then in this case, volume fraction radial and axial profiles must be included into the simulations because of the volume, which is further discussed in Section 3.6. Specific surface area (S''') was used for considering wall-surface reactions in the porous zone. Radiation was considered using the P-1 model [55] since it plays a crucial role as a heat transfer mechanism inside the porous zone of the reactor. Convective terms, species, and energy were discretized using an upwind second-order scheme. The under-relaxation factors were set at 0.5 for momentum, energy 0.8, and species 0.5, except for carbon dioxide (0.7), and oxygen (0.3), as the kinetic scheme involved in the process has a critical effect on these species' conservation. The iterations were stopped when the residual for all equations was less than 10^{-6}, which required approximately 10^5 iterations until convergence. The software was validated against both experimental data [19, 42, 56] and analytical solutions [18], considering a two-film model [57], and the same kinetic scheme implemented in the present work. Functions for effective diffusivity and thermal conductivity in the porous zone were implemented into the software through a user-defined-function (UDF), where the DEFINE macros of DEFINE_DIFFUSIVITY and DEFINE_PROPERTY were used respectively.

4.4 Results and discussion

4.4.1 Effect of heterogeneous chemical reactions and Reynolds number

Reynolds numbers based on particle size (Re_{in}) of 50, 75, and 100 were numerically studied in the reactor. From an elemental perspective, as Re_{in} increases, a higher inlet velocity ($\vec{u}_{in}$) is observed. When comparing 3D CFD particle-resolved simulations against the porous media model in terms of the effect of the heterogeneous chemical reactions in the species concentration, Figure 4.2 depicts the volume-averaged temperature (Fig. 4.2a) and mass fractions of oxygen (Fig. 4.2b), hydrogen (Fig. 4.2c), carbon monoxide (Fig. 4.2d), and carbon dioxide (Fig. 4.2e). It can be observed how Re_{in} affects the profiles, particularly observing for oxygen how the concentration decreases with inflow gas temperature, reaching almost full consumption in the porous zone at high inlet temperature. The highest deviation observed for the temperature inside the porous zone (T_{pz}) is presented for $Re_{in} = 100$, with 12.8%. The effect of R3 and R5 could be observed in Figure 4.2c, where the hydrogen mass fraction increases with the inflow gas temperature. Here the order of magnitude of the mass fraction of hydrogen (Y_{H_2}) increases from an average of $5 \cdot 10^{-6}$ to $1.2 \cdot 10^{-5}$. Moreover, the effect of R4 and R5 could be seen in Figure 4.2d, where between 1300 K and 1500 K, the mass fraction of CO does not increase with a positive slope as compared with hydrogen or carbon dioxide. It could be highlighted that carbon dioxide is quite accurate in all simulations, with a deviation below 12.3% in all cases when comparing PRS and PMM. From 1100 K and higher temperatures, the slope of the curve representing the mass fraction of CO_2 increases remarkably, which could be attributed to R2 and R4, dominant chemical reactions in the semi-global kinetic scheme used for this work. In general terms, the 2D axisymmetric approach is in agreement with results obtained in the literature for 3D PRS modeling [28], specially for low Reynolds number and low inflow gas temperature, where the profiles follow a relatively linear behaviour as the temperature increases. The exception is $T_{in} = 1300$ K, where the highest deviation between the 2D PMM and 3D PRS approaches occurs, which is consistent with the literature when evaluating the effect of inflow gas temperature on the

heterogeneous combustion of carbon [58]. Furthermore, the effect of $\mathrm{Re_{in}}$ can be clearly observed, where the higher the inflow velocity, the higher the deviation exists between the two numerical approaches under study.

This tendency can also be observed in Figure 4.3, where the intention was to evaluate the effect of the continuum model against a particle-resolved simulation approach, without considering homogeneous reactions taking place after the porous zone. To evaluate the accuracy of the porous media model, the following results of the aforementioned figure are calculated at the outlet of the bed zone ($z = 6.88$ cm). The area-weighted averaged temperature ($\mathrm{T_{out-pz}}$) and concentration of main species involved in the kinetic scheme show the same behaviour as for the volume-averaged values, with higher maximum concentration of hydrogen (See Figure 4.3c), carbon monoxide (See Figure 4.3d), and carbon dioxide (See Figure 4.3e) when compared these two results. Again, deviation between PRS and PMM increases with $\mathrm{Re_{in}}$, where a particular control point might be found at $T_{\mathrm{in}} = 1300$ K. At this temperature, most of the available O_2 is consumed, CO_2 presents deviation smaller than 16.7% for all cases, where exact values are 7.7%, 5.5%, and 16.7% for $\mathrm{Re_{in}} = 50$, 75, and 100, respectively. It can also be observed a minimum deviation of 8.1% at H_2 $T_{\mathrm{in}} = 1100$ K, which is a negligible value since the order of magnitude of $\mathrm{Y_{H_2}}$ is 10^{-7}. The effects of the Boudouard reaction (R2) and the oxidation of CO (R4) are remarkable for these species since this is evaluated at the outlet of the porous zone. The effect of the PMM approach was evaluated at the outlet of the porous zone since after the packed-bed, changes in flow velocity, formation of velocity gradients, generation of eddies or recirculation zones may affect the comparison with a 3D PRS approach. Regarding the mass flow, there must be a difference between outflow and inflow mass. There has been a minimal difference between these two approaches. Figure 4.3f shows the highest difference for $\mathrm{Re_{in}} = 100$, $T_{\mathrm{in}} = 1300$ K, with $3.36 \cdot 10^{-6} \mathrm{kg \cdot s^{-1}}$. The tendency of the results is similar to those reported previously, where the higher the Reynolds number, the more deviation with results when comparing 2D PMM and 3D PRS.

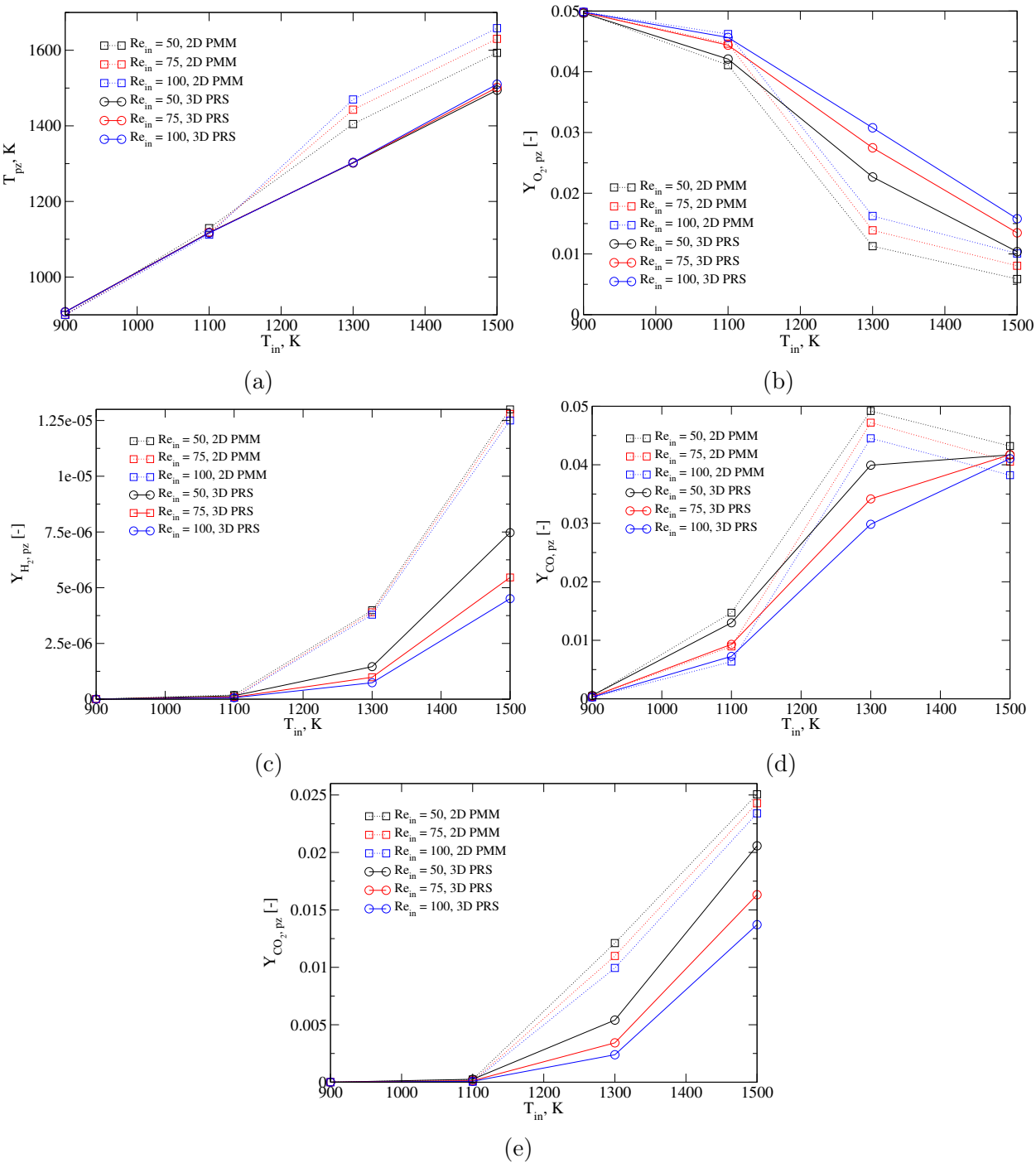

Figure 4.2: Volume-averaged T_{pz} (a), Y_{O_2} (b), Y_{H_2} (c), Y_{CO} (d), and Y_{CO_2} (e) inside porous zone for $\text{Y}_{\text{O}_2,\text{in}} = 0.05$ and Re_{in}= 50, 75 and 100.

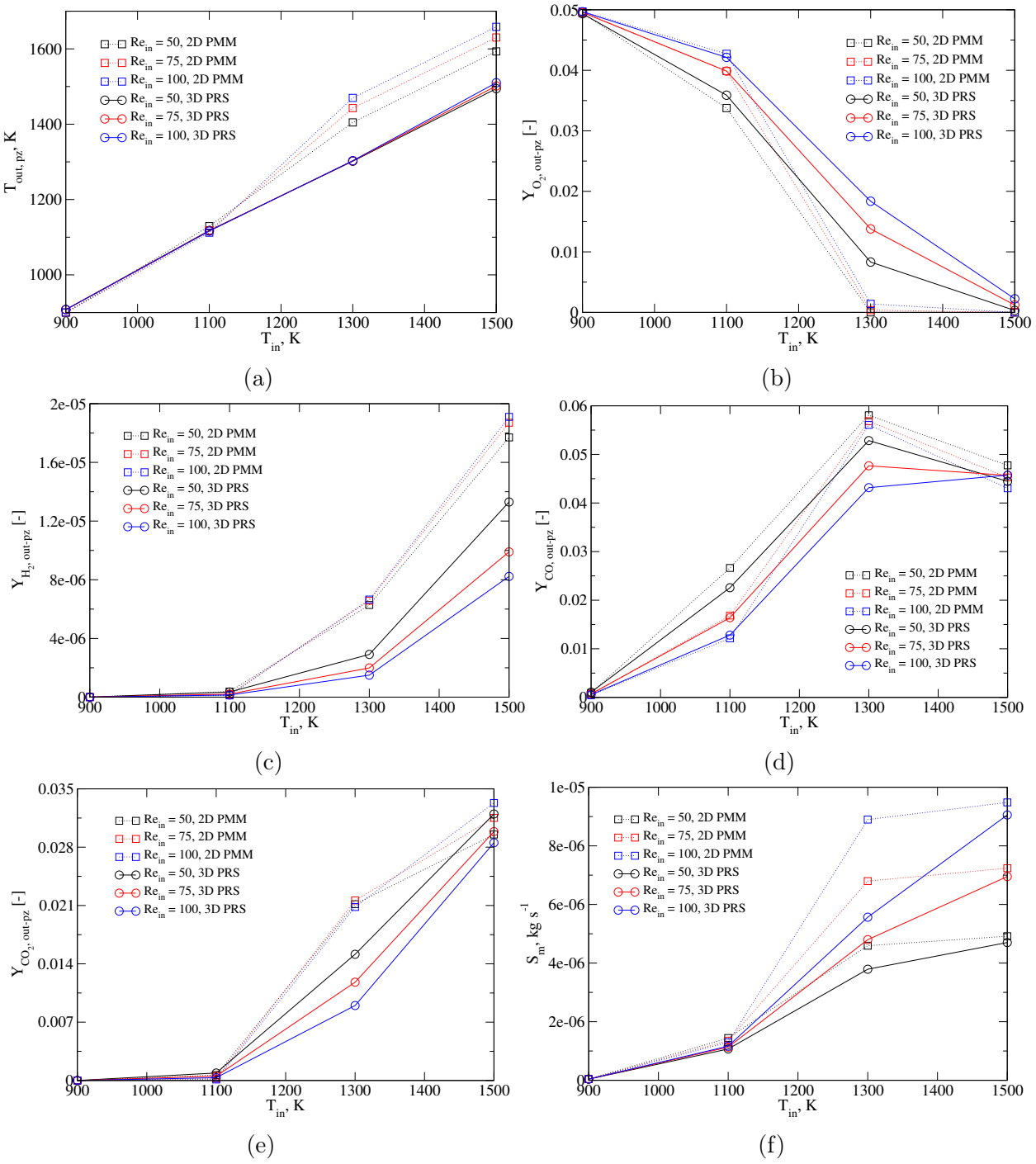

Figure 4.3: Area-weighted averaged $T_{\mathrm{out-pz}}$ (a), $\mathrm{Y_{O_2}}$ (b), $\mathrm{Y_{H_2}}$ (c), $\mathrm{Y_{CO}}$ (d), and $\mathrm{Y_{CO_2}}$ (e) at outlet of the porous zone. $\mathrm{S_m}$ (f) for $\mathrm{Y_{O_2,in}} = 0.05$ and $\mathrm{Re_{in}}$= 50, 75 and 100.

4.4.2 Effect of oxidative atmosphere

Two different gasifying conditions were evaluated during this research. Thermochemical processes using an ambient mass fraction of oxygen $Y_{O_2} = 0.05$, and 0.11 were used to assess the behaviour of the domain, and performance of the heterogeneous combustion of the fixed-bed reactor. Figure 4.4 shows the volume-averaged temperature (Fig. 4.4a) and mass fractions of oxygen (Fig. 4.4b), hydrogen (Fig. 4.4c), carbon monoxide (Fig. 4.4d), and carbon dioxide (Fig. 4.4e). It can be observed a good agreement between both 2D axisymmetric PMM and PRS numerical approaches for all the presented profiles. In particular, and as discussed in the previous section, the highest deviation could be observed for an inflow gas temperature of 1300 K, while the higher this variable, the higher deviation between 2D and 3D models might be seen for all curves. Most probably, the effect of a higher volume-averaged temperature inside the porous zone leads to both a decrease of the oxygen concentration (See Figure 4.4b), and greater production of carbon dioxide (See Figure 4.4e). Deviation on average does not get higher than 10% for temperature, whereas for the lowest inflow temperature, the deviation is below 1%, showing a good fit of curves. In particular, minimum deviations for $T_{\text{in}} = 900$ K are 0.85%, and 0.76% for $Y_{O_2,\text{in}} = 0.05$ and 0.11, respectively. On the other hand, maximum deviations are observed at $T_{\text{in}} = 1300$ K, with 7.9% and 16.1% for the aforementioned case. Also, oxygen and carbon monoxide (See Figure 4.4d) show the best fit in terms of tendency, achieving a remarkable accuracy for low inflow gas temperatures (900-1100 K). In particular, minimum deviations occur at $T_{\text{in}} = 1500$ K, with 3.6% and 6.6% for $Y_{O_2,\text{in}} = 0.05$ and 0.11, respectively. As evaluated in the previous section with Re_{in} as the crucial parameter to assess, Figure 4.5 depicts the effect of the PMM approach against PRS at the outlet of the porous zone ($z = 6.88$ cm), avoiding any constrain due to the abrupt transition between the porous zone and the outlet zone of the unit, comparing $Y_{O_2,\text{in}} = 0.05$ and 0.11 at a constant value of $Re_{\text{in}} = 50$. Figures 4.5b and 4.5d show excellent agreement between both PMM and PRS, in particular for oxygen leading to the entire conversion of oxygen at high inflow gas temperatures, and the highest production of CO for inflow gas temperature of 1300 K for all cases under study.

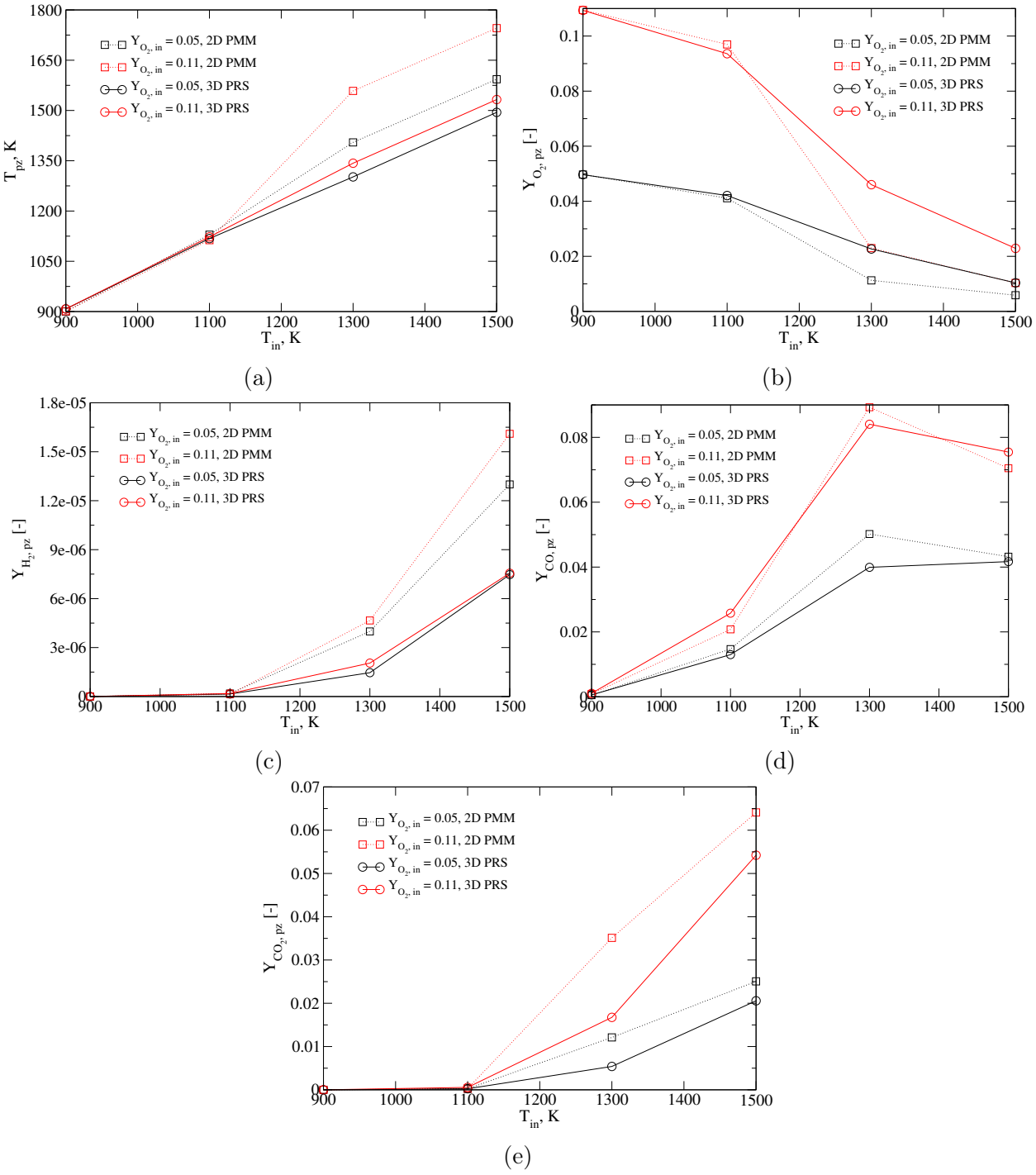

Figure 4.4: Volume-averaged T_{pz} (a), Y_{O_2} (b), Y_{H_2} (c), Y_{CO} (d), and Y_{CO_2} (e) inside porous zone for Re_{in}= 50, and $Y_{O_2,in}$ = 0.05 and 0.11.

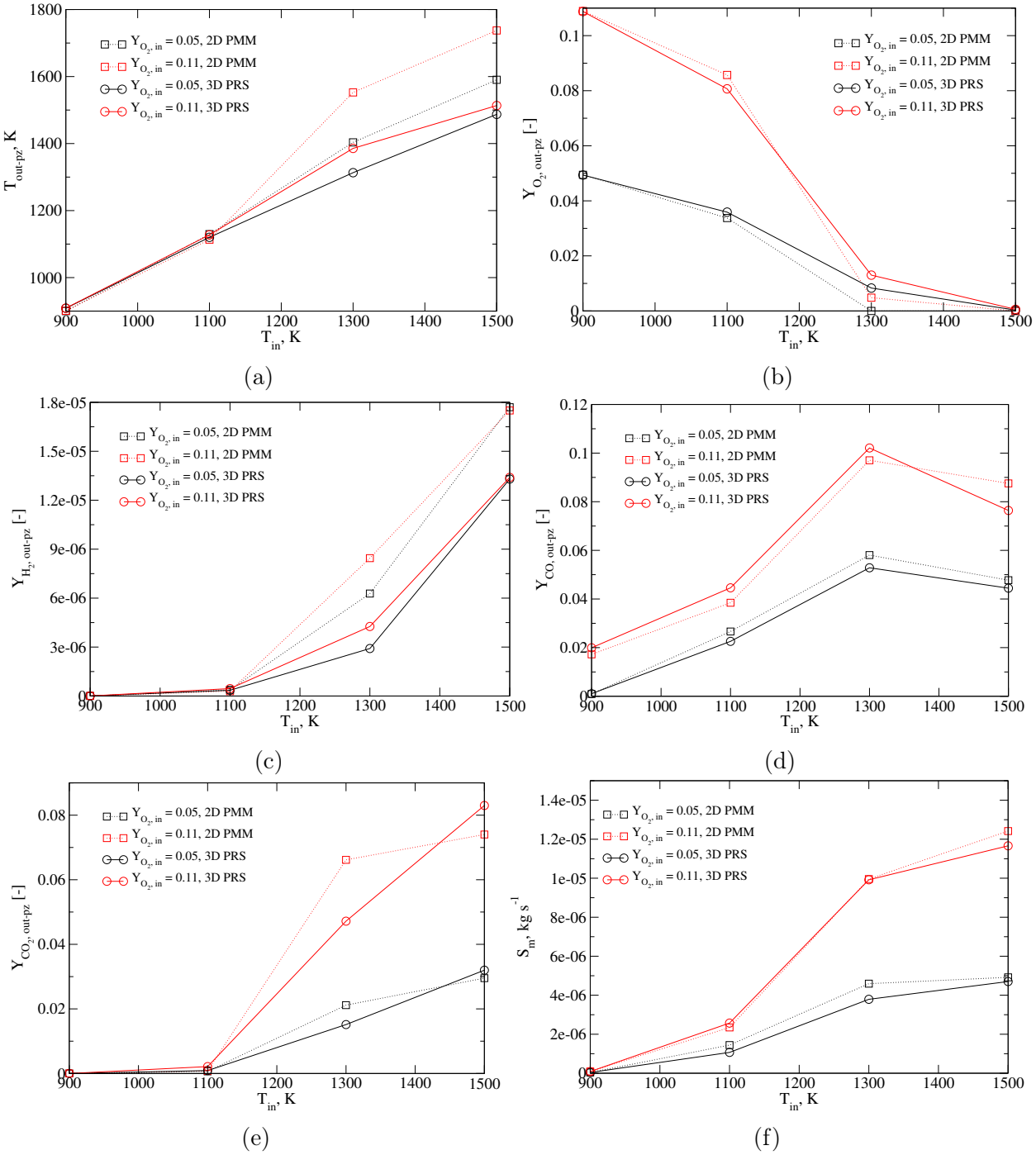

Figure 4.5: Area-weighted averaged $T_{\text{out-pz}}$ (a), Y_{O_2} (b), Y_{H_2} (c), Y_{CO} (d), and Y_{CO_2} (e) at outlet of the porous zone. S_m (f) for for Re_{in}= 50, and $Y_{O_2,in}$ = 0.05 and 0.11.

4.4.3 Effect of homogeneous chemical reactions

As observed in the previous subsections of this article, the porous media model is specially different when compared to a 3D CFD particle-resolved simulation in terms of the fluid dynamics inside the fixed-bed. Figure 4.6 shows the temperature and species concentration along the reactor under both 3D PRS (top view) and 2D PMM (bottom view) at $\mathrm{Re_{in}} = 50$, $\mathrm{Y_{O_2,in}} = 0.05$, and $T_{\mathrm{in}} = 1500$ K. It could be observed how the effect of homogeneous chemical reactions after the porous zone plays a crucial role. In particular, and for hydrogen (See Figure 4.6c), hydrogen is consumed in the 2D PMM approach after the porous zone. Moreover, the profiles are relatively accurate for oxygen and carbon monoxide but do not show a good agreement for temperature, hydrogen, and carbon dioxide. On the other hand, for a lower inflow gas temperature, such as $T_{\mathrm{in}} = 1100$ K, Figure 4.7 depicts again temperature, and main species mass fractions along the reactor using both numerical approaches, observing an excellent agreement between 3D PRS and 2D PMM, not only in the magnitude but also in the position along the reactor, which represents the effect of both heterogeneous and homogeneous chemical reactions.

4.4.4 Effect of thermal conductivity of solid phase

The heterogeneous combustion of carbon char particles inside a fixed-bed is a continuous interaction between the solid and gas phases. The thermal conductivity of the solid phase is an important parameter to assess. Figure 4.8 shows the effect of the variation of thermal conductivity of the solid phase inside the porous zone (λ_s) on the volume-averaged temperature and species concentration. This test was done considering $\mathrm{Y_{O_2,in}} = 0.05$ and $\mathrm{Re_{in}} = 75$, and adding a third plot, considering $\lambda_s = 0.02$ W/m $\cdot$ K. In general, it can be observed how the lower λ_s value used for simulations, better accuracy of the 2D PMM model is achieved, due to the surface-based reaction model studied by Arriagada et al. [28], where no mesh inside solid phase existed. In particular, for the critical inlet temperature of $T_{\mathrm{in}} = 1300$ K, when the thermal conductivity of the solid phase was treated near air conditions (hollow spheres), the curves fit better decreasing the gap between 3D PRS and 2D PMM. Results are consistent with those reported in the literature, where λ_s plays a crucial role in the heat

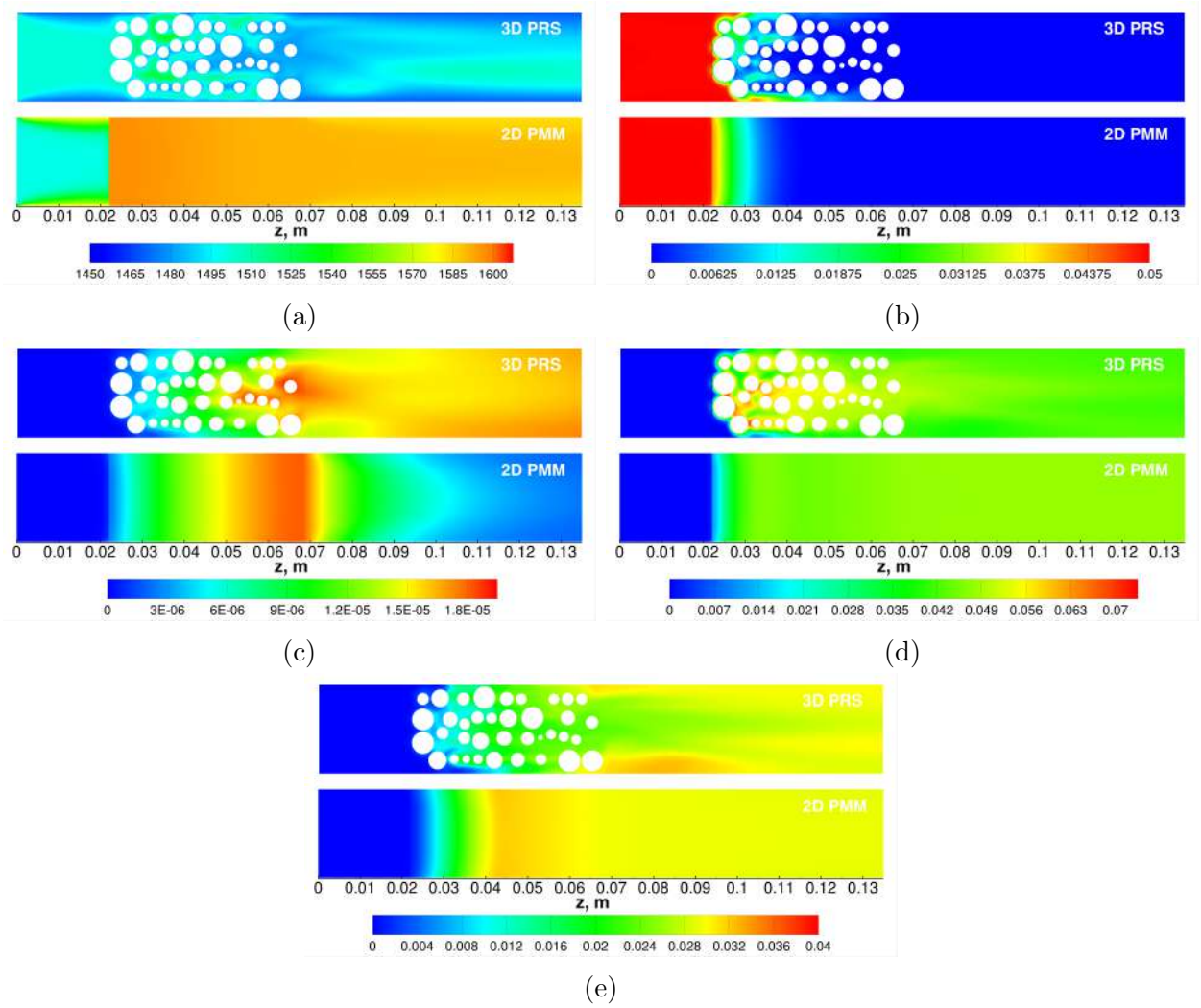

Figure 4.6: Temperature (a), Y_{O_2} (b), Y_{H_2} (c), Y_{CO} (d), and Y_{CO_2} (e) inside fixed-bed reactor for Re_{in}= 50, $Y_{O_2,in}$ = 0.05, and T_{in} = 1500 K.

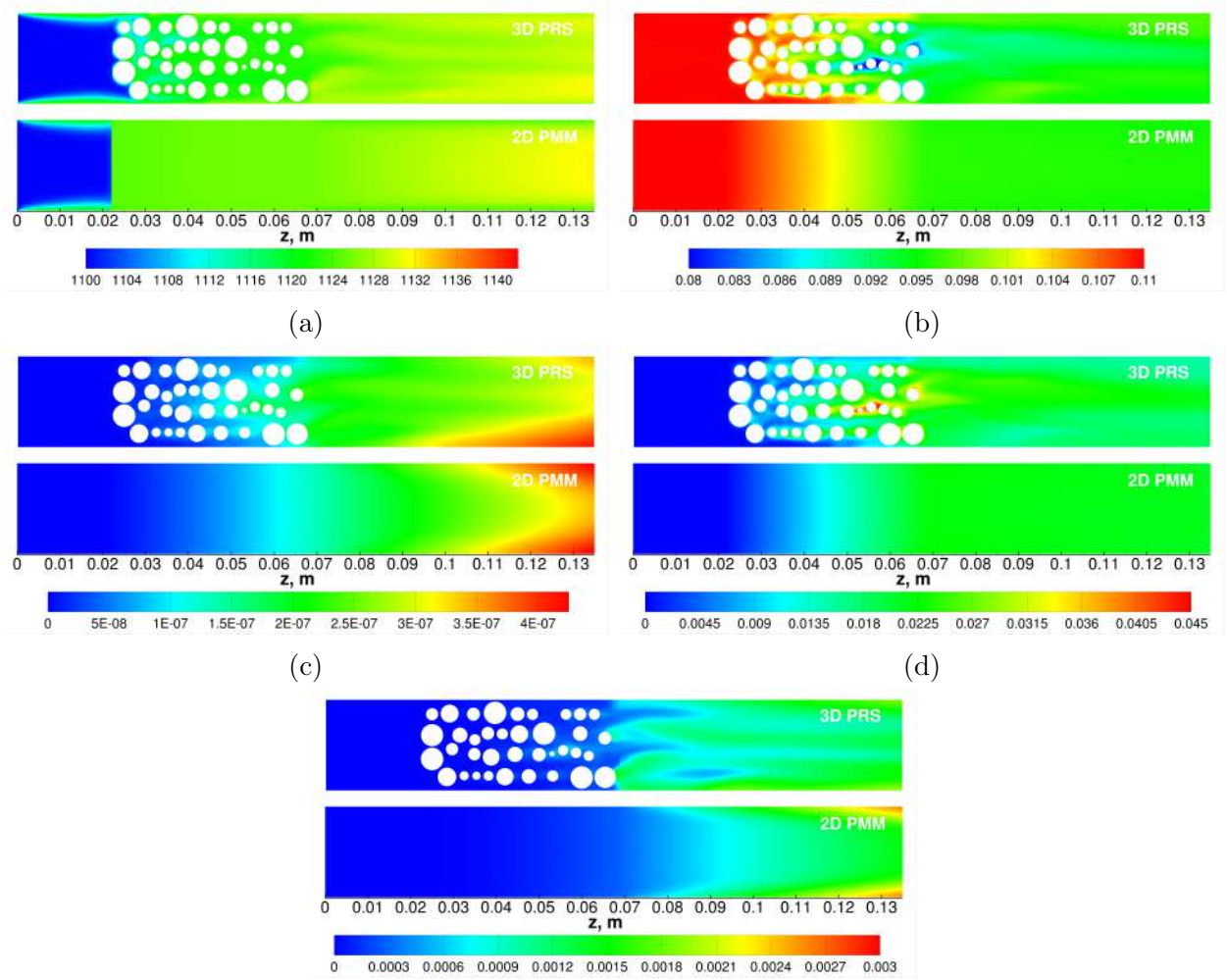

Figure 4.7: Temperature (a), Y_{O_2} (b), Y_{H_2} (c), Y_{CO} (d), and Y_{CO_2} (e) inside fixed-bed reactor for Re_{in}= 100, $Y_{O_2,in}$ = 0.11, and T_{in} = 1100 K.

transfer inside packed-bed reactors [32].

4.4.5 Effect of dispersion coefficient

The dispersion coefficient might play a relevant role in reaction phenomena inside a packed-bed reactor, depending on their geometrical features, such as D_t/d_p ratio, L_t/d_p ratio, Peclet number ($\mathrm{Pe_m}$), among others. This parameter has been widely studied in the literature with several approaches depending on the operational conditions and dimensions of a packed-bed reactor [59–62]. To assess the effect of the dispersion coefficient in the performance of the 2D PMM approach, the longitudinal dispersion coefficient D_L, described by Equation 4.28, was implemented using the macros DEFINE_DIFFUSIVITY in a user-defined-function [62–64]:

$$D_L = 0.7 D_{ij} + u r_p \tag{4.28}$$

The effect of D_L is depicted in Figure 4.9, where the volume-averaged temperature (Figure 4.9a), $\mathrm{Y_{O_2}}$ (Figure 4.9b), $\mathrm{Y_{H_2}}$ (Figure 4.9c), $\mathrm{Y_{CO}}$ (Figure 4.9d), and $\mathrm{Y_{CO_2}}$ (Figure 4.9e) inside the porous zone are presented. It can be observed negligible deviation between 2D PMM (constant ε, no consideration of D_L) and 2D PMM (constant ε, including D_L) is negligible in the range of 900-1100 K. Deviation gets considerable for higher inflow gas temperatures (T_{in} = 1300-1500 K) for all figures. Considering the axial dispersion coefficient is significant for the partial oxidation of a chemically reacting fixed-bed, thus should be considered when using a 2D PMM numerical approach.

4.4.6 Effect of porosity variation

The porosity plays a crucial role when working with continuum models such as the porous media model (PMM) as it depends on the D_t/d_p ratio [65]. Moreover, the porosity inside a packed-bed reactor varies with the radius ($\varepsilon(r)$) depending as well on the D_t/d_p ratio, showing different mathematical correlations [66–70]. A derivation of a particular mathematical representation of $\varepsilon(r)$ considering the specific features of the reactor (D_t/d_p = 3.78) under study is described in Equation 4.29 [67]. In this case, a refined mesh was necessary to perform simulations since the profile in the radial direction behaves in a non-structured

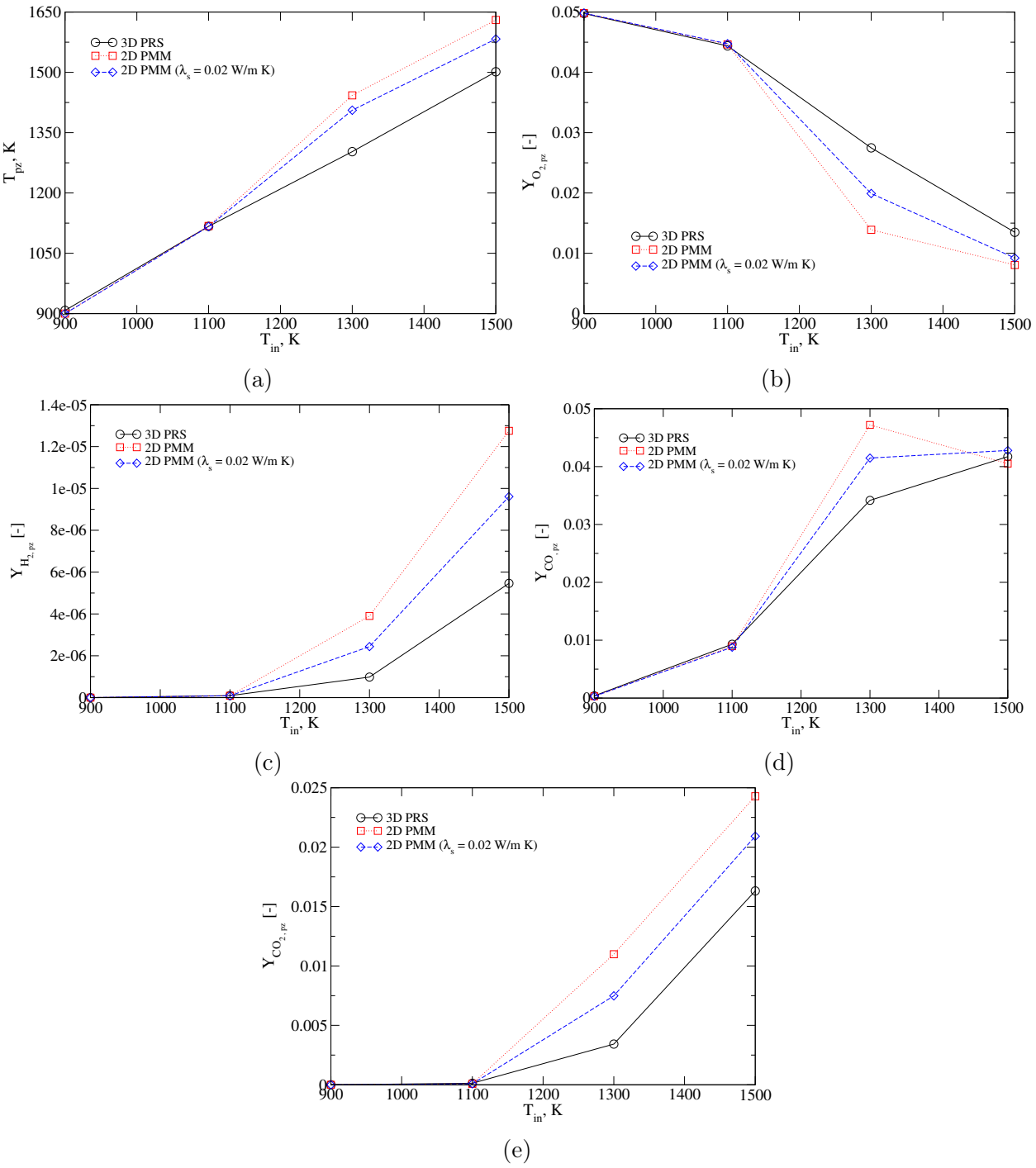

Figure 4.8: Effect of thermal conductivity of solid (λ_s) on the volume-averaged T_{pz} (a), $\mathrm{Y_{O_2}}$ (b), $\mathrm{Y_{H_2}}$ (c), $\mathrm{Y_{CO}}$ (d), and $\mathrm{Y_{CO_2}}$ (e) inside porous zone for $\mathrm{Y_{O_2,in}} = 0.05$ and $\mathrm{Re_{in}} = 75$.

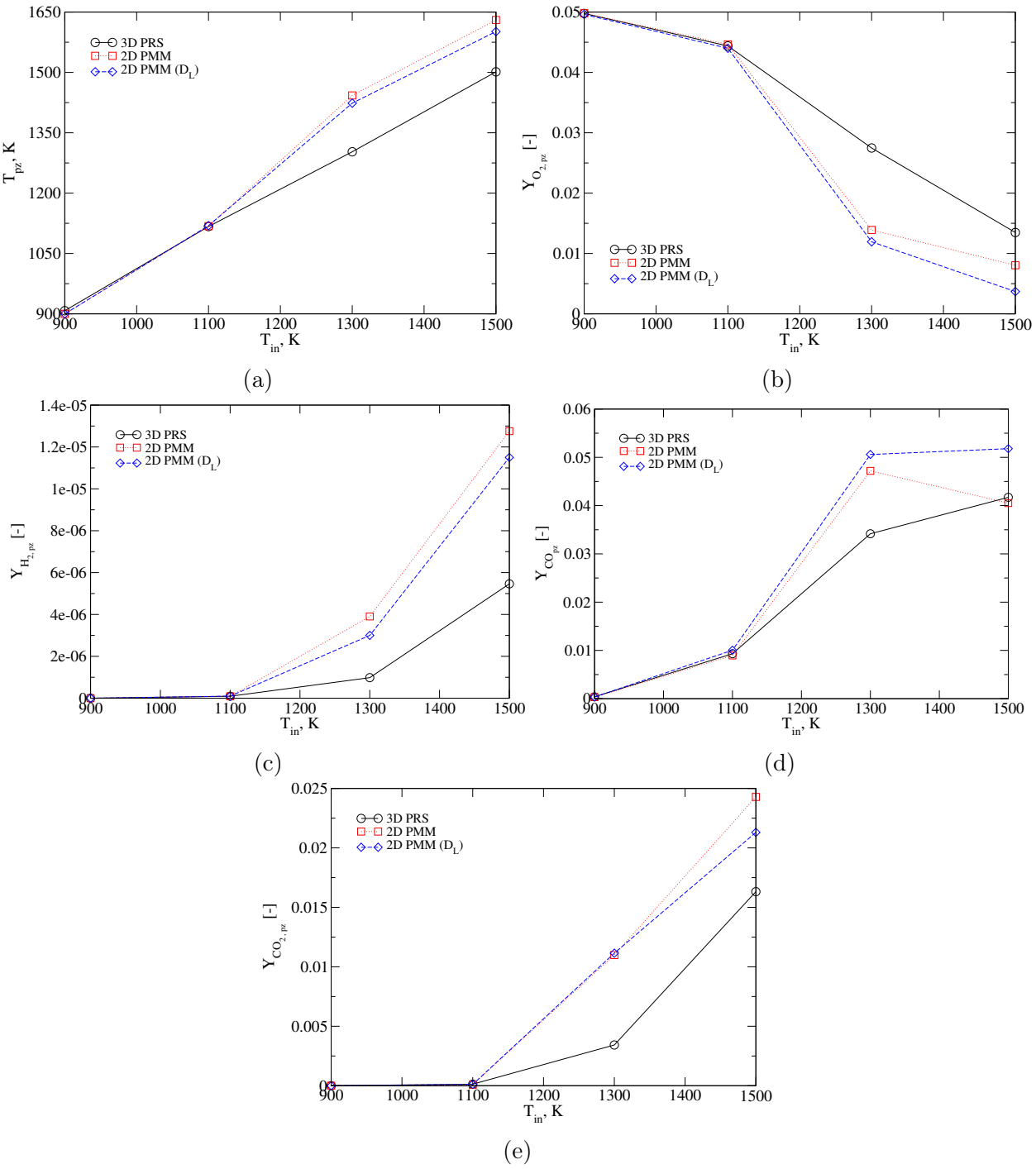

Figure 4.9: Effect of dispersion coefficient (D_L) on the volume-averaged T_{pz} (a), Y_{O_2} (b), Y_{H_2} (c), Y_{CO} (d), and Y_{CO_2} (e) inside porous zone for $\text{Y}_{\text{O}_2,\text{in}} = 0.05$ and $\text{Re}_{\text{in}} = 75$.

way.

$$\varepsilon(r) = \begin{cases} 2.14z^2 - 2.53z + 1; & z \leq 0.637 \\ \varepsilon_b + 0.29\exp(-0.6z)[\cos(2.3\pi(z - 0.16))] + 0.15\exp(-0.9z); & z > 0.637 \end{cases} \tag{4.29}$$

where $z = (R_t - r)/d_p$, r is the radius, d_p is particle diameter, $R_t = 10.6$ mm is the tube radius, and ε_b is bulk porosity, which in this case takes the value of 0.37. The function of $\varepsilon(r)$ was implemented into the software through a user-defined-function (UDF), where the DEFINE_PROFILE macros was used. Since there is a continuous change in the value of porosity over radius of the reactor, a refined mesh was used, refining the whole domain, specially at the wall, obtaining a 18500 cell mesh. Figure 4.10 shows the effect of incorporating a function of $\varepsilon(r)$ in the numerical simulations. Figure 4.10a shows a comparison of $\varepsilon(r)$ using the approach of De Klerk [67] and Mueller [70]. The latter was not later considered due to the sharpness of the function at a near value of z = 1. For figures representing volume-averaged temperature (Figure 4.10b), Y_{O_2} (Figure 4.10c), Y_{H_2} (Figure 4.10d), Y_{CO} (Figure 4.10e), and Y_{CO_2} (Figure 4.10f), an important deviation comparing with using constant porosity, i.e., $\varepsilon = 0.5063$, can be observed. The consideration of a function of porosity for narrow tubes, in this case, $D_t/d_p = 3.78$, plays a crucial role in how the gasification process occurs inside the fixed-bed.

Adding a function for $\varepsilon(r)$ improved the accuracy of the 2D PMM fitting to the 3D PRS case, even for an inlet temperature of 1300 and 1500 K. Figure 4.11 depicts contour plots of temperature (Figure 4.11a), Y_{O_2} (Figure 4.11b), Y_{H_2} (Figure 4.11c), Y_{CO} (Figure 4.11d), and Y_{CO_2} (Figure 4.11e) showing the effect of considering a function for porosity on the most critical inflow gas temperature discussed in this study ($T_{\text{in}} = 1300$ K). The difference between 2D PMM and 2D PMM $\varepsilon(r)$ is evident since including porosity as a function of radius leads to the models to be in good agreement. Moreover, the 2D PMM model including $\varepsilon(r)$ shows consistency with chemical kinetics, showing consumption of oxygen, and generation of H_2, CO, and CO_2 at different rates. At high temperatures, the 2D PMM captures the gasification performance accurately inside the porous zone, deviating in some of the species (H_2 and CO) due to the effect of the oxidation of carbon monoxide and

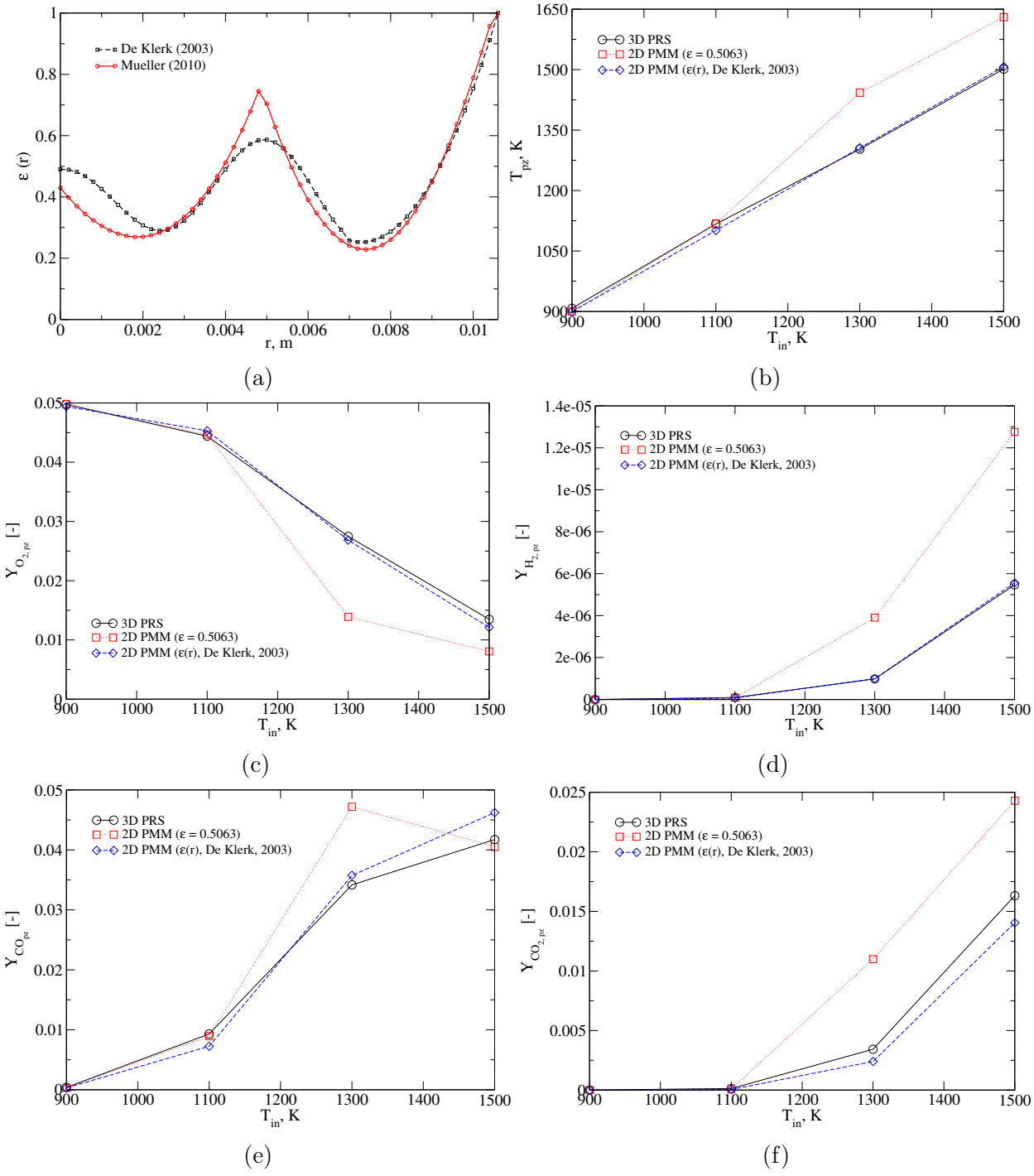

Figure 4.10: Porosity function over reactor radius ($\varepsilon(r)$) (a), effect of $\varepsilon(r)$ on volume-averaged T_{pz} (b), Y_{O_2} (c), Y_{H_2} (d), Y_{CO} (e), and Y_{CO_2} (f) inside porous zone for $\text{Y}_{\text{O}_2,\text{in}} = 0.05$ and $\text{Re}_{\text{in}} = 75$.

water-gas-shift reaction. Results highlight the relevance of geometrical features of the unit. If the diameter of the tube increases accordingly with the number of particles, a reduction of the effect of wall channeling would be expected, both decreasing the temperature of the solid particles along Z axis and increasing Y_{CO} faster. Moreover, for inert porous media reactors, where normally alumina spheres are used for enhancing heat transfer mechanism inside the fixed-bed, decreasing the particle size will lead to higher temperatures inside the unit.

4.5 Concluding remarks

In this work, the filtration combustion of carbon char particles under a laminar flow regime was investigated using a 2D axisymmetric porous media CFD-based model. The PMM approach was verified against 3D CFD surface-based particle-resolved simulations (PRS) for the partial oxidation of a chemically reacting fixed-bed, assessing critical parameters of flow regime (Re_{in}), oxidative atmosphere ($Y_{O_2,in}$), inflow gas temperature (T_{in}), thermal conductivity of solid phase (λ_s), variable porosity ($\varepsilon(r)$), and axial dispersion coefficient (D_L).

Results showed the significant role of the inflow gas temperature T_{in} in the gasification process. In particular, an important activation of chemical reactions is observed for high inlet temperatures (1300 K), showing considerable deviations when compared with the 3D PRS model. Minimum deviations were observed for $Y_{O_2,in} = 0.05$, being 3.6% for CO, 5.5% for CO_2 and 0.76% for the temperature inside the porous zone at different operating conditions. The effect of the axial dispersion coefficient (D_L) was also assessed, showing a considerable effect on the performance of the partial oxidation at high inflow gas temperatures (T_{in} = 1300-1500 K), when comparing 2D PMM approaches, thus, becoming a significant parameter to consider when simulating this phenomenon, where it is also crucial to consider geometrical features of the reactor, such as D_t/d_p and L_t/d_p. Furthermore, the effect of the thermal conductivity of the solid phase (λ_s) was discussed, fitting with good accuracy to the 3D PRS baseline model, incorporating a negligible value for λ_s, assuming hollow spheres (surface-based model).

Finally, the use of a uniform porosity value along the fixed-bed was validated by simulat-

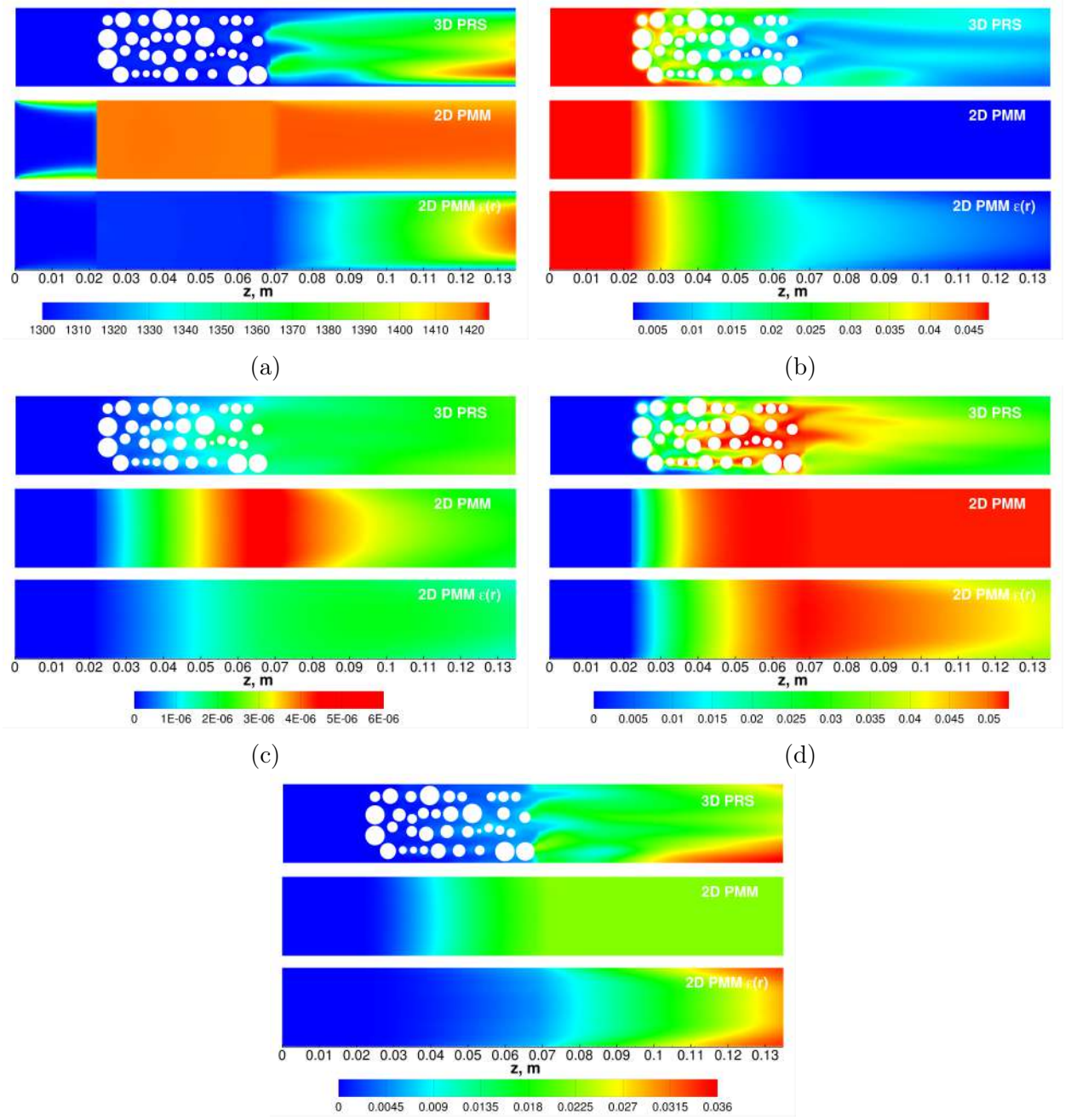

Figure 4.11: Contour plots of chemical species mass fractions (Y_i) predicted numerically using 3D PRS, 2D PMM, and 2D PMM for non-constant volume fraction of solid ($\varepsilon = f(r)$), see Fig. 4.10a) for $\mathrm{Re_{in}}$= 75, $\mathrm{Y_{O_2,in}}$ = 0.05, and T_{in} = 1300 K: T_{pz} (a), $\mathrm{Y_{O_2}}$ (b), $\mathrm{Y_{H_2}}$ (c), $\mathrm{Y_{CO}}$ (d), and $\mathrm{Y_{CO_2}}$ (e). Top plot shows results of 3D PRS, down plot depicts 2D PMM with $\varepsilon = f(r)$ and the middle plot shows 2D PMM with constant ε.

ing under the same conditions a variable porosity over radius $\varepsilon(r)$. Variation of the porosity showed significant differences with those using constant porosity due to the narrow D_t/d_p ratio used for this study, achieving good agreement with the 3D PRS model. In addition, results highlighted the relevance of geometrical features of the reactor, distinguishing effects of wall channeling and mass fraction dynamics of carbon monoxide and on heat transfer mechanism inside inert porous media reactors.

There is an important space to explore regarding numerical approaches for thermochemical conversion processes. Further studies are necessary to assess intrinsic chemical reactions (macro and micro-pore-level numerical studies, tracking of porosity and particle radius) for a single particle and for fixed-bed reactor problems, variation of the converted fuel and gasifying agent, geometrical features of the unit (D_t/d_p), and hybridization of the porous zone.

Acknowledgments

The authors would like to thank the National Agency for Research and Development (ANID) / Scholarship Program / DOCTORADO BECAS CHILE/2021 – 21211230, FONDECYT Project N°1241030, and the Natural Science and Engineering Research Council of Canada (NSERC) for their support.

References

[1] V.S. Babkin. Filtrational combustion of gases. present state of affairs and prospects. *Pure and Applied Chemistry*, 65:335–344, 1993.

[2] E. A. Salgansky, A. Yu Zaichenko, D. N. Podlesniy, M. V. Salganskaya, and M. Toledo. Coal dust gasification in the filtration combustion mode with syngas production. *International Journal of Hydrogen Energy*, 42:11017–11022, 4 2017. ISSN 03603199.

[3] J. Wang, S. Wei, Q. Wang, and B. Sunden. Transient numerical modeling and model

predictive control of an industrial-scale steam methane reforming reactor. *International Journal of Hydrogen Energy*, 46:15241–15256, 2021.

[4] A.G. Dixon. Local transport and reaction rates in a fixed bed reactor tube: Endothermic steam methane reforming. *Chemical Engineering Science*, 168:156–177, 2017.

[5] Zhiqing Zhang, Jiedong Ye, Dongli Tan, Zhiqiang Feng, Jianbin Luo, Yan Tan, and Yuanxing Huang. The effects of fe2o3 based doc and scr catalyst on the combustion and emission characteristics of a diesel engine fueled with biodiesel. *Fuel*, 290:120039, 2021.

[6] S. Manigandan, P. Vinoth Kumar, P. Arivalagan, S. Nižetić, and T. Praveenkumar. Production and utilization of pyrolysis oil from solidplastic wastes: A review on pyrolysis process and influence of reactors design. *Journal of environmental management*, 302: 114046, 2022.

[7] A.G. Dixon, M. Nijemeisland, and E.H. Stitt. Packed tubular reactor modeling and catalyst design using computational fluid dynamics. *Advances in Chemical Engineering*, 31:307–389, 2006.

[8] J. Wang, S. Hu, and X. Liu. Kinetic modelling and experimental validation of single large particle combustion of coal char. *Chemical Engineering Journal*, 450, 12 2022. ISSN 13858947.

[9] R. Meijer, H.J. Miihlen, F. Kapteijn, and J.A. Moulijn. Burn-off behaviour in alkali-catalysed co2 gasification of bituminous coal char: A comparison of tga and fixed-bed reactor. *Fuel Processing Technology*, 28:5–17, 1991.

[10] D.K. Park, S.D. Kim, S. Hoon Lee, and J. Goo Lee. Co-pyrolysis characteristics of sawdust and coal blend in tga and a fixed bed reactor. *Bioresource Technology*, 101: 6151–6156, 8 2010. ISSN 09608524.

[11] F. J. Weinberg. Combustion temperatures: The future? *Nature*, 233:239–241, 1971. ISSN 00280836.

[12] M.A. Mujeebu, M.Z. Abdullah, M.Z. Abu Bakar, A.A. Mohamad, R.M.N. Muhad, and M.K. Abdullah. Combustion in porous media and its applications - a comprehensive survey. *Journal of Environmental Management*, 90:2287–2312, 2009. ISSN 03014797.

[13] M.A. Mujeebu, M.Z. Abdullah, A.A. Mohamad, and M.Z. Abu Bakar. Trends in modeling of porous media combustion. *Progress in Energy and Combustion Science*, 36: 627–650, 2010. ISSN 03601285.

[14] M. Toledo, A. Arriagada, N. Ripoll, E. Salgansky, and M. Mujeebu. Hydrogen and syngas production by hybrid filtration combustion: Progress and challenges. *Renewable and Sustainable Energy Reviews*, 177:113213, 5 2023. ISSN 18790690.

[15] E. A. Salgansky, V. P. Fursov, S. V. Glazov, M. V. Salganskaya, and G. B. Manelis. Model of vapor-air gasification of a solid fuel in a filtration mode. *Combustion, Explosion and Shock Waves*, 42:55–62, 2006. ISSN 00105082.

[16] E.A. Salgansky, V.M. Kislov, S.V. Glazov, A.F. Zholudev, and G.B. Manelis. Filtration combustion of a carbon-inert material system in the regime with superadiabatic heating. *Combustion, Explosion and Shock Waves*, 44:273–280, 2008. ISSN 00105082.

[17] V.S. Gururajan, T.F. Wall, R.P. Gupta, and J.S. Truelove. Mechanisms for the ignition of pulverized coal particles. *Combustion and Flame*, 81(2):119–132, 1990. ISSN 0010-2180.

[18] D. Safronov, M. Kestel, P. Nikrityuk, and B. Meyer. Particle resolved simulations of carbon oxidation in a laminar flow. *Canadian Journal of Chemical Engineering*, 92: 1669–1686, 10 2014. ISSN 1939019X.

[19] A. Richter, P. Nikrityuk, and M. Kestel. Numerical investigation of a chemically reacting carbon particle moving in a hot o2/co2 atmosphere. *Industrial and Engineering Chemistry Research*, 52:5815–5824, 4 2013. ISSN 08885885.

[20] C. Hasse, P. Debiagi, X. Wen, K. Hildebrandt, M. Vascellari, and T. Faravelli. Advanced modeling approaches for cfd simulations of coal combustion and gasification. *Progress in Energy and Combustion Science*, 86:100938, 9 2021. ISSN 03601285.

[21] P.A. Libby and T.R. Blake. Burning carbon particles in the presence of water vapor. *Combustion and Flame*, 41:123–147, 1981.

[22] J.C. Lee, R.A. Yetter, and F.L. Dryer. Transient numerical modeling of carbon particle ignition and oxidation. *Combustion and Flame*, 101:387–398, 1995.

[23] S.Y. Cho, R.A. Yetter, and F.L. Dryer. A computer model for one-dimensional mass and energy transport in and around chemically reacting particles, including complex gas-phase chemistry, multicomponent molecular diffusion, surface evaporation, and heterogeneous reaction. *Journal of Computational Physics*, 102:160–179, 1992.

[24] R. Stauch and U. Maas. Transient detailed numerical simulation of the combustion of carbon particles. *International Journal of Heat and Mass Transfer*, 52:4584–4591, 9 2009. ISSN 00179310.

[25] Y. Qian, Y. Yu, G. Xu, and X. Liu. Cfd modeling of coal pyrolysis in externally heated fixed-bed reactor. *Fuel*, 233:685–694, 12 2018. ISSN 00162361.

[26] Y. Qian, J. Zhan, Y. Yu, G. Xu, and X. Liu. Cfd model of coal pyrolysis in fixed bed reactor. *Chemical Engineering Science*, 200:1–11, 6 2019. ISSN 00092509.

[27] C.B. Nguyen, M. Massoudi Farid, J. Scherer, Q. Guo, M. Gräbner, and A. Richter. A hybrid particle model with advanced conversion parameters and dynamic drag model applied for the cfd modeling of an entrained-flow gasifier. *Combustion and Flame*, 240, 6 2022. ISSN 15562921.

[28] A. Arriagada, M. Toledo, R.E. Hayes, and P.A. Nikrityuk. 3d study of a chemically reacting fixed-bed under gasification conditions for non-porous char: Laminar flow. *Journal of the Energy Institute*, 112:101489, 2 2024. ISSN 17439671.

[29] B. Vardhan Reddy Kuncharam and A.G. Dixon. Multi-scale two-dimensional packed bed reactor model for industrial steam methane reforming. *Fuel Processing Technology*, 200:106314, 2020.

[30] G.H. Fong, S. Jorgensen, and S.L. Singer. Pore-resolving simulation of char particle gasification using micro-ct. *Fuel*, 224:752–763, 7 2018. ISSN 00162361.

[31] S. Liu, F. Xu, B. Lu, W. Wang, Z. Liu, and Y. Wang. Porous-media model based particle-resolved simulation of a fixed bed with olefin catalytic cracking reaction. *Powder Technology*, 431:119099, 1 2024. ISSN 1873328X.

[32] C. Baliga and P. Nikrityuk. Convective heat transfer coefficient for the side-wall in a fixed bed. *Canadian Journal of Chemical Engineering*, 101(11):6151–6169, 2023.

[33] M. Toledo and C. Rosales. Hybrid filtration combustion. In *Hydrogen Energy - Challenges and Perspectives*, pages 201–222. IntechOpen, London, United Kingdom, 2012. ISBN 978-953-51-0812-2.

[34] N. Hanchate, S. Ramani, C.S. Mathpati, and V.H. Dalvi. Biomass gasification using dual fluidized bed gasification systems: A review. *Journal of Cleaner Production*, 280: 123148, 1 2021. ISSN 09596526.

[35] S. Safarian, R. Unnpórsson, and C. Richter. A review of biomass gasification modelling. *Renewable and Sustainable Energy Reviews*, 110:378–391, 8 2019. ISSN 18790690.

[36] J. A. Ruiz, M. C. Juárez, M. P. Morales, P. Muñoz, and M. A. Mendívil. Biomass gasification for electricity generation: Review of current technology barriers. *Renewable and Sustainable Energy Reviews*, 18:174–183, 2013. ISSN 13640321.

[37] R. Luque and J.G. Speight. *Gasification for Synthetic Fuel Production: Fundamentals, Processes and Applications*. Woodhead Publishing Series in Energy, 2015. ISBN 978-0-85709-802-3.

[38] M. Toledo and N. Ripoll. *Syngas Fuel Production from Carbonaceous Feedstocks Using Hybrid Porous Media*. IntechOpen, 9 2019.

[39] M. Toledo, N. Ripoll, J. Céspedes, A. Zbogar-Rasic, N. Fedorova, V. Jovicic, and A. Delgado. Syngas production from waste tires using a hybrid filtration reactor under different gasifier agents. *Energy Conversion and Management*, 172:381–390, 9 2018. ISSN 01968904.

[40] S.R. Turns. *An Introduction to Combustion: Concepts and Applications*. McGraw-Hill, New York City, USA, 2006. ISBN 9780072350449.

[41] W.P. Jones and R.P. Lindstedt. Global reaction schemes for hydrocarbon combustion. *Combustion and Flame*, 73(3):233–249, 1988.

[42] S. Schulze, P. Nikrityuk, F. Compart, A. Richter, and B. Meyer. Particle-resolved numerical study of char conversion processes in packed beds. *Fuel*, 207:655–662, 2017. ISSN 00162361.

[43] P. Nikrityuk and B. Meyer. Pseudo-steady-state approach for carbon particle combustion/gasification. In *Gasification Processes: Modeling and Simulation*, pages 205–244. Willey-VCH Verlag GmbH & Co, Weinheim, Germany, 9 2014. ISBN 9783527335503.

[44] A. Richter, M. Vascellari, P. Nikrityuk, and C. Hasse. Detailed analysis of reacting particles in an entrained-flow gasifier. *Fuel Processing Technology*, 144:95–108, 4 2016. ISSN 03783820.

[45] P.A. Nikrityuk, M. Gräbner, M. Kestel, and B. Meyer. Numerical study of the influence of heterogeneous kinetics on the carbon consumption by oxidation of a single coal particle. *Fuel*, 114:88–98, 2013. ISSN 0016-2361. Advances in Coal Science and Technology, ICCS&T 2011.

[46] J. Yu, K. Zhou, and W. Ou. Effects of stefan flow and co oxidation on char particle combustion in o2/co2 atmosphere. *Fuel*, 106:576–585, 2013. ISSN 00162361.

[47] C. Nguyen, J. Scherer, M. Hartwich, and A. Richter. The morphology evolution of char particles during conversion processes. *Combustion and Flame*, 226:117–128, 4 2021. ISSN 15562921.

[48] S. Kriebitzsch and A. Richter. Les simulation of char particle gasification at reynolds numbers up to 1000. *Combustion and Flame*, 211:185–194, 1 2020. ISSN 15562921.

[49] Inc. ANSYS. ANSYS-FLUENT™ V 2022R2 – Commercially available CFD software package based on the Finite Volume method. Southpointe, 275 Technology Drive, Canonsburg, PA 15317, U.S.A., 2022.

[50] S. Ergun. Fluid flow through packed columns. *Chemical Engineering Progress*, 48(2): 89–94, 1952.

[51] R.E. Hayes and J.P. Mmbaga. *Introduction to Chemical Reactor Analysis*. CRC Press, Taylor & Francis Group, Boca Raton, Florida, 2nd. edition, 2012. ISBN 9780429071515.

[52] E. Fuller, P. Schettler, and J. Giddings. New method for prediction of binary gas-phase diffusion coefficients. *Industrial & Engineering Chemistry*, 58(5):18–27, 1966.

[53] R.J. Kee, M.E. Coltrin, and P. Glarborg. *Chemically Reacting Flow: Theory and Practice*. John Wiley & Sons, 2005. ISBN 9780471461302.

[54] S.V. Patankar. *Numerical heat transfer and fluid flow*. Series on Computational Methods in Mechanics and Thermal Science. Hemisphere Publishing Corporation (CRC Press, Taylor & Francis Group), Florida, USA, 1980. ISBN 978-0891165224.

[55] G. Krishnamoorthy, R. Rawat, and P. Smith. Parallelization of the p-1 radiation model. *Numerical Heat Transfer, Part B: Fundamentals*, 49:1–17, 1 2006. ISSN 10407790.

[56] P.A. Bejarano and Y.A. Levendis. Single-coal-particle combustion in o2/n2 and o2/co2 environments. *Combustion and Flame*, 153:270–287, 4 2008. ISSN 00102180.

[57] S.P. Burke and T.E. Schumann. Kinetics of a type of heterogeneous reactions' the mechanism of combustion of pulverized fuel. *Industrial and Engineering Chemistry*, 23, 1931.

[58] F. Yi, J. Fan, D.Li, S. Lu, and K. Luo. Three-dimensional time-dependent numerical simulation of a quiescent carbon combustion in air. *Fuel*, 90:1522–1528, 4 2011. ISSN 00162361.

[59] M. Edwards and J. Richardson. Gas dispersion in packed beds. *Chemical Engineering Science*, 23(2):109–123, 1968.

[60] J. Delgado. A critical review of dispersion in packed beds. *Heat and Mass Transfer*, 42: 279–310, 2006.

[61] A. Jourak, J. Hellstrom, T. Lundstrom, and V. Frishfelds. Numerical derivation of dispersion coefficients for flow through three-dimensional randomly packed beds of monodisperse spheres. *AIChE Journal*, 60(2):749–761, 2014.

[62] S. Rastegar and T. Gu. Empirical correlations for axial dispersion coefficient and peclet number in fixed-bed columns. *Journal of Chromatography A*, 1490:133–137, 2017.

[63] R. Haghpanah, A. Majumder, R. Nilam, A. Rajendran, S. Farooq, I. Karimi, and M. Amanullah. Multiobjective optimization of a four-step adsorption process for post-combustion co2 capture via finite volume simulation. *Industrial & Engineering Chemistry Research*, 52(11):4249–4265, 2013.

[64] H. Ramos, C. Baliga, A. Rajendran, and P. Nikrityuk. Cfd-based model of adsorption columns: Validation. *Chemical Engineering Science*, 285:119606, 2024.

[65] Z. Guo, Z. Sun, N. Zhang, X. Cao, and M. Ding. Mean porosity variations in packed bed of monosized spheres with small tube-to-particle diameter ratios. *Powder Technology*, 354:842–853, 2019.

[66] R.E. Hayes. Simulation of mixed convection heat transfer at the wall of a packed bed. *Numerical Heat Transfer*, 17(2):217–230, 1990.

[67] A. De Klerk. Voidage variation in packed beds at small column to particle diameter ratio. *AIChE journal*, 49(8):2022–2029, 2003.

[68] G.E. Mueller. Radial void fraction distributions in randomly packed tied beds of uniformly sized spheres in cylindrical containers. *Powder Technology*, 72:269–275, 1992.

[69] S. Schulze, P.A. Nikrityuk, and B. Meyer. Porosity distribution in monodisperse and polydisperse fixed beds and its impact on the fluid flow. *Particulate Science and Technology*, 33(1):23–33, 2015.

[70] G.E. Mueller. Radial porosity in packed beds of spheres. *Powder Technology*, 203: 626–633, 11 2010.

Chapter 5

Solar-driven gasification for syngas production at low temperatures using a rotary hybrid porous media reactor[*]

[*]This chapter is based on the manuscript published in A. Arriagada, R. Mena, N. Ripoll, R.E. Hayes, P. Nikrityuk and M. Toledo, Chemical Engineering Journal, **2024**.

5.1 Abstract

Solar-based technologies play a crucial role in the energy transition towards a green circular economy. This work investigates the solar-driven steam gasification of carbon char particles at low temperatures using an indirectly irradiated rotary hybrid porous media reactor. The solar concentration system consists of a heliostat and parabolic dish with a focus on the emitter plate located at the bottom of the reactor, allowing allothermal conditions for hydrogen (H_2) and syngas production. The hybrid bed is composed of carbon and alumina particles randomly mixed in a 50/50 proportion in mass. Three sets were tested varying rotation speed of the unit, i.e., Set A (0 rpm), Set B (15 rpm), and Set C (20 rpm). Numerical simulations were performed using a one-dimensional model assessing mass, energy and chemical conservation equations, considering a semi-global kinetic scheme, including three homogeneous and four heterogeneous chemical reactions. The optical design configuration of the solar system, in addition to the high heat recirculation enhanced by the rotation of the reactor, allowed maximum temperatures of 662 K (outer surface) and 573 K (reaction chamber). At this low-temperature range, a good agreement between numerical simulations and experiments was achieved, observing a H_2/CO ratio of 0.088 (Set B) and 0.163 (Set C), representing a 5.7% and 3.1% deviation, respectively. Numerical results (1D approach) show an increase in the temperature would lead to a higher H_2/CO ratio production. Finally, a 3D-CFD based porous media model including char reacting particles is mathematically described. Further studies are necessary to assess hydrogen and syngas production under these operating conditions at high temperatures.

Keywords: Fixed-bed reactor, Gasification, Hybrid porous media, Hydrogen, Solar energy.

Nomenclature

Symbol	Definition
B_f	Solid fuel combustion rate, $\mathrm{kg} \cdot \mathrm{m}^{-3} \cdot \mathrm{s}^{-1}$
b	Arrhenius pre-exponential constant, -
C_p	Specific heat at constant pressure, $\mathrm{J} \cdot \mathrm{kg}^{-1} \cdot \mathrm{K}^{-1}$
D	Mass diffusion coefficient, $\mathrm{m}^2 \cdot \mathrm{s}^{-1}$
F	Ratio between the particles surface to the porous media volume, m^{-1}
H_v	Enthalpy release source term, $\mathrm{J} \cdot \mathrm{m}^{-3} \cdot \mathrm{s}^{-1}$
$k_\beta^{(v)}$	Pyrolysis kinetic rate, s^{-1}
Le	Lewis number, -
$\eta'_{j\alpha}$	Stoichiometric coefficient for reactants in homogeneous reactions, -
$\eta''_{j\alpha}$	Stoichiometric coefficient for products in homogeneous reactions, -
N_{SP}	Number of species considered, -
N_{HO}	Number of homogeneous reactions, -
N_{HE}	Number of heterogeneous reactions, -
p_0	Pressure on standard conditions, kPa
Q_{r_γ}	Standard heat of reaction, $\mathrm{J} \cdot \mathrm{mol}^{-1}$
$r_{b\alpha}$	Backward reaction rate, $\mathrm{mol} \cdot \mathrm{m}^{-3} \cdot \mathrm{s}^{-1}$
$r_{f\alpha}$	Forward reaction rate, $\mathrm{mol} \cdot \mathrm{m}^{-3} \cdot \mathrm{s}^{-1}$
$r_\gamma^{(H)}$	Heterogeneous reaction rate, $\mathrm{mol} \cdot \mathrm{m}^{-3} \cdot \mathrm{s}^{-1}$
S_j	Source term for j-th species, $\mathrm{mol} \cdot \mathrm{m}^{-3} \cdot \mathrm{s}^{-1}$
t	Time, s
T	Temperature, K
u_x	Filtration velocity, $\mathrm{m} \cdot \mathrm{s}^{-1}$
v_x	Combustion front propagation rate, $\mathrm{m} \cdot \mathrm{s}^{-1}$
$\nu'_{j\alpha}$	Stoichiometric coefficient for reactants in heterogeneous reactions
$\nu''_{j\alpha}$	Stoichiometric coefficient for products in heterogeneous reactions, -
W	Molecular weight, $\mathrm{kg} \cdot \mathrm{mol}^{-1}$
$\mathrm{y_j}$	Molar fraction of the j-th species in gaseous phase
μ	Molar fraction of volatiles released from the solid fuel, -
σ_j	Mass fraction of the j-th species in the volatiles, -
θ	Porosity, -
ρ	Density, $\mathrm{kg} \cdot \mathrm{m}^{-3}$
λ	Thermal conductivity, $\mathrm{W} \cdot \mathrm{m}^{-1} \cdot \mathrm{K}^{-1}$
ε	Fraction of heat retained in the solid phase, -
ξ	Global heat transfer coefficient, $\mathrm{W} \cdot \mathrm{m}^{-2} \cdot \mathrm{K}^{-1}$

5.2 Introduction

The development of solar-based technologies aligned with the Sustainable Development Goals (SDGs) of the United Nations (UN), in particular with affordable and clean energy (SDG 7),

still represents moderate and significant challenges for most of the OECD countries [1, 2]. In this scenario, solar-driven gasification has been demonstrated as a promising technology to use solar energy for the production of syngas [3], being a forceful path to utilize coal in a low-carbon way for the production of chemical feedstocks.

Coal, known for its abundance and energy density, continues to be a crucial solid fuel, supplying more than one-third of the world's electricity generation. Nevertheless, its constant use as a fuel has resulted in a global coal demand record high in 2022, rising by 4% year-on-year to 8.42 billion tonnes, and it is expected to reach a new record for 2023 (an increase of 1.4%) [4]. As a consequence, the low-carbon emission utilization of coal has gained interest as an essential research topic, coupling the process to carbon capture and development of renewable energy [5, 6].

Synthesis gas, commonly referred to as syngas, constitutes a significant blend of hydrogen (H_2), carbon monoxide (CO), and minor hydrocarbon components. Typically derived from the thermal degradation of carbonaceous feedstock, the production process varies based on the feedstock's form—gaseous, liquid, or solid—each requiring specific processes and technologies. Gaseous and liquid feedstocks are mostly processed by steam reforming, partial oxidation, and autothermal reforming or oxidative steam reforming [7, 8]. While with solid feedstock like coal, petroleum coke, or biomass, a previous stage is required: gasification, which usually occurs under autothermal conditions, where the same fuel is used to provide heat for the highly endothermic reactions, being partial oxidation the most common method used [9]. In general, the conventional gasification process does not meet a carbon-neutral requirement, which could be potentially addressed using renewable energy sources such as solar energy, and feedstocks, for driving the partial oxidation process.

Allothermal gasifiers, also known as indirect gasifiers, use an external source of energy to transform their feedstock into a gaseous fuel. In conventional gasifiers, one part of the carbonaceous fuel is burned with oxygen (O_2) to provide energy to drive the endothermic gasification reactions for syngas production. This results in syngas mixed with combustion products and other impurities, reducing its quality in the process. On the other side, high-quality syngas, produced by solar gasification has a higher energy output per unit of feedstock (with a theoretical energy upgrade of 33% [10]), up to 50% lower specific carbon

dioxide (CO_2) emissions and low (or no) tar content at gasification temperatures exceeding 1400 K [11, 12]. Therefore, the process becomes simpler in post-processing terms, however, an allothermal reactor requires an in-depth thermal design of the exchange surface/heat exchanger, as well as additional parts that are not needed in conventional autothermal gasifiers. Design configurations of allothermal gasifiers are similar to their autothermal counterparts, existing fixed-bed, fluidized bed, entrained flow, molten salt and rotary kiln gasifiers [13–16]. Replacing conventional gasification with concentrated solar radiation driven gasification has the following benefits: (1) The calorific value of syngas can be greater than that of the gasified fuel; (2) The gaseous products are not mixed with combustion products; (3) Pollutant emissions to the environment are reduced [12, 17, 18]; and (4) Solar energy is stored chemically, transforming an intermittent resource into an energy carrier available on demand, among other benefits [19].

In order to facilitate the design process, Steinfeld and Palumbo [20] proposed a classification centred on the interaction of the chemical reactions with solar energy. Two groups are singled, where the first considers directly irradiated reactors i.e., the chemical reactants are directly exposed to the concentrated solar radiation, and the second group considers the indirectly irradiated reactors, which use opaque external walls exposed to the concentrated solar radiation to transfer the absorbed heat into the reaction chamber. Heat transfer in allothermal gasifiers is a limiting condition to drive the endothermic reactions at a desired operational temperature. When operated on directly irradiated reactors, having a porous structure in the reaction zone (packed-bed, fluidized bed or porous foam), the main limiting heat transfer mechanism is the optical thickness of the media [21] and the heat transfer surface [22]. On the other hand, indirectly irradiated reactors are limited by the optical and thermal properties of the emitter plate. Heat is absorbed at the emitter plate and then transferred, through conduction, to the reaction chamber where heat is transferred mainly by radiation to the reactants [11].

Directly irradiated reactor designs have been proposed and implemented for the heating and/or thermochemical processing of particles, but, to the best of the authors' knowledge, have not been used for the gasification of carbonaceous feedstocks. A design approach of great interest to this study is the use of rotation in the reaction chamber. However, Alonso

et al. [23, 24] performed a critical review of the solar rotary kiln technology and reported that its application has only considered water-splitting thermochemical interactions, energy storage by chemical reduction of metals, thermal energy storage in sands, the detoxification of hazardous materials and aluminum recycling. Rotary reactors for the solar gasification of carbonaceous feedstocks have been only theoretically studied. In particular, Lu et al. [25–27] performed an analytical and numerical study on a novel centrifugal fluidized bed reactor for the steam gasification of char particles. Main findings of these studies are: (1) Rotational speed is the most relevant operating parameter to control particle residence time and conversion; (2) Increasing radiation had a positive net effect on the overall conversion, throughout rate and capital intensification; (3) The reactor inner diameter has a strong influence on the distribution of particles and the probability of particles deposition in the reactor's window; and (4) particle deposition rate in the window can be strongly correlated to the ratio of centrifugal to Stokes drag forces. Further works on rotary reactors for solar gasification of carbonaceous feedstocks were not found.

Like the directly irradiated designs, packed-bed and fluidized bed reactors have their equivalent indirectly irradiated design. Piatkowski et al. [28, 29] were the first to perform studies on the solar gasification of carbonaceous feedstocks in an indirectly irradiated packed-bed reactor. This reactor features an opaque emitter plate of SiC-coated graphite fibers to absorb the concentrated solar radiation and reradiate it to the reaction chamber, while remaining inert to the reducing atmosphere at the reactor's interior. To enhance the amount of radiation entering the cavity receiver, a CPC was incorporated at the reactor's aperture, and a fused quartz window was used to reduce reradiation losses to the environment. A benefit of the emitter plate is that it acts as a thermal shock absorber for possible variations on the energy input (intrinsic to solar energy).

An indirectly irradiated molten salt reactor design was theorized earlier by Trombe as a possible solution for stable gasification of carbonaceous feedstocks [30]. Gregg et al. analyzed its technical feasibility [31] and Bruckner presented a detailed account of the layout required for continuous operation [32] while Tamaura et al. performed experimental studies on a molten salt gasifier for the production of syngas using coal and CO_2 powered by electricity [33]. The first operational solar molten-salt indirectly irradiated reactor for the

dry gasification of cellulose was studied by Hathaway et al. in a fully allothermal mode [15] confirming the benefits of utilizing molten carbonate salts as a reaction interphase for the dry gasification of biomass. Later a hybrid autothermal operation was tested in the same reactor to produce hydrogen-rich syngas from the steam gasification of cellulose [34].

To the best of the authors' knowledge, there is no reported experimental research regarding solar-driven steam or dry gasification using an indirectly irradiated rotary hybrid porous media reactor. These units contain a mixture of solid fuel and inert particles composing a discrete porous bed for the simultaneous conversion of solid and gaseous fuels to H_2 and syngas [35], using air, steam, carbon dioxide, and premixed air/fuel flows as gasifying agents. During the autothermal process, the reaction wave propagates through the hybrid porous bed, sustaining simultaneous homogeneous and heterogeneous chemical reactions, naturally including the inherent features of porous media combustion [36–39].

This study aims to evaluate syngas production from sub-bituminous coal and steam at low temperatures using a pioneering coupled system, integrating concentrated solar energy and hybrid porous media technology, assessing air/steam supply ratio, and solar power, to better understand the behaviour of the allothermal indirectly irradiated reactor for improving the generation of syngas.

5.3 Materials and methods

In this section, the experimental setup and procedures are detailed through three subsections: solar field and solid fuel characterization, experimental apparatus, and experimental procedure. The construction of the reactor and the solar field design and setup configuration is provided in the Appendix of this thesis.

5.3.1 Solar field and solid fuel characterization

Experiments were conducted in a solar field consisting of a heliostat and a parabolic concentrator dish located at the Renewable Energy Laboratory (LER) from the Department of Mechanical Engineering of the Universidad Técnica Federico Santa María, in Viña del Mar, Chile (33°02'23.0"S, 71°29'09.3"W) (See Appendix section A.1). The optical design

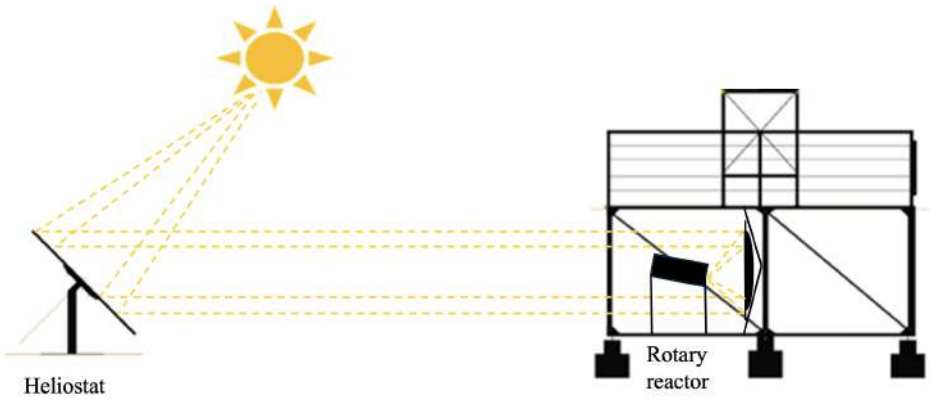

Figure 5.1: Optical design configuration of solar system.

configuration of the solar system is depicted in Figure 5.1. Tests were conducted using a flat-plate calorimeter to characterize temperature, irradiation, and power measurements of the tested experimental conditions (See Appendix section A.2).

The sub-bituminous coal sample was collected from Mina Invierno, located in the Riesco Island, in the local municipality of Rio Verde, Region of Magallanes and Chilean Antarctica. Ultimate analysis of the sub-bituminous coal was conducted using a Thermo Finnigan Flash EA Series 1112. Proximate analysis was performed following standards ASTM D-3173-11 (Moisture content), ASTM D3174-12 (Ash), and ASTM D3175-11 (Volatile matter). Values are summarized in Table 5.1, also comparing results with values reported in the literature.

Table 5.1: Comparison of ultimate and proximate analyses with literature data.

Solid fuel	C	H	O	N	S	MC	Ash	VM	FC
Measured	56.2±0.6	3.44±0.05	18.1±0.3	1.43±0.03	<0.45	6.71±0.01	12.7±0.3	38.8±0.8	41.79
[40]	44.0	3.5	11.6	1.2	0.8	3.6	37.3	23.6	35.5
[41]	74.9	5.33	16.96	2.28	0.47	17.14	6.84	34.2	41.82
[42]	54.41	5.19	32.40	1.15	0.99	13.54	5.86	42.62	37.98

5.3.2 Experimental apparatus

Figures 5.2 shows the schematics of the experimental setup, which consists of six main parts: supply and control lines; an atmospheric reactor; parabolic dish concentrator; thermocouples and data acquisition module; high precision steam generator; and finally, the reaction products sampling system. An actual picture of the experimental setup is shown in Figure 5.3 for future reference. The rotary reactor, depicted in Figure 5.4, has a reaction chamber

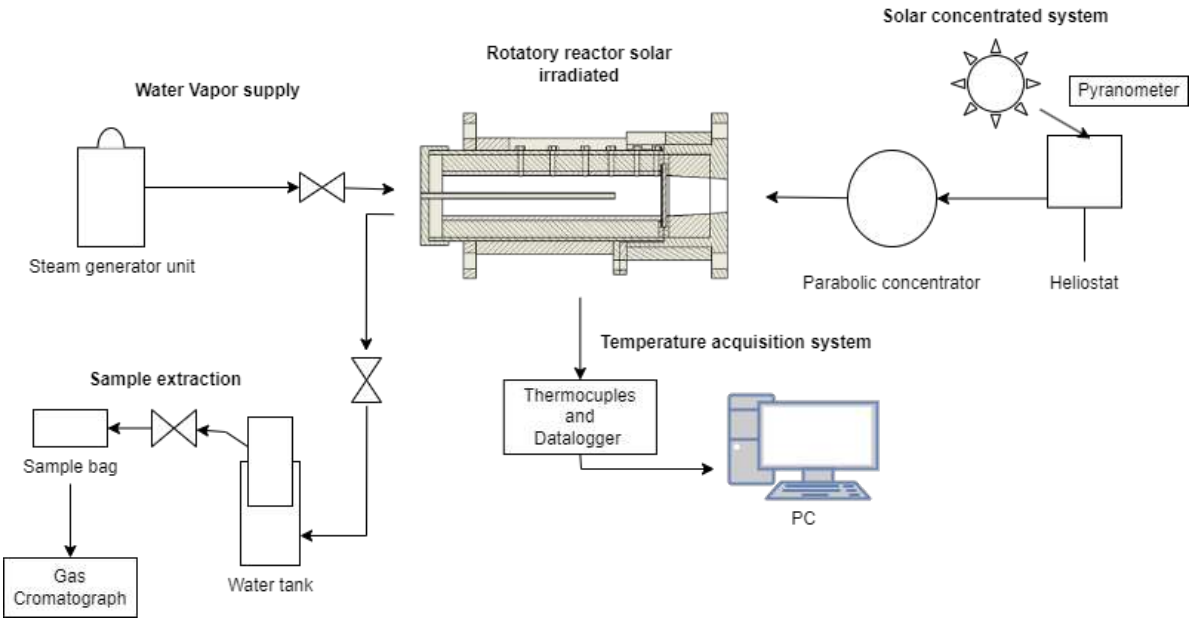

Figure 5.2: Schematic of the experimental setup.

of 1.062 L volume, and an inner diameter of 62 mm, where its cavity receiver inlet diameter is 50 mm. The rotary drive and supporting structure were designed to sustain inclinations from 0° to 60°. A stepper motor and a chain drive were used to rotate the reactor, while the control of the rotary system was performed by an Arduino UNO shield. The system can rotate from 5 rpm to 60 rpm and security mechanisms were incorporated to protect the user and the facility. Thermocouples are distributed over the reactor from a point near the emitting plate to the reactor seal cover (See Figure 5.4), registering the temperature every second during the experimental tests. T1 and T2 correspond to type S thermocouples, and T3 and T4 to type K thermocouples. The reactor was preliminarily characterized using an external heat source (replacing solar heat) to assess thermal profiles inside the unit (See Appendix section A.3).

5.3.3 Experimental procedure

In the first stage of the solar field's construction, a series of experiments were carried out, with the main focus on the analysis of the temperature recorded by the thermocouples and modifications of the solar concentration field, which can be seen in more detail in sections A.1 and A.2 of the Appendix. For each test, crucial parameters must be defined in order

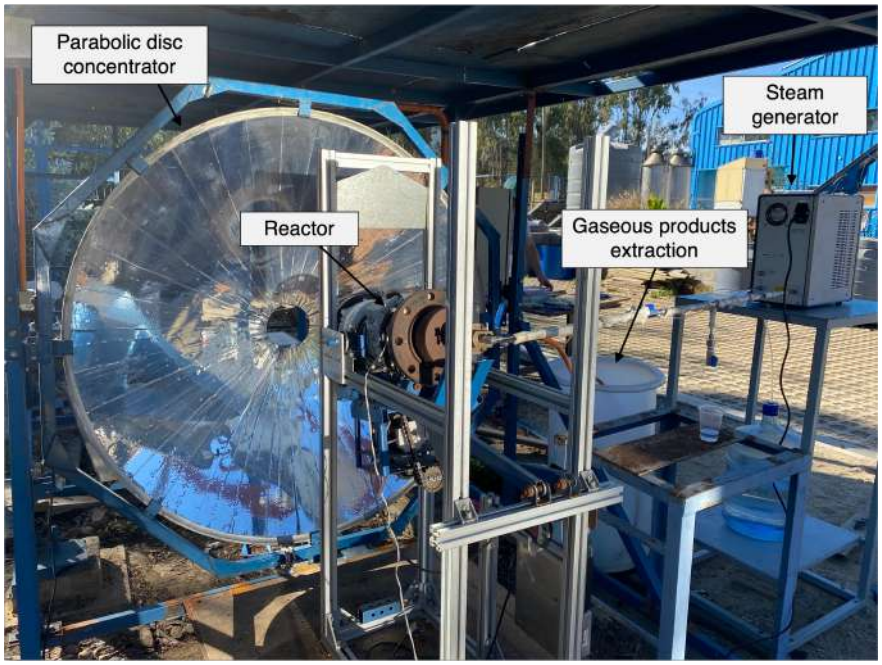

Figure 5.3: Experimental setup.

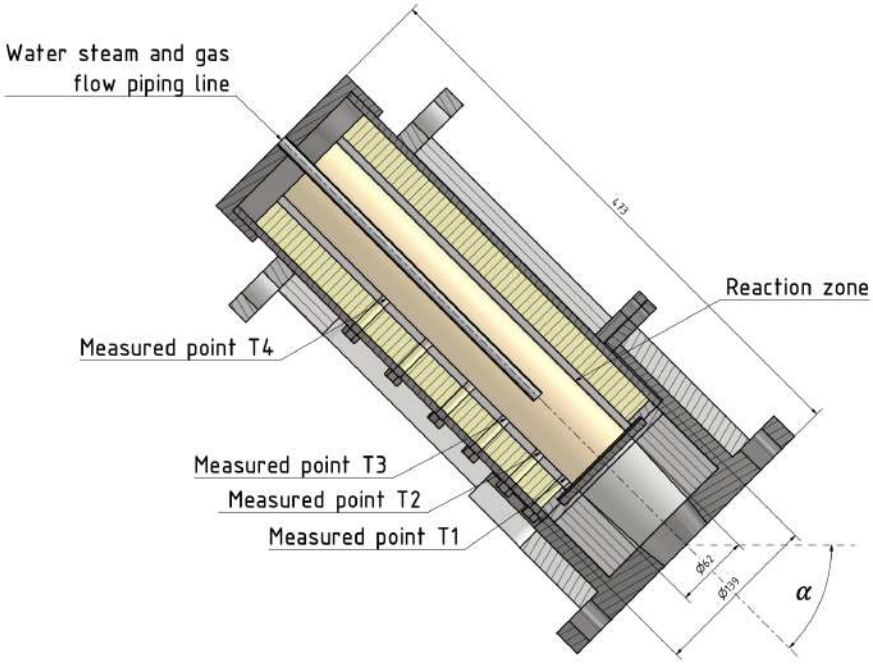

Figure 5.4: Reactor dimensions and thermocouples positions, measures in mm.

to prepare the system for conducting experiments, e.g., operating time, rotation speed, inclination, volume of carbonaceous material/alumina, and steam flow. The heliostat field, high-precision steam generator, and the reaction products sampling system for further gas chromatography follow an independent protocol for their proper functioning. Exhaust gases are captured using Tedlar bags, and subsequently analyzed in a Gas Chromatograph Series 600 GOW-MAC for the detection of H_2, CO, CH_4, CO_2 and hydrocarbons (HC) expressed as C_2H_6. Temperature acquisition within the reactor was performed wirelessly by means of an MCC134 shield coupled to a Raspberry Pi 3 B+ using four thermocouple holders. Datalogging was performed by custom software and allowed data measurement rates of 1 sample per second per channel on four analogue channels.

This study will cover three sets of experiments varying the rotation speed of the system: Set A (0 rpm), Set B (15 rpm), and Set C (20 rpm). An inclination angle of 15° was used for all experiments. The gasification of sub-bituminous coal inside the hybrid porous media reactor operates using batch mode. This reactor sets a baseline for continuous operation, considering its rotation and the feed of fuel at the top of the unit. The proportion between alumina and coal is 50% each from a mass perspective.

5.4 One-dimensional numerical model

This section will present a 1D numerical contrast with experiments, based on the hybrid filtration combustion (HFC) presented, and validated by Ripoll et al. [43]. To simulate the conditions within an allothermal reactor, a Dirichlet boundary condition was set at the "inlet" of the reactor, where the emitter plate is, and a Von Neumann boundary condition was set at the outlet of the reactor. The model considers the following assumptions:

1. There are no heat losses through the reactor walls.
2. The pressure drop across the reactor is negligible.
3. The porosity of the porous matrix is constant, and it is not affected by the local rearrangements of the fuel particles.

4. The linear combustion velocity of the reaction wave is considerably smaller than the filtration velocity of the gases.

5. There is no thermal equilibrium between the gaseous and solid phases.

6. Since it is an atmospheric reactor, methane is not considered in the volatiles.

7. The solid residue of the volatilization of coal is considered to be pure carbon (C).

8. The combustion wave velocity was lowered by two orders of magnitude to assimilate the lower reaction rate of a fully endothermic reaction led by the energy supplied from the emitter plate.

The governing equations of the hybrid porous media reactor model are described by Equations 5.1 to 5.4 as follows:

Conservation of mass for gaseous species:

$$\frac{\partial y_j}{\partial t} + u_x \frac{\partial y_j}{\partial x} - D \frac{\partial^2 y_j}{\partial x^2} = \frac{S_j}{\theta \rho_g} \tag{5.1}$$

Conservation of energy for gaseous species:

$$\frac{\partial T_g}{\partial t} + u_x \frac{\partial T_g}{\partial x} - LeD \frac{\partial^2 T_g}{\partial x^2} = \frac{H_V}{\theta c_{p_g} \rho_g} \tag{5.2}$$

Conservation of mass for solid species:

$$\frac{\partial \rho_f}{\partial t} + \boldsymbol{v_x} \frac{\partial \rho_f}{\partial x} = -\frac{B_f}{(1-\theta)} \tag{5.3}$$

Conservation of energy for solid species:

$$\frac{\partial T_S}{\partial t} + \boldsymbol{v_x} \frac{\partial T_S}{\partial x} - \frac{\lambda_S}{\left(\rho_f C_{P_f} + \rho_i C_{P_i}\right)} \frac{\partial^2 T_S}{\partial x^2} = -\frac{\varepsilon \sum_{\gamma=1}^{N_{HE}} r_\gamma^{(H)} Q_{R_\gamma} + \xi F \left(T_S - T_g\right)}{(1-\theta)\left(\rho_f C_{P_f} + \rho_i C_{P_i}\right)} \tag{5.4}$$

where the mass source term for the j-th gaseous species (S_j) and the enthalpy release term (H_V) are given by Equations 5.5 and 5.6, respectively, where thermal decomposition of

the solid fuel (I), formation of gaseous species due to homogeneous (II) and heterogeneous chemical reactions (III) are included.

$$S_j = \underbrace{\frac{(1-\theta)\cdot\rho_f}{W_j}\cdot k_\beta^{(v)}\cdot\mu\cdot\sigma_j}_{I} + \underbrace{\sum_{\alpha=1}^{N_{HO}}\left(\eta''_{j\alpha}-\eta'_{j\alpha}\right)\cdot\left(r_{f\alpha}-r_{b\alpha}\right)}_{\text{II}} + \underbrace{\frac{1}{W_S}\cdot\sum_{\gamma=1}^{N_{HE}}\left(v''_{j\gamma}-v'_{j\gamma}\right)\cdot r_\gamma^{(H)}}_{\text{III}} \tag{5.5}$$

$$H_V = \underbrace{-(1-\varepsilon)\frac{1}{W_S}\sum_{\gamma=1}^{N_{HE}} r_\gamma^{(H)} Q_{R\gamma}}_{I} + \underbrace{\sum_{j=1}^{N_{SP}} S_{j,v}\cdot h_j\left(T_S\right)}_{II} + \underbrace{\xi\cdot \mathrm{F}\cdot\left(T_S-T_g\right)}_{III} \tag{5.6}$$

Regarding the chemical kinetics, a simplified semi-global scheme was used, being composed of seven reactions, i.e., four heterogeneous, and three homogeneous. R2.1 represents the oxidation of carbon monoxide, R2.2 is the forward and backward water gas shift reaction, R2.6 is the Boudouard reaction. In addition, the kinetic parameters are shown in Table 5.2:

Table 5.2: Reaction mechanism and chemical kinetics factors [44].

	Reaction	ΔH^0 (MJ/kmol)	A ($\mathrm{mol/m^3\cdot s}$)	b $(-)$	E ($\mathrm{J/mol\cdot K}$)
R2.1	$2CO + O_2 \rightarrow 2CO_2$	-283	$3\cdot10^7$	0	118,832
R2.2	$CO + H_2O \leftrightarrow CO_2 + H_2$	-41	$2.78\cdot10^3$	0	104,423
R2.3	$H_2 + O_2 \rightarrow 2H_2O$	-242	$8.8\cdot10^4$	0	99,768
R2.4	$2C + O_2 \rightarrow 2CO$	-221	$2.5\cdot10^6$	0	131,000
R2.5	$C + O_2 \rightarrow CO_2$	-393	$1.6\cdot10^4$	0	98,000
R2.6	$C + CO_2 \rightarrow 2CO$	+172	$4.6\cdot10^2$	0	140,000
R2.7	$C + H_2O \rightarrow CO + H_2$	+131	$7.2\cdot10^4$	0	180,000

Simulations were performed using a one-dimensional model of hybrid porous media combustion considering 7 reactions and 6 species [43]. The experimental conditions consider a hybrid bed of 100 g of sub-bituminous coal and 100 g of alumina spheres with an average diameter of 5.6 mm. Therefore, considering their densities and assuming a porosity of 40%, the volumetric fraction of fuel in the hybrid bed is given by Equation 5.7:

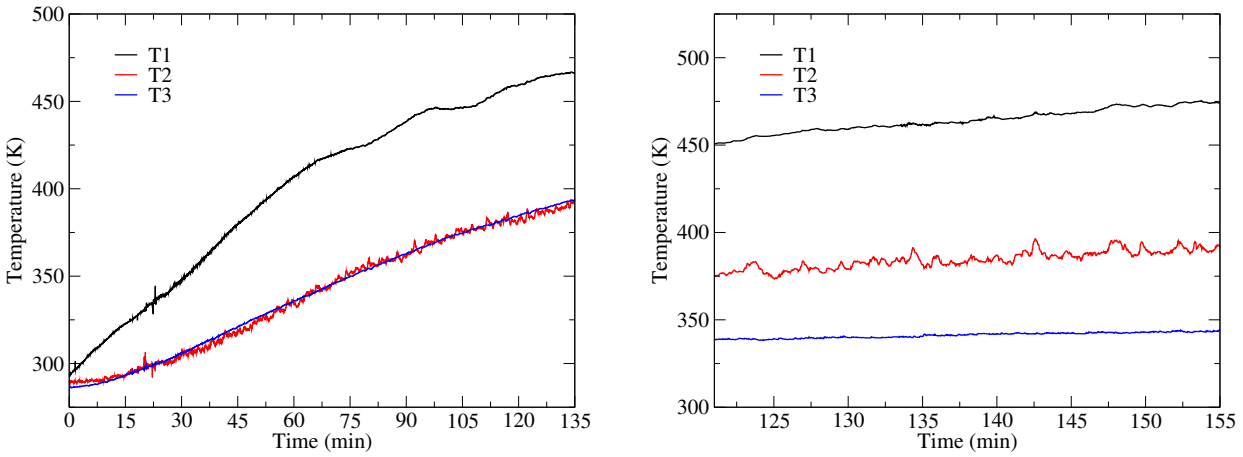

Figure 5.5: Temperature profile. (a) Set A (no rotation). (b) Set B (rotation).

$$\%_{\text{Fuel}} = \frac{\frac{100g}{850g/L} \cdot \frac{1}{0.4}}{\frac{100g}{850g/L} \cdot \frac{1}{0.4} + \frac{100g}{3987\frac{g}{L}} \cdot \frac{1}{0.4}} = 82.43\% \tag{5.7}$$

5.5 Results and discussion

5.5.1 Experimental tests

Firstly, Figure 5.5 shows the transient and stationary thermal profiles measured by thermocouples inside the reactor. Figure 5.5a shows a typical temperature profile of the reactor (Set A, no rotation) that takes approximately 135 min. T1 temperature profile presents the maximum temperature due to its near location close to the solar heating spot (emitter plate). T2 and T3 show similar behaviour in terms of achieved values for temperature, which could be attributed to the absence of rotation. Figure 5.5b shows that T1 presents the highest temperature (around 473 K) where the gasification process takes place due to the catalyst action of air/water vapour. T1 is higher than T2, and T2 is higher than T3, confirming the heat recirculation due to hybrid porous media and rotation of the system.

Thermographic camera TESTO 868 was used to evaluate the accuracy of the focal irradiation in the emitter plate of the reactor. Figure 5.6 shows images from the thermographic camera on the reactor plate and front flange. The maximum (PC1) and average (AV1) temperatures achieved are presented in Table 5.3. The left hand side of Figure 5.6 shows these

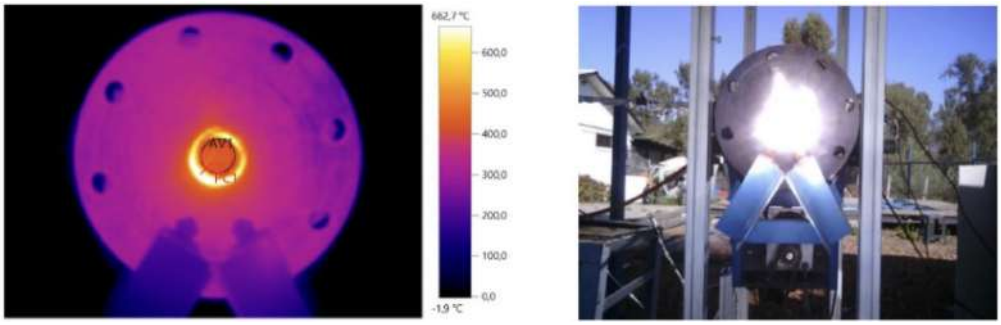

(a)

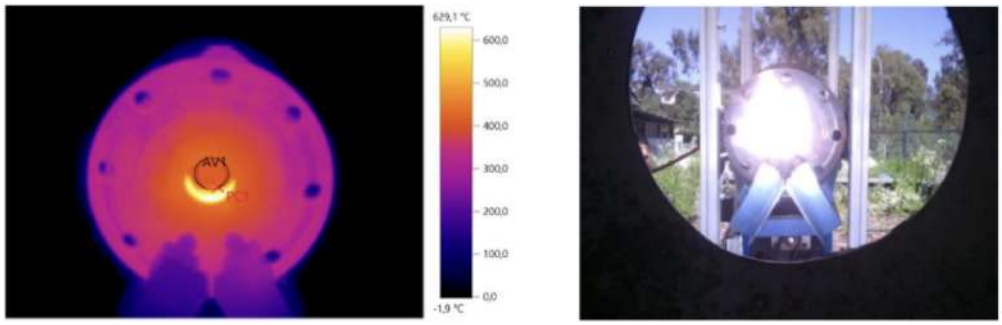

(b)

Figure 5.6: Thermographic camera images on reactor plate and front flange. Emissivity = 0.79. (a) Set A (no rotation) (b) Set B (rotation, 15 rpm).

reference points, where the software incorporated by the thermographic camera (Testo 868 Thermal Imager) reports the obtained values. Set A and Set B consider no rotation and rotation of the reactor, respectively, showing that the plate and front flange take similar high temperatures. These results confirm that the coal is gasified in the range of 473 K and 673 K approximately.

Table 5.3: Results of thermographic camera for different solar tests.

Parameter	Set A	Set B
Maximum temperature, K (PC1)	662.7	654.2
Average temperature, K (AV1)	622.5	610.6

Table 5.4 shows the gases produced (H_2, CO, CH_4 and CO_2) from the process according to the methodology. The majority of the products mixture is represented by carbon dioxide (CO_2) with values of 82.73%, 86.73%, and 90.46% for sets A, B, and C, respectively. The highest share of hydrogen (H_2) was achieved for set C, with a value of 1.27%. These results confirm syngas production at low temperatures for different configurations.

Table 5.4: Gaseous emissions for different solar tests.

Species	Set A (%)	Set B (%)	Set C (%)
Hydrogen (H_2)	0.5	1.02	1.27
Carbon monoxide (CO)	16.45	11.56	7.75
Carbon dioxide (CO_2)	82.73	86.73	90.46
Methane (CH_4)	0.19	0.51	0.39
HC expressed as C_2H_6	0.13	0.17	0.13

5.5.2 Numerical simulations and contrast with experiments

Taking into consideration the experimental conditions, the following set of numerical experiments was performed, using an 82.43% fuel, and 90% steam concentration (See Table 5.5). H_2/CO ratio is calculated on a basis of 100 moles of sample. These values are obtained directly from the gas chromatography as stated in Table 5.4. Differences between experiments and simulations regarding the H_2/CO ratio are 5.7% and 3.1% for sets B, and C, respectively. This shows a better accuracy of the model when the rotation system is active. On the other hand, when operating with a static reactor (Set A, no rotation), there is not a good agreement between experiments and numerics.

Table 5.5: Contrast experiments and numerical simulations of the process.

Set	AV1	H_2/CO exp.	H_2/CO sim.
A	622.5 K	0.030	0.088
B	610.6 K	0.088	0.093
C	496.5 K	0.163	0.158

Figures 5.7 and 5.8 present the simulated temperature distribution and species concentration profile within the reactor respectively, where each graph has a zoomed box with details on the solid (inert particles) and gas temperature near the emitter plate. Figure 5.7 shows higher solid temperature than gas temperature near the emitter plate. That is due to the stronger effect of conduction and radiation between the emitter plate and the solid phase of the reactants in immediate contact. After the first 5 mm, the solid and gas phase temperature profiles seemed to be perfectly aligned, this behaviour showcases the range of

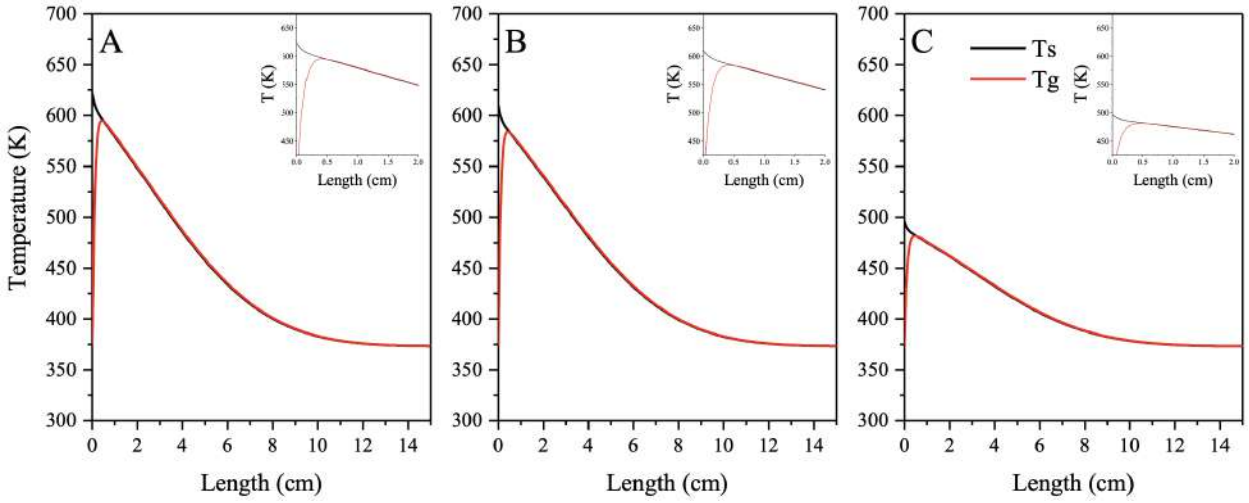

Figure 5.7: Temperature distribution inside the reactor for each test (Simulation).

effect of the emitter plate within the reactor and the increase of relevance of advection as a heat transfer mechanism within the reactor. A compact high-temperature zone is identified within the first 7 cm between the emitter plate and the porous bed, which can be explained by the limited heat transfer performance of the packed-bed at lower temperatures, observing an almost constant temperature profile after this point. Ng and Lipiński [45] highlighted in their theoretical study that for temperatures below 700 K, intermediate reactions do not take place, and is in the range from 700 K to 1,200 K that components such as C, CH_4, CO_2 and H_2O become unstable and their concentration decreases. Moreover, Figure 5.8 shows species concentrations along the reactor, where hydrogen and carbon monoxide were produced in the first part of the reactor (where the emitter plate is located). However, carbon dioxide (CO_2) presents the major concentration, which can be supported by the low availability of high temperature heat to drive the Water Gas Shift and the Boudouard reactions, both highly endothermic reactions that consume CO_2.

An additional set of numerical experiments was performed to observe the behaviour of syngas production, as well as H_2/CO ratio in the range of 400-1200 K within the reaction zone near the emitter plate, (See Figure 5.9). It is observed that the simulated data is in good agreement with the experimental measurements at low temperatures and that a minimum in the H_2/CO is expected to occur between 800 K and 900 K. This could be attributed to a change in the syngas production mechanism from the devolatilization process of coal to

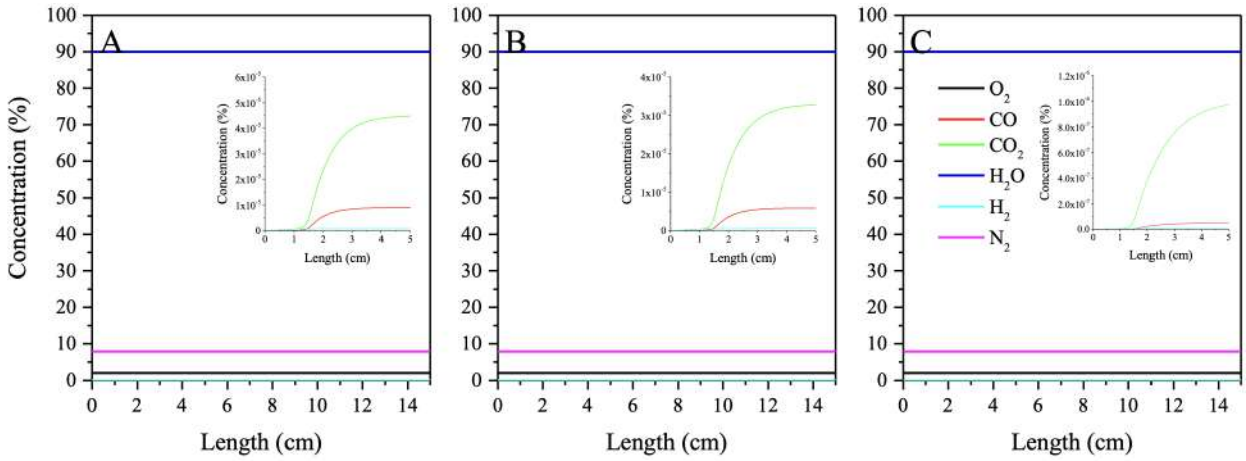

Figure 5.8: Species concentration profile inside the reactor for each test (Simulation).

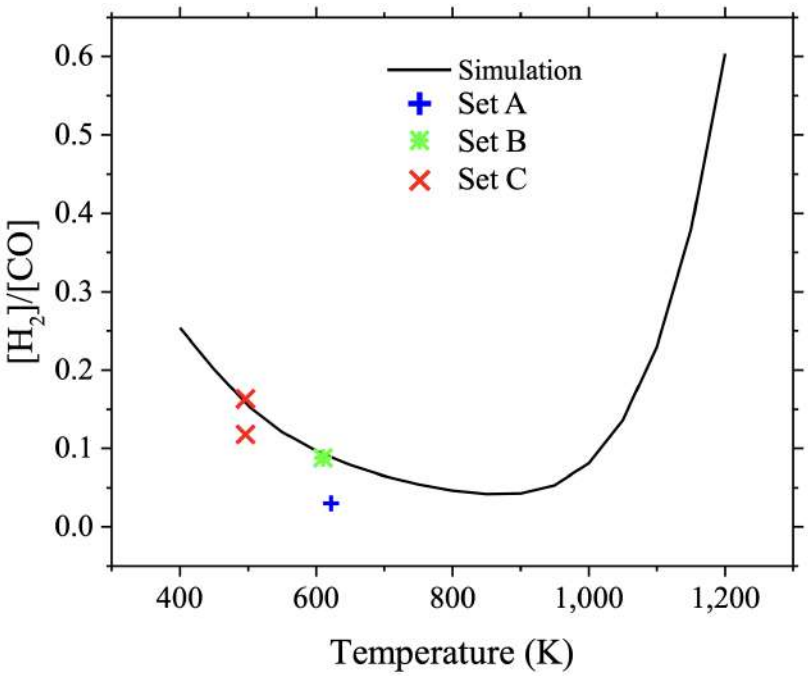

Figure 5.9: H_2/CO ratio for each test.

the steam gasification of the available coke, as well as to the WGS reaction favoured by the wide availability of steam inside the reactor. Results shown in Figure 5.8, and supported by experimental data from Figure 5.9 are of interest, illustrating the possible interactions at temperatures lower than 700 K within a hybrid porous bed.

5.6 Three-dimensional modeling of a hybrid porous media reactor

An extension of the mathematical modeling of a hybrid porous media reactor is now formulated using a 3D-CFD based porous media model including char reacting particles treated as porous, and inert solid particles. It is important to mention that this pseudo-steady-state (PSS) approach would require a significant amount of computational resources (+100 million cells). Just as a comparison, the 3D-CFD based particle-resolved simulations investigated in Chapter 2 were performed using 1.97 million cells regarding the mesh size. Thus, the solution of this model is not performed within this thesis. In addition, formulation of in-house user-defined-functions (UDFs) would be required for porosity, thermal conductivity, effective diffusivity. Considering an unsteady-state approach of the model would also require UDF for specific surface area (S''') and local porosity ($\varepsilon(X_C)$), based on carbon consumption rates (X_C). It is crucial to mention that converting this model into a solar-driven gasification process representation requires a solar boundary condition imposed at the inlet of the reactor.

5.6.1 Governing equations

The conservation equations (Equations 5.8 to 5.11) are described based on the following assumptions, as outlined in the literature [46, 47]:

- The porous zone is composed of monosized spherical carbon char particles and alumina spheres.
- Solid fuel particles as a continuously porous medium with initially isotropic properties.

- The ambient gas phase is considered isobaric with $p = 10^5$ Pa.
- The flow is laminar within the fluid domain.
- Devolatilization of the particles is not included due to the steady-state feature of the model.
- Porosity inside each solid fuel particle (ε_p) is considered as a constant value.
- The radiation model considered for simulations is the P-1 model.
- Thermal equilibrium is assumed for solid (inert, reacting particles) and gas phases.
- The influence of the wall channelling effect on the heat and mass transfer near the wall is neglected.
- The buoyancy effect is neglected.

Taking into account all assumptions made, the final system of equations has the following form [48, 49]:

Conservation equation for mass transport:

$$\nabla \cdot (\varepsilon \rho_g \vec{u}) = S_m \tag{5.8}$$

Conservation equation for momentum transport:

$$\nabla \cdot (\varepsilon \rho_g \vec{u}\vec{u}) = -\varepsilon \nabla p + \nabla \cdot (\varepsilon \overline{\overline{\tau}}) - \left(\frac{\varepsilon^2 \mu}{\alpha} \vec{u} + \frac{\varepsilon^3 C_2}{2} \rho_g |\vec{u}| \vec{u} \right) + S_m \vec{u} \tag{5.9}$$

Conservation equation for species transport:

$$\nabla \cdot (\varepsilon \rho_g \vec{u} Y_i) = \nabla \cdot (\varepsilon \rho_g D_{eff} \nabla Y_i) + \varepsilon R_i + S_{HO} \tag{5.10}$$

Conservation equation for energy transport:

$$\nabla \cdot (\varepsilon \rho_g \vec{u} h_g) = \nabla \cdot (\lambda_{eff} \nabla T) - \sum_i \varepsilon \frac{h_i^0}{M_i} R_i + Q_{HO} \tag{5.11}$$

where ε is the bed porosity, $\overline{\overline{\tau}} = \mu\left(\nabla\vec{u} + \nabla\vec{u}^{\mathrm{T}}\right)$ is the stress tensor. Species i is any reacting participant involved in the heterogeneous combustion process (HE), i.e., H_2O, O_2, H_2, CO, CO_2, D_{eff} is the mass diffusion coefficient, λ is the thermal conductivity, h_i is enthalpy, h^0 is the enthalpy of formation, M_i is molecular weight, Y_i is mass fraction, S_{HO} and Q_{HO} are the species and heat source terms due to homogeneous chemical reactions, respectively. R_i is the net production rate, and $\widehat{R}_{i,r}$ is the Arrhenius molar rate of creation/destruction for species i, respectively. These terms are described below, where $v''_{i,r}$ and $v'_{i,r}$ are the stoichiometric coefficients for reactants and products in the reaction r, $\eta'_{j,r}$ and $\eta''_{j,r}$ are the forward and backward rate exponents in the reaction r for each chemical species j.

$$R_i = M_i \sum_r \widehat{R}_{i,r} \tag{5.12}$$

$$\widehat{R}_{i,r} = \left(v''_{i,r} - v'_{i,r}\right)\left[k_r \prod_{j=1}^{N} C_{j,r}^{\left(\eta'_{j,r} - \eta''_{j,r}\right)}\right] \tag{5.13}$$

The source term incorporated in the continuity equation is calculated depending on the selected kinetic scheme (S''' is different in Chapters 3 and 4 since three heterogeneous chemical reactions were considered), and may be expressed in this case as:

$$S_m = S'''\left(\rho\frac{2M_{\mathrm{C}}}{M_{\mathrm{O_2}}}k_{\mathrm{R4}}Y_{\mathrm{O_2}} + \rho\frac{M_{\mathrm{C}}}{M_{\mathrm{O_2}}}k_{\mathrm{R5}}Y_{\mathrm{O_2}} + \rho\frac{M_{\mathrm{C}}}{M_{\mathrm{CO_2}}}k_{\mathrm{R6}}Y_{\mathrm{CO_2}} + \rho\frac{M_{\mathrm{C}}}{M_{\mathrm{H_2}O}}k_{\mathrm{R7}}Y_{\mathrm{H_2}O}\right) \tag{5.14}$$

The species source term due to homogeneous reactions (r, HO) can be calculated as:

$$S_{HO} = \varepsilon \sum_r \left(v'_{i,r} - v''_{i,r}\right) R_{r,HO} \tag{5.15}$$

The heat source term due to homogeneous reactions (r, HO) can be estimated as:

$$Q_{HO} = -\varepsilon \sum_r \Delta H_{r,HO} R_{r,HO} \tag{5.16}$$

The density of the gaseous mixture can be calculated as stated in Equation 5.17. Viscosity

and thermal conductivity are calculated using the kinetic theory [48].

$$\rho = \frac{P}{RT\sum_i \frac{Y_i}{M_i}} \tag{5.17}$$

The bed porosity (ε) can be described as a spatial distribution function as:

$$\varepsilon(r) = \begin{cases} 2.14z^2 - 2.53z + 1; & z \leq 0.637 \\ \varepsilon_b + 0.29\exp(-0.6z)[\cos(2.3\pi(z-0.16))] + 0.15\exp(-0.9z); & z > 0.637 \end{cases} \tag{5.18}$$

where $z = (R_t - r)/d_p$, r is the radius, d_p is particle diameter, R_t is the tube radius, and ε_b is the bulk porosity, which normally takes the value of 0.37.

The Blake-Kozeny equation may be used for calculating pressure drop, as described in Equation 5.19 [50]. The permeability (α) and inertial loss coefficient of flow (C_2) in the porous zone are described by Equation 5.20 and 5.21, respectively.

$$\frac{|\Delta p|}{L} = \frac{150\mu}{D_p^2}\frac{(1-\varepsilon)^2}{\varepsilon^3}v_\infty \tag{5.19}$$

$$\alpha = \frac{D_p^2}{150}\frac{\varepsilon^3}{(1-\varepsilon)^2} \tag{5.20}$$

$$C_2 = \frac{3.5}{D_p}\frac{(1-\varepsilon)}{\varepsilon^3} \tag{5.21}$$

The effective diffusivity ($D_{m,i}^{eff}$) can be calculated using Equation 5.22:

$$D_{m,i}^{eff} = \frac{\varepsilon_p}{\tau}\frac{1-x_i}{\sum \frac{x_i}{D_{ij}}} \tag{5.22}$$

where ε_p is particle porosity; τ is particle tortuosity; x_i is molar fraction of i th species; D_{ij} is binary diffusivity for $i-j$ th pair. D_{ij} is calculated from the Fuller correlation [51]:

$$D_{ij} = \frac{0.01013T^{1.75}}{p_t M^{0.5}\left(V_i^{1/3} + V_j^{1/3}\right)^2} \tag{5.23}$$

where $V_{i,j}$ - diffusion volume for i,j th species [52], i.e., $V_{\mathrm{CO_2}} = 26.9$, $V_{\mathrm{CO}} = 18.9$, $V_{\mathrm{H_2}} = 7.07$,

$V_{N_2} = 17.9$, $V_{O_2} = 16.6$, $V_{H_2O} = 12.7$. The thermal conductivity (λ_{eff}) inside the porous zone can be calculated using the porosity of the fixed-bed:

$$\lambda_{eff} = \varepsilon\lambda_g + (1-\varepsilon)\lambda_p \tag{5.24}$$

5.6.2 Boundary conditions

At the inlet of the fixed-bed reactor, the following Dirichlet boundary conditions are considered for inflow gas velocity, species mass fractions, and temperature, respectively:

$$\vec{u} = \vec{u}_{\text{in}}, \quad Y_i = Y_{i,\text{in}}, \quad T = T_{\text{in}} \tag{5.25}$$

where $\vec{u}_{\text{in}} = f(\text{Re}_{\text{in}})$, T_{in}, and $Y_{i,\text{in}}$ vary depending on the oxidative atmosphere ($\text{Y}_{\text{O}_2,\text{in}}$). At the outlet of the fixed-bed reactor, the so-called outflow boundary conditions with an overall mass balance correction would be implemented [48].

The convective heat transfer between the wall and ambient air can be calculated using Equation 5.26 [53]:

$$-\lambda_{\text{wr}} \left.\frac{\partial T_{\text{wr}}}{\partial n}\right|_{\text{wr}} = q''_{\Sigma} = (h_{\text{conv}} + h_{\text{rad}})\,(T_{\text{wr}} - T_{\infty}) \tag{5.26}$$

where h_{conv} and h_{rad} are the convective and radiative heat transfer coefficients, respectively. wr states for the wall of the reactor, and ∞ is ambient conditions.

Since there is an important interaction between gaseous and solid phases on the surface of the particles, mass and energy balance at the interface are affected by the heterogeneous chemical reactions (R4 to R7), due to the production and destruction rates of gaseous species caused by these reactions along with convective and diffusive mass fluxes of the gas phase species at the surface of particles [54]. A crucial parameter for heterogeneous chemical reactions is the specific surface area of the porous zone (S'''), which would be an input value obtained from analytical determination. Functions for effective diffusivity and thermal conductivity in the porous zone must be implemented into the software through a user-defined-function (UDF), where the DEFINE macros of DEFINE_DIFFUSIVITY and

DEFINE_PROPERTY should be used respectively.

5.7 Conclusions

In this work, hydrogen and syngas production from sub-bituminous coal and steam at low temperatures using a pioneering coupled system, integrating concentrated solar energy and hybrid porous media technology was assessed. A facility for concentrated solar thermochemistry applications was developed to study a novel design of a rotary kiln using solid fuels mixed with inert particles. The optical design configuration of the solar system (two-axis heliostat and a parabolic concentrator dish) allowed allothermal gasification conditions in an indirectly irradiated process.

Three sets were experimentally tested varying rotation speed of the unit, i.e., Set A (0 rpm), Set B (15 rpm), and Set C (20 rpm). Results showed gasification temperatures in the range of 496.5 K and 662.7 K achieving H_2/CO ratios of 0.030, 0.088, and 0.163 for Set A, B and C, respectively. Numerical simulations at low temperatures showed the conversion of sub-bituminous coal into hydrogen and syngas in the range of 400-700 K within the reaction zone near the emitter plate, observing a good agreement with experiments. These numerical and experimental results confirm the effects of the heat transfer mechanisms inside the reaction chamber and the consistency of the kinetic scheme used in this study.

An increase in the temperature process (>900 K) would lead to a higher H_2/CO ratio production mainly due to the activation of the kinetic scheme, specially homogeneous chemical reactions, e.g., carbon monoxide oxidation. Thus, further studies are recommended to assess a better integration between the solar experimental setup and the reactor to improve its performance, achieving higher gasification temperatures and a larger H_2/CO ratio.

Acknowledgments

The authors would like to thank the support of the National Agency for Research and Development (ANID) / Scholarship Program / DOCTORADO BECAS CHILE/2021 – 21211230, FONDECYT Project N°1241030, SERC Chile FONDAP 1523A0006, and the Natural Sci-

ence and Engineering Research Council of Canada (NSERC).

References

[1] J. He, Y. Yang, Z. Liao, A. Xu, and K. Fang. Linking sdg 7 to assess the renewable energy footprint of nations by 2030. *Applied Energy*, 317:119167, 2022.

[2] J. Sachs, G. Lafortune, G. Fuller, and E. Drumm. Implementing the sdg stimulus. *Sustainable development report*, 2023.

[3] P.G. Loutzenhiser and A.P. Muroyama. A review of the state-of-the-art in solar-driven gasification processes with carbonaceous materials. *Solar Energy*, 156:93–100, 2017.

[4] IEA International Energy Agency. Coal 2023 - analysis and forecast to 2026, 2023. URL `www.iea.org`.

[5] X. Zhao, X. Ma, B. Chen, Y. Shang, and M. Song. Challenges toward carbon neutrality in china: Strategies and countermeasures. *Resources, Conservation and Recycling*, 176: 105959, 2022.

[6] T. Wilberforce, A.G. Olabi, E.T. Sayed, K. Elsaid, and M.A. Abdelkareem. Progress in carbon capture technologies. *Science of The Total Environment*, 761:143203, 2021.

[7] A. Haryanto, S. Fernando, N. Murali, and S. Adhikari. Current status of hydrogen production techniques by steam reforming of ethanol: a review. *Energy & Fuels*, 19(5): 2098–2106, 2005.

[8] L. Braga, J. Silveira, M. Da Silva, C. Tuna, E. Machin, and D. Pedroso. Hydrogen production by biogas steam reforming: A technical, economic and ecological analysis. *Renewable and Sustainable Energy Reviews*, 28:166–173, 2013.

[9] K. Liu, C. Song, and V. Subramani. *Hydrogen and syngas production and purification technologies*. John Wiley & Sons, 2010.

[10] N. Piatkowski, C. Wieckert, A.W. Weimer, and A. Steinfeld. Solar-driven gasification of carbonaceous feedstock—a review. *Energy & Environmental Science*, 4(1):73–82, 2011.

[11] N. Piatkowski and A. Steinfeld. Solar gasification of carbonaceous waste feedstocks in a packed-bed reactor—dynamic modeling and experimental validation. *AIChE Journal*, 57(12):3522–3533, 2011.

[12] C. Wieckert, A. Obrist, P. Von Zedtwitz, G. Maag, and A. Steinfeld. Syngas production by thermochemical gasification of carbonaceous waste materials in a 150 kwth packed-bed solar reactor. *Energy & Fuels*, 27(8):4770–4776, 2013.

[13] C. Higman and S. Tam. Advances in coal gasification, hydrogenation, and gas treating for the production of chemicals and fuels. *Chemical Reviews*, 114(3):1673–1708, 2014.

[14] A. Donatelli, P. Iovane, and A. Molino. High energy syngas production by waste tyres steam gasification in a rotary kiln pilot plant. experimental and numerical investigations. *Fuel*, 89(10):2721–2728, 2010.

[15] B.J. Hathaway and J.H. Davidson. Demonstration of a prototype molten salt solar gasification reactor. *Solar Energy*, 142:224–230, 2017.

[16] J. Li, Y. Xie, K. Zeng, G. Flamant, H. Yang, X. Yang, D. Zhong, Z. Du, and H. Chen. Biomass gasification in molten salt for syngas production. *Energy*, 210:118563, 2020.

[17] D. Trommer and A. Steinfeld. Kinetic modeling for the combined pyrolysis and steam gasification of petroleum coke and experimental determination of the rate constants by dynamic thermogravimetry in the 500- 1520 k range. *Energy & Fuels*, 20(3):1250–1258, 2006.

[18] S.D. Kenarsari and Y. Zheng. Co2 gasification of coal under concentrated thermal radiation: A numerical study. *Fuel Processing Technology*, 118:218–227, 2014.

[19] T. Kodama, S. Bellan, N. Gokon, and H.S. Cho. Particle reactors for solar thermochemical processes. *Solar Energy*, 156:113–132, 2017.

[20] A. Steinfeld and R. Palumbo. Solar thermochemical process technology. *Encyclopedia of Physical Science and Technology*, 15(1):237–56, 2001.

[21] P. Furler, J. R. Scheffe, D. Marxer, and A. Steinfeld. Solar thermochemical CO2 splitting using a reticulated porous ceria redox system. *Energy & Fuels*, 26:7051–7059, 2012.

[22] T. Kodama, S. Enomoto, T. Hatamachi, and N. Gokon. Application of an Internally Circulating Fluidized Bed for Windowed Solar Chemical Reactor with Direct Irradiation of Reacting Particles. *Journal of Solar Energy Engineering*, 130(1):014504, 2008. ISSN 01996231.

[23] E. Alonso, A. Gallo, M. I. Roldán, C. A. Pérez-Rábago, and E. Fuentealba. Use of rotary kilns for solar thermal applications: Review of developed studies and analysis of their potential. *Solar Energy*, 144:90–104, 2017.

[24] E. Alonso and M. Romero. Review of experimental investigation on directly irradiated particles solar reactors. *Renewable and Sustainable Energy Reviews*, 41:53–67, 2015. ISSN 18790690.

[25] Z. Lu, M. Jafarian, M. Arjomandi, and G. J. Nathan. Analytical assessment of a novel rotating fluidized bed solar reactor for steam gasification of char particles. *Solar Energy*, 140:113–123, 2016.

[26] Z. Lu, M. Jafarian, A. Chinnici, M. Arjomandi, and G. J. Nathan. Flow behavior inside a novel rotating fluidized bed for solar gasification of biomass. *AIP Conference Proceedings*, 1850, 2017. ISSN 15517616.

[27] Z. Lu, A. Chinnici, M. Jafarian, M. Arjomandi, and G. J. Nathan. Numerical investigation of the isothermal flow field and particle deposition behaviour in a rotating fluidized bed solar receiver. *Solar Energy*, 182:348–360, 2019.

[28] N. Piatkowski, C. Wieckert, and A. Steinfeld. Experimental investigation of a packed-bed solar reactor for the steam-gasification of carbonaceous feedstocks. *Fuel Processing Technology*, 90(3):360–366, 2009. ISSN 03783820.

[29] N. Piatkowski and A. Steinfeld. Solar-driven coal gasification in a thermally irradiated packed-bed reactor. *Energy & Fuels*, 22(3):2043–2052, 2008. ISSN 08870624.

[30] F. Trombe. Solar furnaces and their applications. *Solar Energy*, 1(2-3):9–15, 1957.

[31] D. W. Gregg, R. W. Taylor, J. H. Campbell, and W. R. Aiman. Solar Coal Gasification. *Solar Energy*, 24(3):313–321, 1980. ISSN 0146955X.

[32] A. P. Bruckner. Continuous duty solar coal gasification system using molten slag and direct-contact heat exchange. *Solar Energy*, 34(3):239–247, 1985.

[33] Y. Tamaura, M. Tsuji, S. Yoshida, O. Yokota, and T. Sano. Solar gasification of coal using carbonate molten salt reactor. *Journal De Physique. IV : JP*, 9(3):0–5, 1999. ISSN 11554339.

[34] B. J. Hathaway and J. H. Davidson. Autothermal hybridization and controlled production of hydrogen-rich syngas in a molten salt solar gasifier. *International Journal of Hydrogen Energy*, 46(29):15257–15267, 2021. ISSN 03603199.

[35] M. Toledo, A. Arriagada, N. Ripoll, E. Salgansky, and M. Mujeebu. Hydrogen and syngas production by hybrid filtration combustion: Progress and challenges. *Renewable and Sustainable Energy Reviews*, 177:113213, 5 2023. ISSN 18790690.

[36] M.A. Mujeebu, M.Z. Abdullah, M.Z. Abu Bakar, A.A. Mohamad, R.M.N. Muhad, and M.K. Abdullah. Combustion in porous media and its applications - a comprehensive survey. *Journal of Environmental Management*, 90:2287–2312, 2009. ISSN 03014797.

[37] M.A. Mujeebu, M.Z. Abdullah, M.Z. Abu Bakar, A.A Mohamad, and M.K. Abdullah. A review of investigations on liquid fuel combustion in porous inert media. *Progress in Energy and Combustion Science*, 35(2):216–230, 2009.

[38] S. Wood and A.T. Harris. Porous burners for lean-burn applications. *Progress in Energy and Combustion Science*, 34(5):667–684, 2008.

[39] F. J. Weinberg. Combustion temperatures: The future? *Nature*, 233:239–241, 1971. ISSN 00280836.

[40] I. Rodilla, M.L. Contreras, and A. Bahillo. Thermogravimetric and mass spectrometric (tg-ms) analysis of sub-bituminous coal-energy crops blends in n2, air and co2/o2 atmospheres. *Fuel*, 215:506–514, 2018.

[41] H. Liu, Z. Li, Y. Yang, G. Miao, and Y. Han. Effects of oxidation on physical and chemical structure of a low rank sub-bituminous coal during the spontaneous combustion latency. *Energy*, 272:127122, 2023.

[42] J. Rizkiana, H.N. Firdausi, R. Pranata, G. Aulia, S.F. Maulana, W. Wulandari, and D. Sasongko. Pretreatment of coal by acid leaching as feedstock preparation for co-gasification with biomass. In *IOP Conference Series: Materials Science and Engineering*, volume 543, page 012067. IOP Publishing, 2019.

[43] N. Ripoll, E. Salgansky, and M. Toledo. Volatiles effects on the thermal and chemical structures of h2 production in a hybrid porous media reactor using solar steam. *International Journal of Heat and Mass Transfer*, 177:121472, 2021.

[44] E. A. Salgansky, V. M. Kislov, S. V. Glazov, A. F. Zholudev, and G. B. Manelis. Filtration combustion of a carbon-inert material system in the regime with superadiabatic heating. *Combustion, Explosion and Shock Waves*, 44:273–280, 2008. ISSN 00105082.

[45] Y.C. Ng and W. Lipiński. Thermodynamic analyses of solar thermal gasification of coal for hybrid solar-fossil power and fuel production. *Energy*, 44(1):720–731, 2012. ISSN 03605442.

[46] C. Nguyen, J. Scherer, M. Hartwich, and A. Richter. The morphology evolution of char particles during conversion processes. *Combustion and Flame*, 226:117–128, 4 2021. ISSN 15562921.

[47] S. Kriebitzsch and A. Richter. Les simulation of char particle gasification at reynolds numbers up to 1000. *Combustion and Flame*, 211:185–194, 1 2020. ISSN 15562921.

[48] Inc. ANSYS. ANSYS-FLUENT™ V 2022R2 – Commercially available CFD software package based on the Finite Volume method. Southpointe, 275 Technology Drive, Canonsburg, PA 15317, U.S.A., 2022.

[49] A. Arriagada-Romero, M. Toledo, R.E. Hayes, D. Pashchenko, and P.A. Nikrityuk. Verification of a porous media model for the partial oxidation of a chemically reacting fixed-bed. *Fuel*, 375:132582, 2024.

[50] S. Ergun. Fluid flow through packed columns. *Chemical Engineering Progress*, 48(2): 89–94, 1952.

[51] R.E. Hayes and J.P. Mmbaga. *Introduction to Chemical Reactor Analysis*. CRC Press, Taylor & Francis Group, Boca Raton, Florida, 2nd. edition, 2012. ISBN 9780429071515.

[52] E. Fuller, P. Schettler, and J. Giddings. New method for prediction of binary gas-phase diffusion coefficients. *Industrial & Engineering Chemistry*, 58(5):18–27, 1966.

[53] H. Fabian-Ramos, C. Baliga, A. Rajendran, and P.A. Nikrityuk. Cfd-based studies of scaled-up adsorption columns. *Chemical Engineering Journal*, 500:156797, 2024.

[54] R.J. Kee, M.E. Coltrin, and P. Glarborg. *Chemically Reacting Flow: Theory and Practice*. John Wiley & Sons, 2005. ISBN 9780471461302.

Chapter 6

Conclusions and Recommendations

As general conclusion, a comprehensive study of the solar thermochemical gasification of solid fuels in a hybrid porous media reactor and a chemically reacting fixed-bed was undertaken. The investigation encompassed experimental and numerical modeling, with special emphasis on the complexity of heterogeneous chemical reactions, temperature and concentration profiles, oxidative regimes, and the effect of crucial parameters for further experiment designing, along with experimental results regarding hydrogen production at low temperatures within a solar gasifier. Particularly, each chapter is specifically summarized in the following paragraphs:

This doctoral thesis starts with an extended literature review regarding hydrogen (H_2) and syngas production by thermochemical processes, focusing on inert porous media combustion (IPM) and hybrid filtration combustion (HFC), which were identified as viable approaches for operating in autothermal and allothermal conditions for hydrogen and syngas production. The heat recirculation inside porous media reactors enables high temperatures in the reaction wave, thus sustaining simultaneous homogeneous and heterogeneous reactions. The latter takes place on the gas-solid interface for the gasification of solid carbonaceous materials, which is the focus of Chapters 2, 4, and 3.

The subsequent section of this work focused on a computational investigation of the combustion of char particles in a fixed-bed using a three-dimensional model. Numerical simulations were carried out using the commercial software Ansys® Fluent, implementing a six semi-global kinetic scheme, where carbon monoxide combustion, forward and backward water-gas-shift reaction (WGS), Boudouard reaction, and two other heterogeneous reactions take place inside the reactor composed of 85 spherical particles. The diameter of the particles was 5.6 mm, following experimental data from the literature. Laminar flow regime ($Re_{in} = 50$, 75 and 100), inflow gas temperature in the range of 900-1500 K, and mass fraction of oxygen at the inlet ($Y_{O_2,in}$) of 0.05, 0.11, and 0.233 were the parameters of interest to study the heterogeneous combustion of carbon char particles inside the unit. The Boudouard reaction and oxidation of carbon monoxide were dominant among heterogeneous and homogeneous chemical reactions, respectively, being the inflow gas temperature a critical parameter to assess, since the kinetic scheme is dramatically activated at higher temperatures. A linear dependency has been found for species concentration and temperature profile in most of the

simulations using $Y_{O_2,in} = 0.05$.

In the following study, the feasibility of a 2D axisymmetric porous media model to represent a 3D particle-resolved fixed-bed model was numerically investigated. The simulation conditions and parameters under study were as implemented in the previous work. Important deviations were observed at T_{in} = 1300 K. Minimum deviations when comparing 3D PRS and 2D PMM models were observed for $Y_{O_2,in} = 0.05$, being 3.6% for CO, 5.5% for CO_2 and 0.76% for temperature inside the porous zone at different operating conditions. Thermal conductivity of the solid material, axial dispersion coefficient, and radial variation of porosity are analysed and discussed, showing good agreement between numerical models, remarking the role of geometrical features of the unit in the gasification process.

Then, a comparative computational study of the heterogeneous combustion of a single spherical carbon char particle in hot atmospheres with different O_2 concentrations using porous media model (PMM) and macro-pore-resolved simulations (PRS) was numerically investigated. A two-dimensional axisymmetric computational fluid dynamics model (2D CFD) in a pseudo-steady-state approach (PSS) was performed. Several Reynolds numbers (Re_{in} = 10, 50, and 100), inflow gas temperatures (T_{in} = 1100-2000 K), and inlet mass fractions of oxygen ($Y_{O_2,in}$ = 0.05 and 0.11) are assessed. Results showed good agreement between PMM and PRS, specially for T_{in} = 2000 K, where the deviation in the values for species was not higher than 8.3%. Maximum deviation for CO_2 was 1.54% when evaluating the maximum values for species concentration. In addition, the effects of the gasifying conditions, oxidative regime, and tortuosity on the partial oxidation process were discussed.

On the other hand, the experimental results of solar-driven gasification had the main purpose of investigating the use of an indirectly irradiated rotary hybrid porous media reactor for hydrogen production, located at Renewable Energy Laboratory (LER) of the Department of Mechanical Engineering at the UTFSM, Chile. The solar concentration system consists of a heliostat and parabolic dish with a focus on the emitter plate located at the bottom of the reactor, allowing allothermal conditions for hydrogen (H_2) and syngas production. The hybrid bed was composed of carbon and alumina particles randomly mixed in a 50/50 proportion in mass. Three sets were tested varying rotation speed of the unit, i.e., Set A (0 rpm), Set B (15 rpm), and Set C (20 rpm). Numerical simulations were performed using

a one-dimensional model assessing mass, energy and chemical conservation equations, considering a semi-global kinetic scheme, including three homogeneous and four heterogeneous chemical reactions. The optical design configuration of the solar system, in addition to the high heat recirculation enhanced by the rotation of the reactor, allowed maximum temperatures of 662 K (outer surface) and 573 K (reaction chamber). At this low-temperature range, a good agreement between numerical simulations and experiments was achieved, observing a H_2/CO ratio of 0.088 (Set B) and 0.163 (Set C), representing a 5.7% and 3.1% deviation, respectively. Finally, numerical results show an increase in the temperature would lead to a higher H_2/CO ratio production.

Specific conclusions for the result of each chapter were thoroughly presented at the end of each section.

6.1 Future Steps and Recommendations

The standard Computational Fluid Dynamics (CFD) simulation approach moves from a simplified scenario to more realistic conditions. It is clear that the ultimate numerical simulation suggests a fully three-dimensional resolved model for solar-driven gasification, including a fully rotating device, tracking of the local porosity of each single carbon/biomass particles inside the chemically reacting fixed-bed, the use of solar energy as a boundary condition. In the context of inert porous media, hybrid filtration combustion, and solar-driven gasification processes, the following steps can be undertaken to better understand these phenomena:

- With the improvement of user-based computational systems, more accurate simulations would be possible. In particular, transitioning from 2D axisymmetric to 3D particle-resolved simulations considering intrinsic heterogeneous chemical reactions represents a balance between computational costs and the complexity of the model.

- Although all the numerical studies were focused on coal and solid fuel particles, it is necessary to transition towards the hybridization of the porous bed to get a realistic hybrid filtration combustion configuration of the reactor, where part of the solid particles are also inert.

- The dimensions of the implemented reactor in the numerical studies are a smaller version of those generally used at lab-scale. Thus, implementing HFC reactors with the usual dimensions would be important as a new layer of complexity for the model.

- From the theory of HFC and solar-driven gasification, it is well-known that to avoid the instability of the combustion wave, the rotation of the system must be included. This was not considered in the numerical studies due to their steady-state feature.

- The last step to evolve from HFC to solar-driven gasification would be including the solar boundary condition to create a realistic setup inside the numerical model.

- One of the important assumptions was adiabatic conditions at the wall of the reactor. It would be a relevant improvement to add a user-defined-function (UDF) for heat flux through the wall.

- Although char coal particles are more manageable regarding their kinetic mechanism (use of global and semi-global schemes), the main goal of the future project will be to explore the use of two renewable sources (solar and biomass energy) to produce hydrogen and syngas. Thus, the variation of the solid fuel to gasify inside the reactor is a relevant parameter to assess. This can be extended for the numerical simulation of new blends, including hydrogen (H_2), methane (CH_4), and ammonia (NH_3) as interesting gaseous fuels to assess.

- The transient simulation of the gasification of char particles inside a chemically reacting fixed-bed or a hybrid porous media reactor requires tracking of the local porosity along the process inside each solid fuel particle.

In terms of the experimental studies, future steps consider the design of a new reactor concept for solar-driven gasification, and the improvement of the setup (heliostat) to get higher gasification temperatures, also varying the solid fuel under study and other operational parameters, such as equivalence ratio, rotation speed, inclination angle, share of fuel/inert particles inside the reactor, continuity of the operation, among others. Specific recommendations can be found below:

- Extend the use of several solid fuels inside the gasifier concept. In particular, the use of *Radiata Pine* and *Eucalyptus Globulus*, two of the most abundant forest species available in Chile. This would suggest the use of more complex kinetic schemes to represent the heat and mass transfer processes of biomass gasification. An extension to other gaseous fuels can be implemented using hydrogen (H_2) or ammonia (NH_3), where if only volumetric reactions take place inside the reactor, a detailed mechanism should be evaluated to perform numerical simulations.

- Regarding the last point, it would be interesting to assess the composition of the hybrid bed, including experimental tests using layers of solid fuel and inert particles and several configurations inside the porous bed (particle sizes, amount of solid fuel particles included inside the reactor).

- The use of different D_t/d_p ratio for the evaluation of the geometrical features of the reactor. This must be analyzed simultaneously with the CFD approach to assess the relevance of these parameters in the performance inside a porous medium.

- Improve the design of a solar gasifier for future solar-driven gasification tests, including geometrical aspects, inclination and rotations peed. This must be aligned with the control and monitoring of variables throughout the experiments.

General Bibliography

Acar, C., Bicer, Y., Demir, M., and Dincer, I. (2019). "Transition to a new era with light-based hydrogen production for a carbon-free society: An overview". In: *International Journal of Hydrogen Energy* 44 (47), pp. 25347–25364. ISSN: 03603199.

Ahrenfeldt, J., Egsgaard, H., Stelte, W., Thomsen, T., and Henriksen, U. (2013). "The influence of partial oxidation mechanisms on tar destruction in TwoStage biomass gasification". In: *Fuel* 112, pp. 662–680. ISSN: 00162361.

Al-Hamamre, Z. and Al-Zoubi, A. (Mar. 2010). "The use of inert porous media based reactors for hydrogen production". In: *International Journal of Hydrogen Energy* 35 (5), pp. 1971–1986. ISSN: 03603199.

Al-Rahbi, A. and Williams, P. (2017). "Hydrogen-rich syngas production and tar removal from biomass gasification using sacrificial tyre pyrolysis char". In: *Applied Energy* 190, pp. 501–509. ISSN: 03062619.

Aldushin, A., Bayliss, A., and Matkowsky, B. (May 2006). "On the transition from smoldering to flaming". In: *Combustion and Flame* 145 (3), pp. 579–606. ISSN: 00102180.

Aldushin, A., Bayliss, A., and Matkowsky, B. (2007). "On the mechanism of triggering the transition from smoldering to flaming". In: *Proceedings of the Combustion Institute* 31 II (2), pp. 2661–2668. ISSN: 15407489.

Aldushin, A. and Braverman, B. (2009). "Hydrodynamic instability of filtration combustion wave". In: *Doklady Physical Chemistry* 427 (1), pp. 125–128. ISSN: 00125016.

Aldushin, A. and Ivleva, T. (2013). "Hydrodynamic instability of the coflow filtration combustion: Numerical simulation". In: *Doklady Physical Chemistry* 451 (1), pp. 157–160. ISSN: 00125016.

Aldushin, A. and Ivleva, T. (2015a). "Counterflow infiltration combustion in conditions of fluid-dynamic instability: Fingering in low gas flow". In: *International Journal of Self-Propagating High-Temperature Synthesis* 24 (4), pp. 182–186. ISSN: 1934788X.

Aldushin, A. and Ivleva, T. (2015b). "Simulation of the hydrodynamic instability of a filtration combustion wave in a porous medium". In: *Combustion, Explosion and Shock Waves* 51 (1), pp. 107–115. ISSN: 15738345.

Aldushin, A. and Matkowsky, B. (1998). "Instabilities, Fingering and the saffman - Taylor problem in filtration combustion". In: *Combustion Science and Technology* 133 (4-6), pp. 293–341. ISSN: 00102202.

Aldushin, A., Merzhanov, A., and Seplyarskii, B. (1976). "Theory of filtration combustion of metals". In: *Combustion, Explosion, and Shock Waves* 12 (3), pp. 285–294.

Aldushin, A., Seplyarskii, B., and Shkadinskii, K. (1980). "Theory of filtrational combustion". In: *Combustion, Explosion, and Shock Waves* 16 (1), pp. 33–40. ISSN: 00105082.

Alonso, E., Gallo, A., Roldán, M. I., Pérez-Rábago, C. A., and Fuentealba, E. (2017). "Use of rotary kilns for solar thermal applications: Review of developed studies and analysis of their potential". In: *Solar Energy* 144, pp. 90–104.

Alonso, E. and Romero, M. (2015). "Review of experimental investigation on directly irradiated particles solar reactors". In: *Renewable and Sustainable Energy Reviews* 41, pp. 53–67. ISSN: 18790690.

Amelin, I., Salgansky, E., Volkova, N., Zholudev, A., Alekseev, A., Polianczyk, E., and Manelis, G. (2011). "Parametric domain of the stationary filtration combustion wave in the charge with a low carbon content". In: *Izvestiya Akademii Nauk. Seriya Khimicheskaya* 60 (6), pp. 1125–1132.

Andrews, J. and Shabani, B. (2014). "The role of hydrogen in a global sustainable energy strategy". In: *Wiley Interdisciplinary Reviews: Energy and Environment* 3 (5), pp. 474–489. ISSN: 2041840X.

ANSYS, I. (2022). *ANSYS-FLUENT™ V 2022R2 – Commercially available CFD software package based on the Finite Volume method. Southpointe, 275 Technology Drive, Canonsburg, PA 15317, U.S.A., www.ansys.com.*

A.P-Aldushin (1996). "Filtration Combustion". In: 1st ed., pp. 95–115. ISBN: 9781600866456.

Appl, M. (2007). *Ammonia: Principles and Industrial Practice*. Wiley-VCH, p. 310. ISBN: 978-3-527-61388-5.

Aramouni, N., Touma, J., Tarboush, B., Zeaiter, J., and Ahmad, M. (Feb. 2018). "Catalyst design for dry reforming of methane: Analysis review". In: *Renewable and Sustainable Energy Reviews* 82, pp. 2570–2585. ISSN: 18790690.

Araus, K., Reyes, F., and Toledo, M. (2014). "Syngas production from wood pellet using filtration combustion of lean natural gas-air mixtures". In: *International Journal of Hydrogen Energy* 39 (15), pp. 7819–7825. ISSN: 03603199.

Arriagada, A., Mena, R., Ripoll, N., Hayes, R., Nikrityuk, P., and Toledo, M. (2024a). "Solar-driven gasification for syngas production at low temperatures using a rotary hybrid porous media reactor". In: *Chemical Engineering Journal*, p. 153011.

Arriagada, A., Toledo, M., Hayes, R., and Nikrityuk, P. (Feb. 2024b). "3D study of a chemically reacting fixed-bed under gasification conditions for non-porous char: Laminar flow". In: *Journal of the Energy Institute* 112, p. 101489. ISSN: 17439671.

Arriagada-Romero, A., Toledo, M., Hayes, R., Pashchenko, D., and Nikrityuk, P. (2024). "Verification of a porous media model for the partial oxidation of a chemically reacting fixed-bed". In: *Fuel* 375, p. 132582.

Babkin, V. (1993). "Filtrational combustion of gases. Present state of affairs and prospects". In: *Pure and Applied Chemistry* 65 (2), pp. 335–344.

Baliga, C. and Nikrityuk, P. (2023). "Convective heat transfer coefficient for the side-wall in a fixed bed". In: *Canadian Journal of Chemical Engineering* 101.11, pp. 6151–6169.

Banerjee, D., Kushwaha, N., Shetti, N., Aminabhavi, T., and Ahmad, E. (Oct. 2022). "Green hydrogen production via photo-reforming of bio-renewable resources". In: *Renewable and Sustainable Energy Reviews* 167. ISSN: 18790690.

Baykara, S. (2018). "Hydrogen: A brief overview on its sources, production and environmental impact". In: *International Journal of Hydrogen Energy* 43 (23), pp. 10605–10614. ISSN: 03603199.

Bejarano, P. and Levendis, Y. (Apr. 2008). "Single-coal-particle combustion in O2/N2 and O2/CO2 environments". In: *Combustion and Flame* 153 (1-2), pp. 270–287. ISSN: 00102180.

Bellouard, Q., Abanades, S., and Rodat, S. (2017). "Biomass Gasification in an Innovative Spouted-Bed Solar Reactor: Experimental Proof of Concept and Parametric Study". In: *Energy & Fuels* 31.10, pp. 10933–10945. ISSN: 15205029.

Bellouard, Q., Abanades, S., Rodat, S., and Dupassieux, N. (2017). "Solar thermochemical gasification of wood biomass for syngas production in a high-temperature continuously-fed tubular reactor". In: *International Journal of Hydrogen Energy* 42.19, pp. 13486–13497. ISSN: 03603199.

Bellouard, Q., Rodat, S., Abanades, S., Ravel, S., and Frayssines, P. (2018). "Design, simulation and experimental study of a directly-irradiated solar chemical reactor for hydrogen and syngas production from continuous solar-driven wood biomass gasification". In: *International Journal of Hydrogen Energy*, pp. 1–13. ISSN: 03603199.

Benkorichi, S., Fateh, T., Richard, F., Consalvi, J., and Nadjai, A. (2017). "Investigation of thermal degradation of pine needles using multi-step reaction mechanisms". In: *Fire Safety Journal* 91 (February), pp. 811–819. ISSN: 03797112.

Bergman, T., Lavine, A., Incropera, F., and Dewitt, D. (2011). *Fundamentals of Heat and Mass Transfer*. 7th ed. John Wiley & Sons.

Bhatia, S. and Perlmuiter, D. (1980). *A Random Pore Model for Fluid-Solid Reactions : II. Diffusion and Transport Effects*.

Bhatia, S. and Perlmutter, D. (1981). "A Random Pore Model for Fluid-Solid Reactions : II. Diffusion and Transport Effects". In: *AlChE Journal* 27, pp. 247–254.

Bingue, J., Saveliev, A., and Kennedy, L. (2004). "Optimization of hydrogen production by filtration combustion of methane by oxygen enrichment and depletion". In: *International Journal of Hydrogen Energy* 29 (13), pp. 1365–1370. ISSN: 03603199.

Blasi, C. D. (Feb. 2008). "Modeling chemical and physical processes of wood and biomass pyrolysis". In: *Progress in Energy and Combustion Science* 34 (1), pp. 47–90. ISSN: 03601285.

Blinderman, M. and Klimenko, A. (Aug. 2007). "Theory of reverse combustion linking". In: *Combustion and Flame* 150 (3), pp. 232–245. ISSN: 00102180.

Blinderman, M., Saulov, D., and Klimenko, A. (2008). "Forward and reverse combustion linking in underground coal gasification". In: *Energy* 33 (3), pp. 446–454. ISSN: 03605442.

Braga, L., Silveira, J., Silva, M. D., Tuna, C., Machin, E., and Pedroso, D. (2013). "Hydrogen production by biogas steam reforming: A technical, economic and ecological analysis". In: *Renewable and Sustainable Energy Reviews* 28, pp. 166–173.

Bruckner, A. P. (1985). "Continuous duty solar coal gasification system using molten slag and direct-contact heat exchange". In: *Solar Energy* 34.3, pp. 239–247.

Burke, S. and Schumann, T. (1931). "Kinetics of a Type of Heterogeneous Reactions' The Mechanism of Combustion of Pulverized Fuel". In: *Industrial and Engineering Chemistry* 23 (4).

Burra, K. and Gupta, A. (Feb. 2019). "Modeling of biomass pyrolysis kinetics using sequential multi-step reaction model". In: *Fuel* 237, pp. 1057–1067. ISSN: 00162361.

Caram, H. and Amundson, N. (1977). "Diffusion and reaction in a stagnant boundary layer about a carbon particle". In: *Industrial & Engineering Chemistry Fundamentals* 12 (2), pp. 171–181.

Caro, S., Torres, D., and M.Toledo (2015). "Syngas production from residual biomass of forestry and cereal plantations using hybrid filtration combustion". In: *International Journal of Hydrogen Energy* 40 (6), pp. 2568–2577. ISSN: 03603199.

Carvalho, T., Costa, M., Casaca, C., Catapan, R. C., and Oliveira, A. A. (Feb. 2015). "Destruction of the tar present in syngas by combustion in porous media". In: *Energy and Fuels* 29 (2), pp. 1130–1136. ISSN: 15205029.

Cetrulo, T., Marques, R., Malheiros, T., and Cetrulo, N. (July 2020). "Monitoring inequality in water access: Challenges for the 2030 Agenda for Sustainable Development". In: *Science of the Total Environment* 727. ISSN: 18791026.

Chandrasekhara, B. and Vortmeyer, D. (1979). "Flow model for velocity distribution in fixed porous beds under isothermal conditions". In: *Wärme und Stoffübertragung* 12.2, pp. 105–111.

Cho, S., Yetter, R., and Dryer, F. (1992). "A Computer Model for One-Dimensional Mass and Energy Transport in and around Chemically Reacting Particles, Including Complex

Gas-Phase Chemistry, Multicomponent Molecular Diffusion, Surface Evaporation, and Heterogeneous Reaction". In: *Journal of Computational Physics* 102, pp. 160–179.

Cincinelli, A., Guerranti, C., Martellini, T., and Scodellini, R. (2019). "Residential wood combustion and its impact on urban air quality in Europe". In: *Current Opinion in Environmental Science and Health* 8, pp. 10–14. ISSN: 24685844.

Ciuta, S., Tsiamis, D., and Castaldi, M. (Jan. 2017). *Fundamentals of gasification and pyrolysis*. Elsevier, pp. 13–36. ISBN: 9780128127162.

Dawood, F., Anda, M., and Shafiullah, G. (Feb. 2020). "Hydrogen production for energy: An overview". In: *International Journal of Hydrogen Energy* 45 (7), pp. 3847–3869. ISSN: 03603199.

Delgado, J. (2006). "A critical review of dispersion in packed beds". In: *Heat and Mass Transfer* 42, pp. 279–310.

Dierich, F., Richter, A., and Nikrityuk., P. (2018). "A fixed-grid model to track the interface and porosity of a chemically reacting moving char particle". In: *Chemical Engineering Science* 175, pp. 296–305.

Dieterich, V., Buttler, A., Hanel, A., Spliethoff, H., and Fendt, S. (Oct. 2020). "Power-to-liquid via synthesis of methanol, DME or Fischer–Tropsch-fuels: a review". In: *Energy and Environmental Science* 13 (10), pp. 3207–3252. ISSN: 17545706.

Dincer, I. (Jan. 2012). "Green methods for hydrogen production". In: *International Journal of Hydrogen Energy* 37 (2), pp. 1954–1971. ISSN: 03603199.

Dincer, I. and Acar, C. (June 2017). "Innovation in hydrogen production". In: *International Journal of Hydrogen Energy* 42 (22), pp. 14843–14864. ISSN: 03603199.

Dixon, A. (2017). "Local transport and reaction rates in a fixed bed reactor tube: Endothermic steam methane reforming". In: *Chemical Engineering Science* 168, pp. 156–177.

Dixon, A., Nijemeisland, M., and Stitt, E. (2006). "Packed tubular reactor modeling and catalyst design using computational fluid dynamics". In: *Advances in Chemical Engineering* 31, pp. 307–389.

Dixon, A., Nijemeisland, M., and Stitt, E. (2013). "Systematic mesh development for 3D CFD simulation of fixed beds: contact points study". In: *Comput. Chem. Eng.* 48, 135–153.

Dobrego, K., Gnesdilov, N., Lee, S., and Choi, H. (2008). "Overall chemical kinetics model for partial oxidation of methane in inert porous media". In: *Chemical Engineering Journal* 144 (1), pp. 79–87. ISSN: 13858947.

Donatelli, A., Iovane, P., and Molino, A. (2010). "High energy syngas production by waste tyres steam gasification in a rotary kiln pilot plant. Experimental and numerical investigations". In: *Fuel* 89.10, pp. 2721–2728.

Dorofeenko, S., Polianczyk, E., and Manelis, G. (Oct. 2008). "Numerical simulation of bidisperse granular material flow in a rotating reactor". In: *Doklady Physics* 53 (10), pp. 510–512. ISSN: 10283358.

Dou, B., Zhang, H., Song, Y., Zhao, L., Jiang, B., He, M., Ruan, C., Chen, H., and Xu, Y. (2019). "Hydrogen production from the thermochemical conversion of biomass: Issues and challenges". In: *Sustainable Energy and Fuels* 3 (2), pp. 314–342. ISSN: 23984902.

Drayton, M., Saveliev, A., Kennedy, L., Fridman, A., and Li, Y. (1998). "Syngas production using superadiabatic combustion of ultra-rich methane-air mixtures". In: *Symposium (International) on Combustion*. Vol. 27. 1. Elsevier, pp. 1361–1367.

Dutta, S. (2014). "A review on production, storage of hydrogen and its utilization as an energy resource". In: *Journal of Industrial and Engineering Chemistry* 20 (4), pp. 1148–1156. ISSN: 22345957.

Edwards, M. and Richardson, J. (1968). "Gas dispersion in packed beds". In: *Chemical Engineering Science* 23.2, pp. 109–123.

Ellzey, J., Belmont, E., and Smith, C. (2019). "Heat recirculating reactors: Fundamental research and applications". In: *Progress in Energy and Combustion Science* 72, pp. 32–58.

Epelle, E., Desongu, K., Obande, W., Adeleke, A., Ikubanni, P., Okolie, J., and Gunes, B. (June 2022). "A comprehensive review of hydrogen production and storage: A focus on the role of nanomaterials". In: *International Journal of Hydrogen Energy* 47 (47), pp. 20398–20431. ISSN: 03603199.

Ergun, S. (1952). "Fluid flow through packed columns". In: *Chemical Engineering Progress* 48.2, pp. 89–94.

Ermoline, A., Yildiz, D., and Dreizin, E. (Dec. 2013). "Model of heterogeneous combustion of small particles". In: *Combustion and Flame* 160 (12), pp. 2982–2989. ISSN: 00102180.

Espegren, K., Damman, S., Pisciella, P., Graabak, I., and Tomasgard, A. (July 2021). "The role of hydrogen in the transition from a petroleum economy to a low-carbon society". In: *International Journal of Hydrogen Energy* 46 (45), pp. 23125–23138. ISSN: 03603199.

Farzad, S., Mandegari, M., and Görgens, J. (2016). "A critical review on biomass gasification, co-gasification, and their environmental assessments". In: *Biofuel Research Journal* 3 (4), pp. 483–495. ISSN: 22928782.

Fong, G., Jorgensen, S., and Singer, S. (July 2018). "Pore-resolving simulation of char particle gasification using micro-CT". In: *Fuel* 224, pp. 752–763. ISSN: 00162361.

Fuller, E., Schettler, P., and Giddings, J. (1966). "New method for prediction of binary gas-phase diffusion coefficients". In: *Industrial & Engineering Chemistry* 58.5, pp. 18–27.

Furler, P., Scheffe, J. R., Marxer, D., and Steinfeld, A. (2012). "Solar thermochemical CO2 splitting using a reticulated porous ceria redox system". In: *Energy & Fuels* 26, pp. 7051–7059.

Gentillon, P. and M.Toledo (July 2013). "Hydrogen and syngas production from propane and polyethylene". In: *International Journal of Hydrogen Energy* 38 (22), pp. 9223–9228. ISSN: 03603199.

Gerandi, G., Tihay-Felicelli, V., Santoni, P., Leroy-Cancellieri, V., and Cancellieri, D. (Sept. 2019). "Multi-scale modeling of the degradation of thermally thin wood plates". In: *Fire Safety Journal* 108. ISSN: 03797112.

Gielen, D., Boshell, F., Saygin, D., Bazilian, M., Wagner, N., and Gorini, R. (Apr. 2019). "The role of renewable energy in the global energy transformation". In: *Energy Strategy Reviews* 24, pp. 38–50. ISSN: 2211467X.

Glazov, S., Kislov, V., Salgansky, E., Rabinovich, O., Malinouski, A., Salganskaya, M., Pilipenko, E., and Kolesnikova, Y. (2017). "Effect of local rearrangements in the particle bed on the stability of filtration combustion of solid fuel". In: *International Journal of Heat and Mass Transfer* 108, pp. 1602–1609. ISSN: 00179310.

Gómez, J., Mmbaga, J., Hayes, R., Toledo, M., and Gracia, F. (2016). "Modelling hydrogen production by the rich combustion of heavy fuel oil". In: *International Journal of Hydrogen Energy* 41.40, pp. 17933–17943.

González, H., Caro, S., Toledo, M., and Olguin, H. (Mar. 2018). "Syngas production from polyethylene and biogas in porous media combustion". In: *International Journal of Hydrogen Energy* 43 (9), pp. 4294–4304. ISSN: 03603199.

Grange, N., Chetehouna, K., Gascoin, N., Coppalle, A., Reynaud, I., and Senave, S. (Apr. 2018). "One-dimensional pyrolysis of carbon based composite materials using FireFOAM". In: *Fire Safety Journal* 97, pp. 66–75. ISSN: 03797112.

Gregg, D. W., Taylor, R. W., Campbell, J. H., and Aiman, W. R. (1980a). "Solar Coal Gasification". In: *Solar Energy* 24.3, pp. 313–321. ISSN: 0146955X.

Gregg, D. W., Taylor, R. W., Campbell, J. H., Taylor, J. R., and Cotton, A. (1980b). "Solar gasification of coal, activated carbon, coke and coal and biomass mixtures". In: *Solar Energy* 25.4, pp. 353–364.

Grinchuk, P. and Rabinovich, O. (2007). "Critical phenomena and structural effects in combustion of disordered heterogeneous mixtures". In: *Heat Transfer Research* 38 (1), pp. 57–69. ISSN: 10642285.

Gudkova, I., Lempert, D., and Rozenberg, A. (2011). "Burning chromium-containing compounds in the filtration combustion mode". In: *Russian Journal of Applied Chemistry* 84 (11), pp. 1855–1859. ISSN: 10704272.

Guerrero, F., Arriagada, A., Muñoz, F., Silva, P., Ripoll, N., and Toledo, M. (Apr. 2021). "Particulate matter emissions reduction from residential wood stove using inert porous material inside its combustion chamber". In: *Fuel* 289. ISSN: 00162361.

Gug, J., Cacciola, D., and Sobkowicz, M. (2015). "Processing and properties of a solid energy fuel from municipal solid waste (MSW) and recycled plastics". In: *Waste Management* 35, pp. 283–292. ISSN: 18792456.

Guo, F., Li, X., Liu, Y., Peng, K., Guo, C., and Rao, Z. (July 2018). "Catalytic cracking of biomass pyrolysis tar over char-supported catalysts". In: *Energy Conversion and Management* 167, pp. 81–90. ISSN: 01968904.

Guo, Z., Sun, Z., Zhang, N., Cao, X., and Ding, M. (2019). "Mean porosity variations in packed bed of monosized spheres with small tube-to-particle diameter ratios". In: *Powder Technology* 354, pp. 842–853.

Gururajan, V., Wall, T., Gupta, R., and Truelove, J. (1990). "Mechanisms for the ignition of pulverized coal particles". In: *Combustion and Flame* 81.2, 119–132. ISSN: 0010-2180.

Gómez, J., Mmbaga, J., Hayes, R., Toledo, M., and Gracia, F. (2016). "Modelling hydrogen production by the rich combustion of heavy fuel oil". In: *International Journal of Hydrogen Energy* 41 (40), pp. 17933–17943. ISSN: 03603199.

Gómez, J., Mmbaga, J., Hayes, R., Toledo, M., and Gracia, F. (2018). "Modeling hydrogen production in a catalytic-inert packed bed reactor by rich combustion of heavy fuel oil". In: *International Journal of Hydrogen Energy* 43 (5), pp. 2677–2688. ISSN: 03603199.

Haghpanah, R., Majumder, A., Nilam, R., Rajendran, A., Farooq, S., Karimi, I., and Amanullah, M. (2013). "Multiobjective optimization of a four-step adsorption process for postcombustion CO2 capture via finite volume simulation". In: *Industrial & Engineering Chemistry Research* 52.11, pp. 4249–4265.

Hammi, Z., Labjar, N., Dalimi, M., El Hamdouni, Y., and El Hajjaji, S. (2024). "Green hydrogen: A holistic review covering life cycle assessment, environmental impacts, and color analysis". In: *International Journal of Hydrogen Energy* 80, pp. 1030–1045.

Han, J. and Kim, H. (Feb. 2008). "The reduction and control technology of tar during biomass gasification/pyrolysis: An overview". In: *Renewable and Sustainable Energy Reviews* 12 (2), pp. 397–416. ISSN: 13640321.

Hanchate, N., Ramani, S., Mathpati, C., and Dalvi, V. (Jan. 2021). "Biomass gasification using dual fluidized bed gasification systems: A review". In: *Journal of Cleaner Production* 280. ISSN: 09596526.

Hardesty, D. and Weinberg, F. (Dec. 1973). "Burners producing large excess enthalpies". In: *Combustion Science and Technology* 8 (5-6), pp. 201–214. ISSN: 1563521X.

Haryanto, A., Fernando, S., Murali, N., and Adhikari, S. (2005). "Current status of hydrogen production techniques by steam reforming of ethanol: a review". In: *Energy & Fuels* 19.5, pp. 2098–2106.

Hasse, C., Debiagi, P., Wen, X., Hildebrandt, K., Vascellari, M., and Faravelli, T. (Sept. 2021). "Advanced modeling approaches for CFD simulations of coal combustion and gasification". In: *Progress in Energy and Combustion Science* 86, p. 100938. ISSN: 03601285.

Hathaway, B. J. and Davidson, J. H. (2021). "Autothermal hybridization and controlled production of hydrogen-rich syngas in a molten salt solar gasifier". In: *International Journal of Hydrogen Energy* 46.29, pp. 15257–15267. ISSN: 03603199.

Hathaway, B. and Davidson, J. (2017). "Demonstration of a prototype molten salt solar gasification reactor". In: *Solar Energy* 142, pp. 224–230.

Haugen, N., Loong, B., and Mitchell, R. (July 2022). "Numerical approaches for thermochemical conversion of char". In: *Progress in Energy and Combustion Science* 91. ISSN: 03601285.

Hayes, R. (1990). "Simulation of mixed convection heat transfer at the wall of a packed bed". In: *Numerical Heat Transfer* 17.2, pp. 217–230.

Hayes, R. and Mmbaga, J. (2012). *Introduction to Chemical Reactor Analysis*. 2nd. Boca Raton, Florida: CRC Press, Taylor & Francis Group. ISBN: 9780429071515.

He, J., Yang, Y., Liao, Z., Xu, A., and Fang, K. (2022). "Linking SDG 7 to assess the renewable energy footprint of nations by 2030". In: *Applied Energy* 317, p. 119167.

Henneke, M. and Ellzey, J. (1999). "Modeling of filtration combustion in a packed bed". In: *Combustion and Flame* 117 (4), pp. 832–840. ISSN: 00102180.

Herce, C., Caprariis, B. D., Stendardo, S., Verdone, N., and Filippis, P. D. (2014). "Comparison of global models of sub-bituminous coal devolatilization by means of thermogravimetric analysis". In: *Journal of Thermal Analysis and Calorimetry* 117 (1), pp. 507–516. ISSN: 13886150.

Higman, C. (2003). *Gasification. Elsevier*. Gulf Professional Publishing, pp. 1–21.

Higman, C. and Tam, S. (2014). "Advances in coal gasification, hydrogenation, and gas treating for the production of chemicals and fuels". In: *Chemical Reviews* 114.3, pp. 1673–1708.

Higuera, F. (Jan. 2008). "Combustion of a coal char particle in a stream of dry gas". In: *Combustion and Flame* 152 (1-2), pp. 230–244. ISSN: 00102180.

Holladay, J., Hu, J., King, D., and Wang, Y. (2009). "An overview of hydrogen production technologies". In: *Catalysis Today* 139, pp. 244–260.

Hopkins, M. W., DeJenga, C., and Antal, M. J. (1984). "The flash pyrolysis of cellulosic materials using concentrated visible light". In: *Solar Energy* 32.4, pp. 547–551.

Hosseini, S. and Thévenin, D. (2023). "Toward pore-scale simulation of combustion in porous media using a low-Mach hybrid lattice Boltzmann/finite-difference solver". In: *Physics of Fluids* 35.6.

Hosseini, S., Barzegaravval, H., Chehroudi, B., and Wahid, M. (2018). "Hybrid solar flameless combustion system: Modeling and thermodynamic analysis". In: *Energy Conversion and Management* 166 (December 2017), pp. 146–155. ISSN: 01968904.

Howell, J., Hall, M., and Ellzey, J. (1996). "Combustion of hydrocarbon fuels within porous inert media". In: *Progress in Energy and Combustion Science* 22 (2), pp. 121–145. ISSN: 03601285.

Hurley, M., Gottuk, D., Hall, J., Harada, K., Kuligowski, E., Puchovsky, M., Torero, J., Watts, J., and Wieczorek, C. (Jan. 2016). *SFPE handbook of fire protection engineering, fifth edition*. Springer New York, pp. 1–3493. ISBN: 9781493925650.

IEA (2019). *International Energy Agency - The Future of Hydrogen*. URL: `www.iea.org`.

IEA (2022). *International Energy Agency - CO2 Emissions in 2022*. URL: `www.iea.org`.

IEA (2023). *International Energy Agency - Coal 2023 - Analysis and forecast to 2026*. URL: `www.iea.org`.

Jayawickrama, T., Chishty, M., Haugen, N., Babler, M., and Umeki, K. (Sept. 2023). "The effects of Stefan flow on the flow surrounding two closely spaced particles". In: *International Journal of Multiphase Flow* 166, 104499. ISSN: 03019322.

Johansen, J., Gadsbøll, R., Thomsen, J., Jensen, P., Glarborg, P., Ek, P., Martini, N. D., Mancini, M., Weber, R., and Mitchell, R. (2016). "Devolatilization kinetics of woody biomass at short residence times and high heating rates and peak temperatures". In: *Applied Energy* 162, pp. 245–256. ISSN: 03062619.

Jones, W. and Lindstedt, R. (1988). "Global reaction schemes for hydrocarbon combustion". In: *Combust. Flame; (United States)* 73.

Jourak, A., Hellstrom, J., Lundstrom, T., and Frishfelds, V. (2014). "Numerical derivation of dispersion coefficients for flow through three-dimensional randomly packed beds of monodisperse spheres". In: *AIChE Journal* 60.2, pp. 749–761.

Jovicic, V., Fedorova, N., Zbogar-Rasic, A., Nloka, D., and Delgado, A. (2017a). "Combustion of solid fuel in a hybrid porous reactor". In: *Energy Procedia* 120, pp. 431–438. ISSN: 18766102.

Jovicic, V., Fedorova, N., Zbogar-Rasic, A., Toledo, M., and Delgado, A. (2017b). "Experimental Investigation of Solid Fuel Combustion Process in a Hybrid Porous Reactor". In: *Journal of Energy and Power Engineering* 11 (9), pp. 589–596. ISSN: 19348975.

Kamal, M. and Mohamad, A. (2006). "Combustion in porous media". In: *Proceedings of the Institution of Mechanical Engineers, Part A: Journal of Power and Energy* 220.5, pp. 487–508.

Kang, J., Wei, Y., Liu, L., R.H., Yu, B., and Wang, J. (Apr. 2020). "Energy systems for climate change mitigation: A systematic review". In: *Applied Energy* 263. ISSN: 03062619.

Kaya, K., Ak, E., Yaslan, Y., and Oktug, S. (June 2021). "Waste-to-Energy Framework: An intelligent energy recycling management". In: *Sustainable Computing: Informatics and Systems* 30. ISSN: 22105379.

Kee, R., Coltrin, M., and Glarborg, P. (2005). *Chemically Reacting Flow: Theory and Practice*. John Wiley & Sons. ISBN: 9780471461302.

Kenarsari, S. and Zheng, Y. (2014a). "CO2 gasification of coal under concentrated thermal radiation: A numerical study". In: *Fuel Processing Technology* 118, pp. 218–227. ISSN: 03783820.

Kenarsari, S. and Zheng, Y. (2014b). "CO2 gasification of coal under concentrated thermal radiation: A numerical study". In: *Fuel Processing Technology* 118, pp. 218–227.

Kennedy, L., Bingue, J., Saveliev, A., Fridman, A., and Foutko, S. (2000). "Chemical structures of methane-air filtration combustion waves for fuel-lean and fuel-rich conditions". In: *Proceedings of the Combustion Institute* 28 (1), pp. 1431–1438. ISSN: 15407489.

Khandelwal, H., Dhar, H., Thalla, A., and Kumar, S. (2019). "Application of life cycle assessment in municipal solid waste management: A worldwide critical review". In: *Journal of Cleaner Production* 209, pp. 630–654. ISSN: 09596526.

Khatoonabadi, M., Prasianakis, N., and Mantzaras, J. (2024). "A pore-level 3D lattice Boltzmann simulation of mass transport and reaction in catalytic particles used for methane synthesis". In: *International Journal of Heat and Mass Transfer* 221, p. 125025.

Kislov, V. M., Glazov, S. V., Chervonnaya, N. A., Patronova, L. I., Salganskaya, M. V., and Manelis, G. B. (2008). "Biomass gasification under combustion conditions with superadiabatic heating". In: *Solid Fuel Chemistry* 42 (3), pp. 135–139. ISSN: 03615219.

Kislov, V., Glazov, S., Salgansky, E., Kolesnikova, Y., and Salganskaya, M. (2016). "Coal gasification by a mixture of air and carbon dioxide in the filtration combustion mode". In: *Combustion, Explosion and Shock Waves* 52 (3), pp. 320–325. ISSN: 15738345.

Klerk, A. D. (2003). "Voidage variation in packed beds at small column to particle diameter ratio". In: *AIChE journal* 49.8, pp. 2022–2029.

Kodama, T. (2003). "High-temperature solar chemistry for converting solar heat to chemical fuels". In: *Progress in Energy and Combustion Science* 29.6, pp. 567–597. ISSN: 03601285.

Kodama, T., Bellan, S., Gokon, N., and Cho, H. (Nov. 2017a). "Particle reactors for solar thermochemical processes". In: *Solar Energy* 156, pp. 113–132. ISSN: 0038092X.

Kodama, T., Bellan, S., Gokon, N., and Cho, H. (2017b). "Particle reactors for solar thermochemical processes". In: *Solar Energy* 156, pp. 113–132.

Kodama, T., Enomoto, S., Hatamachi, T., and Gokon, N. (2008). "Application of an Internally Circulating Fluidized Bed for Windowed Solar Chemical Reactor with Direct Irradiation of Reacting Particles". In: *Journal of Solar Energy Engineering* 130.1, p. 014504. ISSN: 01996231.

Kodama, T., Kondoh, Y., Tamagawa, T., Funatoh, A., Shimizu, K.-I., and Kitayama, Y. (2002). "Fluidized Bed Coal Gasification with CO 2 under Direct Irradiation with Concentrated Visible Light". In: *Energy & Fuels* 16.5, pp. 1264–1270. ISSN: 0887-0624.

Kozicki, J. and Donze, F. V. (2009). "YADE-OPEN DEM: An open-source software using a discrete element method to simulate granular material". In: *Engineering Computations* 26.7, 786 – 805.

Kriebitzsch, S. and Richter, A. (Jan. 2020). "LES simulation of char particle gasification at Reynolds numbers up to 1000". In: *Combustion and Flame* 211, pp. 185–194. ISSN: 15562921.

Krishna, B., Biswas, B., and Bhaskar, T. (2019). *Gasification of lignocellulosic biomass*. 2nd ed. Elsevier Inc., pp. 285–300. ISBN: 9780128168561.

Krishnamoorthy, G., Rawat, R., and Smith, P. (Jan. 2006). "Parallelization of the P-1 radiation model". In: *Numerical Heat Transfer, Part B: Fundamentals* 49 (1), pp. 1–17. ISSN: 10407790.

Kumar, A., Jones, D., and Hanna, M. (Sept. 2009). "Thermochemical biomass gasification: A review of the current status of the technology". In: *Energies* 2 (3), pp. 556–581. ISSN: 19961073.

Lapuerta, M., J.Hernández, and Rodríguez, J. (2007). "Comparison between the kinetics of devolatilisation of forestry and agricultural wastes from the middle-south regions of Spain". In: *Biomass and Bioenergy* 31 (1), pp. 13–19. ISSN: 09619534.

Lautenberger, C. (2017). "Gpyro : A Three Dimensional Generalized Pyrolysis Model Gpyro - Open source pyrolysis model". In: *IAFSS Workshop on MaCFP (Condensed Phase Subgroup)*.

Lebedev, A., Sukhov, G., and Yarin, P. (1977). "Theory of filtration combustion". In: *Combustion Explosion Schock and Waves* 4 (4), pp. 7–11.

Lee, J., Yetter, R., and Dryer, F. (1995). "Transient Numerical Modeling of Carbon Particle Ignition and Oxidation". In: *Combustion and Flame* 101, pp. 387–398.

Lempert, D., Glazov, S., and Manelis, G. (2011). "Mass Transfer in Filtration Combustion Processes". In: *Mass Transfer in Multiphase Systems and its Applications*.

Levin, V. and Lutsenko, N. (Sept. 2017). "Two-dimensional gas flows under heterogeneous combustion of solid porous media". In: *Doklady Physics* 62 (9), pp. 425–429. ISSN: 10283358.

Li, J., Xie, Y., Zeng, K., Flamant, G., Yang, H., Yang, X., Zhong, D., Du, Z., and Chen, H. (2020). "Biomass gasification in molten salt for syngas production". In: *Energy* 210, p. 118563.

Li, K. and Lin, B. (2015). "Impacts of urbanization and industrialization on energy consumption/CO2 emissions: Does the level of development matter?" In: *Renewable and Sustainable Energy Reviews* 52, pp. 1107–1122. ISSN: 18790690.

Li, X., Chen, J., Hu, Q., Chu, P., Dai, Y., and Wang, C. (2021). "Solar-driven gasification in an indirectly-irradiated thermochemical reactor with a clapboard-type internally-circulating fluidized bed". In: *Energy Conversion and Management* 248, p. 114795. ISSN: 01968904.

Libby, P. and Blake, T. (1981). "Burning Carbon Particles in the Presence of Water Vapor". In: *Combustion and Flame* 41, p. 123.

Liu, G., Rezaei, H., Lucas, J., Harris, D., and Wall, T. (2000). "Modelling of a pressurised entrained flow coal gasifier: the effect of reaction kinetics and char structure". In: *Fuel* 79.14, pp. 1767–1779.

Liu, H., Li, Z., Yang, Y., Miao, G., and Han, Y. (2023). "Effects of oxidation on physical and chemical structure of a low rank sub-bituminous coal during the spontaneous combustion latency". In: *Energy* 272, p. 127122.

Liu, K., Song, C., and Subramani, V. (2010). *Hydrogen and syngas production and purification technologies*. John Wiley & Sons, p. 533. ISBN: 9780471719755.

Liu, L., Huang, Y., Cao, J., Liu, C., Dong, L., Xu, L., and Zha, J. (2018). "Experimental study of biomass gasification with oxygen-enriched air in fluidized bed gasifier". In: *Science of the Total Environment* 626, pp. 423–433. ISSN: 18791026.

Liu, S., Xu, F., Lu, B., Wang, W., Liu, Z., and Wang, Y. (Jan. 2024). "Porous-media model based particle-resolved simulation of a fixed bed with olefin catalytic cracking reaction". In: *Powder Technology* 431, p. 119099. ISSN: 1873328X.

Loutzenhiser, P. and Muroyama, A. (2017). "A review of the state-of-the-art in solar-driven gasification processes with carbonaceous materials". In: *Solar Energy* 156, pp. 93–100.

Lu, C. and Yortsos, Y. (Sept. 2005). "Pattern formation in reverse filtration combustion". In: *Physical Review E - Statistical, Nonlinear, and Soft Matter Physics* 72 (3). ISSN: 15393755.

Lu, Y. and Nikrityuk, P. (2022). "DEM-based model for steam methane reforming". In: *Chemical Engineering Science* 247, p. 116903.

Lu, Z., Chinnici, A., Jafarian, M., Arjomandi, M., and Nathan, G. J. (2019). "Numerical investigation of the isothermal flow field and particle deposition behaviour in a rotating fluidized bed solar receiver". In: *Solar Energy* 182, pp. 348–360.

Lu, Z., Jafarian, M., Arjomandi, M., and Nathan, G. J. (2016). "Analytical assessment of a novel rotating fluidized bed solar reactor for steam gasification of char particles". In: *Solar Energy* 140, pp. 113–123.

Lu, Z., Jafarian, M., Chinnici, A., Arjomandi, M., and Nathan, G. J. (2017). "Flow behavior inside a novel rotating fluidized bed for solar gasification of biomass". In: *AIP Conference Proceedings* 1850. ISSN: 15517616.

Luque, R. and Speight, J. (2015). *Gasification for Synthetic Fuel Production: Fundamentals, Processes and Applications*. Woodhead Publishing Series in Energy, p. 348. ISBN: 978-0-85709-802-3.

Ma, W., Wenga, T., Frandsen, F., Yan, B., and Chen, G. (2020). "The fate of chlorine during MSW incineration: Vaporization, transformation, deposition, corrosion and remedies". In: *Progress in Energy and Combustion Science* 76, p. 100789. ISSN: 03601285.

Ma, X., Zhao, X., Gu, J., and Shi, J. (Mar. 2019). "Co-gasification of coal and biomass blends using dolomite and olivine as catalysts". In: *Renewable Energy* 132, pp. 509–514. ISSN: 18790682.

Mahari, W., Azwar, E., Foong, S., Ahmed, A., Peng, W., Tabatabaei, M., Aghbashlo, M., Park, Y., Sonne, C., and Lam, S. (Oct. 2021). "Valorization of municipal wastes using co-pyrolysis for green energy production, energy security, and environmental sustainability: A review". In: *Chemical Engineering Journal* 421. ISSN: 13858947.

Malinuski, A. and Rabinovich, O. (2016). "Modelling of Inclined Wave of Filtration Solid Fuel Combustion Using CFD-DEM Technique". In: *Procedia Engineering* 157, pp. 422–427. ISSN: 18777058.

Manelis, G. B., Glazov, S. V., Lempert, D. B., and Salgansky, E. A. (2011). "Filtration combustion of solid fuel in countercurrent reactors". In: *Russian Chemical Bulletin* 60 (7), pp. 1301–1317. ISSN: 10665285.

Manelis, G. B., Glazov, S. V., Salgansky, E. A., Lempert, D. B., Gudkova, I. Y., Domashnev, I. A., Kolesnikova, A. M., Kislov, V. M., and Kolesnikova, Y. Y. (2016). "Extraction of molybdenum-containing species from heavy oil residues using the filtration combustion method". In: *International Journal of Heat and Mass Transfer* 92, pp. 744–750. ISSN: 00179310.

Manelis, G., Glazov, S., Salgansky, E., and Lempert, D. (2012). "Autowave processes in the filtration combustion in counterflow systems". In: *Russian Chemical Reviews* 81 (9), pp. 855–873. ISSN: 0036-021X.

Manigandan, S., Kumar, P. V., Arivalagan, P., Nižetić, S., and Praveenkumar, T. (2022). "Production and utilization of pyrolysis oil from solidplastic wastes: A review on pyrolysis process and influence of reactors design". In: *Journal of environmental management* 302, p. 114046.

Marazziti, D., Cianconi, P., Mucci, F., Foresi, L., Chiarantini, I., and Vecchia, A. D. (June 2021). "Climate change, environment pollution, COVID-19 pandemic and mental health". In: *Science of the Total Environment* 773. ISSN: 18791026.

Martínez, M., Toledo, M., and Cabrera, M. (2016). "Molybdenum oxide reduction using syngas and heat from an inert porous media reactor". In: *International Journal of Hydrogen Energy* 41 (30), pp. 12747–12761. ISSN: 03603199.

Medwell, P., Nathan, G., Chan, Q., Alwahabi, Z., and Dally, B. (2011). "The influence on the soot distribution within a laminar flame of radiation at fluxes of relevance to concentrated solar radiation". In: *Combustion and Flame* 158 (9), pp. 1814–1821. ISSN: 00102180.

Meijer, R., Miihlen, H., Kapteijn, F., and Moulijn, J. (1991). "Burn-off behaviour in alkali-catalysed CO2 gasification of bituminous coal char: A comparison of TGA and fixed-bed reactor". In: *Fuel Processing Technology* 28, pp. 5–17.

Mitchell, R., Kee, R., Glarborg, P., and Coltrin, M. (1991). "The effect of CO conversion in the boundary layers surrounding pulverized-coal char particles". In: *Symposium (International) on Combustion* 23.1. Twenty-Third Symposium (International) on Combustion, 1169–1176. ISSN: 0082-0784.

Mohammadi, A. and Jazayeri, A. (Sept. 2012). *Numerical Simulation of Combustion in Porous Media*. IntechOpen, pp. 529–556. ISBN: 978-953-51-0749-1.

Mohr, S. H., Wang, J., Ellem, G., Ward, J., and Giurco, D. (2015). "Projection of world fossil fuels by country". In: *Fuel* 141, pp. 120–135. ISSN: 00162361.

Mondal, P., Dang, G. S., and Garg, M. O. (2011). "Syngas production through gasification and cleanup for downstream applications - Recent developments". In: *Fuel Processing Technology* 92 (8), pp. 1395–1410. ISSN: 03783820.

Mueller, G. (1992). "Radial void fraction distributions in randomly packed tied beds of uniformly sized spheres in cylindrical containers". In: *Powder Technology* 72, pp. 269–275.

Mueller, G. (Nov. 2010). "Radial porosity in packed beds of spheres". In: *Powder Technology* 203 (3), pp. 626–633.

Mujeebu, M. (July 2016). "Hydrogen and syngas production by superadiabatic combustion - A review". In: *Applied Energy* 173, pp. 210–224. ISSN: 03062619.

Mujeebu, M., Abdullah, M., Bakar, M. A., Mohamad, A., and Abdullah, M. (2009a). "A review of investigations on liquid fuel combustion in porous inert media". In: *Progress in Energy and Combustion Science* 35.2, pp. 216–230.

Mujeebu, M., Abdullah, M., Bakar, M. A., Mohamad, A., and Abdullah, M. (2009b). "Applications of porous media combustion technology - A review". In: *Applied Energy* 86 (9), pp. 1365–1375. ISSN: 03062619.

Mujeebu, M., Abdullah, M., Bakar, M. A., Mohamad, A., Muhad, R., and Abdullah, M. (2009c). "Combustion in porous media and its applications - A comprehensive survey". In: *Journal of Environmental Management* 90 (8), pp. 2287–2312. ISSN: 03014797.

Munir, M. T., Mardon, I., Al-Zuhair, S., Shawabkeh, A., and Saqib, N. U. (Dec. 2019). "Plasma gasification of municipal solid waste for waste-to-value processing". In: *Renewable and Sustainable Energy Reviews* 116. ISSN: 18790690.

Muroyama, A. P., Guscetti, I., Schieber, G. L., Haussener, S., and Loutzenhiser, P. G. (2018). "Design and demonstration of a prototype 1.5 kWth hybrid solar/autothermal steam gasifier". In: *Fuel* 211, pp. 331–340. ISSN: 00162361.

Murray, J. P. and Fletcher, E. A. (1994). "Reaction of steam with cellulose in a fluidized bed using concentrated sunlight". In: *Energy* 19.10, pp. 1083–1098. ISSN: 03605442.

Nathan, G. J., Jafarian, M., Dally, B. B., Saw, W. L., Ashman, P. J., Hu, E., and Steinfeld, A. (2018). "Solar thermal hybrids for combustion power plant: A growing opportunity". In: *Progress in Energy and Combustion Science* 64, pp. 4–28. ISSN: 03601285.

Ng, Y. and Lipiński, W. (2012). "Thermodynamic analyses of solar thermal gasification of coal for hybrid solar-fossil power and fuel production". In: *Energy* 44.1, pp. 720–731. ISSN: 03605442.

Ngoh, S. and Njomo, D. (Dec. 2012). "An overview of hydrogen gas production from solar energy". In: *Renewable and Sustainable Energy Reviews* 16 (9), pp. 6782–6792. ISSN: 13640321.

Nguyen, C., Scherer, J., Guo, Q., Kriebitzsch, S., and Richter, A. (Mar. 2020). "The shape development of spherical and non-spherical char particles in the flame zone of an entrained-flow gasifier – A numerical study". In: *International Journal of Heat and Mass Transfer* 149. ISSN: 00179310.

Nguyen, C., Scherer, J., Hartwich, M., and Richter, A. (Apr. 2021). "The morphology evolution of char particles during conversion processes". In: *Combustion and Flame* 226, pp. 117–128. ISSN: 15562921.

Nguyen, C., Farid, M., Scherer, J., Guo, Q., Gräbner, M., and Richter, A. (June 2022). "A hybrid particle model with advanced conversion parameters and dynamic drag model applied for the CFD modeling of an entrained-flow gasifier". In: *Combustion and Flame* 240. ISSN: 15562921.

Nikolaidis, P. and Poullikkas, A. (Jan. 2017). "A comparative overview of hydrogen production processes". In: *Renewable and Sustainable Energy Reviews* 67, pp. 597–611. ISSN: 18790690.

Nikrityuk, P. and Meyer, B. (Sept. 2014a). "Pseudo-Steady-State Approach for Carbon Particle Combustion/Gasification". In: *Gasification Processes: Modeling and Simulation*. Weinheim, Germany: Willey-VCH Verlag GmbH & Co, pp. 205–244. ISBN: 9783527335503.

Nikrityuk, P. and Meyer, B. (Sept. 2014b). "Unsteady Char Gasification/Combustion". In: *Gasification Processes: Modeling and Simulation*. Weinheim, Germany: Willey-VCH Verlag GmbH & Co, pp. 143–171. ISBN: 9783527335503.

Nikrityuk, P., Gräbner, M., Kestel, M., and Meyer, B. (2013). "Numerical study of the influence of heterogeneous kinetics on the carbon consumption by oxidation of a single coal particle". In: *Fuel* 114, pp. 88–98. ISSN: 00162361.

Nusselt, W. (1924). "Der Verbrennungsvorgang in der Kohlenstaubfeuerung". In: *Zeitschrift des Vereines Deutscher Ingenieure* 68.

Oka, K., Mizutani, W., and Ashina, S. (June 2020). "Climate change impacts on potential solar energy production: A study case in Fukushima, Japan". In: *Renewable Energy* 153, pp. 249–260. ISSN: 18790682.

Olah, G., Goeppert, A., and Prakash, G. (Jan. 2009). "Chemical recycling of carbon dioxide to methanol and dimethyl ether: From greenhouse gas to renewable, environmentally carbon neutral fuels and synthetic hydrocarbons". In: *Journal of Organic Chemistry* 74 (2), pp. 487–498. ISSN: 00223263.

Ong, B. C., Kamarudin, S. K., and Basri, S. (Apr. 2017). "Direct liquid fuel cells: A review". In: *International Journal of Hydrogen Energy* 42 (15), pp. 10142–10157. ISSN: 03603199.

Orihuela, M., Espinoza, L., Ripoll, N., Chacartegui, R., and Toledo, M. (Apr. 2021). "Natural gas-supported gasification of polyethylene and wood mixtures in a porous medium reactor". In: *Energy Conversion and Management* 233. ISSN: 01968904.

Osinga, T., Olalde, G., and Steinfeld, A. (2004). "Solar carbothermal reduction of ZnO: Shrinking packed-bed reactor modeling and experimental validation". In: *Industrial and Engineering Chemistry Research* 43.25, pp. 7981–7988. ISSN: 08885885.

Otterstedt, J., Zhu, Y., and Sterte, J. (1988). "Catalytic cracking of heavy oil over catalysts containing different types of zeolite Y in active and inactive matrices". In: *Applied Catalysis* 38 (1), pp. 143–155. ISSN: 01669834.

Pala, L., Wang, Q., Kolb, G., and Hessel, V. (Feb. 2017). "Steam gasification of biomass with subsequent syngas adjustment using shift reaction for syngas production: An Aspen Plus model". In: *Renewable Energy* 101, pp. 484–492. ISSN: 18790682.

Palacios, P., Toledo, M., and Cabrera, M. (2015). "Iron ore reduction by methane partial oxidation in a porous media". In: *International Journal of Hydrogen Energy* 40 (31), pp. 9621–9633. ISSN: 03603199.

Park, D., Kim, S., Lee, S. H., and Lee, J. G. (Aug. 2010). "Co-pyrolysis characteristics of sawdust and coal blend in TGA and a fixed bed reactor". In: *Bioresource Technology* 101 (15), pp. 6151–6156. ISSN: 09608524.

Pastore, A. and Mastorakos, E. (Apr. 2010). "Rich n-heptane and diesel combustion in porous media". In: *Experimental Thermal and Fluid Science* 34 (3), pp. 359–365. ISSN: 08941777.

Pastore, A. and Mastorakos, E. (2011). "Syngas production from liquid fuels in a non-catalytic porous burner". In: *Fuel* 90.1, pp. 64–76.

Patankar, S. (1980). *Numerical heat transfer and fluid flow*. Series on Computational Methods in Mechanics and Thermal Science. Hemisphere Publishing Corporation (CRC Press, Taylor & Francis Group). ISBN: 978-0891165224.

Pereira, E., Silva, J. D., Oliveira, J. D., and MacHado, C. (2012). "Sustainable energy: A review of gasification technologies". In: *Renewable and Sustainable Energy Reviews* 16 (7), pp. 4753–4762. ISSN: 13640321.

Piatkowski, N. and Steinfeld, A. (May 2008). "Solar-driven coal gasification in a thermally irradiated packed-bed reactor". In: *Energy and Fuels* 22 (3), pp. 2043–2052. ISSN: 08870624.

Piatkowski, N. and Steinfeld, A. (2011). "Solar gasification of carbonaceous waste feedstocks in a packed-bed reactor—Dynamic modeling and experimental validation". In: *AIChE Journal* 57.12, pp. 3522–3533.

Piatkowski, N., Wieckert, C., and Steinfeld, A. (2009). "Experimental investigation of a packed-bed solar reactor for the steam-gasification of carbonaceous feedstocks". In: *Fuel Processing Technology* 90.3, pp. 360–366. ISSN: 03783820.

Piatkowski, N., Wieckert, C., Weimer, A., and Steinfeld, A. (2011). "Solar-driven gasification of carbonaceous feedstock—a review". In: *Energy & Environmental Science* 4.1, pp. 73–82.

Pichler, M., Haddadi, B., Jordan, C., Norouzi, H., and Harasek, M. (2021). "Effect of particle contact point treatment on the CFD simulation of the heat transfer in packed beds". In: *Chem. Eng. Res. and Design* 165, 242–253.

Pinilla, J., Utrilla, R., Lázaro, M., Suelves, I., Moliner, R., and Palacios, J. (Oct. 2009). "A novel rotary reactor configuration for simultaneous production of hydrogen and carbon

nanofibers". In: *International Journal of Hydrogen Energy* 34 (19), pp. 8016–8022. ISSN: 03603199.

Podlesniy, D., Zaichenko, A., Salgansky, E., and Salganskaya, M. (Nov. 2017). "Stability of the Front of Filtration Combustion of Bidisperse Fuel Mixture in an Inclined Rotating Gas Generator". In: *Russian Journal of Applied Chemistry* 90 (11), pp. 1783–1788. ISSN: 10704272.

Préndez, M., Carvajal, V., Corada, K., Morales, J., Alarcón, F., and Peralta, H. (2013). "Biogenic volatile organic compounds from the urban forest of the Metropolitan Region, Chile." In: *Environmental pollution (Barking, Essex : 1987)* 183 (x), pp. 143–150. ISSN: 18736424.

Puig-Arnavat, M., Tora, E. A., Bruno, J. C., and Coronas, A. (2013). "State of the art on reactor designs for solar gasification of carbonaceous feedstock". In: *Solar Energy* 97, pp. 67–84.

Qian, Y., Yu, Y., Xu, G., and Liu, X. (Dec. 2018). "CFD modeling of coal pyrolysis in externally heated fixed-bed reactor". In: *Fuel* 233, pp. 685–694. ISSN: 00162361.

Qian, Y., Zhan, J., Yu, Y., Xu, G., and Liu, X. (June 2019). "CFD model of coal pyrolysis in fixed bed reactor". In: *Chemical Engineering Science* 200, pp. 1–11. ISSN: 00092509.

Raksha, T., Bünger, U., Albrecht, U., Michalski, J., and Zerhusen, J. (2020). *International Hydrogen Strategies: A study commissioned by and in cooperation with the World Energy Council Germany.*

Ramos, H., Baliga, C., Rajendran, A., and Nikrityuk, P. (2024). "CFD-based model of adsorption columns: Validation". In: *Chemical Engineering Science* 285, p. 119606.

Rastegar, S. and Gu, T. (2017). "Empirical correlations for axial dispersion coefficient and Peclet number in fixed-bed columns". In: *Journal of Chromatography A* 1490, pp. 133–137.

Rein, G. (2009). "Smouldering Combustion Phenomena in Science and Technology". In: *International Review of Chemical Engineering* 1, pp. 3–18.

Richter, A., Kestel, M., and Nikrityuk, P. (2014). "Pore-resolved simulation of char particle combustion/gasification". In: *Gasification Processes: Modeling and Simulations*. Ed. by P.

Nikrityuk and B. Meyer. Weinheim, Germany: Wiley-VCH, Verlag GmbH & Co. KGaA, pp. 243–270.

Richter, A., Nikrityuk, P., and Kestel, M. (Apr. 2013). "Numerical investigation of a chemically reacting carbon particle moving in a hot O2/CO2 atmosphere". In: *Industrial and Engineering Chemistry Research* 52 (16), pp. 5815–5824. ISSN: 08885885.

Richter, A., Vascellari, M., Nikrityuk, P., and Hasse, C. (Apr. 2016). "Detailed analysis of reacting particles in an entrained-flow gasifier". In: *Fuel Processing Technology* 144, pp. 95–108. ISSN: 03783820.

Ripoll, N., Salgansky, E., and Toledo, M. (2021). "Volatiles effects on the thermal and chemical structures of H2 production in a hybrid porous media reactor using solar steam". In: *International Journal of Heat and Mass Transfer* 177, p. 121472.

Ripoll, N., Silvestre, C., Paredes, E., and Toledo, M. (2017). "Hydrogen production from algae biomass in rich natural gas-air filtration combustion". In: *International Journal of Hydrogen Energy* 42 (8), pp. 5513–5522. ISSN: 03603199.

Rivero, M., Rodrigues, D., Pinheiro, C., Cardoso, J., and Mendes, L. (2022). "Solid – gas reactors driven by concentrated solar energy with potential application to calcium looping : A comparative review". In: *Renewable and Sustainable Energy Reviews* 158, p. 112048. ISSN: 1364-0321.

Rizkiana, J., Firdausi, H., Pranata, R., Aulia, G., Maulana, S., Wulandari, W., and Sasongko, D. (2019). "Pretreatment of coal by acid leaching as feedstock preparation for co-gasification with biomass". In: *IOP Conference Series: Materials Science and Engineering*. Vol. 543. 1, p. 012067.

Rodilla, I., Contreras, M., and Bahillo, A. (2018). "Thermogravimetric and mass spectrometric (TG-MS) analysis of sub-bituminous coal-energy crops blends in N2, air and CO2/O2 atmospheres". In: *Fuel* 215, pp. 506–514.

Romero, M. and Steinfeld, A. (2012). "Concentrating solar thermal power and thermochemical fuels". In: *Energy & Environmental Science* 5.11, p. 9234.

Rozenberg, A. S., Grigor'Yan, L. A., Gudkova, I. Y., Lempert, D. B., and Manelis, G. B. (Oct. 2009). "Mass transfer of zinc-containing compounds during filtration combustion in the counterflow regime: 3. Mass transfer at a low content of the zinc-containing component in

the initial stock". In: *Russian Journal of Physical Chemistry B* 3 (5), pp. 802–806. ISSN: 19907931.

Ruiz, G., Ripoll, N., Fedorova, N., Zbogar-Rasic, A., Jovicic, V., Delgado, A., and Toledo, M. (2019). "Experimental and numerical analysis of the heat transfer in a packed bed exposed to the high thermal radiation flux". In: *International Journal of Heat and Mass Transfer* 136, pp. 383–392. ISSN: 00179310.

Ruiz, J. A., Juárez, M. C., Morales, M. P., Muñoz, P., and Mendívil, M. A. (2013). "Biomass gasification for electricity generation: Review of current technology barriers". In: *Renewable and Sustainable Energy Reviews* 18, pp. 174–183. ISSN: 13640321.

Sachs, J., Lafortune, G., Fuller, G., and Drumm, E. (2023). "Implementing the SDG stimulus". In: *Sustainable development report*.

Safarian, S., Unnþórsson, R., and Richter, C. (Aug. 2019). "A review of biomass gasification modelling". In: *Renewable and Sustainable Energy Reviews* 110, pp. 378–391. ISSN: 18790690.

Safronov, D., Kestel, M., Nikrityuk, P., and Meyer, B. (Oct. 2014). "Particle resolved simulations of carbon oxidation in a laminar flow". In: *Canadian Journal of Chemical Engineering* 92 (10), pp. 1669–1686. ISSN: 1939019X.

Saidi, M., Gohari, M., and Ramezani, A. (Sept. 2020). "Hydrogen production from waste gasification followed by membrane filtration: a review". In: *Environmental Chemistry Letters* 18 (5), pp. 1529–1556. ISSN: 16103661.

Salganskaya, M. V., Glazov, S. V., Salganskii, E. A., and Zholudev, A. F. (2010). "Filtration combustion of charcoal-polyethylene systems". In: *Russian Journal of Physical Chemistry B* 4 (6), pp. 928–933. ISSN: 1990-7931.

Salganskaya, M., Glazov, S., Salganskii, E., Kislov, V., Zholudev, A., and Manelis, G. (2008). "Filtration combustion of humid fuels". In: *Russian Journal of Physical Chemistry B* 2 (1), pp. 71–76. ISSN: 19907923.

Salganskii, E., Fursov, V., Glazov, S., Salganskaya, M., and Manelis, G. (2006). "Model of vapor-air gasification of a solid fuel in a filtration mode". In: *Combustion, Explosion and Shock Waves* 42 (1), pp. 55–62. ISSN: 00105082.

Salgansky, E. A., Kislov, V. M., Glazov, S. V., and Salganskaya, M. V. (2016). "Formation of liquid products at the filtration combustion of solid fuels". In: *Journal of Combustion* 2016. ISSN: 20901976.

Salgansky, E. A., Zaichenko, A. Y., Podlesniy, D. N., Salganskaya, M. V., and Toledo, M. (Apr. 2017). "Coal dust gasification in the filtration combustion mode with syngas production". In: *International Journal of Hydrogen Energy* 42 (16), pp. 11017–11022.

Salgansky, E. A., Zaichenko, A. Y., Podlesniy, D. N., Salganskaya, M. V., Tsvetkov, M. V., and Chub, A. V. (2020). "Gasification of oil shale dust in a counterflow moving bed filtration combustion reactor". In: *International Journal of Hydrogen Energy* 45 (35), pp. 17270–17275. ISSN: 03603199.

Salgansky, E., Kislov, V., Glazov, S., Zholudev, A., and Manelis, G. (2008). "Filtration combustion of a carbon-inert material system in the regime with superadiabatic heating". In: *Combustion, Explosion and Shock Waves* 44 (3), pp. 273–280. ISSN: 00105082.

Salgansky, E., Lutsenko, N., and Toledo, M. (Nov. 2020). "The Model of the Extraction Process of Rare Metals Under Condition of Filtration Combustion Wave". In: *Frontiers in Chemistry* 8. ISSN: 22962646.

Schmidt, R., Wittig, K., and Nikrityuk, P. (2014). "Single Particle Heating and Drying". In: *Gasification Processes: Modeling and Simulation*. Ed. by P. Nikrityuk and B. Meyer. Weinheim, Germany: Willey-VCH Verlag GmbH & Co, pp. 105–142.

Schult, D., Bayliss, A., Matkowsky, B., and Siam (1998). "Traveling waves in natural counterflow filtration combustion and theri stability". In: *and Applied Mathematics* 58 (3), pp. 806–852.

Schulze, S., Kestel, M., D., S., and Nikrityuk, P. (2013). "From detailed description of chemical reacting coal particles to subgrid models for CFD: model development and validation". In: *Oil & Gas Science and Technology* 68, pp. 1007–1026.

Schulze, S. and Nikrityuk, P. (2016). "A New Subgrid Model for the Heat and Mass Transfer Between a Hot Gas and Char Particles in Dense-Bed Reactors". In: *Journal of Energy Resources Technology* 138, p. 042206.

Schulze, S., Nikrityuk, P., Compart, F., Richter, A., and Meyer, B. (2017). "Particle-resolved numerical study of char conversion processes in packed beds". In: *Fuel* 207, pp. 655–662. ISSN: 00162361.

Schulze, S., Nikrityuk, P., and Meyer, B. (2015). "Porosity distribution in monodisperse and polydisperse fixed beds and its impact on the fluid flow". In: *Particulate Science and Technology* 33.1, pp. 23–33.

Schulze, S., Schmidt, R., and Nikrityuk, P. (2014). "Subgrid models for particle devolatilization-combustion-gasification". In: *Gasification Processes: Modeling and Simulation*. Ed. by P. Nikrityuk and B. Meyer. Weinheim, Germany: Willey-VCH Verlag GmbH & Co, pp. 271–304.

Scott, D. (2008). *Smelling Land: The Hydrogen Defense Against Climate Catastrophe*. Queen's Printer Publishing, p. 485. ISBN: 9780980967401.

Sengodan, S., Lan, R., Humphreys, J., Du, D., Xu, W., Wang, H., and Tao, S. (2018). "Advances in reforming and partial oxidation of hydrocarbons for hydrogen production and fuel cell applications". In: *Renewable and Sustainable Energy Reviews* 82, pp. 761–780. ISSN: 18790690.

Shareefdeen, Z., Elkamel, A., and Tse, S. (Oct. 2015). "Review of current technologies used in municipal solid waste-to-energy facilities in Canada". In: *Clean Technologies and Environmental Policy* 17 (7), pp. 1837–1846. ISSN: 16189558.

Shi, J., Mao, M., Liu, Y., and Lv, J. (2020). "Theoretical analysis of superadiabatic combustion for non-stationary filtration combustion by excess enthalpy function". In: *Royal Society Open Science* 7.10, p. 201038.

Sikarwar, V., Zhao, M., Clough, P., Yao, J., Zhong, X., Memon, M., Shah, N., Anthony, E., and Fennell, P. (2016). "An overview of advances in biomass gasification". In: *Energy and Environmental Science* 9 (10), pp. 2939–2977. ISSN: 17545706.

Siwal, S., Zhang, Q., Sun, C., Thakur, S., Gupta, V., and Thakur, V. (Feb. 2020). "Energy production from steam gasification processes and parameters that contemplate in biomass gasifier – A review". In: *Bioresource Technology* 297. ISSN: 18732976.

Slimane, R., Lau, F., Khinkis, M., Bingue, J., Saveliev, A., and Kennedy, L. (Nov. 2004). "Conversion of hydrogen sulfide to hydrogen by superadiabatic partial oxidation: Thermo-

dynamic consideration". In: *International Journal of Hydrogen Energy* 29 (14), pp. 1471–1477. ISSN: 03603199.

Smith, C., Pineda, D., Zak, C., and Ellzey, J. (2013). "Conversion of jet fuel and butanol to syngas by filtration combustion". In: *International Journal of Hydrogen Energy* 38.2, pp. 879–889.

Soglasnova, S. I., Rozenberg, A. S., and Lempert, D. B. (2009). "Mass transfer of zinc-containing compounds during filtration combustion in the counterflow regime. 1. Mass transfer in the ZnO-inert component system during CO filtration". In: *Russian Journal of Physical Chemistry B* 3 (4), pp. 615–619. ISSN: 19907931.

Stauch, R. and Maas, U. (Sept. 2009). "Transient detailed numerical simulation of the combustion of carbon particles". In: *International Journal of Heat and Mass Transfer* 52 (19-20), pp. 4584–4591. ISSN: 00179310.

Steinfeld, A. (2005). "Solar thermochemical production of hydrogen - A review". In: *Solar Energy* 78 (5), pp. 603–615. ISSN: 0038092X.

Steinfeld, A. and Palumbo, R. (2001). "Solar thermochemical process technology". In: *Encyclopedia of Physical Science and Technology* 15.1, pp. 237–56.

Stoliarov, S. and Lyon, R. (2008). "Thermo-kinetic model of burning for pyrolyzing materials". In: pp. 1141–1152.

Su, Y., Luo, Y., Chen, Y., Wu, W., and Zhang, Y. (Aug. 2011). "Experimental and numerical investigation of tar destruction under partial oxidation environment". In: *Fuel Processing Technology* 92 (8), pp. 1513–1524. ISSN: 03783820.

Subramani, K. (2010). "Hydrogen and Syngas Production and Purification Technologies". In: *Focus on Catalysts* 2010 (7), p. 533. ISSN: 13514180.

Swain, D., Singh, D., Touma, D., and Diffenbaugh, N. (June 2020). "Attributing Extreme Events to Climate Change: A New Frontier in a Warming World". In: *One Earth* 2 (6), pp. 522–527. ISSN: 25903322.

Tamaura, Y., Tsuji, M., Yoshida, S., Yokota, O., and Sano, T. (1999). "Solar gasification of coal using carbonate molten salt reactor". In: *Journal De Physique. IV : JP* 9.3, pp. 0–5. ISSN: 11554339.

Taylor, R. W., Berjoan, R., and Coutures, J. P. (1983). "Solar Gasification of Carbonaceous Materials". In: *Solar Energy* 30.6, pp. 513–525.

Tihay, V. and Gillard, P. (2010). "Pyrolysis gases released during the thermal decomposition of three Mediterranean species". In: *Journal of Analytical and Applied Pyrolysis* 88 (2), pp. 168–174. ISSN: 01652370.

Toledo, M., Araus, K., and Vasconcelo, D. (2015). "Syngas production from coal in presence of steam using filtration combustion". In: *International Journal of Hydrogen Energy* 40 (19), pp. 6340–6345. ISSN: 03603199.

Toledo, M., Arriagada, A., Ripoll, N., Salgansky, E., and Mujeebu, M. (May 2023). "Hydrogen and syngas production by hybrid filtration combustion: Progress and challenges". In: *Renewable and Sustainable Energy Reviews* 177. ISSN: 18790690.

Toledo, M. and Ripoll, N. (Sept. 2019). *Syngas Fuel Production from Carbonaceous Feedstocks Using Hybrid Porous Media*. IntechOpen.

Toledo, M., Ripoll, N., Céspedes, J., Zbogar-Rasic, A., Fedorova, N., Jovicic, V., and Delgado, A. (2018). "Syngas production from waste tires using a hybrid filtration reactor under different gasifier agents". In: *Energy Conversion and Management* 172 (April), pp. 381–390. ISSN: 01968904.

Toledo, M. and Rosales, C. (Oct. 2012). "Hybrid Filtration Combustion". In: *Hydrogen Energy - Challenges and Perspectives*.

Toledo, M., Rosales, C., Silvestre, C., and Caro, S. (Dec. 2016). "Numerical simulation of the hybrid filtration combustion of biomass". In: *International Journal of Hydrogen Energy* 41 (46), pp. 21131–21139. ISSN: 03603199.

Toledo, M., Utria, K., González, F., Zuñiga, J., and Saveliev, A. (2012a). "Hybrid filtration combustion of natural gas and coal". In: *International Journal of Hydrogen Energy* 37 (8), pp. 6942–6948. ISSN: 03603199.

Toledo, M., Utria, K., González, F., Zuñiga, J., and Saveliev, A. (2012b). "Hybrid filtration combustion of natural gas and coal". In: *International Journal of Hydrogen Energy* 37 (8), pp. 6942–6948. ISSN: 03603199.

Toledo, M., Vergara, E., and Saveliev, A. (Mar. 2011). "Syngas production in hybrid filtration combustion". In: *International Journal of Hydrogen Energy* 36 (6), pp. 3907–3912. ISSN: 03603199.

Tomboulides, A., Lee, J., and Orszag, S. (1997). "Numerical simulation of low Mach number reactive flows". In: *Journal of Scientific Computing* 12, pp. 139–167.

Torero, J., Gerhard, J., Martins, M., Zanoni, M., Rashwan, T., and Brown, J. (Nov. 2020). "Processes defining smouldering combustion: Integrated review and synthesis". In: *Progress in Energy and Combustion Science* 81. ISSN: 03601285.

Trombe, F. (1957). "Solar furnaces and their applications". In: *Solar Energy* 1.2-3, pp. 9–15.

Trommer, D. and Steinfeld, A. (2006a). "Kinetic modeling for the combined pyrolysis and steam gasification of petroleum coke and experimental determination of the rate constants by dynamic thermogravimetry in the 500- 1520 K range". In: *Energy & Fuels* 20.3, pp. 1250–1258.

Trommer, D. and Steinfeld, A. (May 2006b). "Kinetic modeling for the combined pyrolysis and steam gasification of petroleum coke and experimental determination of the rate constants by dynamic thermogravimetry in the 500-1520 K range". In: *Energy and Fuels* 20 (3), pp. 1250–1258. ISSN: 08870624.

Turns, S. (2006). *An Introduction to Combustion: Concepts and Applications*. McGraw-Hill. ISBN: 9780072350449.

Vardhan Reddy Kuncharam, B. and Dixon, A. (2020). "Multi-scale two-dimensional packed bed reactor model for industrial steam methane reforming". In: *Fuel Processing Technology* 200, p. 106314.

Volkov, R. and Strizhak, P. (2017). "Planar laser-induced fluorescence diagnostics of water droplets heating and evaporation at high-temperature". In: *Applied Thermal Engineering* 127, pp. 141–156. ISSN: 13594311.

Wang, J., Hu, S., and Liu, X. (Dec. 2022). "Kinetic modelling and experimental validation of single large particle combustion of coal char". In: *Chemical Engineering Journal* 450. ISSN: 13858947.

Wang, J., Wei, S., Wang, Q., and Sundén, B. (Apr. 2021). "Transient numerical modeling and model predictive control of an industrial-scale steam methane reforming reactor". In: *International Journal of Hydrogen Energy* 46 (29), pp. 15241–15256. ISSN: 03603199.

Warsi, Y., Kabanov, V., Zhou, P., and Sinha, A. (Oct. 2020). "Novel Carbon Dioxide Utilization Technologies: A Means to an End". In: *Frontiers in Energy Research* 8. ISSN: 2296598X.

Weinberg, F. (1971). "Combustion temperatures: The future?" In: *Nature* 233 (5317), pp. 239–241. ISSN: 00280836.

Wernberg, T., Russell, B., Moore, P., Ling, S., Smale, D., Campbell, A., Coleman, M., Steinberg, P., Kendrick, G., and Connell, S. (Apr. 2011). "Impacts of climate change in a global hotspot for temperate marine biodiversity and ocean warming". In: *Journal of Experimental Marine Biology and Ecology* 400 (1-2), pp. 7–16. ISSN: 00220981.

Wieckert, C., Obrist, A., Zedtwitz, P. V., Maag, G., and Steinfeld, A. (2013). "Syngas production by thermochemical gasification of carbonaceous waste materials in a 150 kWth packed-bed solar reactor". In: *Energy & Fuels* 27.8, pp. 4770–4776.

Wilberforce, T., Olabi, A., Sayed, E., Elsaid, K., and Abdelkareem, M. (2021). "Progress in carbon capture technologies". In: *Science of The Total Environment* 761, p. 143203.

Wittig, K., Golia, A., and Nikrityuk, P. (2012). "3D Numerical study of the influence of particle porosity on the heat and fluid flow". In: *Progress in Computational Fluid Dynamics* 12, pp. 207–19.

Wittig, K., Nikrityuk, P., Schulze, S., and Richter, A. (May 2017). "Three-dimensional modeling of porosity development during the gasification of a char particle". In: *AIChE Journal* 63 (5), pp. 1638–1647. ISSN: 15475905.

Wittig, K., Nikrityuk, P., and Richter, A. (2017). "Drag coefficient and Nusselt number for porous particles under laminar flow conditions". In: *International Journal of Heat and Mass Transfer* 112, pp. 1005–1016.

Wood, S. and Harris, A. (2008). "Porous burners for lean-burn applications". In: *Progress in Energy and Combustion Science* 34.5, pp. 667–684.

Wu, X. and Ghoniem, A. (2019). "Mixed ionic-electronic conducting (MIEC) membranes for thermochemical reduction of CO2: A review". In: *Progress in Energy and Combustion Science* 74, pp. 1–30. ISSN: 03601285.

Xu, Q., Pang, S., and Levi, T. (May 2011). "Reaction kinetics and producer gas compositions of steam gasification of coal and biomass blend chars, Part 2: Mathematical modelling and model validation". In: *Chemical Engineering Science* 66 (10), pp. 2232–2240. ISSN: 00092509.

Yang, Z., Wu, Y., Zhang, Z., Li, H., Li, X., Egorov, R., Strizhak, P., and Gao, X. (Apr. 2019). "Recent advances in co-thermochemical conversions of biomass with fossil fuels focusing on the synergistic effects". In: *Renewable and Sustainable Energy Reviews* 103, pp. 384–398. ISSN: 18790690.

Yi, F., Fan, J., Li, D., Lu, S., and Luo, K. (Apr. 2011). "Three-dimensional time-dependent numerical simulation of a quiescent carbon combustion in air". In: *Fuel* 90 (4), pp. 1522–1528. ISSN: 00162361.

Younas, M., Rezakazemi, M., Daud, M., Wazir, M., Ahmad, S., Ullah, N., Inamuddin, and Ramakrishna, S. (2020). "Recent progress and remaining challenges in post-combustion CO2 capture using metal-organic frameworks (MOFs)". In: *Progress in Energy and Combustion Science* 80. ISSN: 03601285.

Yu, J., Zhou, K., and Ou, W. (2013). "Effects of Stefan flow and CO oxidation on char particle combustion in O2/CO2 atmosphere". In: *Fuel* 106, pp. 576–585. ISSN: 00162361.

Zaichenko, A., Podlesniy, D., Salganskaya, M., Tsvetkov, M., and Salganskiy, E. (Apr. 2018). "Gasification of Powdered Solid Fuel in the Filtration Combustion Mode". In: *Russian Journal of Applied Chemistry* 91 (4), pp. 611–617. ISSN: 10704272.

Zaichenko, A. Y., Zhirnov, A. A., Manelis, G. B., Polianchik, E. V., and Zholudev, A. F. (2008a). "Filtration combustion front stabilization". In: *Doklady Chemistry* 418.2, pp. 37–39. ISSN: 00125008.

Zaichenko, A. Y., Zhirnov, A. A., Manelis, G. B., Polianchik, E. V., and Zholudev, A. F. (2010). "Filtration combustion of carbon in a non-one-dimensional solid flow". In: *Theoretical Foundations of Chemical Engineering* 44.1, pp. 30–35. ISSN: 00405795.

Zaichenko, A., Zhirnov, A., Manelis, G., Polianchik, E., and Zholudev, A. (2008b). "Filtration combustion front stabilization". In: *Doklady Chemistry* 418 (2), pp. 37–39. ISSN: 0012-5008.

Zandalinas, S., Fritschi, F., and Mittler, R. (June 2021). "Global Warming, Climate Change, and Environmental Pollution: Recipe for a Multifactorial Stress Combination Disaster". In: *Trends in Plant Science* 26 (6), pp. 588–599. ISSN: 13601385.

Zanganeh, J., Moghtaderi, B., and Ishida, H. (2013). "Combustion and flame spread on fuel-soaked porous solids". In: *Progress in Energy and Combustion Science* 39 (4), pp. 320–339. ISSN: 03601285.

Zeng, Y. X., Wang, L., Wu, C. F., Wang, J. Q., Shen, B. X., and Tu, X. (2018). "Low temperature reforming of biogas over K-, Mg- and Ce-promoted Ni/Al2O3 catalysts for the production of hydrogen rich syngas: Understanding the plasma-catalytic synergy". In: *Applied Catalysis B: Environmental* 224, pp. 469–478. ISSN: 09263373.

Z'Graggen, A., Haueter, P., Trommer, D., Romero, M., Jesus, J. C. de, and Steinfeld, A. (2006). "Hydrogen production by steam-gasification of petroleum coke using concentrated solar power-II Reactor design, testing, and modeling". In: *International Journal of Hydrogen Energy* 31.6, pp. 797–811. ISSN: 03603199.

Zhang, Z., Ye, J., Tan, D., Feng, Z., Luo, J., Tan, Y., and Huang, Y. (2021a). "The effects of Fe2O3 based DOC and SCR catalyst on the combustion and emission characteristics of a diesel engine fueled with biodiesel". In: *Fuel* 290, p. 120039.

Zhang, Z., Zhao, Z., Wu, F., Luo, C., Li, X., Chen, Y., Lu, B., Zhang, L., and Zheng, C. (May 2021b). "Reaction behaviors of a single coal char particle affected by oxygen and steam under oxy-fuel combustion". In: *Fuel* 291, p. 120229. ISSN: 00162361.

Zhang, Z., Zhong, Y., Zhao, Z., Zhang, L., Li, X., Zha, X., Luo, C., and Wu, F. (July 2022). "Numerical study on heterogeneous reaction characteristics of a single coal char particle under air- and oxy-fuel combustion: Effects of particle motion". In: *Fuel* 320, p. 123919. ISSN: 00162361.

Zhao, X., Huang, G., Lu, C., Zhou, X., and Li, Y. (2020). "Impacts of climate change on photovoltaic energy potential: A case study of China". In: *Applied Energy* 280 (August), p. 115888. ISSN: 03062619.

Zhao, X., Ma, X., Chen, B., Shang, Y., and Song, M. (2022). "Challenges toward carbon neutrality in China: Strategies and countermeasures". In: *Resources, Conservation and Recycling* 176, p. 105959.

Zheng, C., Cheng, L., Cen, K., Bingue, J., and Saveliev, A. (Mar. 2012). "Partial oxidation of methane in a reciprocal flow porous burner with an external heat source". In: *International Journal of Hydrogen Energy* 37 (5), pp. 4119–4126. ISSN: 03603199.

Zhu, X., Li, S., Shi, Y., and Cai, N. (2019). "Recent advances in elevated-temperature pressure swing adsorption for carbon capture and hydrogen production". In: *Progress in Energy and Combustion Science* 75. ISSN: 03601285.

Zik, O., Olami, Z., and Moses, E. (1998). "Fingering instability in combustion". In: *Physical Review Letters* 81 (18), pp. 3868–3871. ISSN: 10797114.

Appendix: Supplementary material Chapter 5[*]

[*]This appendix is based on the supplementary material of the manuscript published in A. Arriagada, R. Mena, N. Ripoll, R.E. Hayes, P. Nikrityuk and M. Toledo, Chemical Engineering Journal, **2024**.

A.1 Evolution of optical design configuration

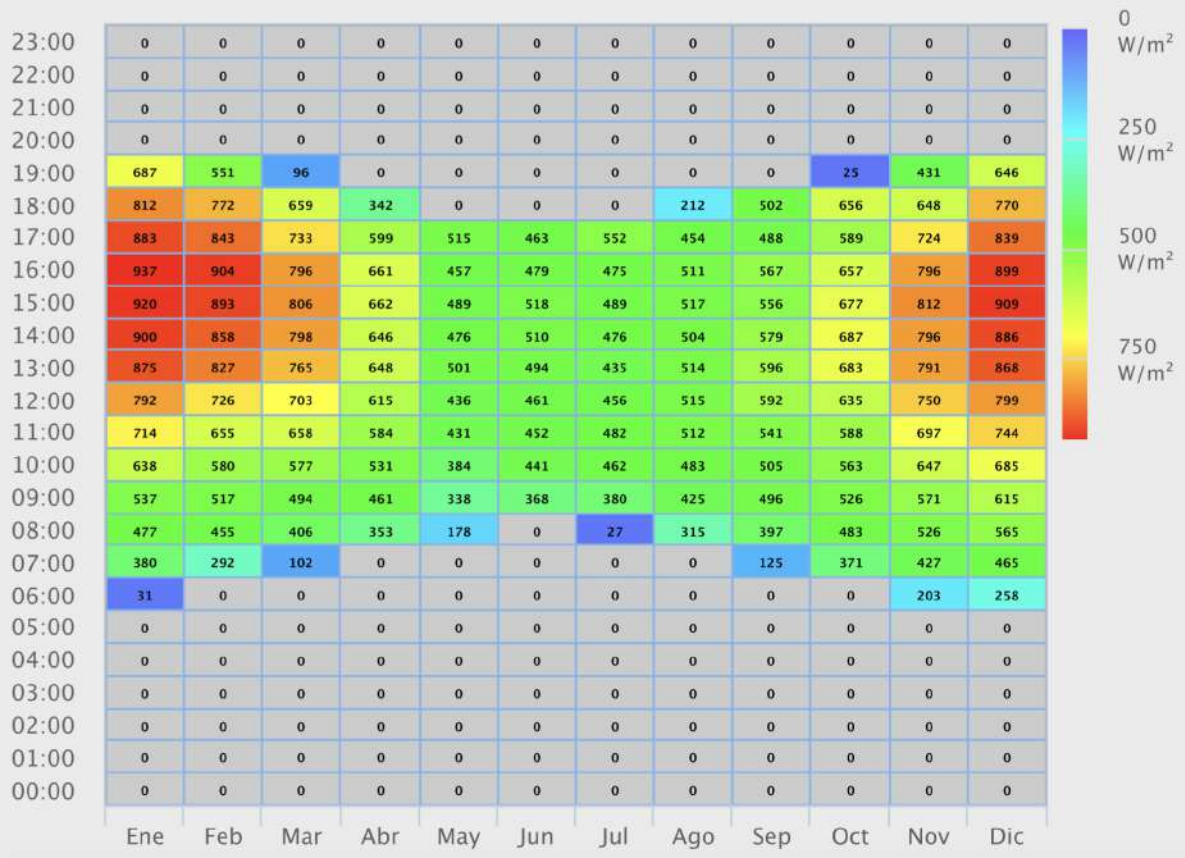

Figure A.1.1: Annual normal radiation at sample site period 2004-2016. Coordinates: 33°02'23.0"S, 71°29'09.3"W.

(a) (b)

(c)

Figure A.1.2: Reactor located behind parabolic disc (a). Reactor located in front of parabolic disc (b). Actual optical configuration (c).

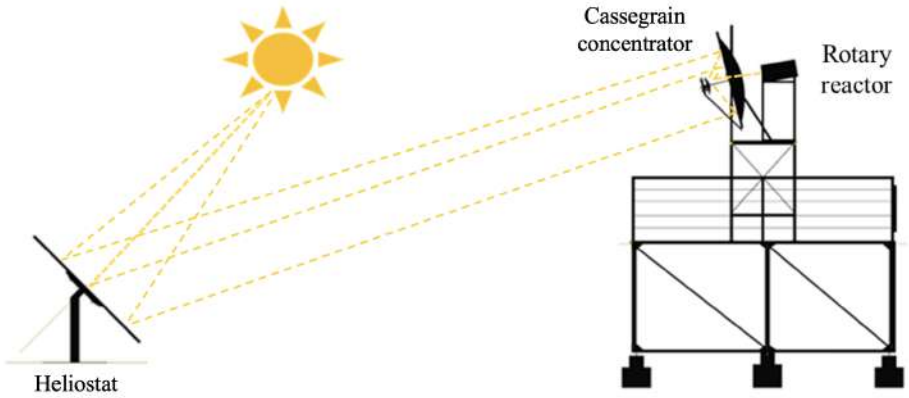

(a)

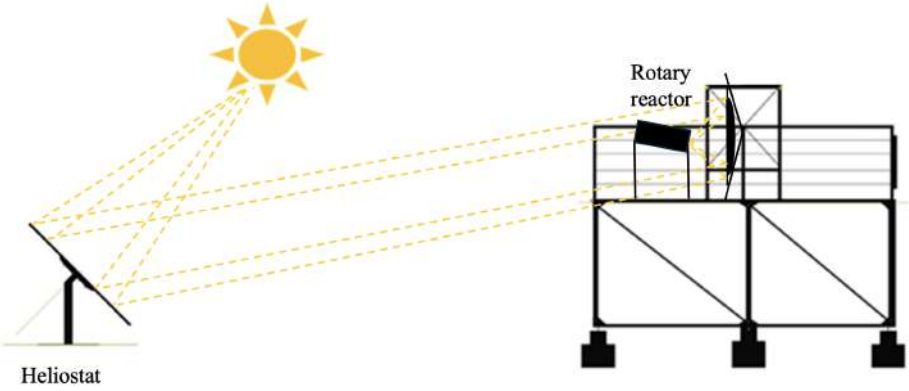

(b)

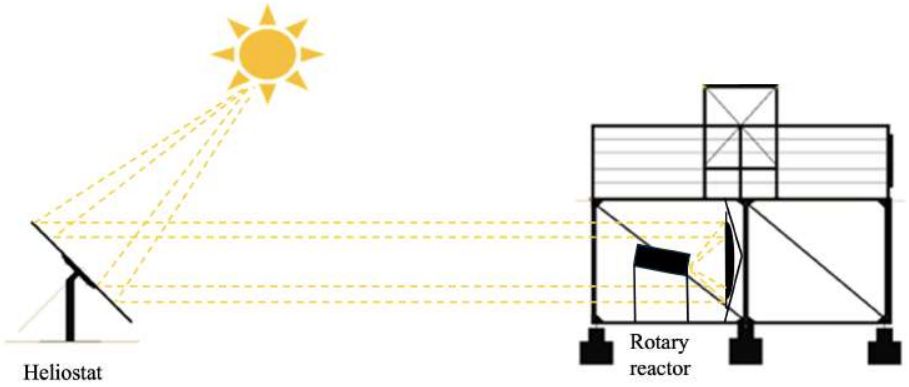

(c)

Figure A.1.3: Schematic of the solar experimental test bench. Yellow dashed lines represent the trajectory of a sun ray across the optical configuration. (a) Cassegrain concentrator configuration. (b) Reactor located at the top of the structure. (c) Real emplacement of the solar experimental test bench.

A.2 Flat-plate calorimeter

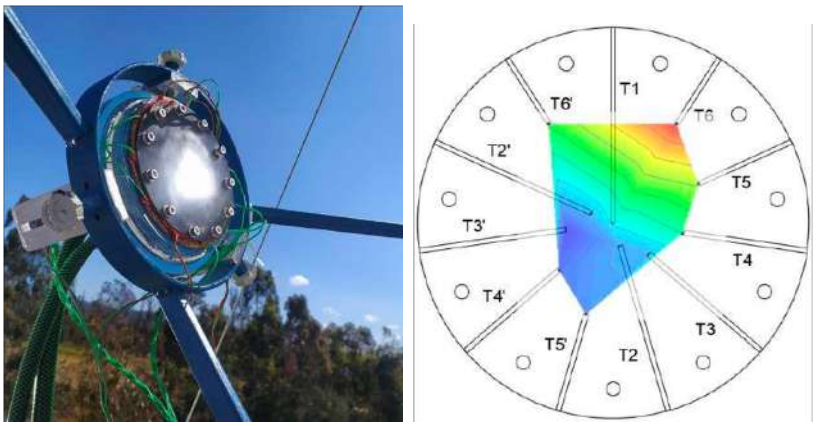

(a) (b)

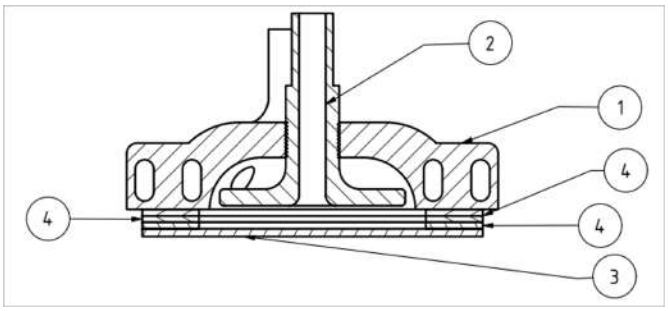

(c)

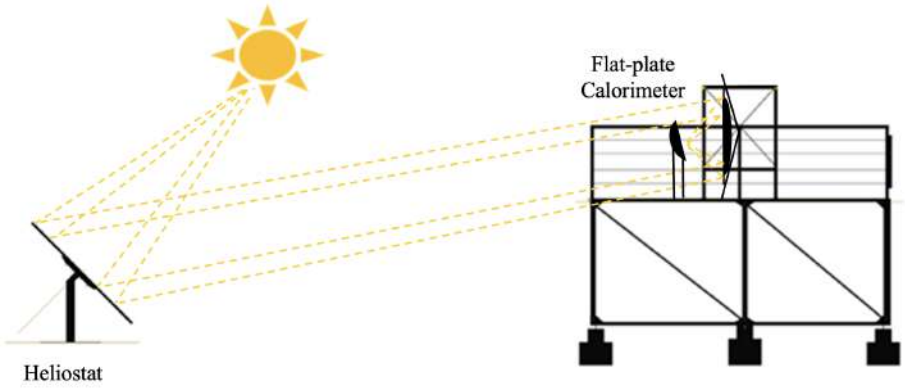

(d)

Figure A.2.1: Flat-plate calorimeter under real operation conditions (a). Distribution of type-K thermocouples and temperature profile obtained from a measurement (lower to higher temperatures go from blue to red) (b). Schematic of flat-plate calorimeter with parallel plates: (1) Calorimeter body, (2) Difusor, (3) Copper plate, (4) Rubber seals (c). Solar experimental test bench using calorimeter (d).

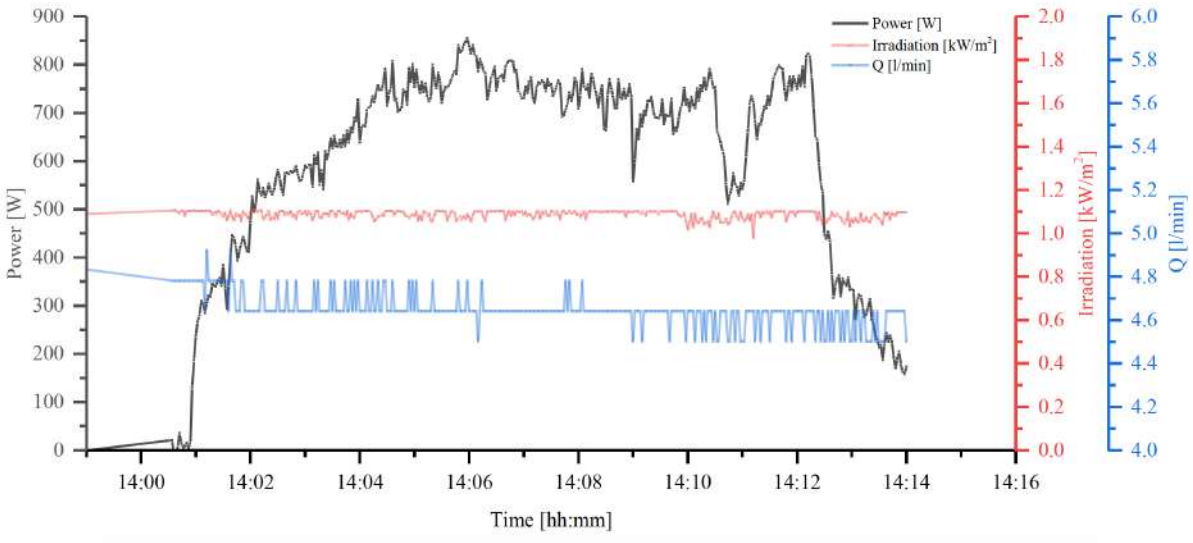

Figure A.2.2: Temperature, irradiation, and power measurements for one of the tested experimental conditions with the custom calorimeter.

A.3 Solar rotary reactor

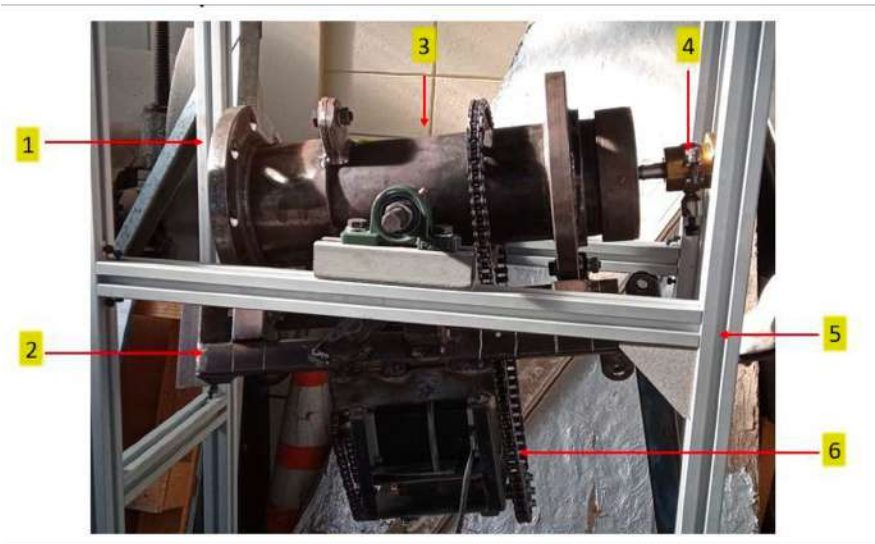

Figure A.3.1: Uninsulated rotary reactor. (1) Cavity receiver; (2) Reactor's cradle; (3) Reactor main body; (4) Two-way high temperature rotary joint; (5) Adjustable support structure; (6) Rotary drive.

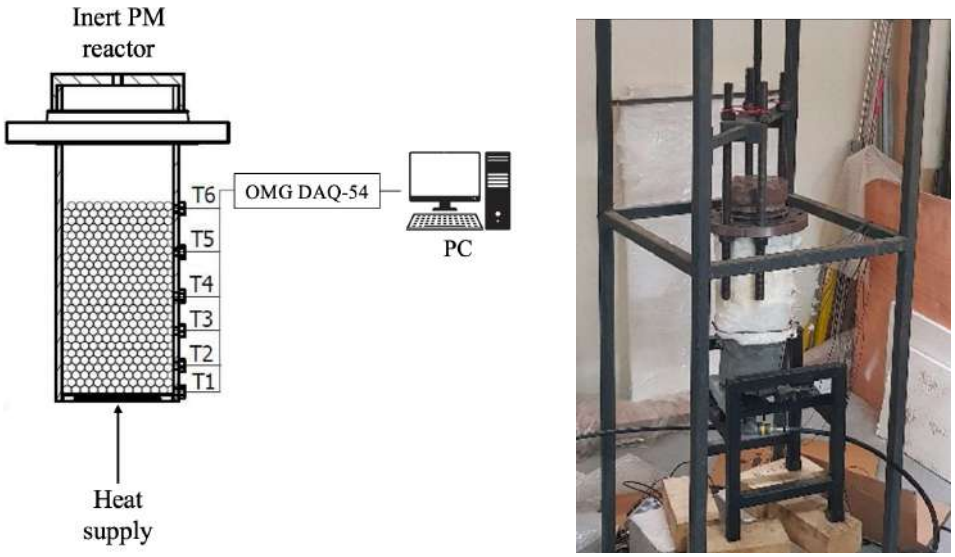

(a) (b)

Figure A.3.2: Schematics (a) and Experimental setup (b) for characterization inert porous media reactor.

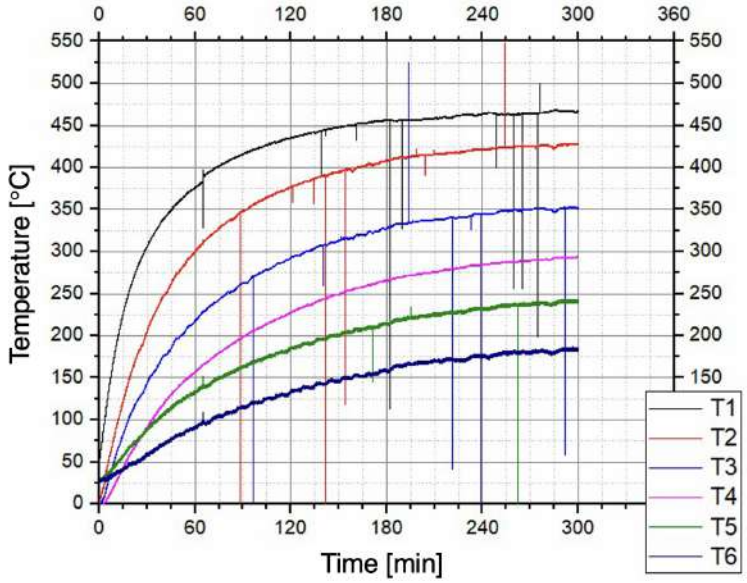

Figure A.3.3: Thermal profile characterization inert porous media reactor.